

The Texas Medical Center Library

DigitalCommons@TMC

The University of Texas MD Anderson Cancer
Center UTHealth Graduate School of
Biomedical Sciences Dissertations and Theses
(Open Access)


The University of Texas MD Anderson Cancer
Center UTHealth Graduate School of
Biomedical Sciences

8-2019

Commissioning of Micro-Cube Thermoluminescent Dosimeters for Small Field Dosimetry Quality Assurance in Radiotherapy

Brandon Luckett

Follow this and additional works at: https://digitalcommons.library.tmc.edu/utgsbs_dissertations

 Part of the [Biological and Chemical Physics Commons](#), [Medicine and Health Sciences Commons](#), and
the [Other Physics Commons](#)

Recommended Citation

Luckett, Brandon, "Commissioning of Micro-Cube Thermoluminescent Dosimeters for Small Field Dosimetry Quality Assurance in Radiotherapy" (2019). *The University of Texas MD Anderson Cancer Center UTHealth Graduate School of Biomedical Sciences Dissertations and Theses (Open Access)*. 951.
https://digitalcommons.library.tmc.edu/utgsbs_dissertations/951

This Thesis (MS) is brought to you for free and open access by the The University of Texas MD Anderson Cancer Center UTHealth Graduate School of Biomedical Sciences at DigitalCommons@TMC. It has been accepted for inclusion in The University of Texas MD Anderson Cancer Center UTHealth Graduate School of Biomedical Sciences Dissertations and Theses (Open Access) by an authorized administrator of DigitalCommons@TMC. For more information, please contact digitalcommons@library.tmc.edu.

The
TMC LIBRARY
Health Sciences Resource Center

COMMISSIONING OF MICRO-CUBE THERMOLUMINESCENT DOSIMETERS
FOR SMALL FIELD DOSIMETRY QUALITY ASSURANCE
IN RADIOTHERAPY

by

Brandon Michael Lockett, B.S.

APPROVED:

Paige Taylor, M.S.
Advisory Professor

David Followill, Ph.D.

Stephen Kry, Ph.D.

Dershan Luo, Ph.D.

Christine Peterson, Ph.D.

APPROVED:

Dean, The University of Texas
MD Anderson Cancer Center UTHHealth Graduate School of Biomedical Sciences

COMMISSIONING OF MICRO-CUBE THERMOLUMINESCENT DOSIMETERS
FOR SMALL FIELD DOSIMETRY QUALITY ASSURANCE
IN RADIOTHERAPY

A

THESIS

Presented to the Faculty of

The University of Texas

MD Anderson Cancer Center UTHHealth

Graduate School of Biomedical Sciences

in Partial Fulfillment

of the Requirements

for the Degree of

MASTER OF SCIENCE

by

Brandon Michael Lockett, B.S.

Houston, TX

August, 2019

Dedication

I would like to dedicate this work to my father, John Paul Lockett Jr. My father was my first mentor and is my greatest critic, my largest motivation, and one of my best friends. There has never been a moment when he did not have my back. A simple thank you will never be enough.

Acknowledgements

First and foremost I would like to thank Paige Taylor, my advisor, for taking me on as her first student. Paige was an incredible advisor to me and did an exceptional job of being a mentor as I conducted my research. Secondly I would like to thank Dr. David Followill for providing my project and helping to develop my skills as a student and physicist. Together, Paige and Dr. Followill developed my abilities and work ethic.

I would also like to extend my thanks to my committee, who spent so much time and energy in ensuring I would complete my project, not only in a timely manner, but also in a way which exhibited fantastic results. Dr. Dershan Luo spent several evenings developing treatment plans and delivering SRS treatments with me, Dr. Christine Peterson conducted statistical analysis during her busy schedule, and Dr. Kry taught me to dive deeper into the meaning behind the results we procured and how to truly think as a physicist.

This thesis work would not be complete if it had not been for the hands of several people outside of my committee. Paola Alavarez arguable spent the most amount of time with me, from countless measurements on Cobalt machines and linacs to equally countless office visits to discuss results, without her help, I would likely have spent another year working on this thesis.

Several IROC Houston staff also had a large hand in the success of this thesis. This study required several custom designed tools, holders, and capsules. John Costales was the genius behind the designs and the talent behind making them a reality. Lynda McDonald taught me how to read TLD, and also took time out of her schedule multiple times to read TLD for my experiment as well. I would like to extend a huge thank you to both of them.

Trang Nguyen deserves a special thanks for being patient with me as we did film analysis across more than 40 experiments. Additionally, Trang loaded multiple phantoms, and made them ready for experiments for me.

Another special thanks to Dr. Ryan Lafratta from St. Luke's. Dr. Ryan took time out of her own day to give me access to their CyberKnife SRS treatment machine. Not only is Dr. Ryan outside of my committee, she is also outside of MD Anderson, so her help was purely out of selflessness.

As you can very well tell, this work was an effort which extended far past my hands. I am incredibly thankful to each individual who made my work possible, and I cannot take full credit.

A final thank you to my family and loved ones, for they are the backbone of my life. They truly are my motivation.

COMMISSIONING OF MICRO-CUBE THERMOLUMINESCENT DOSIMETERS FOR SMALL FIELD
DOSIMETRY QUALITY ASSURANCE
IN RADIOTHERAPY

Brandon Michael Lockett, B.S.

Supervisory Professor: Paige Taylor, M.S.

Abstract

Small field dosimetry presents complications and uncertainties that could be circumvented by using detectors which are smaller than the radiation field. This study evaluates the reproducibility and accuracy of TLD micro-cubes for use in stereotactic radiosurgery (SRS) remote auditing quality assurance (QA) for treatment centers participating in clinical trials. This study tested the hypothesis that TLD micro-cubes could be commissioned to evaluate small field dosimetry, and provide reproducibility within $\pm 3\%$, as well as assure agreement between measured dose and calculated doses to within $\pm 5\%$.

The aims of this thesis were to characterize and commission TLD micro-cubes as well as to develop guidelines for handling micro-cubes. Additionally the micro-cubes were commissioned to evaluate standard single field output dosimetry. Further aims were to adapt IROC Houston SRS head phantoms to use TLD micro-cubes for anthropomorphic phantom quality assurance and to test this design on linac, Gamma Knife, and CyberKnife treatment delivery machines. The final aim was to use TLD micro-cubes to evaluate photon fields which are smaller than 1.25 cm in diameter.

This study was designed by first defining the handling process, including: selection of micro-cubes, annealing parameters, and readout techniques. The micro-cubes were then

characterized based on correction factors for element sensitivity, signal fading, dose response, and energy response.

To test the reproducibility and accuracy of the dosimeters, they were first evaluated under a single small field beam in a simple geometric configuration, then in anthropomorphic SRS head phantoms. Agreement between calculated dose and measured dose was evaluated. Following satisfactory results of these experiments, the micro-cubes were used to evaluate single small fields down to 5 mm fields on the same basis as single field output checks.

TLD micro-cubes showed good accuracy and agreement when compared to beam output, treatment planning system (TPS) dose, and measurements made with TLD powder. For all experiments conducted in this study, measured dose was within 4.1%. For SRS experiments, the average difference in measured and expected dose was within 3.4% with an average difference of 1.0% and an average coefficient of variation of 0.9%. For single field experiments, all measurements were within 4.1% with an average of 2.1% and an average coefficient of variation of 0.6%. These results give us confidence in our ability to accurately measure dose in radiation fields as small as 5 mm in diameter, as well as obtain excellent reproducibility.

Contents

Signature Page.....	i
Title Page.....	ii
Dedication	iii
Acknowledgements.....	iv
Abstract	vi
Tables	xi
Figures	xii
1 Introduction	1
1.1 Statement of the Problem.....	1
1.2 Background.....	3
1.2.1 Stereotactic Radiosurgery	3
1.2.2 Small Field Dosimetry	6
1.2.3 The Imaging and Radiation Oncology Core Houston QA Center Services.....	9
1.2.4 Thermoluminescent Dosimeters	12
1.3 Hypothesis and Specific Aims.....	20
1.3.1 Hypothesis	20
1.3.2 Specific Aims	20
2 Materials and Methods.....	22
2.1 TLD Micro-Cubes	22
2.1.1 TLD-100 Micro-Cube Specifications.....	24
2.2 TLD Micro-Cube Handling	24
2.2.1 Micro-Cube Shape Uniformity.....	24
2.2.2 TLD Annealing.....	25
2.2.3 TLD Signal Reading.....	28
2.3 TLD Micro-Cube Characterization	32
2.3.1 Elemental Correction Factor.....	33
2.3.2 System Calibration Factor: S	36
2.3.3 Linearity Correction: K_L	37
2.3.4 Energy Correction Factor: K_E	39
2.3.5 Fading Correction Factor: K_F	39

2.4 Uncertainty Analysis.....	40
2.5 Single Field Irradiations	41
2.6 SRS Head Phantom Irradiation Experiments.....	48
2.6.1 Varian TrueBeam Treatment Planning and Delivery to SRS Head Phantom.....	53
2.6.2 Elekta Gamma Knife Treatment Planning and Delivery to SRS Head Phantom	56
2.6.3 CyberKnife Treatment Planning and Delivery to SRS Head Phantom	59
2.7 Single Small Field Irradiations	63
2.8 TLD Dose Calculations and Dosimetry Evaluation.....	65
2.8.1 Dose Calculations.....	65
2.8.2 Film Dosimetry Evaluation.....	66
2.9 Statistical Analysis	68
3 Results	69
3.1 Micro-Cube Handling	69
3.1.1 Micro-Cube Shape Uniformity.....	69
3.1.2 TLD Annealing Response	70
3.1.3 Micro-Cube Reading Variability.....	72
3.2 TLD Micro-cube Characterization.....	74
3.2.1 Elemental Correction Factor (ECF)	74
3.2.2 Linearity Correction Factor (K_L)	76
3.2.3 Energy Correction Factor K_E	81
3.3 Uncertainty Analysis.....	81
3.4 Single Field Experiment Results	83
3.4.1 Single Field Film	84
3.5 SRS Head Experiment Results	86
3.5.1 SRS Head Linac Experiment Results.....	86
3.5.2 SRS Head Gamma Knife Experiment Results	90
3.5.3 SRS Head CyberKnife Experiment Results	98
3.6 Single Small Field Output Results.....	101
3.6.1 Small Field Film	103
3.7 Statistical Analysis	105

4 Discussion.....	106
4.1 Characterization	106
4.2 TLD Handling and Reading	106
4.3 Irradiation Experiments.....	107
4.3.1 Single Field Irradiations	107
4.3.2 SRS Linac, Gamma Knife, CyberKnife Experiments	107
4.3.3 Small Field Irradiations	109
4.3.4 Film Analysis	109
4.4 Statistics	110
4.5 Small Field Considerations	110
5 Conclusion.....	111
5.1 Conclusion	111
5.2 Future Work	113
5.2.1 Fading Correction	113
5.2.2 Future Applications.....	113
6 Appendix	114
6.1 SRS Head Phantom Instructions.....	114
6.2 Gamma Knife	116
6.2.1 Gamma Knife Treatment Plan Snapshots.....	116
6.2.2 Gamma Knife Dose Profile.....	119
6.2.3 GammaKnife Film	119
6.2.4 Gamma Knife Film Gamma Analysis.....	120
6.2.5 Gamma Knife Film/TPS dose Line Profiles.....	123
6.3 CyberKnife	126
6.3.1 CyberKnife Treatment Plan Snapshots.....	126
6.3.2 CyberKnife Film.....	130
6.3.3 CyberKnife Film Gamma Analysis	131
6.3.4 CyberKnife Film/TPS dose Agreement.....	135
6.4 Linac.....	137
6.4.1 Linac Treatment Plan Snapshots and Isodose Lines.....	137

6.4.2 Linac Film	141
6.4.3 Linac Film Gamma Analysis	142
6.4.3 Linac Film/TPS dose Line Profiles	145
6.5 Small Field Film Line Profiles	147
Bibliography	153
Vita	157

Tables

Table 1: Various commercially available forms of TLD-100 from ThermoScientific™	14
Table 2: TLD annealing times	28
Table 3: WinREMS software TTP parameters for reading TLD micro-cubes	30
Table 4: Energy Correction factors for ⁶⁰ Cobalt, 6MV, and 18MV photon beams.	81
Table 5: Single field output results	83
Table 6: Single filed output average dose, coefficient of variation, and average ratio of measured dose: expected dose	84
Table 7: TLD micro-cube and TLD powder agreement	84
Table 8: Linac SRS head phantom dose measurement compared to TPS doses. Letter A, B, and C refer to the experiment trial	87
Table 9: Linac micro-cube reproducibility	87
Table 10: TLD micro-cube and TLD powder comparison for SRS linac experiments.....	87
Table 11: Summary of Gamma Knife experiment dose calculations. Letter A, B, and C refer to the experiment trial.	91
Table 12: Gamma Knife micro-cube reproducibility.....	91
Table 13: TLD micro-cube versus TLD powder for Gamma Knife SRS head experiments	91
Table 14: TLD micro-cube differences in Gamma Knife experiment.....	96
Table 15: CyberKnife measured dose evaluation	99
Table 16: CyberKnife experiment reproducibility.....	99
Table 17: Comparison of micro-cube and TLD powder	99
Table 18: Single small field irradiation results.....	103
Table 19: Single small field irradiation results.....	103

Figures

Figure 1: Horsley-Clarke Frame <i>Used with permission from the American Association of Neurological Surgeons: "A Short History of Stereotactic Neurosurgery", Robert Levy, MD</i>	Figure 1
Figure 2: Partial occlusion of the primary photon source (B) causes the penumbra from both field edges to overlap. (Aspradakis et al., 2010) <i>Copyright: Institute of Physics and Engineering in Medicine 2010. Reproduced with Permission</i>	8
Figure 3: 4mm dose profile for Gamma Knife. See Appendix for more profiles.	9
Figure 4: IROC SRS Head Phantom.....	11
Figure 5: Capsules used to contain TLD-100 Powder.	12
Figure 6 : The crystal lattice contains two energy levels of importance: the valence band, and the conduction band. The valence band is low energy, and electrons contained in the valence band are bound to the lattice. Electrons in the higher energy conduction band are free to migrate about the crystal lattice. In between is the band gap, in which electrons are forbidden to occupy. Added impurities create activator sites in the forbidden band gap, which permit electron occupation.	16
Figure 7: The impurities added to TLD provide electron/hole trapping centers in the band gap. Trapping centers permit the use of TLD as a dosimeter that can be read out at a later time after irradiation. Trapping centers have different escape energies (depth), and are therefore cleared at different temperatures upon readout.....	17
Figure 8: TLD-100 is linear out to about 400cGy; where there is an over-response as dose increases.	18
Figure 9: Harshaw TLD-100 Micro-Cubes from ThermoScientific	23
Figure 10: Radiation Products Design Inc. annealing planchet	26
Figure 11: Radiation Products Design Inc. Model 168 TLD Annealing Furnace.....	26
Figure 12: Blue M Electric Company Stabil-Therm Gravity Oven	27
Figure 13: Glow curve captured from TLD-100 micro-cube using Harshaw reader and WinRems software	29
Figure 14: A) Harshaw 3500 TLD annealing planchet B) TLD Micro-cube in the center of the heating planchet	31
Figure 15 A) ECF irradiation disc B) Irradiation disc with buildup.	35
Figure 16: IROC Cobalt mini-phantoms 4.5 x 3 x 1.6 cm ³ , 6.8 mm buildup cap, TLD micro-cube numbered insert for cube identification.	37
Figure 17: Single field phantom: A) Block with gantry direction indicator B) Dimensions 14.8 x 14.8 x 16.5 cm ³ C) Unassembled single field phantom D) Single field phantom with top plate removed	42
Figure 18: Gantry direction indicator and laser alignment indicators on the single field phantom	43
Figure 19: Single field phantom insert.....	44

Figure 20: TLD micro-cube capsule for single field phantom Dimensions: Diameter= 4.55mm Length= 5.14mm	45
Figure 21: TLD micro-cube capsules for single field phantom.....	46
Figure 22: Single field irradiation linac set-up.	47
Figure 23: Single small field irradiation setup. A) 10 x 10 cm ² B) 10 x 10 cm ² C) 3 x 3 cm ² D) 2 x 2 cm ²	48
Figure 24: SRS Head Phantom	50
Figure 25: SRS Head Phantom	51
Figure 26: Solid water tumor simulator, TLD capsule insert indicated by the blue ovals, and the center of the solid water ball is indicated by the green crosshairs.....	52
Figure 27: SRS micro-cube capsules, constructed with polycarbonate. Each capsule holds 3 TLD micro-cubes.....	53
Figure 28: RayStation treatment planning dose constraint goals	54
Figure 29: RayStation treatment planning dose to volume. CTV2mm = Clinical Target Volume, InfTLD = inferior TLD capsule active volume (powder or micro-cubes), SupTLD = superior TLD capsule active volume.....	55
Figure 30: Varian TrueBeam SRS head treatment setup	56
Figure 31: Gamma Knife setup.....	58
Figure 32: Gamma Knife image co-registration applied correction	59
Figure 33: Gamma Knife Treatment Plan Dose Map	59
Figure 34: Minimum, Mean, and Maximum dose to CTV (Tumor), Inferior TLD Capsule (Cap 1), and Superior Capsule (Cap 2).....	61
Figure 35. TOP: DVH of relative dose BOTTOM: Min, Max, and Mean dose to volumes. Cap 1 = superior capsule Cap 2 = inferior capsule.....	61
Figure 36: CyberKnife treatment plan. See Appendix	62
Figure 37: CyberKnife treatment plan isodose lines to treatment volume. See Appendix.....	63
Figure 38: Small Fied CyberKnife set-up 78.5cm SSD	64
Figure 39: CyberKnife internal laser alignment for small field experiments.....	65
Figure 40: Film Densitometer, Model CCD100 CCD Microdensitometer for Radiochromic Film (Photoelectron Corporation, Lexington, Massachusetts, USA).....	67
Figure 41: <i>Left</i> : Coronal film loaded using MatLab program <i>Right</i> : Pin breaks registered for positioning, labeled 1, 2, and 3.....	68
Figure 42: The film dose profile is co-registered on the CT simulation.....	68
Figure 43: Irregularly shaped TLD-100 micro-cubes from ThermoScientific.....	70
Figure 44: TLD Annealing Response: Legend reads: Time at 400°C, Time cooling; Time at 100°C	71
Figure 45: TLD annealing planchet cooling curve	72
Figure 46: TLD placement effect.....	73
Figure 47: Reader variability	74

Figure 48: Histogram of ECF values for all TLD micro-cubes.	76
Figure 49: TOP) Linearity dose measurement 1 BOTTOM) Linearity measurement 2	77
Figure 50: Dose/Signal (K_L) with respect to dose. 45A show the first experiment for linearity, while 45B shows the second experiment.	79
Figure 51: Normalized linearity plots. 46A show the first experiment for linearity, while 46B shows the second experiment.	80
Figure 52: Linearity correction factors comparison from both measurements	81
Figure 53: 3 x 3 cm ² field film.....	85
Figure 54: 3 x 3 cm ² field line profiles, solid black lines indicate tumor boundaries	85
Figure 55: 2 x 2 cm ² field film.....	85
Figure 56: 2 x 2 cm ² field line profiles, solid black lines indicate tumor boundaries	86
Figure 57: SRS linac film registration	88
Figure 58: Film dose line profiles for Linac. See appendix for all profiles.	89
Figure 59: Gamma analysis for linac coronal plane	90
Figure 60: Superior Capsule TOP: Axial view BOTTOM: Sagittal View	93
Figure 61: Inferior Capsule TOP: Axial View BOTTOM: Sagittal View	94
Figure 63: Film registration using 3 pin breaks for localization in the coronal plane	97
Figure 64: Film dose line profiles for Gamma Knife. See appendix for all profiles.	97
Figure 65: Film and TPS dose agreement	98
Figure 66: CyberKnife film registration in the sagittal plane	100
Figure 67: CyberKnife film line profiles.....	100
Figure 68: Gamma analysis for CyberKnife SRS experiments	101
Figure 69: A) 20 mm B) 15 mm C) 10 mm D) 7.5 mm E) 5 mm	104
Figure 70: 5 mm field line profile, the thick vertical lines represent the boundaries of the micro cubes	105
Figure 71: 5 mm field profile of CyberKnife.....	111
Figure 72 Gamma Knife coronal plane film registration.....	119
Figure 73 Gamma Knife sagittal plane film registration	120
Figure 74 Gamma Knife A Coronal.....	120
Figure 75 Gamma Knife A sagittal.....	121
Figure 76 Gamma Knife B coronal	121
Figure 77 Gamma Knife B sagittal	122
Figure 78 Gamma Knife C coronal	122
Figure 79 Gamma Knife C sagittal	123
Figure 80: CyberKnife Coronal Film	130
Figure 81: CyberKnife Sagittal Film	131
Figure 82. Coronal A.....	131
Figure 83. Sagittal A	132
Figure 84. Coronal B.....	132

Figure 85. Sagittal B	133
Figure 86. Coronal C.....	133
Figure 87. Sagittal C	134
Figure 88: Linac Coronal Film.....	141
Figure 89: Linac Sagittal Film	141
Figure 90: Linac Coronal A	142
Figure 91: Linac Sagittal A	142
Figure 92: Cornal B.....	143
Figure 93: Sagittal A	143
Figure 94: Coronal C.....	144
Figure 95: Sagittal C	144

1 Introduction

Imaging and Radiation Oncology Core of Houston

Mission Statement

Provide integrated radiation oncology and diagnostic imaging quality control programs in support of the NCI's NCTN Network thereby assuring high quality data for clinical trials designed to improve the clinical outcomes for cancer patients worldwide.

The QA programs at IROC Houston are designed to assure NCI and the NCTN Groups that institutions participating in NCTN clinical trials deliver prescribed radiation doses that are clinically comparable and consistent.

We accomplish this by assessing the institution's radiotherapy programs, helping the institutions implement remedial actions, assisting the NCTN Groups by reviewing protocols and QA procedures, and informing the community of our findings.

1.1 Statement of the Problem

In order to advance radiation therapy treatment, it is necessary to answer a foundational question: How can the relationships between dose to tumor and dose to healthy tissue be maximized? Physicists continually seek better answers to this question and recent developments of small field radiotherapy, such as those used in stereotactic radiosurgery (SRS), have partially answered this quandary. Stereotactic radiosurgery utilizes small field photon beams to deliver a high, conformal dose to a tumor with a sharp dose fall off in surrounding healthy tissue. Advances in treatment delivery units such as Brainlab m3 linear accelerator (linac) with microMultileaf Collimator (Brainlab Inc., Feldkirchen, Germany), Gamma Knife (Elekta Instrument, Stockholm, Sweden), and CyberKnife (Accuray Inc., Sunnyvale, CA) have field sizes

as small as 4mm in diameter. The ability to create a highly conformal treatment plan with small radiation fields permits the delivery of a high tumor dose in a low number of fractions: the ideology behind SRS.

As a result of the high dose gradients of SRS treatment, small errors in treatment delivery or dosimetry can result in increased toxicity to normal tissue, while reducing tumor control. Thus the need for dose verification is vital to providing quality treatment (Wowra, Muacevic, & Tonn, 2009). However dosimetric challenges arise with the use of small fields. A small field is defined as fulfilling at least one of the following characteristics: there is a loss of lateral charged particle equilibrium on the beam axis; there is partial occlusion of the primary photon source by the collimating devices on the beam axis; the size of the detector is similar or large compared to the beam dimensions (Palmans et al., 2018). Both the nature of SRS treatment and the considerations of small field dosimetry necessitate an accurate and reliable tool to verify dose delivery plans to ensure both quality and consistency.

SRS treatment verification is particularly important in the context of clinical trials. The Imaging and Radiation Oncology Core (IROC) Houston Quality Assurance (QA) Center provides a simple and efficient remote audit dosimetry program for institutions participating in clinical trials. IROC Houston uses both thermoluminescent dosimeters (TLD) and optically stimulated luminescent dosimeters (OSLD) in their audit programs to evaluate photon, electron, brachytherapy, and proton beams for multiple parameters. These assessments range from simple beam output checks to end-to-end evaluations of treatment delivery using an anthropomorphic phantom. In this work, the anthropomorphic SRS brain phantom is of particular interest.

The aim of this research is to test TLD in the form of a micro-cube ($1 \times 1 \times 1 \text{ mm}^3$) for implementation into a radiotherapy audit program for small field dosimetry. This study seeks to avoid the complications of small field dosimetry, namely partial volume averaging. Micro-cube TLD may be able to fill this niche due to their small size relative to the fields studied.

The output measured by TLD micro-cubes is proportionally small when compared to larger forms of TLD (rods, chips, etc.). This means that small deviations in measured signal result in rather large deviations as a percentage of measured output, thus the accuracy and reproducibility characteristics of TLD-100 are not necessarily expected with TLD-100 micro-cubes, and need to be investigated.

1.2 Background

1.2.1 Stereotactic Radiosurgery

In 1908 Victor Horsley and Robert Henry Clarke developed a stereotactic apparatus (Horsley-Clarke frame, Figure 1) for studying the brains of monkeys (Lasak & Gorecki, 2009). Nearly 30 years later, Earnest A. Spiegel and Henry T. Wycis were the first to apply this technique to the human brain, and introduced stereotactic surgery in 1947 (Gildenberg, 2001). Just two years later, Lars Leksell introduced the Gamma Knife concept, which paired a stereotactic apparatus with radiation treatment, giving birth to stereotactic radiosurgery. Leksell treated the first patient in 1950. Originally developed by Leksell to destroy dysfunctional loci in the brain, stereotactic radiosurgery has become widely used for a variety of treatments with recent advances in technology (Mathieu et al., 2008).

As previously mentioned, stereotactic radiosurgery makes use of a stereotactic apparatus combined with high energy photon beams to irradiate a lesion in a single fraction with

millimeter accuracy (Kano, Niranjana, Kondziolka, Flickinger, & Lunsford, 2009). Similarly, stereotactic radiotherapy uses the same methods, but treatment is typically delivered in multiple fractions. SRS requires precision localization of a cranial lesion and neuroanatomy in the reference frame of the stereotactic frame using a CT, MRI, or angiographic unit (W. Li et al., 2016). A treatment plan is developed and a concentrated dose is delivered to the lesion with a sharp dose fall off in surrounding healthy tissue. This dramatic dose gradient provides substantial sparing of normal brain tissue, decreasing clinical toxicity.

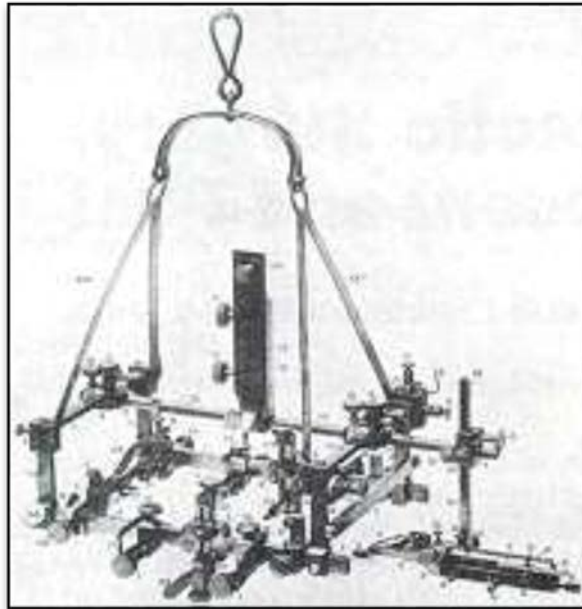


Figure 1: Horsley-Clarke Frame

Used with permission from the American Association of Neurological Surgeons: "A Short History of Stereotactic Neurosurgery", Robert Levy, MD Figure 1

The precision treatment is made possible through a combination of beam size, patient immobilization, and tumor localization. SRS treatments often employ multiple non-coplanar beams or arcs converging about an isocenter. Rotation from the gantry, collimator, and treatment table about their respective axes should coincide about a common point, creating a

central sphere with a radius of 1mm. The use of multiple precision beams (201 individual beams in Gamma Knife) with various isocenters and weights permits customization of dose distribution to the tumor shape (Flickinger et al., 1990).

In SRS treatment, defining a tumor's location is limited by diagnostic imaging technology. Delineation of tumor boundaries using a CT depends strongly on the resolution of the image and the association between the macroscopic view of the lesion with the microscopic range of its borders. The resolution of an image is limited by the size of a voxel. In the early use of SRS, typical voxel dimensions were 0.7 mm x 0.7 mm x 1 mm, or larger, depending on the separation of slices. Consequently, the location of a lesion could not be known better than within 1.5 to 2 mm (Michael C. Schell, 1995).

Patient immobilization considerably reduces uncertainty in dose delivery. Conventional external beam radiotherapy setup has been investigated using differences between simulation and port film. These investigations determined a mean standard deviation of 3 mm in treatment-to-treatment positioning, and an average discrepancy of 5 mm in variability, for cranial treatments. In comparison, SRS treatment can achieve a standard deviation in positional uncertainty of 2.4 mm. This uncertainty is a combination of uncertainty in the stereotactic frame positioning (1.0 mm), isocentric alignment (1.0 mm), CT image resolution (1.7 mm), tissue motion (1.0 mm), and point identification (AAPM Task Group Report No. 54 Table II). The accuracy in target alignment in two SRS studies report uncertainties of 0.2 mm - 0.4 mm in patient position (Michael C. Schell, 1995).

SRS treatment is an intricate procedure involving multiple steps, tools, and technologies. The radiation dose delivered is highly ablative, and requires incredible precision to ensure

satisfactory patient outcome. Implementing SRS treatment into a clinic's repertoire requires a deep understanding of the importance in maintaining a stringent quality assurance program to reach the full potential of this advanced treatment.

1.2.2 Small Field Dosimetry

The increase in use of standard multileaf collimators (MLC) and add-on MLCs has caused a downstream effect in the availability of small static fields for radiation therapy. Additionally, the use of small external beam radiation fields used in SRS treatments has also risen as technology advances and treatment techniques improve. Thus, the uncertainty of clinical dosimetry has increased as the link to conventional dosimetry practice is lost (Palmans et al., 2018). In light of the increase in use of small field beams, it is vital that quality of treatment is insured for patient safety and outcomes. Beam calibration and tumor localization errors as well as machine malfunctions can have severe effects on beam output and dose delivery. When considering that a SRS treatment can deliver 20 to 40 Gy (Schulz, Maryanski, Ibbott, & Bond, 1993) in a single fraction, any error could be severe for healthy tissue.

Differences in detector type, setup, and orientation can play significant roles in dosimetric measurements. Detector type alone can reflect a discrepancy as large as 10% (Godson et al., 2016). Even detector orientation can cause an overestimation in percent depth dose at 10 cm (PDD_{10}) of 5.7% to 8.6%. Detector positioning must be precise as just a 1 mm deviation off central axis can influence percent depth dose (PDD) by 2% (Godson et al., 2016). When observing dosimetric measurements between institutions, parallel inconsistencies were noticed. For $0.6 \times 0.6 \text{ cm}^2$ fields, "the PDD at 10 cm fell outside the 95% confidence level at 63.2% of institutions" (S. Li, Medin, Pillai, & Solberg, 2006).

We remember that the radiation field is defined as *small* when one of three characteristics is observed: loss of lateral charged particle equilibrium (LCPE) on the beam axis; partial occlusion of the primary photon source by the collimating device; the size of the detector is similar or large compared to the beam dimensions (Palmans et al., 2018). Small fields are created by collimation of flattened or unflattened photon beams using jaws, MLCs, or cones. Because the lateral dimensions of small fields are significantly different from conventional fields, the penumbra from both sides of the field overlap (Figure 2), which also leads to dosimetric obstacles.

The first two conditions are characteristics of the photon beam itself. LCPE occurs when half of the beam width is shorter than the maximum range of secondary electrons produced by the primary photon field (Crop et al., 2009). Partial occlusion of the primary photon source is a result the finite size of the source, which is determined by the full width half max (FWHM) of the photon fluence profile exiting the target. The result of collimating the beam to a field size smaller than the size of the source yields a reduced beam output on the CAX when compared to the output of conventional fields. Partial occlusion of the photon source can have a large effect on detector response, as it is a source of steep dose gradients and plays a role in particle spectrum (Aspradakis et al., 2010).

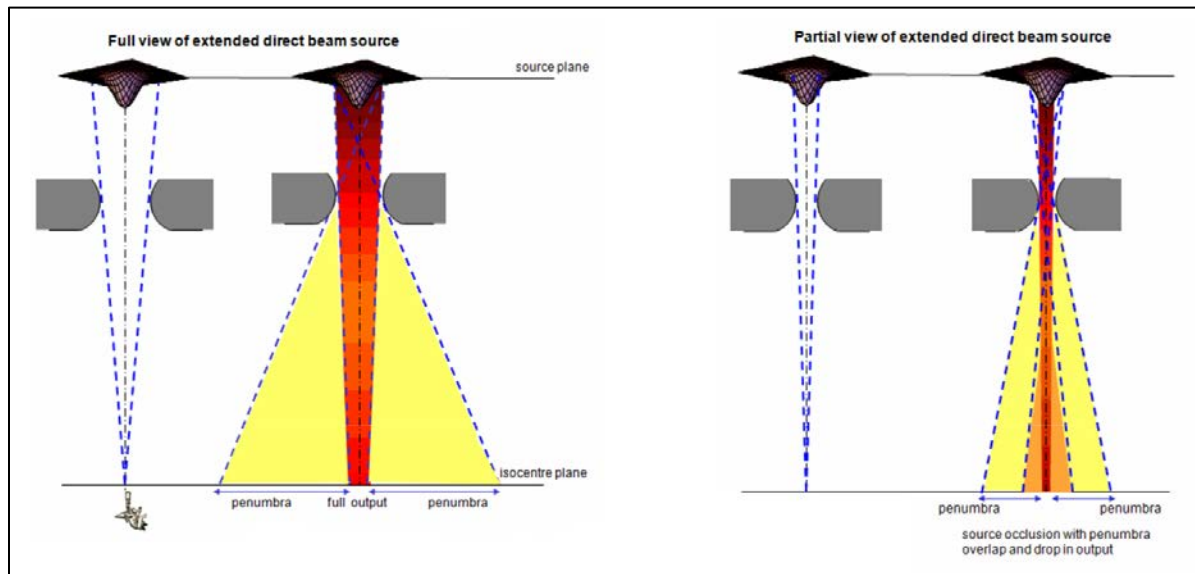


Figure 2: Partial occlusion of the primary photon source (B) causes the penumbra from both field edges to overlap.

Aspradakis, M. M., Byrne, J. P., Palmans, H., Duane, S., Conway, J., Warrington, A. P., & Rosser, K. (2010). *IPEM report 103: Small field MV photon dosimetry*. Retrieved from International Atomic Energy Agency (IAEA), Page 7:

Copyright: Institute of Physics and Engineering in Medicine 2010. Reproduced with Permission

The third condition is a characteristic of the detector size as it pertains to the size of the field. Generally, a detector produces a signal that is proportional to the absorbed dose over the active volume of the detector. Therefore the detected signal is dependent on the homogeneity of the photon field over the volume: volume averaging. This, coupled with perturbations in the charged particle fluence caused by the presence of the detector, characterizes small fields as those where the external edge of the detector volume is closer to the field edge than the range for LCPE in the medium (Agency, 2017).

Small field dosimetry presents many challenges, but there are many detectors designed for this purpose. These detectors include micro-ionization chambers, diodes, film, and solid state detectors. An appropriate detector should be chosen for the particular application. Each has its

own unique advantages, and some are more accurate and reliable than others. Additionally, a great deal of precision is needed to make accurate measurements in small field dosimetry. This can be made clear by looking at a dose profile for a 4 mm Gamma Knife photon beam (Figure 3). We can see that there is no flat area/ plateau of dose on the central axis. We can also observe the steep dose falloff to 90% just 2 mm off the CAX. This means detector placement or localization must be very precise for accurate results.

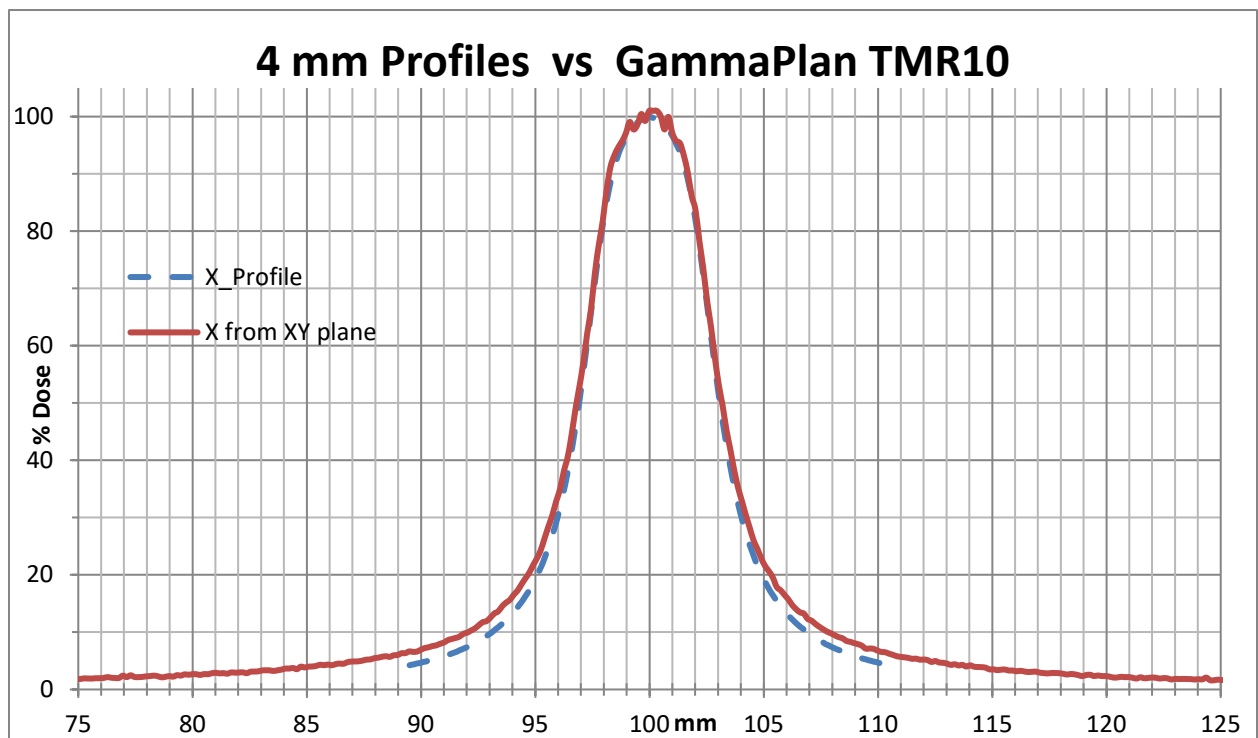


Figure 3: 4mm dose profile for Gamma Knife. See Appendix for more profiles.

1.2.3 The Imaging and Radiation Oncology Core Houston QA Center Services

The Imaging and Radiation Oncology Core (IROC) Houston, originally titled the Radiological Physics Center, was founded in 1968. IROC Houston works with institutions participating in National Cancer Institute (NCI)-sponsored clinical trials to monitor and evaluate beam output, dosimetry data, calculation algorithms used for treatment planning, and quality

control procedures (Ibbott, 2010). The key objective of IROC Houston is to insure quality of treatment as well as congruency of treatment among institutions participating in the same clinical trial.

These evaluations may be performed in person by an IROC Houston physicist, or it may be performed as part of the IROC Houston remote audit program. For remote audit programs, IROC Houston makes use of both TLD and OSLD to evaluate photon, electron, and proton beams. Using these dosimeters, IROC Houston monitors more than 22,600 megavoltage photon and electron beams from 2100 institutions each year. Although OSLD has become the predominate dosimeter, IROC Houston continues to use TLD in their QA programs.

Institutions participating in NCI-sponsored clinical trials using photon beams are monitored on a yearly basis, while electron beams are monitored on a 2-year cycle. For each institution and each radiation beam, an acrylic mini-phantom containing either TLD or OSLD is mailed. The dimensions of the phantom are specific to the beam being evaluated and range from $3 \times 4.5 \times 1.5 \text{ cm}^3$ to $6.5 \times 6.5 \times 5.5 \text{ cm}^3$ for photon beams and 8.5cm cubes for electron beams. Each phantom is designed to produce electronic equilibrium for photon beams and full phantom scatter for electron beams. IROC Houston also uses anthropomorphic phantoms for more in-depth analysis of treatment plans. These phantoms include head (Figure 4), spine, liver and lung, and are generally used as an end-to-end test of the entire treatment process: CT simulation, treatment planning, and treatment delivery.



Figure 4: IROC SRS Head Phantom

The dosimetry auditing program implemented by IROC Houston performs quite well. With regards to TLD, the uncertainty in dose determination for TLD-100 is 1.3% at one sigma level (Alvarez, Kry, Stingo, & Followill, 2017). IROC Houston currently uses TLD-100 powder in capsules for dosimetry measurements (Figure 5). These capsules are placed within phantoms for various QA audits. IROC Houston plans to incorporate TLD-100 micro-cubes into their existing audit program, in hopes to evaluate small field sizes that are currently beyond the limitations of their TLD capsules.

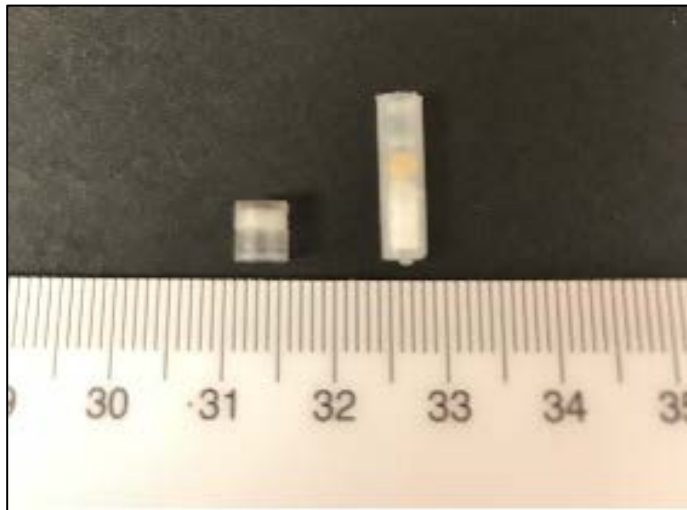


Figure 5: Capsules used to contain TLD-100 Powder.

1.2.4 Thermoluminescent Dosimeters

1.2.4.1 Introduction to Thermoluminescent Dosimeters

TLD are crystals which contain added impurities that can be used to trap electrons in energetic states which can be released through thermal stimulation to produce fluorescent photons. In the realm of dosimetry, TLD have been commonplace for nearly a century. Thermoluminescence was noted by Sir Robert Boyle and Henri Becquerel long before it was used in dosimetry. In 1904, Marie Curie observed the thermoluminescent properties of calcium fluoride (CaF) after exposure to radium. Many years later, Sir John Turton Randall and Maurice Wilkins developed a theory of thermoluminescent dosimetry by interpreting characteristics of measured glow curves (Kron, 1995).

Although one of the first uses of TLD was for archeological and geological dating, Farrington Daniels theorized various applications, including clinical dosimetry using lithium

fluoride (LiF). The first application to clinical dosimetry involved a patient swallowing a crystal, post injection of radioactive isotopes. Upon recovery, the TLD were gauged for accumulation of dose in roentgens, by measuring luminescent intensity. For many years, TLD use in medical dosimetry was not widespread. This was part in due to the stumbling blocks of TLD, namely energy dependence, fading, and ultraviolet light sensitivity. James Cameron, however, was later able to demonstrate importance of added impurities, leading to more efficient dosimeters. Cameron, along with Harshaw Chemical Co., developed TLD-100 (LiF:Mg,Ti), which is the most commonly used TLD.

LiF can be produced in various forms, including a single crystal; however, these crystals can display significant variations in sensitivity. Therefore, LiF is often ground into powder crystals of 100 μm in diameter. This can be utilized in powder form, or pressed into chips, rods, discs, or cubes (Table 1). TLD are compact and easily transported, they have a wide range of sensitivities, and are useful for doses of a few milligray to many gray. Additionally, LiF is nearly tissue equivalent ($Z_{\text{eff}}=8.2$) (Kron, 1995), which makes it suitable for in vivo dosimetry and other patient/personnel related measurements.

Table 1: Various commercially available forms of TLD-100 from ThermoScientific™.

Thermo Scientific™ TLD-100 Shape	Dimensions
Rod	Diameter: 1 x 6 mm, Diameter: 1 x 3 mm, Diameter: 1 x 4 mm, Diameter: 1 x 4 mm, Diameter: 1 x 2 mm
Micro-cube	1 x 1 x 1 mm
Chip	3.2 x 3.2 x 1.5 mm, 3.2 x 3.2 x 0.38 mm, 3.2 x 3.2 x 0.89 mm, 6.35 x 6.35 x 0.89 mm
Disk	Diameter: 3.6 x 0.25 mm, Diameter 3.6 x 0.38 mm

1.2.4.2 Mechanisms of Thermoluminescence

TLD operate on principles similar to inorganic scintillating crystals, which emit prompt fluorescence after absorbing energy from an external source. To explain this property of inorganic crystals, we must first look at the crystal lattice. Within the crystal lattice are two energetic bands, the valence band and the conduction band (Figure 6). The valence band contains electrons in a low energy state, and thus is mostly occupied. Electrons contained in the valence band are inherently bound to lattice sites and are considered immobile. The conduction band is conversely a high energy state that is sparsely occupied by electrons which are free to migrate through the crystal lattice. There is also a third level of the crystal lattice, the band gap, otherwise known as the forbidden band gap. Electrons are mechanically forbidden from residing

within the band gap, and consequently must exist within the conduction band or the valence band (Knoll).

When an electron, bound in the valence band, absorbs sufficient energy, it can be excited up across the band gap into the conduction band. The electron leaves a “hole” behind in the valence band. When excited electrons lose energy, they fall back down to the valence band, and recombine with a hole, which causes an emission of a photon. In pure crystal, the energy difference between the valence and conduction bands is large, and emitted photons lie outside of the visible range. This result leads to the practice of intentionally adding impurities to the crystal called activators. Activators alter the energy band structure of the inorganic crystal, creating energy states within the forbidden gap which excited electrons may occupy (Figure 6). Because these energy states are lower energy than the conduction band, the emitted photons from recombination events are predictably lower energy and within the visible photon range (Knoll).

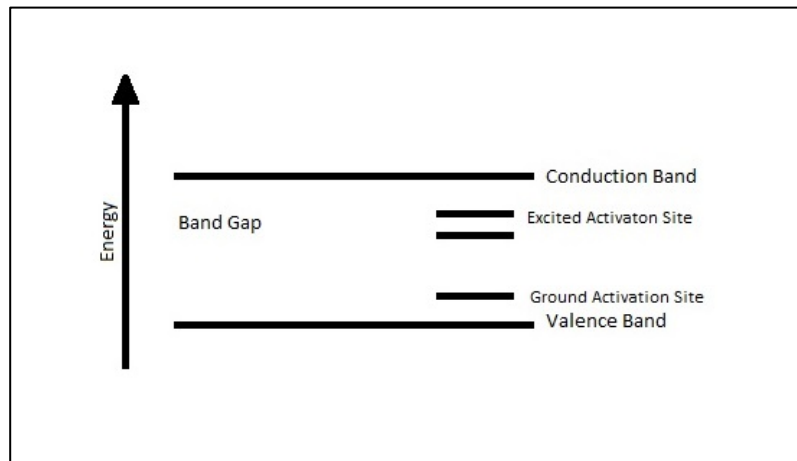


Figure 6 : The crystal lattice contains two energy levels of importance: the valence band, and the conduction band. The valence band is low energy, and electrons contained in the valence band are bound to the lattice. Electrons in the higher energy conduction band are free to migrate about the crystal lattice. In between is the band gap, in which electrons are forbidden to occupy. Added impurities create activator sites in the forbidden band gap, which permit electron occupation.

An important note is that the inorganic crystals create prompt fluorescence. In other words, the excitation of an electron and systematic emission of a photon happen in rapid succession; this is where TLD differ. TLD are inorganic crystals with added impurities similar to the inorganic crystals previously mentioned, however, the impurities added to TLD perform a very different function. The impurities, such as Magnesium in TLD-100 (400 ppm), create trapping centers (Figure 7) in the band gap of the crystal lattice (Knoll).

When an electron is excited up to the conduction band, and falls back to the valence band, there is a probability that the electrons will become trapped in one of the many trapping centers in the band gap. The advantage of trapping electrons in the band gap is that they are stored in the trapped state until sufficient energy is added to the TLD to free them. Once freed from the trapping center, electrons can recombine with holes, which can be trapped and freed in a similar way, and it is this recombination which emits photons in the visible spectrum. It is

worth noting that the Titanium (8 ppm) added to TLD-100 provides luminescent recombination centers at which freed electrons/holes recombine accompanied by emission of a photon.

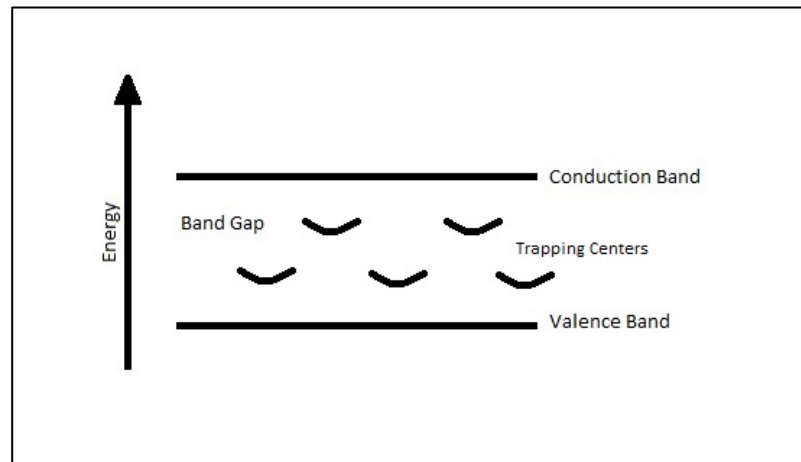


Figure 7: The impurities added to TLD provide electron/hole trapping centers in the band gap. Trapping centers permit the use of TLD as a dosimeter that can be read out at a later time after irradiation. Trapping centers have different escape energies (depth), and are therefore cleared at different temperatures upon readout.

In the practice of medical physics dosimetry, TLD can be irradiated, providing the external energy necessary to jump electrons from the valence to the conduction band, leading to trapped electrons/holes in the band gap. As dose is absorbed by the TLD, more electron/hole traps are filled. In this way, a relationship between the number of trapped electron/hole pairs and absorbed dose can be established. To measure the number of electron hole pairs, the TLD is thermally stimulated to release the electrons and holes from their traps leading to recombination events. The photons released from recombinations can be measured by a photomultiplier tube, converting photons to a charge.

A few characteristics of TLD are fading, dose dependence, energy dependence, and annealing. Fading refers to a concept in which electrons contained in low energy traps have a high probability of escaping due to low energy thermal stimulation such as room temperature,

this results in a rapid fall-off of TLD signal shortly after irradiation. Dose dependence is a relatively evident concept; as higher dose is absorbed by the TLD, more electron hole pairs are created, and more photons are released upon readout. TLD-100 have a linear dose response from about 100 μGy out to 4 Gy, above this dose, response becomes supralinear (Figure 8). Energy dependence refers to the response of TLD-100 as a function of photon energy, where we use 1.25 Mev Cobalt 60 gammas as a reference.

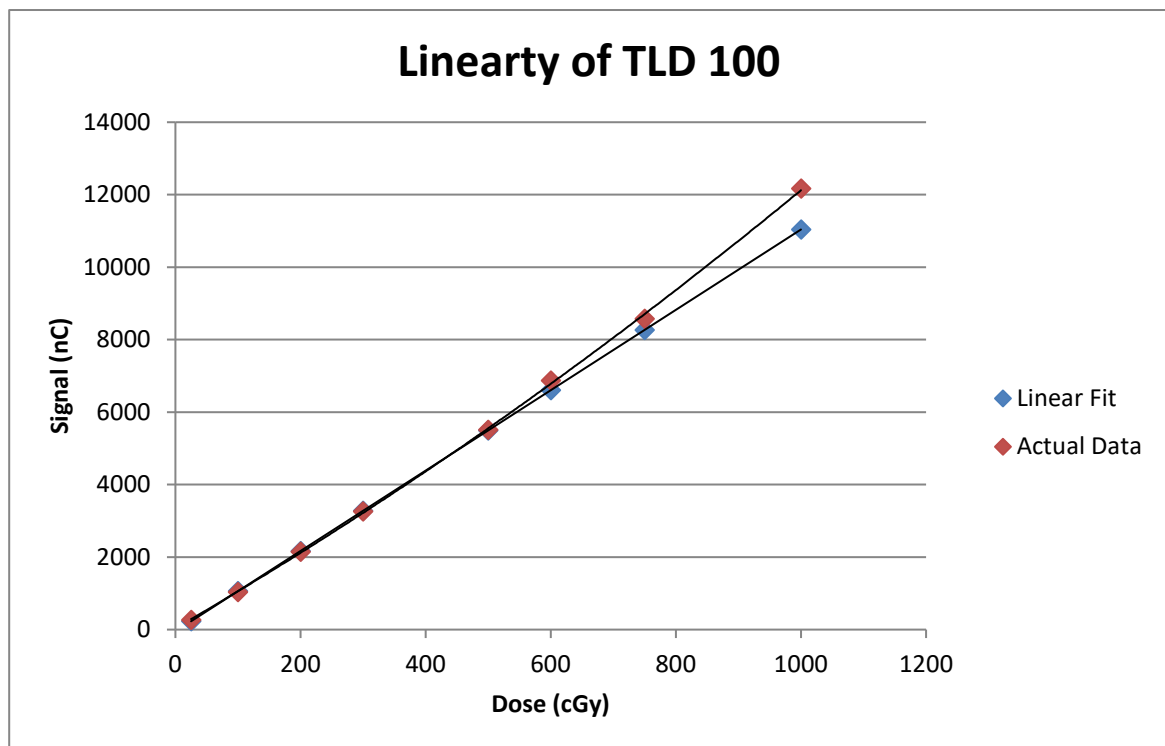


Figure 8: TLD-100 is linear out to about 400cGy; where there is an over-response as dose increases.

The last TLD concept is annealing. Annealing can be described as clearing all electron and hole traps in the crystal lattice through a heating cycle. Not only does annealing clear these traps, it also plays a role in the arrangement of trap levels within the forbidden gap, therefore, the TLD response is dependent on the annealing process and should be kept consistent. Literature also

shows that TLD sensitivity may decrease over time with continued irradiation and annealing (Ogunleye, Richmond, Cash, & Jones, 1987).

1.2.4.3 TLD-100

TLD-100 is the most commonly utilized TLD crystal and, consequently, has been well characterized in the literature. Many of these characteristics have been previously mentioned, but will be concentrated on TLD-100 in this section. TLD-100 is a LiF crystal with impurities of Magnesium (400 ppm) and Titanium (8 ppm). In the case of TLD-100, Magnesium creates the trapping centers in the forbidden gap, and the Titanium creates the recombination centers, which leads to photon production.

The near tissue equivalence of TLD-100 as well as the clinically relevant range of sensitivities for both dose and energy has made it a popular personnel and in vivo dosimeter. The effective atomic number of TLD-100 has been cited as 8.2 by Kron et al. and more precisely as 8.27 by Taylor et al. TLD-100 is linear out to about 4 Gray where it begins to over-respond as dose increases. If Cobalt 60 is taken as the reference energy, TLD-100 energy correction factors are generally not larger than 7% for megavoltage beams. TLD-100 are also reliable in terms of reproducibility and accuracy; uncertainty in dose determination is 1.3% at the one sigma level based on IROC Houston evaluations (Alvarez et al., 2017).

Several companies have made TLD-100 commercially available. Harshaw Chemical Co., perhaps the most well-known company, was the first to formulate the dosimeter in the 1960's with the help of James Cameron (DeWerd, 1983). Today, Harshaw TLD-100 is offered for purchase through ThermoFisher Scientific in numerous configurations.

1.3 Hypothesis and Specific Aims

1.3.2 Hypothesis

The hypothesis developed for this experiment is stated:

Micro-cube TLD can be commissioned to evaluate small field dosimetry, and provide reproducibility within $\pm 3\%$, as well as assure agreement between measured dose and calculated doses to within $\pm 5\%$.

1.3.2 Specific Aims

1. Characterize and commission TLD micro-cubes and develop guidelines for the handling process of TLD micro-cubes.
 - a. Define readout technique
 - b. Define annealing technique
 - c. Determine Elemental Correction Factor (ECF)
 - d. Determine Linearity, Energy, and Fading correction factors
2. Commission the TLD micro-cubes for standard single beam small field output dosimetry.
 - a. Develop capsule inserts which allow identification of TLD micro-cubes
 - b. Develop a method for making standard measurements in Cobalt 60 beam
3. Adapt the IROC Houston SRS phantom to use the TLD micro-cubes for anthropomorphic phantom quality assurance, test the phantom using standard linac, GammaKnife and CyberKnife treatment delivery machines, and compare the measured and calculated doses to determine agreement and precision.

- a. Develop capsule inserts for anthropomorphic head phantom which allow identification of TLD micro-cubes

2 Materials and Methods

2.1 TLD Micro-Cubes

In order to avoid the dosimetric complications of partial volume averaging, a consequence of small field dosimetry, the detector needs to be sufficiently small. The detector type should also be well understood, and well documented in literature. This section will highlight some detector considerations with regards to the needs of this study.

There are many detectors suitable for small field dosimetry that can provide accurate and reliable data for radiotherapy dosimetry. These range from passive detectors like TLD, radiophotoluminescence detectors, and alanine to active detectors such as liquid filled ion chambers, diamond detectors, and diodes. However, because this study is focused on developing a remote radiotherapy QA program for small field dosimetry, the detector needs to be carefully chosen.

The detector, used for remote audits, will be shipped to and from clinics, therefore it would be beneficial if it was free of wires or electronics. It is preferable to use a passive detector so that dose information is stored and can be read back at IROC Houston, eliminating any requirement for the irradiating institution to play a role in readout. Additionally, the detector type should be robust; environmental stressors such as heat (within the range of shipment temperatures) and humidity should not have a degenerative impact on the performance of the detector. In a similar sense the detector will be implemented into an audit program, so the readout should be simple to perform.

An essential idea behind this experiment is to develop a small field audit program that is both accurate and reproducible within the standards set in place at IROC Houston. That is, the

dosimeter should exhibit reproducibility within $\pm 3\%$, showing reliability of a measurement. Additionally, the dosimeter should be accurate to within $\pm 5\%$ when comparing the TLD measured dose to the treatment planning system (TPS) calculated dose.

TLD-100 micro-cubes (Figure 9) display characteristics that satisfy the requirements determined by the nature of the service to be provided. They are sufficiently small ($1 \times 1 \times 1 \text{ mm}^3$), where the smallest field size to be evaluated is 4 mm in diameter, therefore partial volume averaging correction factors are minimized. In terms of reliability, Regulla et al (da Rosa, Regulla, & Fill, 1999) was able to achieve a mean reproducibility of 1.03% in one standard deviation, which is well within the $\pm 3\%$ objective.

These passive detectors are well understood, can be reused multiple times, and can be easily transported. TLD-100 is the original dosimeter through which IROC Houston's services were developed, and implementing micro-cubes into the workflow of IROC Houston should be a smooth transition.

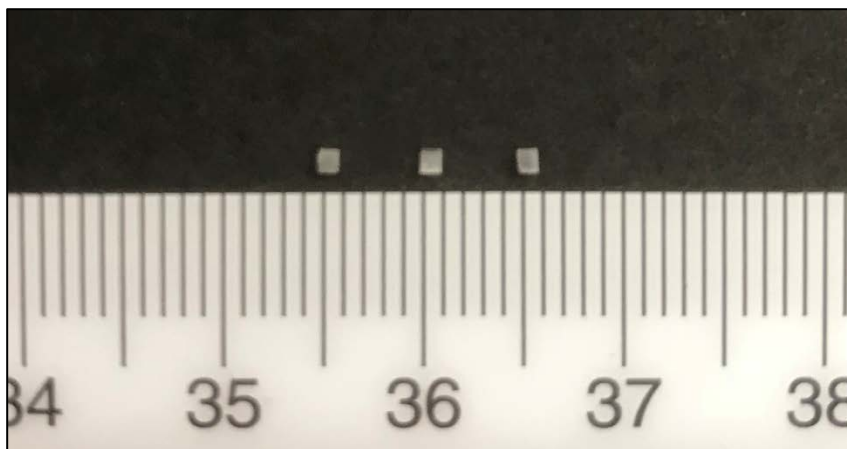


Figure 9: Harshaw TLD-100 Micro-Cubes from ThermoScientific

2.1.1 TLD-100 Micro-Cube Specifications

Dimensions: 1 x 1 x 1 mm³

Material: LiF:Mg,Ti

Z_{eff}: 7.51 (Azangwe et al., 2014)

Density: 2.64 g/cm³

Electron Density (relative to water): 0.833 e⁻/g

Accuracy: ± 15% (± 2 sigma)

Emission Spectra: 3500 to 6000 Å

Measurement Range: 10 pGy to 10 Gy

2.2 TLD Micro-Cube Handling

2.2.1 Micro-Cube Shape Uniformity

In order to obtain satisfactory reproducibility and accuracy, certain measures were taken in preparing TLD-100 micro-cubes for use in an audit program. Despite the name, the micro-cubes are not perfectly cuboidal, and each face is not necessarily a smooth surface. To reduce the likelihood of poor reproducibility, each micro-cube was carefully inspected.

Shape uniformity was an obvious characteristic to keep in mind when inspecting individual cubes. Aspects such as chipped edges or apparent cracks in the crystal were checked and irregularly shaped cubes were removed from service. The color of the cube was also inspected. In this study, some cubes with a yellowish opaque color exhibited poor dosimetry performance. Although discoloration did not appear to affect the signal stability, these cubes had significantly lower response to radiation, and were not suitable for audit use.

Moreover, throughout the course of the experiment, a handful of other detectors were determined to be of poor uniformity and were discarded or discontinued. This included some micro-cubes which had a uniform shape and no apparent physical distortion, but did not produce reliable signal. These steps were important in characterizing and commissioning TLD, as one cannot assume that all micro-cubes will provide the same reproducibility.

2.2.2 TLD Annealing

Annealing refers to the process of clearing electron and hole traps in the crystal lattice through heating cycles. The annealing process is to be performed before irradiation, which allows the dosimeter to be reused multiple times. If the dosimeter is expected to respond the same after each annealing cycle, then the cycle should be identical each time it is performed. The annealing methods used in a TLD dosimetry system need to be well defined, and well implemented.

This experiment followed the guidelines developed by Cameron et al. (Grant & Cameron, 1966):

1. 1 hour and 20 minutes at 400°C
2. 5 minutes rapid cooling between aluminum cooling plates
3. 2 hours at 100°C

For annealing procedures, the micro-cubes were contained within a Radiation Products Design, Inc. aluminum TLD chip annealing planchet (Figure 10). For heating to 400°C, a Radiation Products Design Inc. Model 168 TLD Annealing furnace (Radiation Products Design Inc., Albertville, Minnesota) (Figure 11) was used. For heating the micro-cubes to 100°C, a Blue M Electric Company Stabil-Therm Gravity Oven (Thermal Product Solutions, New Columbia, Pennsylvania) (Figure 12) was used. To rapidly cool the annealing planchets between heating

cycles, two aluminum plates were used. The plate dimensions were approximately 14 x 16 x 1 cm³.

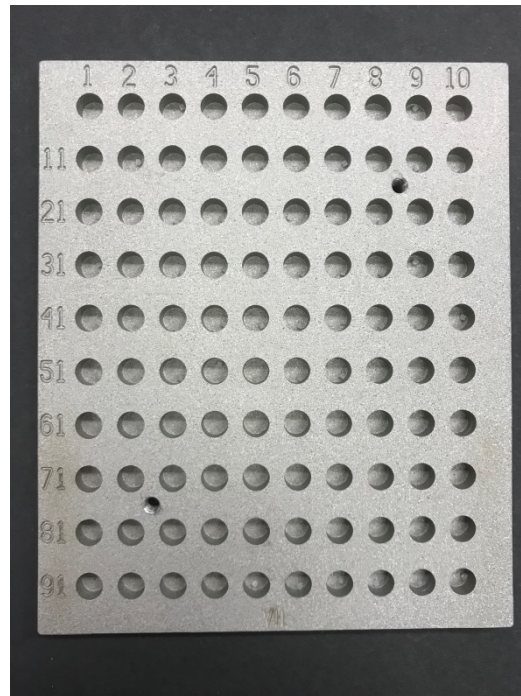


Figure 10: Radiation Products Design Inc. annealing planchet



Figure 11: Radiation Products Design Inc. Model 168 TLD Annealing Furnace



Figure 12: Blue M Electric Company Stabil-Therm Gravity Oven

TLD annealing can have a profound effect on TLD output. To test the sensitivity of the annealing procedure, we tested the TLD response from 500 cGy of absorbed dose using different annealing techniques, and compared them to our standard. The times we tested are in Table 2. The purpose of this test was to expose dependencies on annealing times that may be used as part of human error.

To help define the cooling portion of the annealing cycle, we measured the temperature of the aluminum planchet as a function of time during the five minute cooling period. To make these measurements, an infrared thermometer was used. The aluminum planchet was heated to 400°C, and then placed between the two room-temperature aluminum plates. The room temperature was 20.5°C. . Measurements were then made at various time intervals after removal from the oven. These measurements were repeated multiple time until a consistent trend in the temperature change was measured.

Table 2: TLD annealing times

Annealing Trial	Time at 400°C	Rapid Cooling Time	Time at 100°C
Baseline	1 hour 20 minutes	5 minutes	2 hours
Trial 1	1 hour 30 minutes	5 minutes	2 hours
Trial 2	1 hour 20 minutes	3 minutes	2 hours
Trial 3	1 hour 20 minutes	5 minutes	2 hours 30 minutes
Trial 4	1 hour 20 minutes	0 minutes	2 hours

2.2.3 TLD Signal Reading

To get signal from TLD, external energy needs to be supplied to free the electron and hole traps. This allows for the process of recombination describe in section 1.2.4.2 which releases a photon. To get dose from the TLD, the number of photons released through the reading heating cycle needs to be known, so a photomultiplier tube is coupled to the heating mechanism. This converts photons released to a charge which can then be related to an absorbed dose. Usually, when TLD in powder form are used, the amount of powder irradiated is weighed so a relationship between charge and mass (Coulombs/gram) can be used to relate charge to dose. Because this experiment uses an ECF, knowing the mass of each cube is unnecessary.

The reader used to evaluate the glow curve (Figure 13) of the TLD micro-cubes was a Harshaw model 3500 manual TLD reader (ThermoFisher Scientific, Weltham, Massachusetts).

Although use of the Harshaw 3500 is somewhat labor intensive, when compared to the Harshaw 5500, there is reason to believe the Harshaw 5500 may not be the optimal machine for evaluation of TLD micro-cube signal. A study conducted by de Rosa et al. demonstrated a reproducibility of 3.27% using the Harshaw 5500 automatic reader, and a reproducibility of 2.47% using the Harshaw 3500 manual reader, a significant improvement where all other factors remained constant.

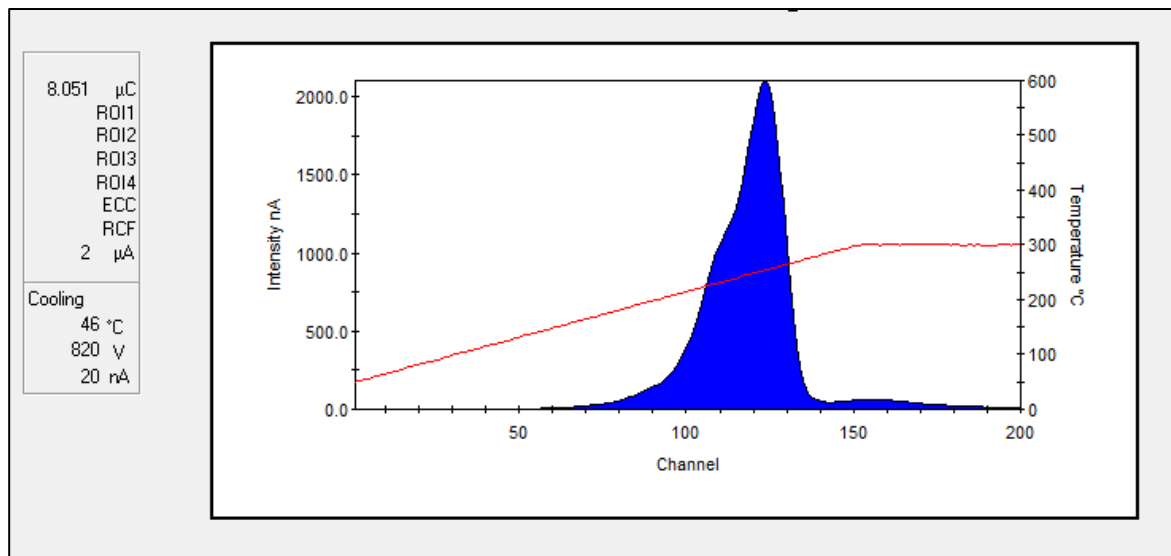


Figure 13: Glow curve captured from TLD-100 micro-cube using Harshaw reader and WinRems software

The software used to read TLD micro-cube signal was WinREMS (ThermoScientific). This software allowed us to define a heating curve for reading TLD micro-cubes which is outlined in Table 3.

Table 3: WinREMS software TTP parameters for reading TLD micro-cubes

Parameter	TTPs
Preheat Temp (°C)	50
Preheat Time (sec.)	0
Acquire Rate (°C/sec.)	10
Acquire Temp (°C)	300
Acquire Time (sec.)	33+1/3
Anneal Temp (°C)	300
Anneal Time (sec.)	0

Because micro-cubes have non-uniform faces, the thermal contact with the heating planchet is slightly different on each face. Therefore, to maintain consistency, the same face of each cube should be read each time signal is measured. This precaution can reduce variation in reproducibility from 4% to 0.9% as demonstrated by Bassinet et al. (Bassinnet et al., 2010). A similar study also showed that establishing a reading face of the cube can improve reproducibility from 2.47% to 1.03% (da Rosa et al., 1999).

Bassinnet also took the following precaution in maximizing reproducibility: “the micro-cube must be positioned with good reproducibility on the heating system (planchet)” (Bassinnet et al., 2010). This is difficult to do as the Harshaw 3500 reader used only has a planchet designed for TLD chips (Figure 14). The dimensions of the reading area of the planchet are approximately 1 cm x 1 cm². The only way to achieve reproducible placement is to guide-by-eye the placement of the micro-cube in the center of the heating planchet using fine point tweezers. This certainly

comes with some uncertainty in placement and is likely user dependent, however, alteration to the surface of the heating planchet could come with consequences in heating or luminescence of the aluminum itself, and it was not desirable to take that risk.

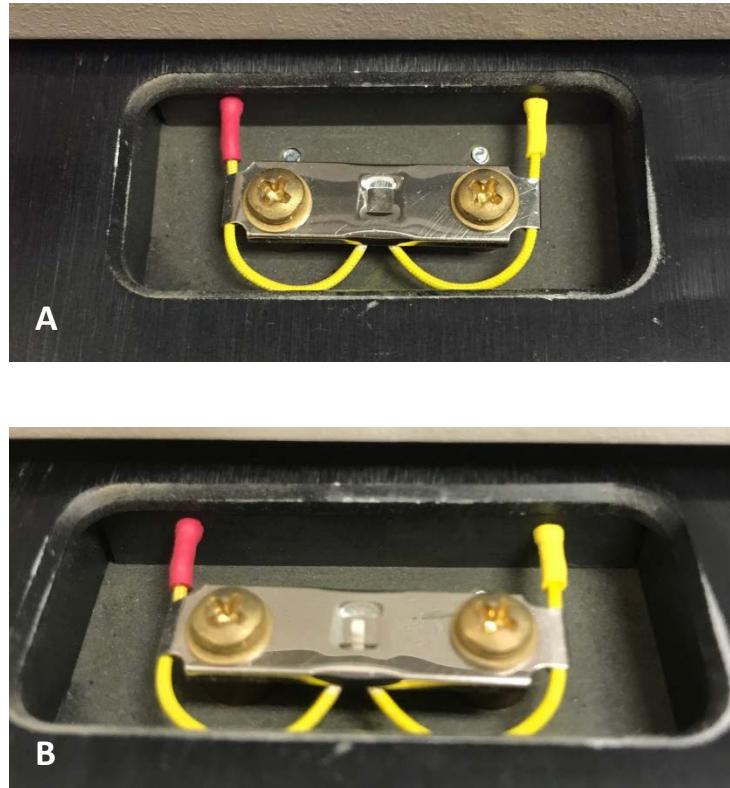


Figure 14: A) Harshaw 3500 TLD annealing planchet B) TLD Micro-cube in the center of the heating planchet

To investigate how TLD placement on the reading planchet might affect TLD micro-cube reproducibility, the micro-cube were read without taking significant care in placing the cube in the center of the reading area. This meant some TLD micro-cubes were placed on the edge/periphery of the central reading area, and some were placed closer to the center. In general, the only criteria followed for this test was placing the cube inside of the 1 cm x 1 cm reading area. This gave some insight into the care that is needed in placing the micro-cube in a reproducible location.

2.3 TLD Micro-Cube Characterization

There are many corrections to the TLD signal that must be applied to get dose. These correction factors account for the absorbed dose response, the energy of the photon beam, the time between irradiation and reading, and the sensitivity of the entire reader system. In defining these parameters, the TLD are characterized, and can then be used as dosimeters.

The dose absorbed by the reference medium at the location of the micro-cube can be calculated using Equation 1 and Equation 2 (Kirby, Hanson, & Johnston, 1992). Thus, the characterization of TLD micro-cubes entails defining each correction and calibration factor.

$$D = TSK_LK_FK_EECF$$

Equation 1

D= absorbed Dose to the reference medium at the location of the TLD

T= thermoluminescence reading (nC)

S= system calibration factor (cGy/nC)

K_L=dose response linearity

K_F=fading correction factor

K_E=energy correction factor

ECF= elemental correction factor

Prime (') denotes reference conditions

$$S = \frac{D'}{T'K_F'K_L'}$$

Equation 2

2.3.1 Elemental Correction Factor

TLD micro-cubes have relatively non-uniform response on a cube-to-cube basis. This can be expected from a batch of micro-cubes, as each cube is unique on a microscopic and macroscopic level. Although the signal from one cube to the next is inconsistent and unpredictable, a single cube can be expected to produce the same response from a given dose. This leads to the establishment of an elemental correction factor (ECF). ECF (Equation 3) is defined as the average signal of a group of TLD micro-cubes, irradiated to the same dose, divided by an individual cube's signal.

$$ECF = \frac{\text{Average Signal (nC)}}{\text{Individual Signal (nC)}}$$

Equation 3

The ECF gives insight as to how an individual micro-cube responds in relation to a batch average of micro-cubes. This batch, population, or group, must be maintained and micro-cube identity within the group must remain known, otherwise, ECF must be re-calculated. These groups should be annealed, irradiated, and read together, so that there is no discrepancy in the annealing cycle, irradiation technique, or reading sensitivity. These are requirements in obtaining reliable ECF values during the characterization and commissioning of TLD micro-cubes.

To establish ECFs for micro-cubes, the following steps were taken:

1. Micro-cubes were annealed
2. Micro-cubes were irradiated to 500 cGy using a Cobalt 60 source
3. Micro-cubes were allowed a minimum of 48 hours to fade

4. Micro-cubes signals were measured in a single session using a Harshaw 3500
5. Measurements were repeated for a total of 3 data sets to establish an average ECF value

For this experiment, we had 5 groups of TLD micro-cubes; 4 groups of 100 and 1 group of 63. An ECF value was measured for each cube in each group three times, where the average was taken across a group. This gave us three measurements to evaluate and allowed us to check TLD reproducibility on a macroscopic level and discard TLD which showed large coefficients of variation (Equation 4).

$$\textit{Coefficient of Variation} = 100\% \times \frac{\textit{Standard Deviation}}{\textit{Average}}$$

Equation 4

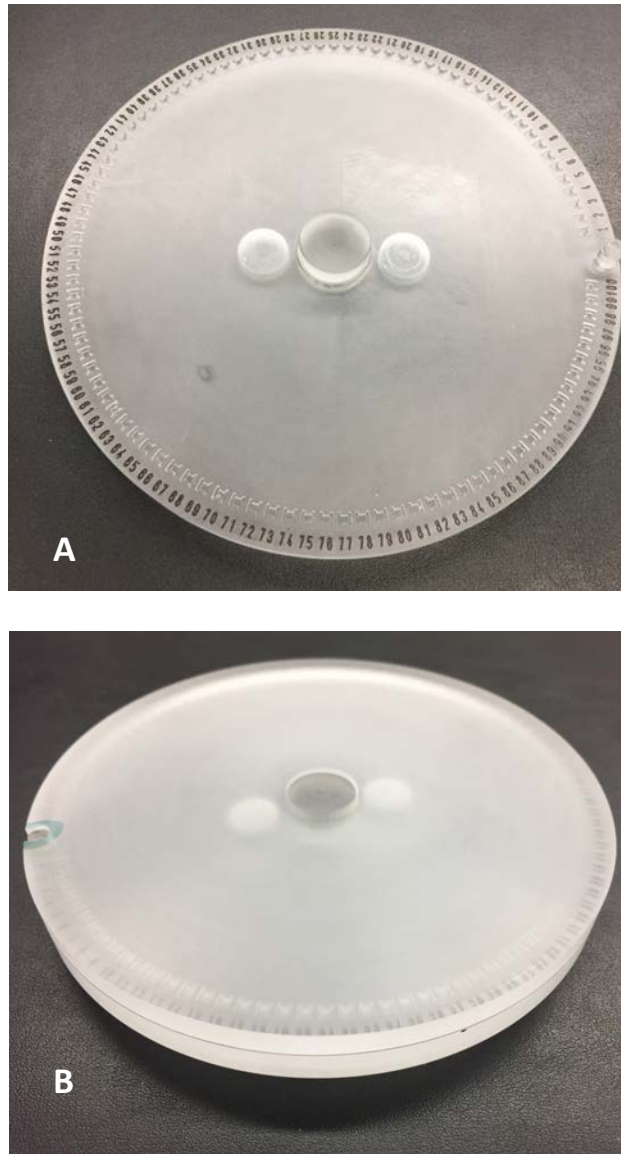


Figure 15 A) ECF irradiation disc B) Irradiation disc with buildup.

Rotating irradiation discs were used to ensure uniform dose delivery among the micro-cubes. The discs are made of acrylic and are centered on the CAX of the 24.5 cm x 24.5 cm Cobalt beam at 80.5 cm (SSD). The ring of cubes sits 5.8 cm from the center of the disc, which slowly rotates beneath the beam during the radiation exposure, ensuring that all TLD are exposed to the same dose, i.e. this reduces effects of any possible hotspots in the field. The buildup is 5.65

mm thick, providing electronic equilibrium for the 1.25 MeV ^{60}Co photons at the depth of the micro-cube (Alvarez et al., 2017).

2.3.2 System Calibration Factor: S

$$S = \frac{D'}{T'K_F K_L'}$$

The calibration factor, which can also be described as the system sensitivity, accounts for changes in reader electronics, optics, planchet characteristics, and heating properties (Kirby et al., 1992). “The system calibration factor is defined as the inverse of the thermoluminescence response of the TLD system per unit dose “(Kirby et al., 1992). Therefore, in Equation 2, D' , T' , K_F , and K_L' , the prime (') denotes values obtained from the standards.

IROC Houston uses 300 cGy as the dose for the standards, delivered with a ^{60}Co unit. However, for this experiment, we used both 300 cGy and 600 cGy as standard doses. Because the dose delivered to the TLD micro-cubes for SRS head phantom audits will be doses closer to 600 cGy, we made our standards closer to that dose to reduce uncertainty in the correction factor used. For these experiments, standards were irradiated on the same day of single field irradiations (Section 2.4) and SRS head phantom irradiations (Section 2.5). Doing the standard irradiations on the same day as the experimental irradiation allowed fading corrections to be ignored.

To irradiate standards in a ^{60}Co beam, we used an acrylic “mini-phantom” (Figure 16) that was originally constructed for OSLD irradiations, but was adapted for micro-cubes. The acrylic mini-phantom is $4.5 \times 3 \times 1.6 \text{ cm}^3$. The micro-cubes sat inside of the mini-phantom under a 6.8 mm buildup cap, providing D_{max} at the location of the TLD. The geometry of these

irradiations was a 10 cm x 10 cm field at 79.3 cm SSD. These conditions were defined to deliver a known dose to the TLD.



Figure 16: IROC Cobalt mini-phantoms

4.5 x 3 x 1.6 cm³, 6.8 mm buildup cap, TLD micro-cube numbered insert for cube identification.

2.3.3 Linearity Correction: K_L

The linearity correction factor relates the signal measured to the dose absorbed by the TLD. We expect the dose and the signal to be proportional, and in general this is a true statement for TLD-100, up until about 400 cGy. Beyond this dose, the signal begins to over-respond as dose increases, as displayed in Figure 8. To make these measurements, we used the same rotating irradiation disc from the ECF irradiations under the same configuration, using the ^{60}Co beam to deliver the doses.

To make these measurements, we used 2 micro-cubes per dose level, with 2 sets of system sensitivity standards irradiated to 300 cGy; one at the beginning and end of each reading session. We repeated this linearity experiment once. The doses used to evaluate linearity were: 100 cGy, 200 cGy, 300 cGy, 500 cGy, 600 cGy, 700 cGy, 1000 cGy. This range of doses gave us a clear picture of how the TLD respond to dose over a wide range, including the supralinear region. The maximum dose used, 1000 cGy, is considered the limit for TLD micro-cubes, as the over-response of the micro-cubes is too significant and requires a large correction factor.

The linearity correction for a given measurement is defined in Equation 5. The raw dose is defined as the reading, in coulombs, from a micro-cube multiplied by the system sensitivity, ECF and fading correction factors (Equation 6). In this experiment, fading was taken to be unity.

$$K_L = m\left(\frac{1}{\text{cGy}}\right) \cdot \text{raw dose}(\text{cGy}) + b$$

m=slope

b=intercept

Equation 5: Linearity correction factor

$$\text{Raw Dose} = T(\text{nC}) \cdot SS \left(\frac{\text{cGy}}{\text{nC}} \right) \cdot \text{ECF} \cdot K_F$$

SS=system sensitivity

ECF=elemental correction factor

T= reading in (nC)

Equation 6: Raw Dose

2.3.4 Energy Correction Factor: K_E

$$K_E = \frac{DT'}{D'T}$$

Equation 7: Energy Correction Factor

The energy correction factor was used to correct the thermoluminescent response of TLD for different energies, with ^{60}Co as a reference in Equation 7. The energies used for this correction factor were ^{60}Co (which defines the reference energy) and 6 MV.

For the ^{60}Co reference, the same conditions for irradiating standards for system sensitivity in section 2.3.2 were held. For this reference, 600 cGy was delivered to the standards.

To make these measurements, we used a 15 x 15 x 19 cm³ high impact polystyrene phantom with capsules containing TLD micro-cubes. Each capsule held 3 TLD micro-cubes, and the phantom held one capsule at 10 cm. The 6 MV photon beam from a Trilogy linear accelerator (Varian Medical Systems, Palo Alto, California) was used. Prior to irradiating the TLD for energy correction measurements, the Trilogy beam was calibrated following the guidelines of TG-51 (Almond et al., 1999). The beam calibration in water was cross-referenced with the beam output at 10 cm depth in the polystyrene phantom used for the energy correction. 600 MU were delivered for a 10 x 10 cm² field. Three irradiations were conducted. For each measurement, the signal per unit dose was evaluated and divided by the signal per unit dose for ^{60}Co .

2.3.5 Fading Correction Factor: K_F

The fading correction factor is used to correct the thermoluminescence for low energy traps that may be cleared at room temperature during the time between irradiation and reading.

The fading correction factor is necessary when there is no pre-read annealing to clear these shallow traps or low temperature peaks. The correction is also needed when standards and samples are irradiated on different dates. For this experiment, standards were always irradiated and read on the same day as the sample, so fading correction was not necessary.

When this system is implemented as an IROC Houston audit program, a fading correction curve must be established if standards and phantom irradiations are conducted on different days. To make these measurements, TLD micro-cubes would be irradiated at given intervals prior to a designated date, on which all TLD from each irradiation session would be read for signal. It is important to read all TLD on the same day so that the system sensitivity correction is the same for all cubes. A fading correction curve should be established for approximately three months to cover a wide range of delays between the irradiation date and the read date.

2.4 Uncertainty Analysis

The uncertainty in determining the dose to TLD micro-cubes needs to be assessed in order to have confidence in their measurements. The guidelines presented by Kirby et al. were followed in assessing the uncertainty of the data collected in this experiment. Because dose to TLD is determined using Equation 1, below, the uncertainty in the constituents of the equation need to be established individually and summed in quadrature. Therefore, the uncertainty to the dose as calculated from the TLD reading is defined in Equation 8 (Kirby et al., 1992).

$$D = TSK_L K_F K_E \text{ECF}$$

Equation 1

$$s_D^2 = (s_T \frac{\delta D}{\delta T})^2 + (s_{D'} \frac{\delta D}{\delta D'})^2 + (s_E \frac{\delta D}{\delta K_E})^2 + (s_{T'} \frac{\delta D}{\delta T'})^2 + (s_F \frac{\delta D}{\delta (F)})^2 + (s_L \frac{\delta D}{\delta L})^2 + (s_{ECF} \frac{\delta D}{\delta ECF})^2$$

Equation 8

Here the subscripts, T and T' denote the thermoluminescent reading from the TLD, D' is the dose to the standards, D is the dose to the sample, K_E is the energy correction factor, F is the fading correction factor, L is the linearity correction factor and ECF is the elemental correction factor. Together, s_D defines the uncertainty in a single dose calculation. For each of these terms, a value for the uncertainty was established, and a final value for the entire system was obtained. For this experiment, the uncertainty in fading was not evaluated.

2.5 Single Field Irradiations

Single small field irradiations are used to check beam output under a simple geometric configuration for 6 MV photon beams. This test serves to assess beam output alone at different field sizes, and is not meant to evaluate the treatment planning process of a clinical trial.

IROC Houston uses a polystyrene block phantom (Figure 17 and Figure 18) (dimensions: 14.8 x 14.8 x 16.5 cm³) with a cylindrical phantom insert (Figure 19) (dimensions: radius: 7.5 cm, height: 8.3 cm) to evaluate linac beam output. The cylinder and block contain a fitting thread, indicated by the arrow in Figure 18A and Figure 19A, to ensure that the cylinder is oriented the same way each time. The phantom insert holds two TLD capsules: one at D_{max} and one at a depth of 7 cm. Both capsules are in the center of the cylinder, indicated by the arrow in Figure 19B. Above the first capsule is a slit in the phantom which holds GAFchromic film (Figure 19C). The film allows us to check the CAX alignment and dose profile. The film also has pin-pricks to indicate orientation information.

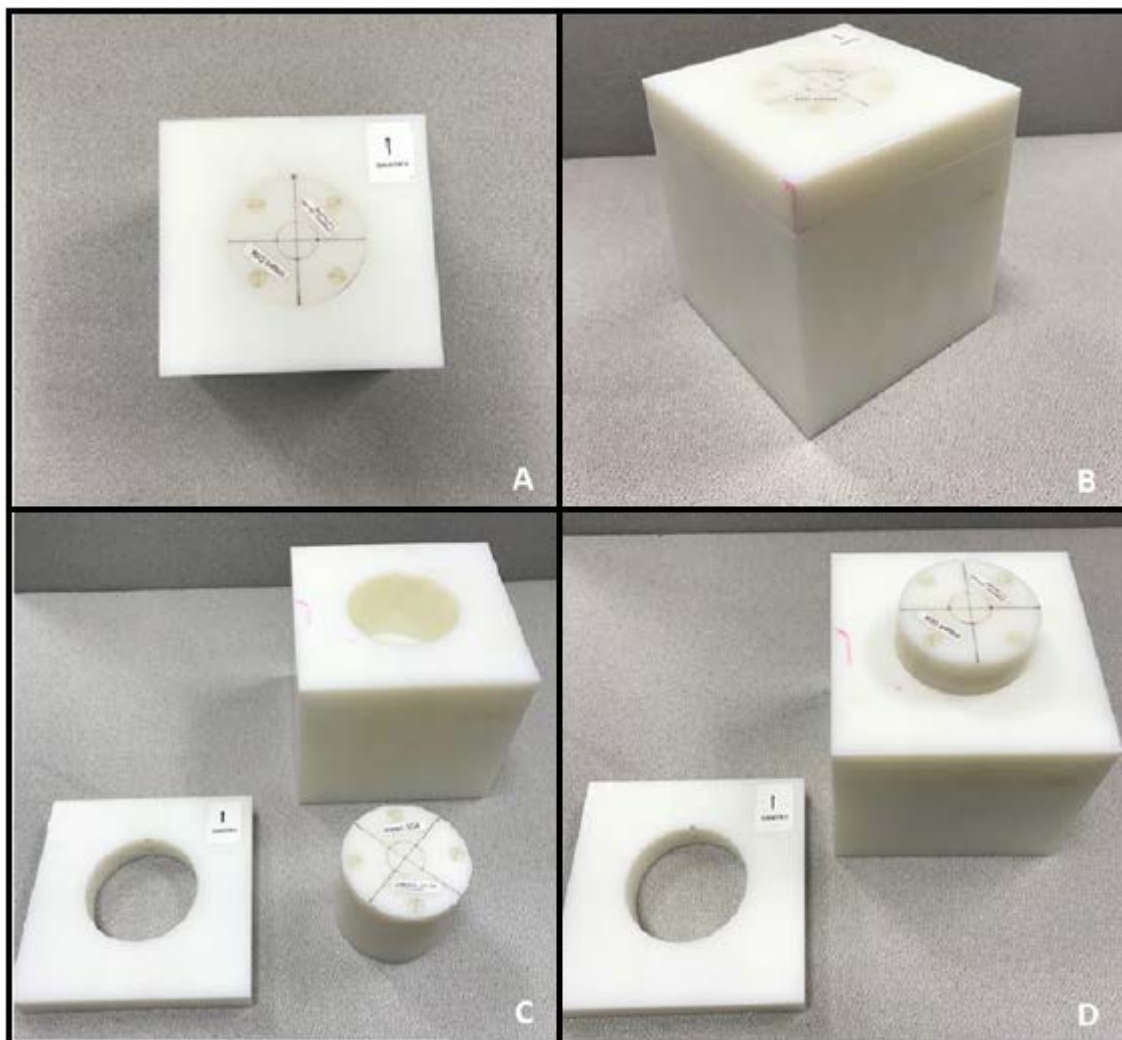


Figure 17: Single field phantom:

- A) Block with gantry direction indicator**
- B) Dimensions 14.8 x 14.8 x 16.5 cm³**
- C) Unassembled single field phantom**
- D) Single field phantom with top plate removed**

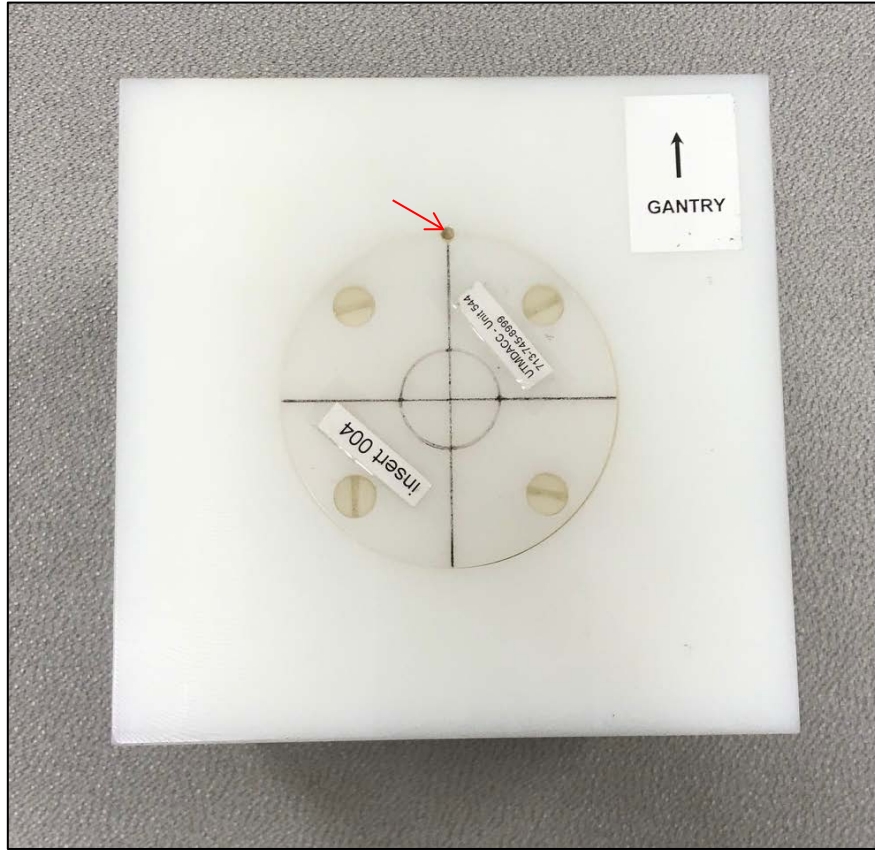


Figure 18: Gantry direction indicator and laser alignment indicators on the single field phantom

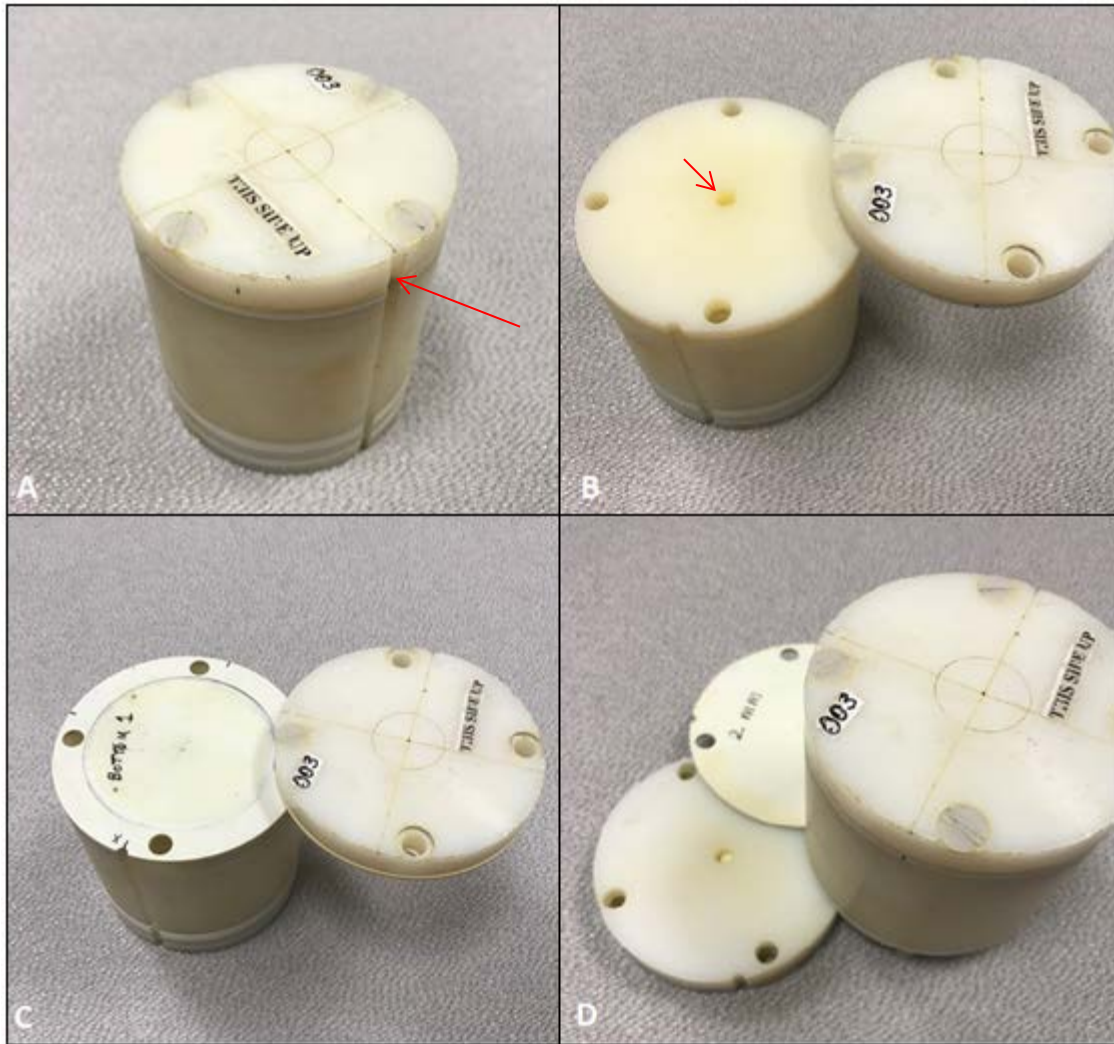


Figure 19: Single field phantom insert

In conducting the single field irradiations, for each field size, we performed four irradiations. Three measurements were made with TLD micro-cubes, and one measurement was made with the IROC Houston standard TLD powder capsules. The TLD powder measurement was used as a reference/ comparison. For each micro-cube irradiation, the cylinder contained 3 micro-cubes (Figure 20 and Figure 21). Each irradiation also used GAFchromic film to check beam alignment and beam profile. We delivered 600 cGy at 3 field sizes: $10 \times 10 \text{ cm}^2$, $3 \times 3 \text{ cm}^2$, and $2 \times 2 \text{ cm}^2$ (Figure 22 and Figure 23).

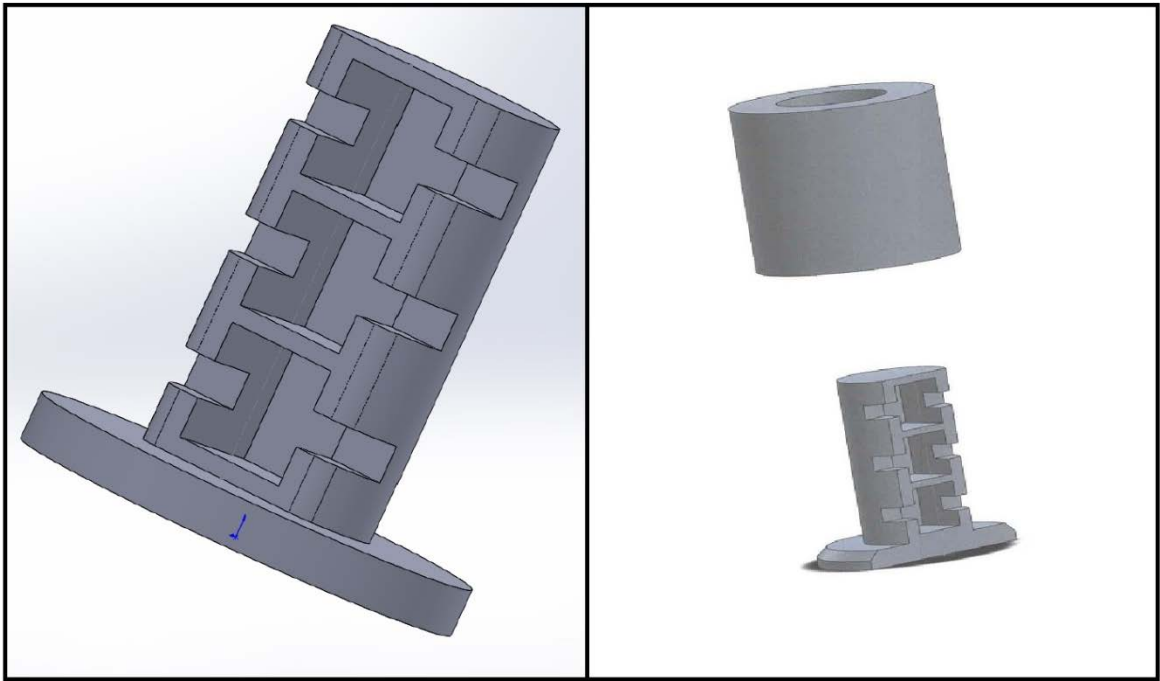


Figure 20: TLD micro-cube capsule for single field phantom

Dimensions: Diameter= 4.55mm Length= 5.14mm

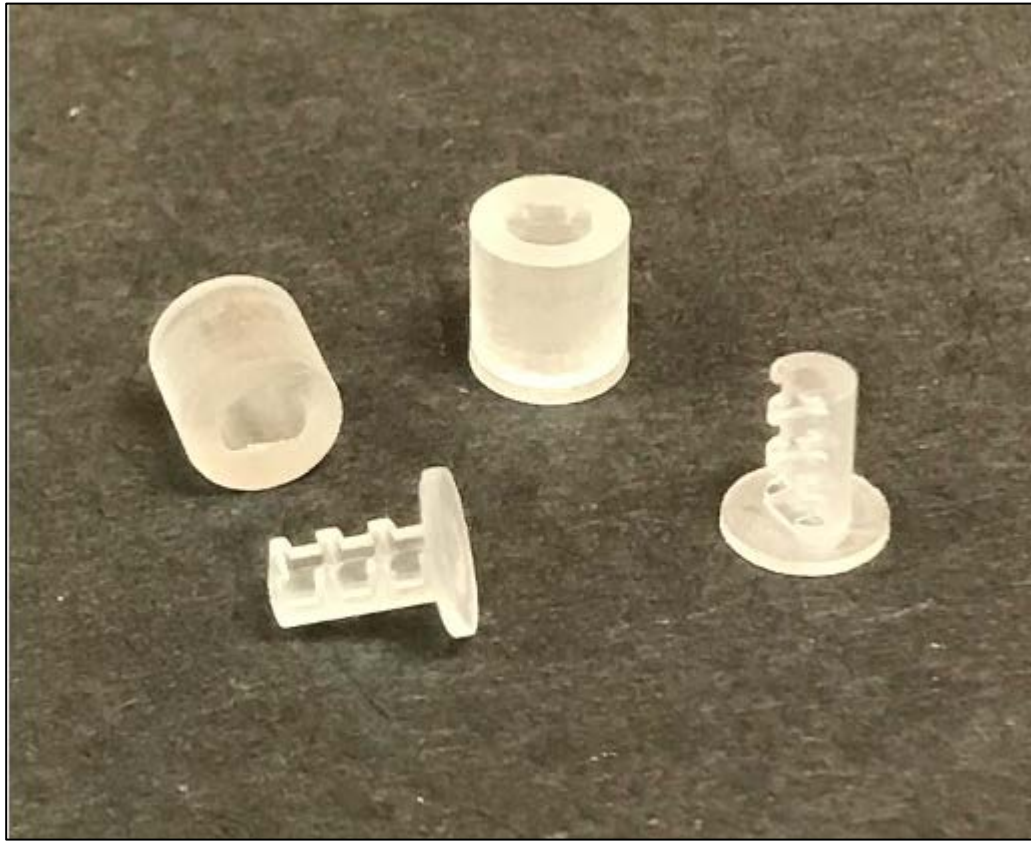


Figure 21: TLD micro-cube capsules for single field phantom.

To deliver the radiation dose, we used a 6 MV photon beam from a Varian TrueBeam linear accelerator, delivered orthogonal to the top face of the phantom block. The block was oriented towards the gantry using the indications on the block itself (Figure 17A). The source to surface distance (SSD) was 100 cm, measured with the optical distance indicator. To ensure congruence of the central axis of the beam with the central axis of the phantom, we aligned the positioning lasers with the crosshairs of the cylindrical phantom insert (Figure 19). The delivery setup is pictured in Figure 22.

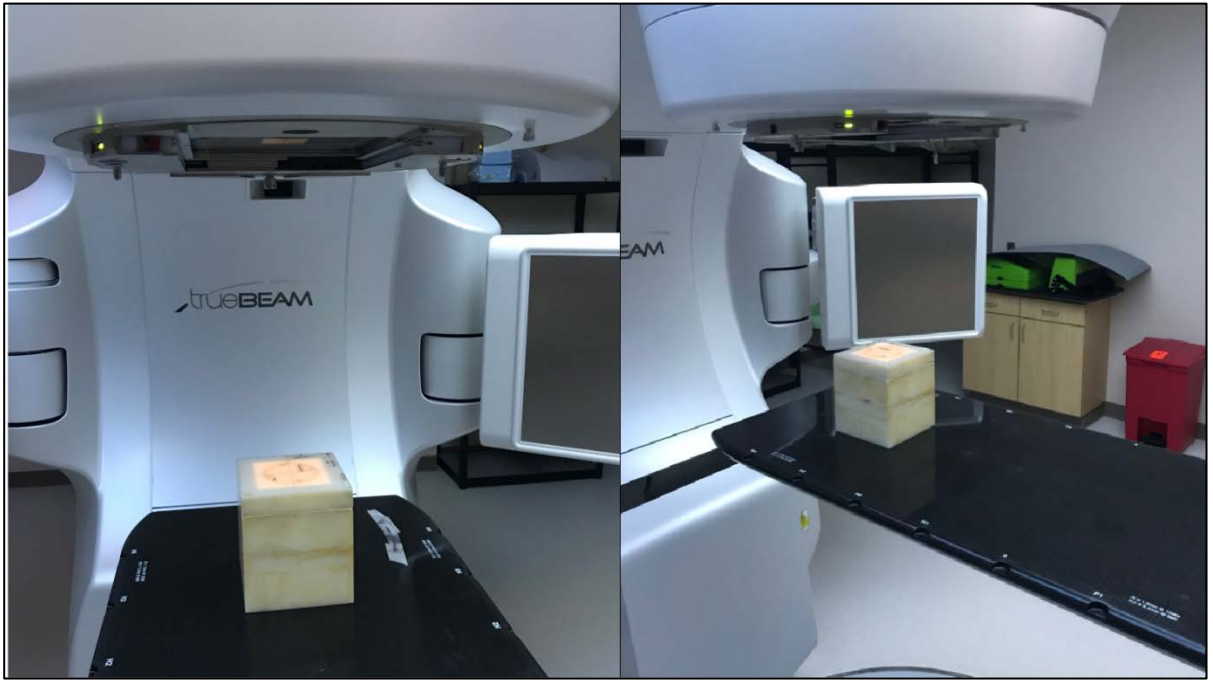


Figure 22: Single field irradiation linac set-up.

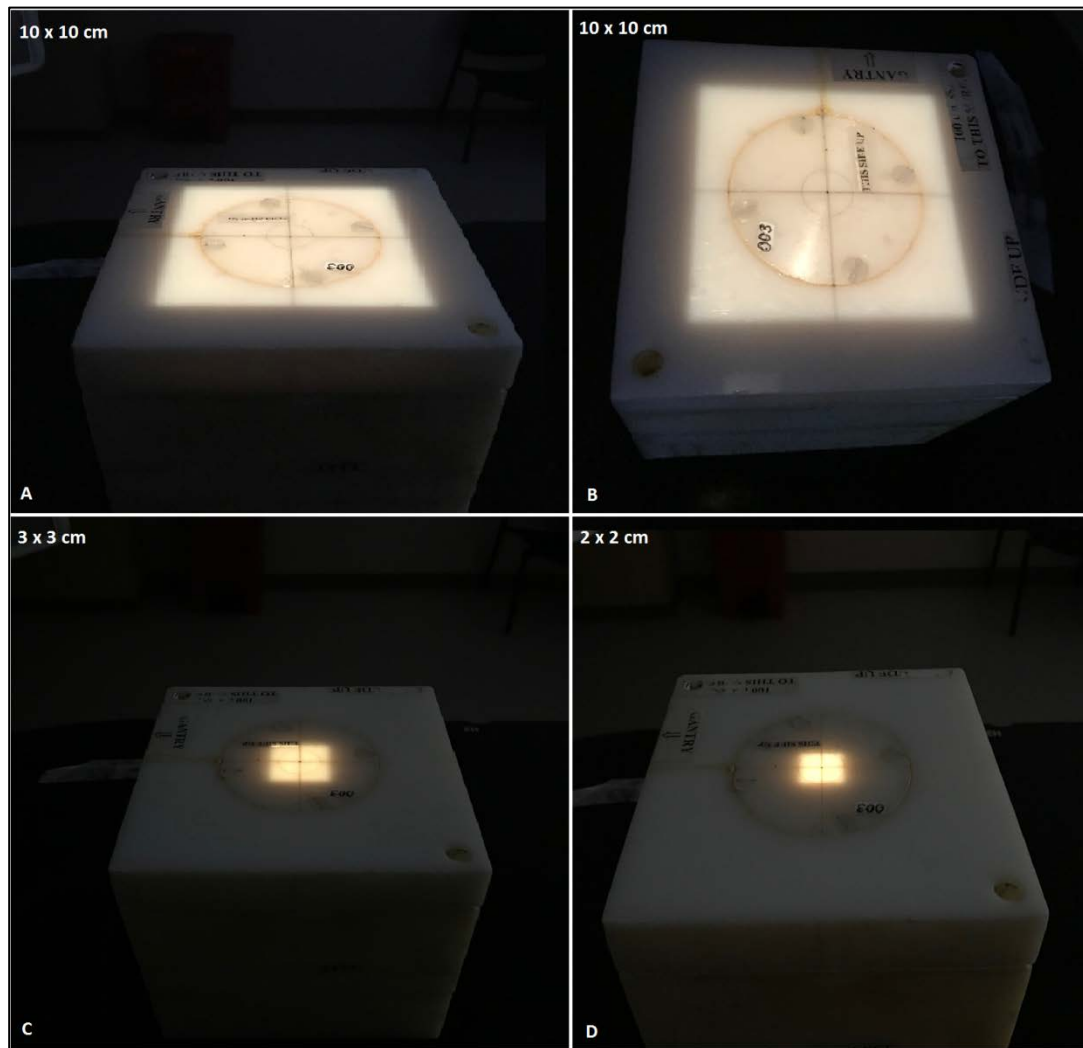


Figure 23: Single small field irradiation setup.

A) $10 \times 10 \text{ cm}^2$

B) $10 \times 10 \text{ cm}^2$

C) $3 \times 3 \text{ cm}^2$

D) $2 \times 2 \text{ cm}^2$

2.6 SRS Head Phantom Irradiation Experiments

To test the efficacy of the micro-cube TLD system, performance was evaluated with respect to three different treatment delivery systems: Varian TrueBeam Linac, Elekta Gamma Knife Icon, and Accuray CyberKnife. The treatment planning system used for each machine was

RayStation 8A, GammaPlan 11.1, and MultiPlan 5.1.2, respectively. Each of these machines are commonly used to treat brain lesions, and are regularly evaluated by IROC Houston.

For these experiments, an SRS head phantom (Figure 24 and Figure 25) constructed in-house at IROC Houston was used. IROC Houston uses this phantom to confirm dose and dose distribution in addition to dose localization in the treatment volume. This portion of the experiment was designed to show congruence between the current powder TLD system used for SRS beam evaluation and the micro-cube system.

This head phantom has been used extensively by IROC Houston for end-to-end evaluations for SRS treatment delivery, and required minor alterations for use with micro-cubes. The head phantom is constructed of high impact polystyrene. The phantom contains an insert, held inside of a sleeve, with a solid water sphere (1.9 cm in diameter) which simulates the tumor volume. Within the tumor volume are two TLD capsules, one superior and one inferior, with the active TLD powder of each within 0.5 cm of the center of the sphere (Figure 26). The phantom insert also permits the use of GAFchromic film for dose profile evaluation. The film planes are orthogonal to each other, in the sagittal and coronal planes of the phantom and pass through the center of the target sphere (Figure 26). Additionally, the phantom contains three fiducials for localization and co-registration purposes. The exterior fiducials, indicated by the arrows in Figure 24, were used for CyberKnife simulation and set-up.

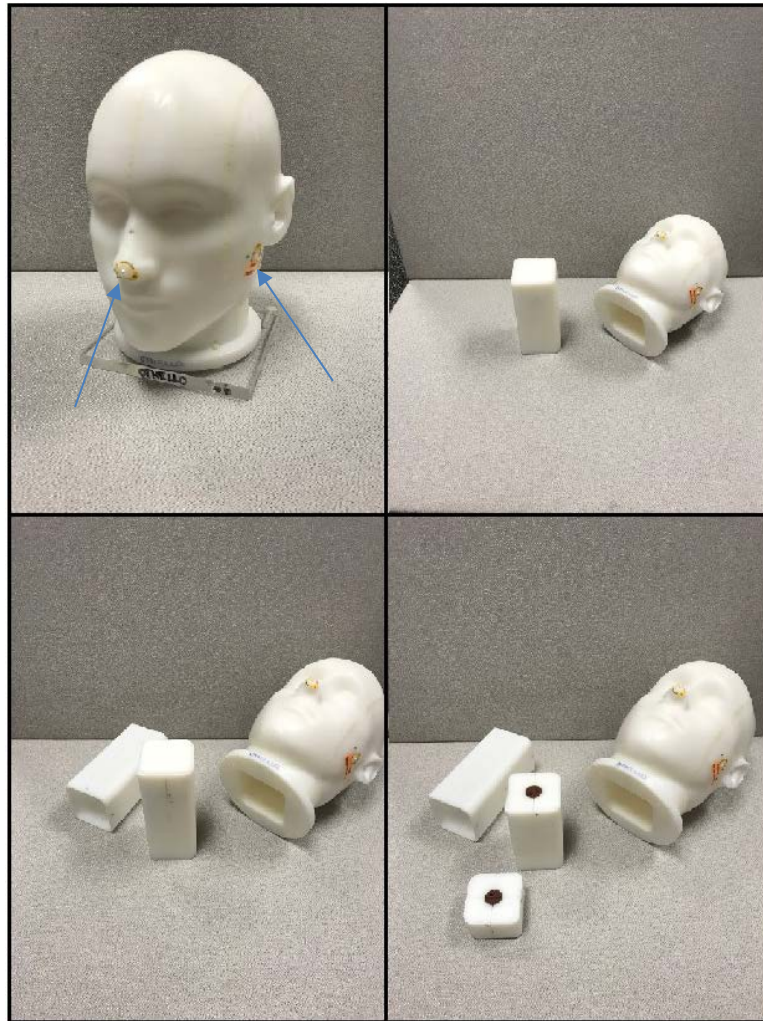


Figure 24: SRS Head Phantom



Figure 25: SRS Head Phantom

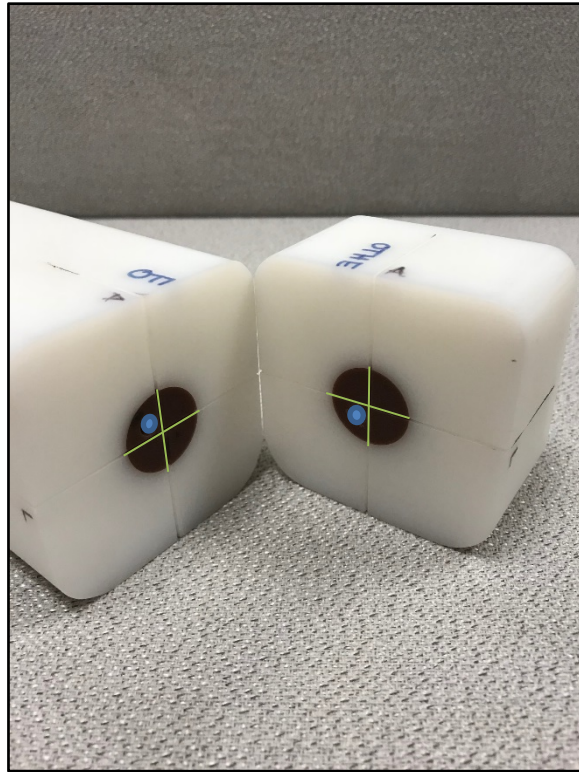


Figure 26: Solid water tumor simulator, TLD capsule insert indicated by the blue ovals, and the center of the solid water ball is indicated by the green crosshairs

When this phantom is sent to an institution or clinic, instructions are included along with the materials, which give information regarding the prescription. The appendix contains the instructions for imaging the phantom, treatment planning, and delivery.

For the purposes of this micro-cube experiment, the TLD capsules and some of the guidelines were slightly altered. Because the dose response of TLD micro-cubes exhibits supralinearity at high doses, this experiment delivered approximately 600 cGy to the tumor volume to minimize dose uncertainty. Additionally, the TLD micro-cube capsules (Figure 27), which replaced the TLD powder, hold three micro-cubes per capsule. We developed treatment plans that were homogeneous over the treatment volume so each micro-cube would receive approximately the same dose.

For each of the three modalities mentioned, four experiments were conducted: one with the standard IROC Houston TLD-100 powder capsules, and three with TLD-100 micro-cubes. The purpose of the standard IROC Houston evaluation with TLD powder is for comparison to the typical phantom results. The work flow for the experiment on each machine included a CT simulation, development of a treatment plan by a medical physicist, and treatment delivery. In the following sections, each modality is discussed separately.

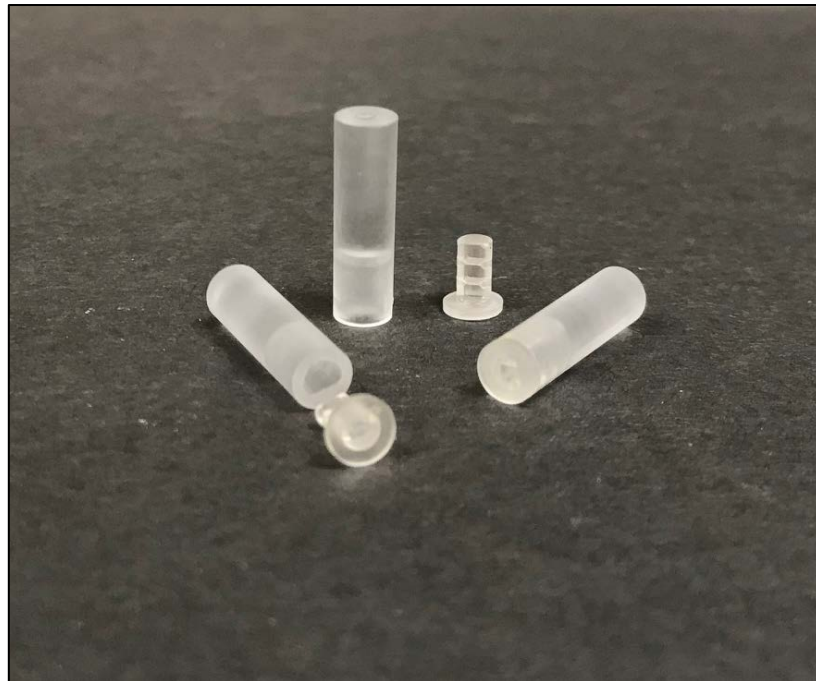


Figure 27: SRS micro-cube capsules, constructed with polycarbonate. Each capsule holds 3 TLD micro-cubes.

2.6.1 Varian TrueBeam Treatment Planning and Delivery to SRS Head Phantom

The IROC Houston SRS head phantom was scanned on a Siemens CT scanner, with 1 mm slice spacing, 530 cm field of view (FOV), and 512 x 512 pixels. The 530 mm FOV accommodates the couch model used during treatment planning for the linac. Additionally, the phantom was loaded with “dummy” film and TLD capsules to simulate the treatment volume for appropriate planning.

Contours of the “lesion” (Gross Tumor Volume (GTV)), represented by a 1.9 cm sphere inside the phantom, as well as the two sets of 3 micro-cube TLDs, which were placed near the center of the sphere (one set is at the inferior-left-anterior, and the other at the superior-right-posterior corner of the center of the sphere), were drawn on RayStation planning based on the CT scan. The GTV was expanded by 2 mm uniformly in all 3 dimensions to define the Clinical Target Volume (CTV). The planning goal was to give 600 cGy to the CTV while minimizing the dose outside CTV. A 6 MV VMAT (Volumetric-modulated Arc Radiotherapy) plan was developed, with a prescription of 600 cGy to 99% of the GTV with 2 arcs: one clock-wise from gantry angle 182° to 178°, and the other counter-clock-wise from 178° to 181°. The (min, max, mean) dose to the CTV, inferior TLD, and superior TLD were (596.7, 609.8, 605.3) cGy, (604.9, 608.2, 605.7) cGy, and (604.5, 609.4, 607.6) cGy, respectively (Figure 28 and Figure 29).













ROI/POI	Clinical goal	Value	Result
 CTV2mm	At least 0 cGy dose at 0.00 % volume	6098 cGy	
 CTV2mm	At most 100000 cGy dose at 100.00 % volume	5967 cGy	
 InfTLD	At least 0 cGy dose at 0.00 % volume	6082 cGy	
 InfTLD	At most 100000 cGy dose at 100.00 % volume	6049 cGy	
 SupTLD	At least 0 cGy dose at 0.00 % volume	6094 cGy	
 SupTLD	At most 100000 cGy dose at 100.00 % volume	6045 cGy	

Figure 28: RayStation treatment planning dose constraint goals






ROI	ROI vol. [cm ³]	Dose [cGy]						
		D99	D98	D95	Average	D50	D2	D1
 *Skull								
 CTV2mm	5.95	5999	6005	6016	6053	6055	6092	6094
 External	4891.53	0	0	0	231	19	2028	2969
 InfTLD	0.06	6049	6049	6050	6057	6055	6078	6079
 SupTLD	0.06	6055	6056	6057	6076	6079	6094	6094

Figure 29: RayStation treatment planning dose to volume. CTV2mm = Clinical Target Volume, InfTLD = inferior TLD capsule active volume (powder or micro-cubes), SupTLD = superior TLD capsule active volume.

For treatment delivery, the head phantom was placed on the treatment couch in the same orientation as the CT simulation. The phantom was loaded with TLD-100 powder capsules, and GAFchromic film, and aligned using both the wall lasers and light field crosshairs (Figure 30). Two TLD-100 powder capsules were taped near the ears of the phantom head. This allowed for subtraction of exposure from onboard images from the measured dose.

The head phantom was then imaged using the Varian TrueBeam cone beam CT (CBCT) with 1 mm slice spacing. Using this CT, the images were co-registered to attain a 3D-3D match, and minor couch adjustments were made to ensure optimum accuracy. Masking tape was then applied to the surface of the head phantom as well as the treatment couch to assist in re-alignment, as the phantom would have to be removed from the treatment position multiple times to replace TLD capsules and film for repeated measurements. The treatment plan was then delivered. This process was repeated three times with TLD-100 micro-cubes and no reference TLD on the ears, with the assumption that the exposure from each CBCT would be consistent. Each time an on-board CBCT was taken, the image was co-registered with the simulation, necessary couch adjustments were made, and treatment was delivered.

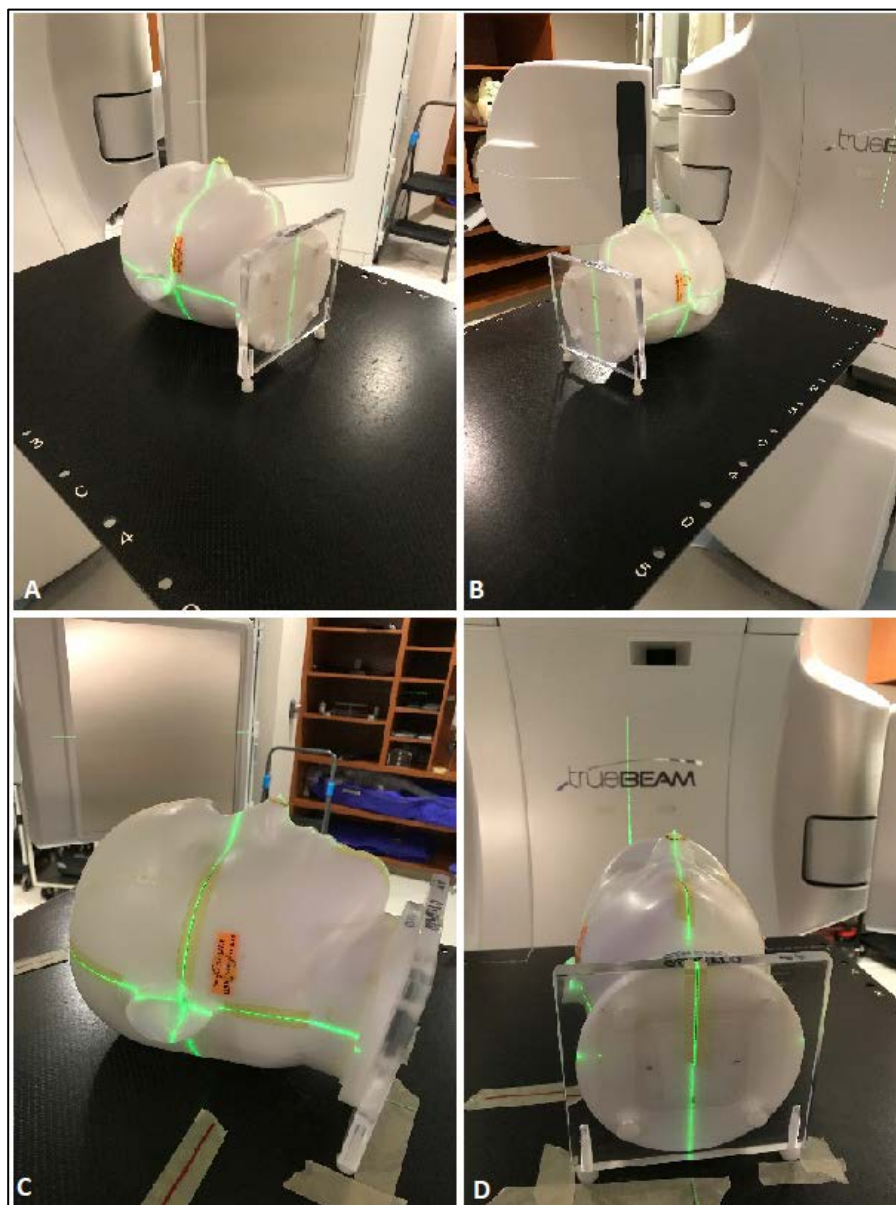


Figure 30: Varian TrueBeam SRS head treatment setup

2.6.2 Elekta Gamma Knife Treatment Planning and Delivery to SRS Head Phantom

The same simulation CT as described in Section 2.6.1, as well as the contours defined in RayStation for the TrueBeam plan, were imported to GammaPlan to create a treatment plan for the Gamma Knife machine. In order to give the TLDs 600 cGy, the prescription was set to 400 cGy to the 60% isodose line using 21 composite shots. The (min, max, mean) dose of the CTV, inferior TLD, and superior TLD were (391,666, 549) cGy, (591, 665, 628) cGy, and (580, 659, 632)

cGy, respectively. Due to characteristics of Gamma Knife, it is very difficult to get dose coverage to the CTV when prescribing a plan with isodose lines (IDL) higher than 60%, which would have resulted in more uniform dose inside CTV.

The phantom was secured inside a mask adaptor using a Moldcare cushion (QFix, Avondale, Pennsylvania) and Orfit mask (Orfit, Wihnegem, Belgium) for positional reproducibility between 4 treatments (Figure 31). For the first setup scan, a stand-alone CBCT acquired without TLDs and films in the phantom, was used as the planning CT, which was registered to the pre-planned (the original simulation) CT. The final plan was delivered 4 times, in the same sequence and TLDs/films configuration as the linac deliveries, with the phantom in the same position as the first CBCT. For each delivery, a treatment-position CBCT was acquired and registration was reviewed and approved, then treatment was delivered. GammaPlan automatically adapted the planned shots according to the registration for delivery. The relative change of the phantom position was presented as a geometrical rotation and translation at the isocenter, which has coordinates of $(x, y, z) = (100, 100, 100)$ in the Leksell stereotactic space. The result of these translational and rotational changes of the four deliveries are shown in Figure 32. They were all less than 0.3 degrees (Rotation) and 0.4 mm (translation).

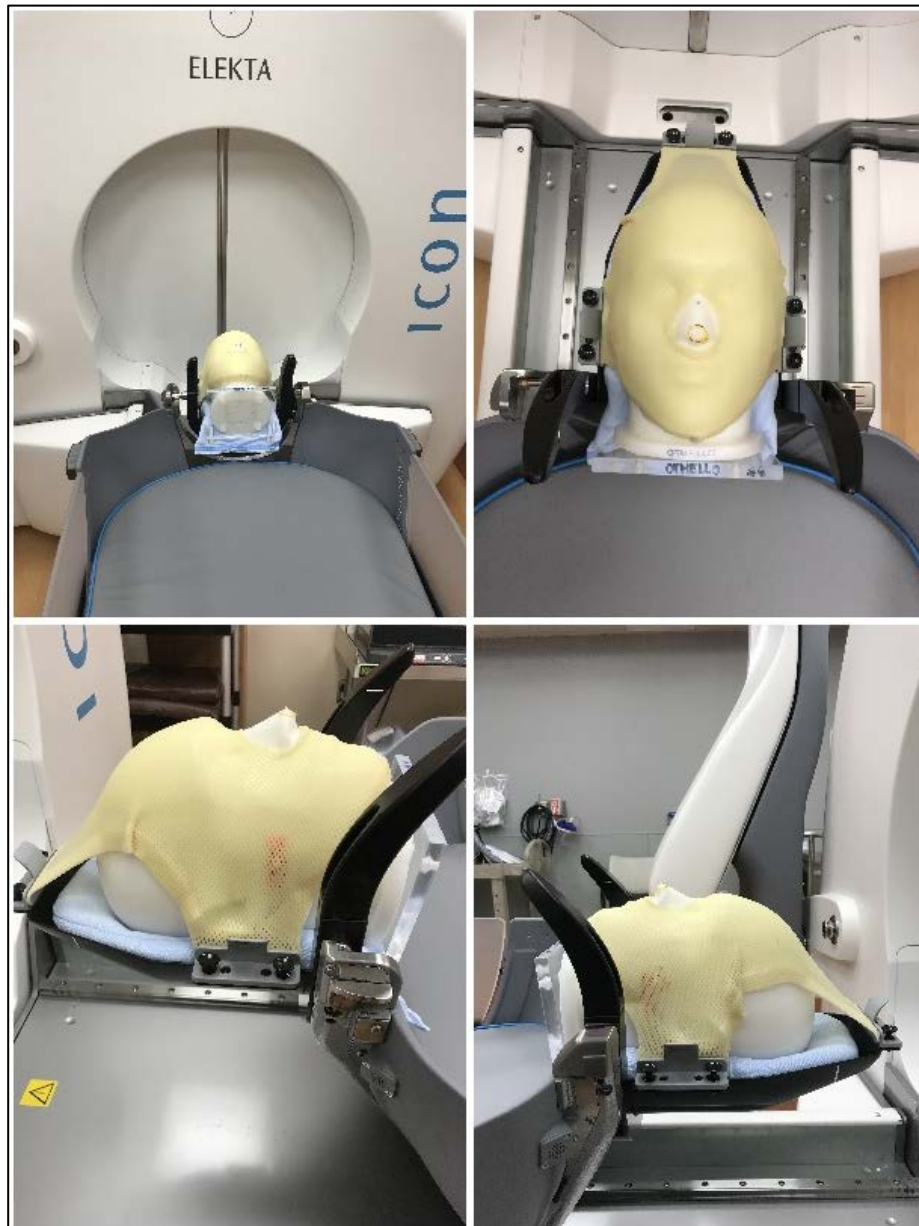


Figure 31: Gamma Knife setup

A	Rotation [degrees]			Translation [mm]		
	X	Y	Z	X	Y	Z
	-0.08	-0.17	0.55	0.11	-0.19	-0.09
B	Rotation [degrees]			Translation [mm]		
	X	Y	Z	X	Y	Z
	-0.20	-0.04	-0.17	-0.01	-0.26	-0.36
C	Rotation [degrees]			Translation [mm]		
	X	Y	Z	X	Y	Z
	-0.13	-0.04	-0.27	0.04	-0.23	-0.36
D	Rotation [degrees]			Translation [mm]		
	X	Y	Z	X	Y	Z
	-0.15	-0.06	0.30	-0.03	-0.23	-0.39

Figure 32: Gamma Knife image co-registration applied correction

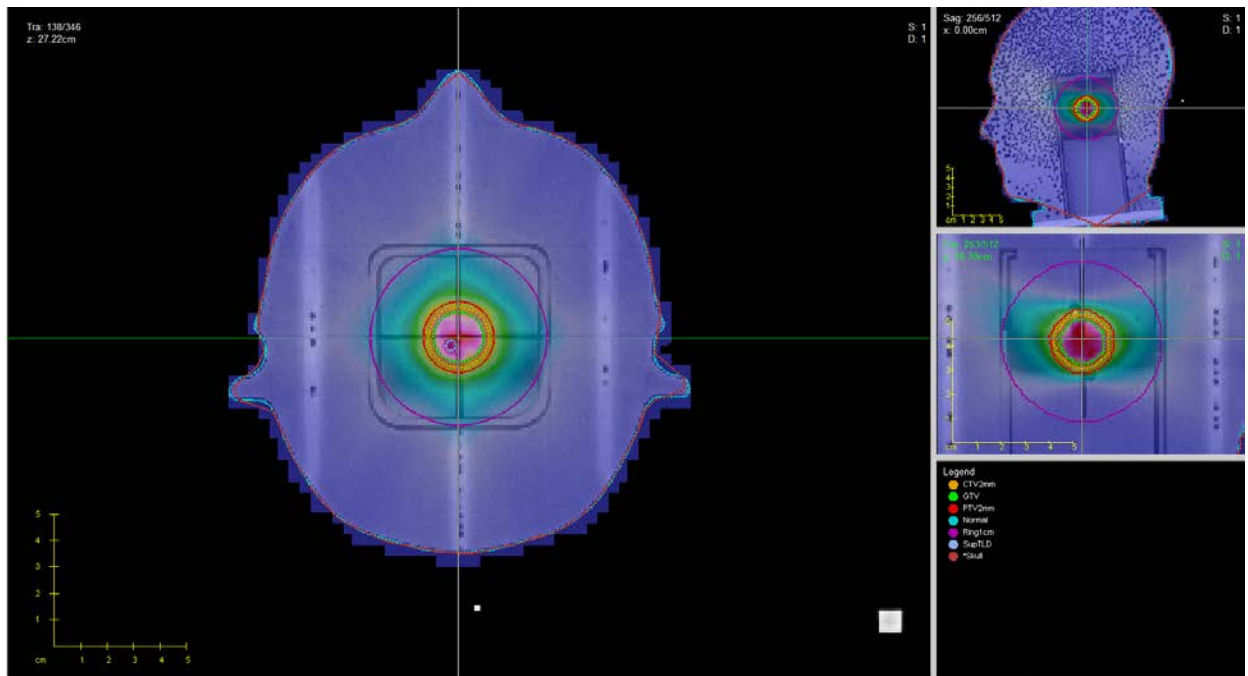


Figure 33: Gamma Knife Treatment Plan Dose Map

2.6.3 CyberKnife Treatment Planning and Delivery to SRS Head Phantom

The simulation CT unit used for the CyberKnife treatment planning was a GE LightSpeed RT 16 (GE Healthcare, USA). The CT used 1.25 mm slice spacing, and 512 x 512 pixels. The images

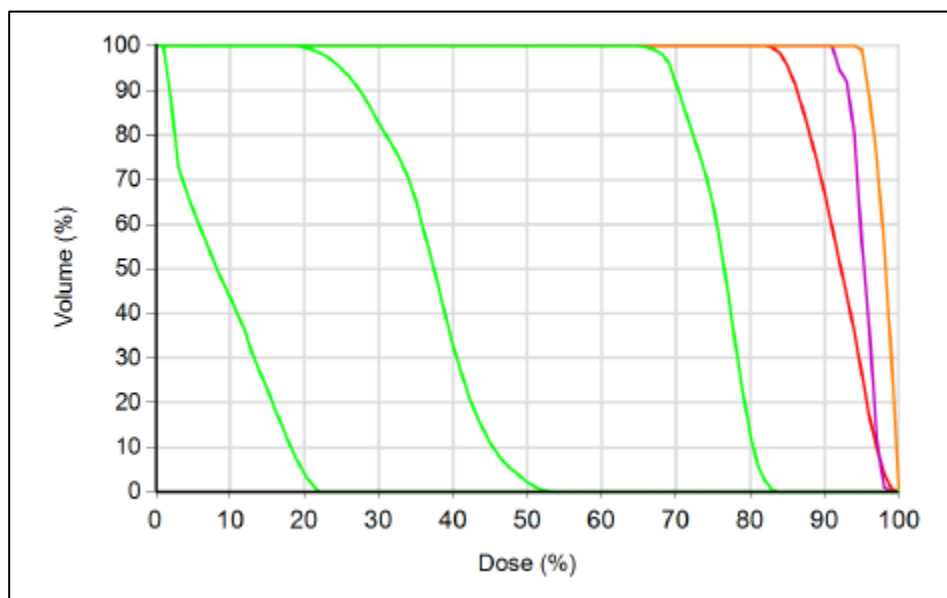
were loaded in to MultiPlan 5.1.2 (Accuray Inc., Sunnyvale, CA, Chicago, Illinois) for treatment planning, using a Sequential Optimization algorithm and Ray Tracing dose calculation algorithm. Contours were drawn around the 1.9 cm tumor volume, forming the CTV and around the active volume of both TLD capsules (superior and inferior). Additionally, three gold fiducials, which were located within the phantom, were identified for phantom positioning during treatment setup.

The treatment plan was developed to deliver 600 cGy to the 83% isodose line using 46 photon beams (Figure 36). The goal of this treatment plan was to deliver a homogeneous dose to both capsules. The (min, mean, max) dose to the CTV, inferior capsule (Cap 1), and superior capsule (Cap 2) were: (582.4cGy, 664.5cGy, 723.0cGy), (658.8cGy, 688.5cGy, 708.9cGy), and (685.9cGy, 708.3cGy, 723.0cGy), respectively (Figure 34).

To deliver treatment, an Accuray CyberKnife with fixed cones was used. The phantom head, loaded with ear TLD, TLD capsules, and film, was set on the treatment couch, and roughly aligned with the wall lasers. This placed the head phantom in the approximate area needed to take positioning radiographs. These radiographs are taken orthogonally from each other and use fixed room geometry to determine the position of the phantom in the reference space of the treatment head. Small adjustments were made to the positioning of the phantom head, and radiograph images were taken again, until an agreeable position of the phantom was achieved (approximately three radiographs were taken). The treatment was then delivered to the phantom head. This process was repeated three more times for a total of four irradiations: one using TLD powder, and three using TLD micro-cubes.

VOI	Min (cGy)	Mean (cGy)	Max (cGy)
Tumor	582.44	664.49	722.89
Cap 1	658.76	688.49	708.88
Cap 2	685.94	708.31	722.89

Figure 34: Minimum, Mean, and Maximum dose to CTV (Tumor), Inferior TLD Capsule (Cap 1), and Superior Capsule (Cap 2)



VOI	Min (cGy)	Mean (cGy)	Max (cGy)
Tumor	582.44	664.49	722.89
Cap 1	658.76	688.49	708.88
Cap 2	685.94	708.31	722.89
[Tumor] Shell 1	458.49	548.79	602.46
[Tumor] Shell 2	130.75	267.02	388.28
[Tumor] Shell 3	10.78	65.95	159.86

Figure 35. TOP: DVH of relative dose BOTTOM: Min, Max, and Mean dose to volumes. Cap 1 = superior capsule Cap 2 = inferior capsule

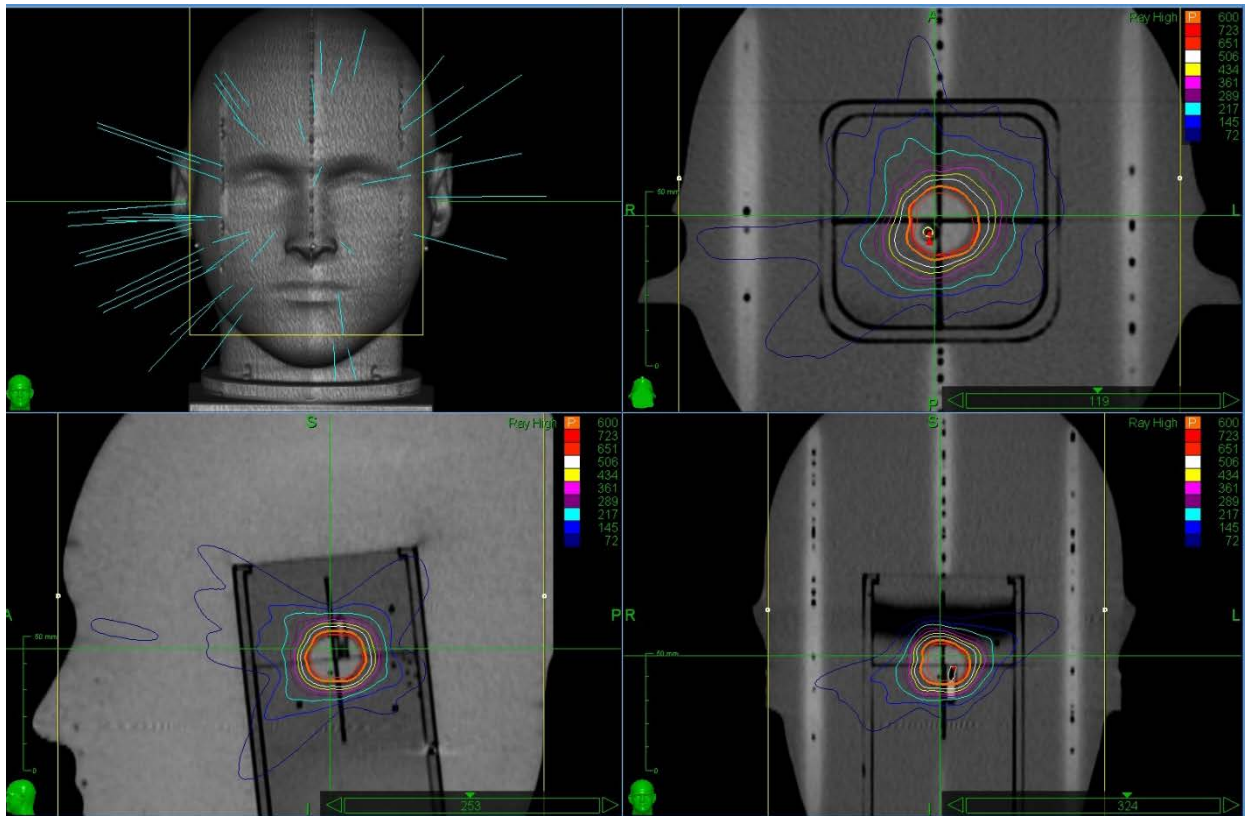


Figure 36: CyberKnife treatment plan. See Appendix

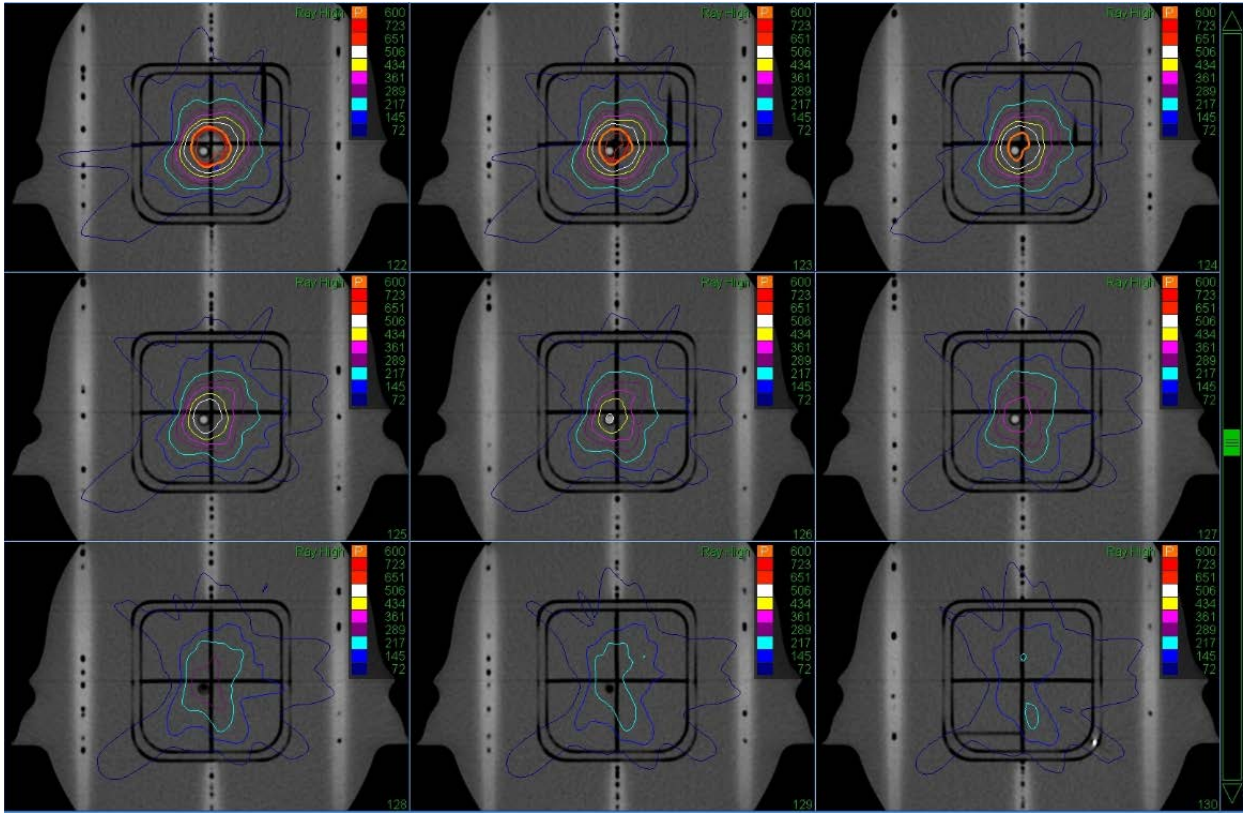


Figure 37: CyberKnife treatment plan isodose lines to treatment volume. See Appendix

2.7 Single Small Field Irradiations

The purpose of this experiment was to evaluate the limitations of TLD micro-cubes in measuring small photon fields. An Accuray CyberKnife was used to deliver the photon beams for the small field experiments. Furthermore, this CyberKnife was used with fixed collimators.

The same single field phantom used for the single field experiments described in section 2.4 was used to hold the TLD capsules. This phantom holds the micro-cubes at D_{\max} and includes GAFchromic film for evaluating field alignment. This phantom was set up at 78.5 cm SSD and 80 cm SAD, where the beam output is defined for CyberKnife (Figure 38). The phantom was aligned using the internal laser of the CyberKnife gantry head (Figure 39).

The field sizes used in this experiment were 60, 20, 15, 10, 7.5, and 5 mm collimator diameters. Three micro-cubes were used to measure each field size, and each field size was measured three times.



Figure 38: Small Field CyberKnife set-up 78.5cm SSD

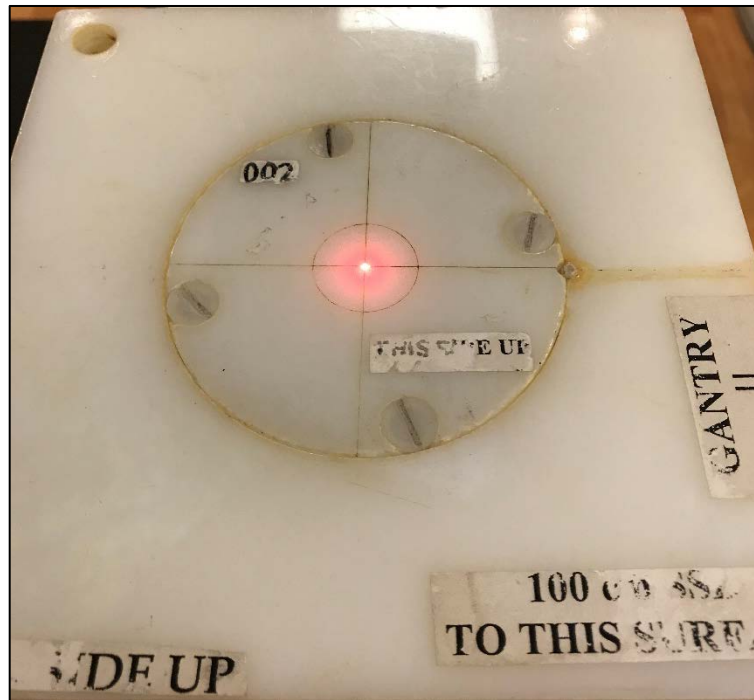


Figure 39: CyberKnife internal laser alignment for small field experiments

2.8 TLD Dose Calculations and Dosimetry Evaluation

2.8.1 Dose Calculations

To calculate dose to TLD micro-cubes for the experiments described above, IROC Houston follows these steps:

1. The TLD standards are irradiated with a Cobalt-60 unit. The dose levels are close to 300 cGy, and 600 cGy (based on the type of session).
2. The standards are read no earlier than 10 days after irradiation.
3. When TLD session begins, a set of standards are read first. Then up to 18 institution TLD capsules can read followed by another set of controls. Another 18 institution TLD capsules can be read followed by another set of controls. This is a continued until all of the TLD sets have been read within a session. A maximum of 54 institution TLD

capsule could be read in a session. The session is then closed out by a set of standards being read.

4. Equation 1 is used to determine dose from TLD for photon energies

2.8.2 Film Dosimetry Evaluation

GAFchromic film is used in the IROC Houston QA services in multiple ways. For single field output dosimetry, the film gives information regarding the alignment of the radiation field with the central axis of the phantom. For this experiment, alignment is increasingly important at field sizes below 2 cm x 2 cm, where misalignment can have a serious effect on output at the location of the micro-cubes. For the SRS head phantoms, the film is used to check phantom alignment and treatment delivery, as well as an additional check for TLD dose agreement.

Each film used in the single field and SRS head phantom irradiations had pin pricks for localization. These pin pricks were at known locations within the phantom, which permitted the evaluation of alignment during film analysis.

Film was read 10 to 14 days after irradiation, which reflects the time post-irradiation in which film are typically read. It is important to wait a similar time period to read film as the calibration (Girard, Bouchard, & Lacroix, 2012). To read the film, a Model CCD100 CCD Microdensitometer for Radiochromic Film (Photoelectron Corporation, Lexington, Massachusetts, USA) was used (Figure 40). The image data was then read into a MatLab program developed by IROC Houston. This program allowed the user to register the pin pricks to get spatial information about the film (Figure 41). The program calculated a dose map of the film, which was normalized to the dose from the TLD.

Following the film registration, the CT images, the radiation therapy dose, plan, and structures were loaded into the program, co-registered with the film (Figure 42). The information from the TPS and the film was evaluated for agreement.



Figure 40: Film Densitometer, Model CCD100 CCD Microdensitometer for Radiochromic Film (Photoelectron Corporation, Lexington, Massachusetts, USA)

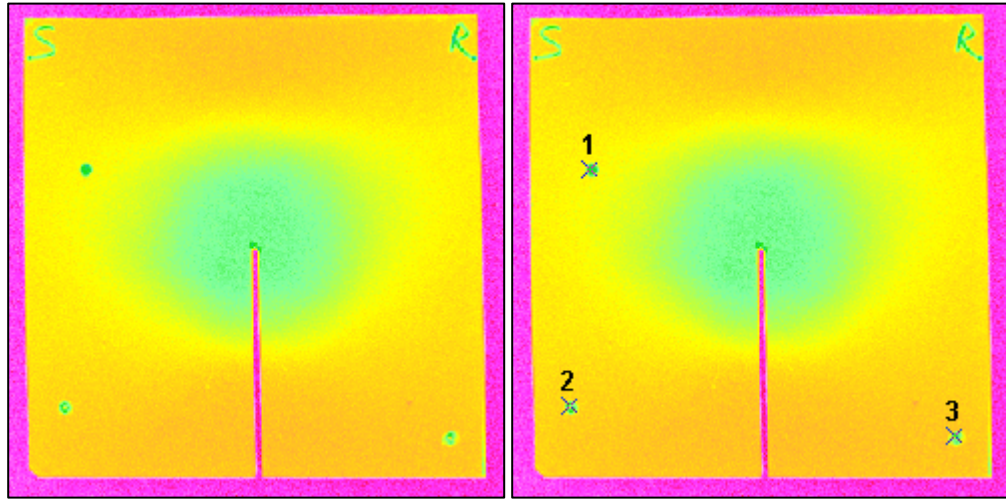


Figure 41: *Left*: Coronal film loaded using MatLab program *Right*: Pin breaks registered for positioning, labeled 1, 2, and 3

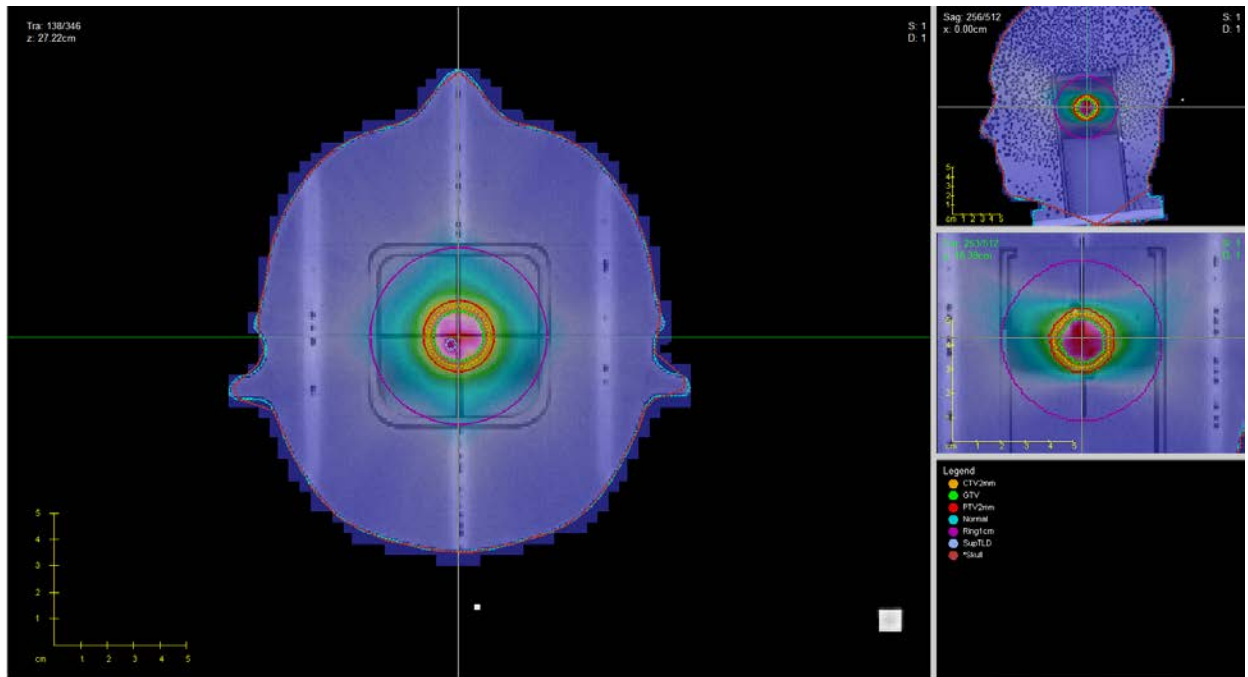


Figure 42: The film dose profile is co-registered on the CT simulation

2.9 Statistical Analysis

To test our hypotheses regarding the consistency of measured and expected dose for the various experimental settings, we used a Two One Sided T-Test (TOST) of equivalence. To perform these t-tests, the `tost()` function from the equivalence package in R statistical software was used. The results of the TOST tests were cross checked by running two t-tests using the `t.test()` function in R.

A TOST test was conducted for four sets/populations of measurement in which the values evaluated were the ratios of measured dose to expected dose. The single field and small field data were held separately as individual populations. Secondly, the data from all three SRS modality experiments were combined to form a population. Lastly, the ratio of micro-cube over powder for both single field and SRS were combined to form the third population to evaluate.

In each of these statistical tests, the composite null hypothesis tested was that the true ratio was ≤ 0.95 and that the true ratio was ≥ 1.05 . With this test, a p-value smaller than 0.05 meant there was strong statistical evidence to reject the null hypotheses, in support that the true ratio was within the bounds.

3 Results

3.1 Micro-Cube Handling

3.1.1 Micro-Cube Shape Uniformity

We began the experiment with 500 micro-cubes, however, after inspection, we determined 37 were not suitable for experiments. These were micro-cubes which did not represent a uniform cubic shape, had chipped edges, or had other apparent malformations

(Figure 43), and were likely to exhibit poor reproducibility and other complications in TLD handling.



Figure 43: Irregularly shaped TLD-100 micro-cubes from ThermoScientific

3.1.2 TLD Annealing Response

The analysis of TLD annealing response was described in Section 2.2.2. There was no noticeable difference in TLD response for leaving TLD in of the oven at 400°C for 10 extra minutes or leaving the TLD in the oven at 100°C for 30 extra minutes. Nor was there an effect on the TLD signal output for shortening the cooling phase, however, there was a noticeably large effect on TLD output when the cooling phase was ignored completely. The decrease in signal output was 29.5% for the group which did not undergo rapid cooling. For the other groups tested with a different annealing cycle, there was no noticeable difference in TLD output.

This test of annealing response lends confidence that TLD output can be trusted if there are small changes to annealing, similar to those differences demonstrated here (Figure 44).

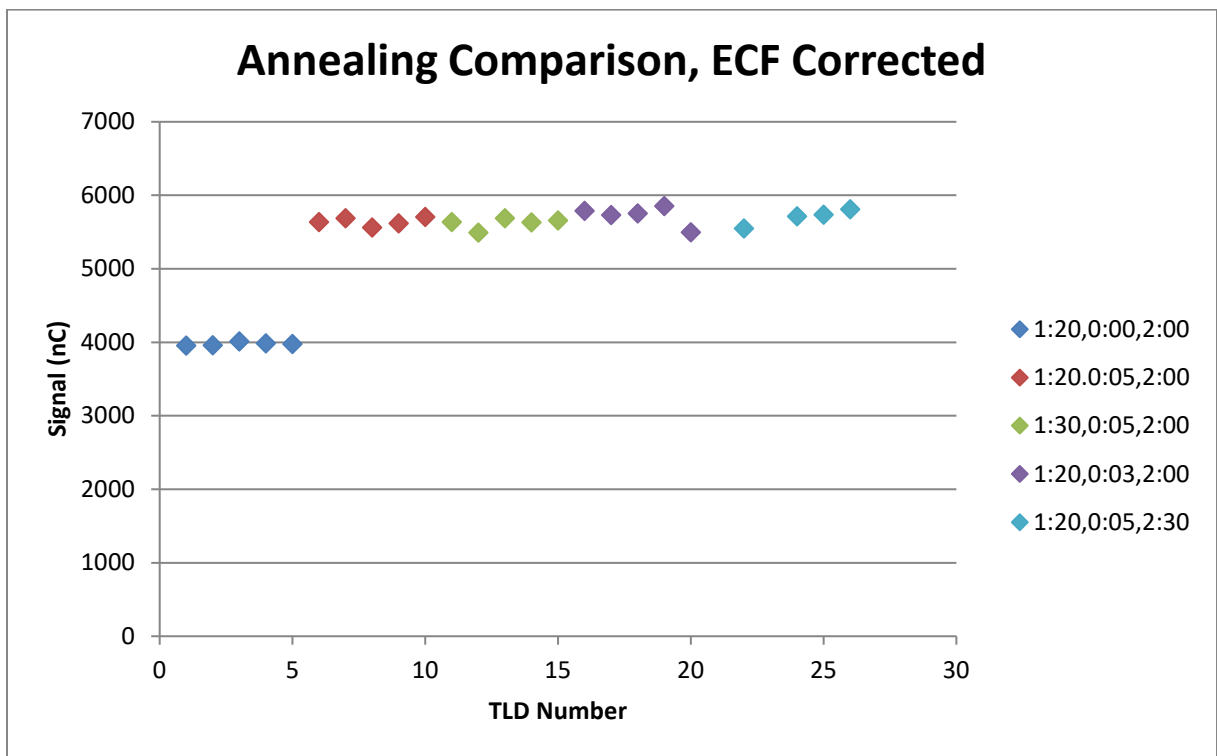


Figure 44: TLD Annealing Response: Legend reads: Time at 400°C, Time cooling; Time at 100°C

Measurements were also conducted to define the rate of cooling, as it is known that this portion of annealing can have a significant effect on the output of TLD. The trend in cooling followed an exponential decay. The temperature reached 60°C in just over a minute, and then gradually decreased to approximately 50°C (Figure 45). After this 50° C was reached, there was no significant decrease in temperature of the annealing planchet for the remainder of the cooling phase.

It seems that once the temperature has decreased to approximately 50°C, the cooling can be stopped, and the annealing planchet can be moved into the next oven. Given the results from the experiments in varying annealing times, this seems viable, as decreasing the cooling period from 5 minutes to 3 minutes did not have an effect on the output of the TLD.

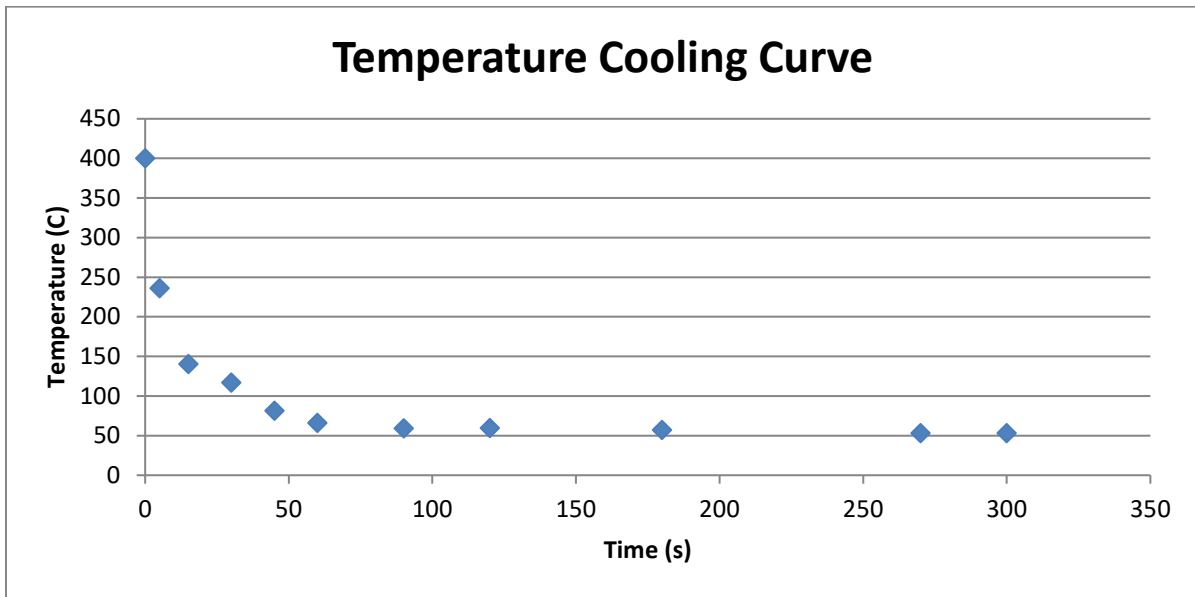


Figure 45: TLD annealing planchet cooling curve

3.1.3 Micro-Cube Reading Variability

3.1.3.1 Placement Variability

67 micro-cubes were read without specific guidelines on placing the cube in a reproducible location in the reading planchet. Three repeated measurements of ECF where the micro-cube was placed as reproducible as possible in the center of the reading planchet were compared to a single measurement of ECF where the micro-cube was not placed reproducibly. This variable placement reading increased the average coefficient of variation from 1.2% to 3.0%. The average difference in measured ECF values was 5%, with a maximum of a 15% change in measured ECF value.

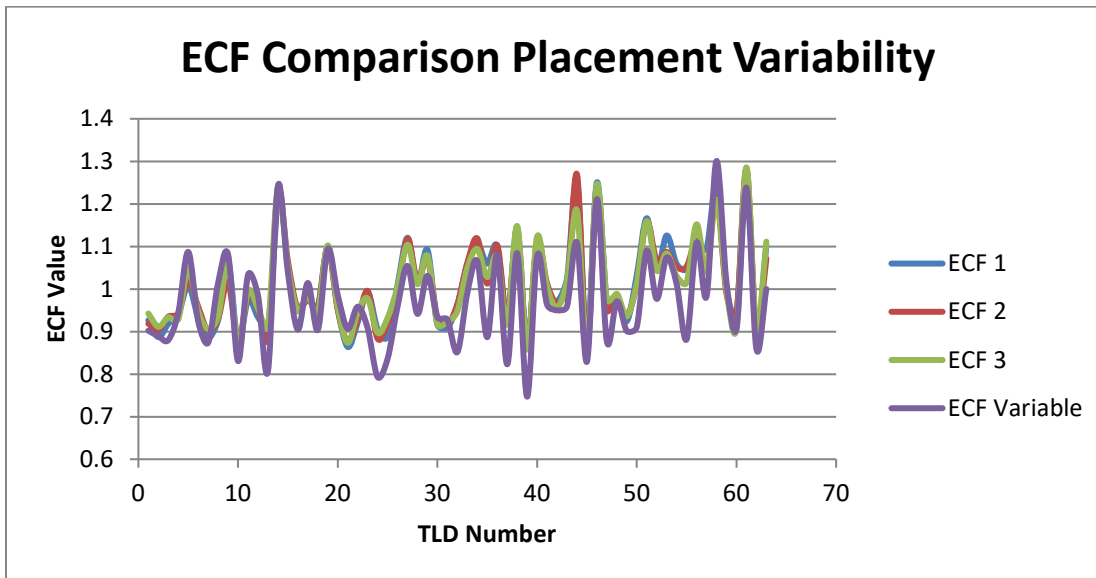


Figure 46: TLD placement effect

3.1.3.2 Reader Variability

The experiment described above was repeated, however the reader was instructed to carefully place the TLD in the center of the reading planchet to the best of their ability. The idea behind this experiment was to gather a perspective on human dependence in evaluating ECF values. This information gives some insight into reader dependence in reproducibility of measurements. This experiment showed that the average coefficient of variation increased from 1.1% to 1.5%. Here, the average difference in the measured ECF was 2.1% with a maximum difference of 5.8%.

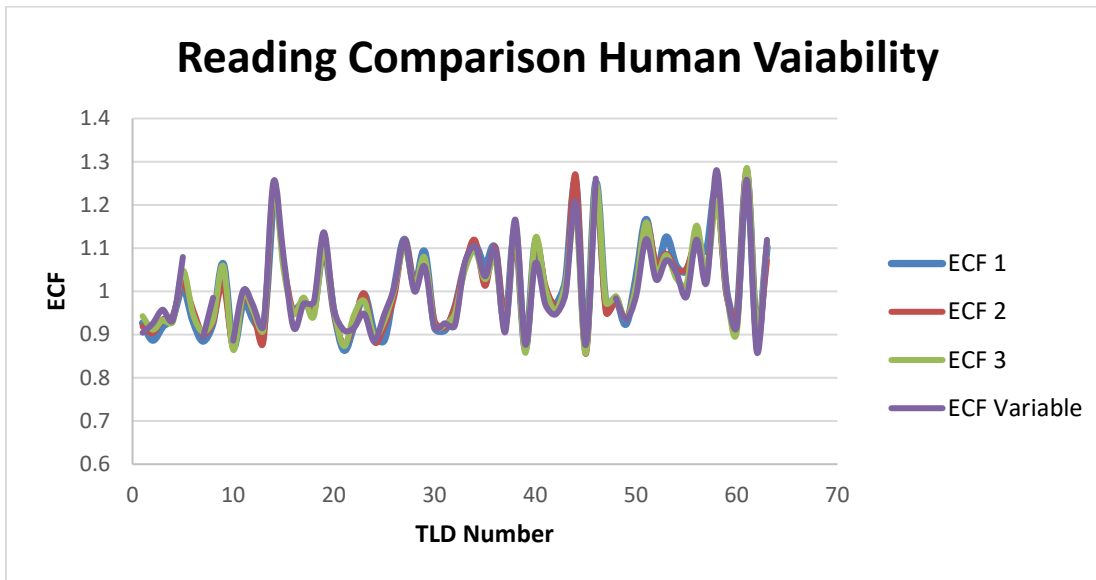


Figure 47: Reader variability

3.2 TLD Micro-cube Characterization

3.2.1 Elemental Correction Factor (ECF)

The average ECF value for 461 micro-cubes was 1.01. Intuitively, the ECF value should be 1, so interest in the result of a 1% difference led to an investigation of this discrepancy. The response from each batch of micro-cubes is expected to be Gaussian in distribution, symmetric about the average. In reality, the ECF values more accurately represent a Poisson distribution (Figure 48), where there is a tail of large ECF values greater than 1, which pushes the average ECF value above unity. This shows that most of the TLD micro-cubes under-respond to dose, when compared to the average signal response of all cubes.

To investigate the stability of the individual cubes, the coefficient of variance, defined in Equation 5, was evaluated for 3 measurements of ECF for each cube. The average coefficient of variance was 1.25% for 461 micro-cubes where the maximum value was 8.98% and the minimum was 0.06%.

For this study, micro-cubes that showed poor reproducibility were banned from use in further experiments. The cut-off reproducibility was 2%, where any micro-cube with a coefficient of variance greater than this value was not used. The tolerance for 2% stability is a stringent request, as TLD micro-cubes have an accuracy of $\pm 15\%$ (± 2 sigma) as specified by ThermoFisher. Across all TLD cubes, 15.40% of cubes were outside of a 2% coefficient of variance, which is a larger portion than preferred, but can only be expected when stability is already stated by the manufacturer as an area of concern. However, only 0.87% were outside of 5%, so if we decided to adopt a looser criteria, a larger proportion of the cubes could be used.

$$\text{Coefficient of Variance} = 100\% \times \frac{\text{Standard Deviation}}{\text{Average}}$$

Equation 4

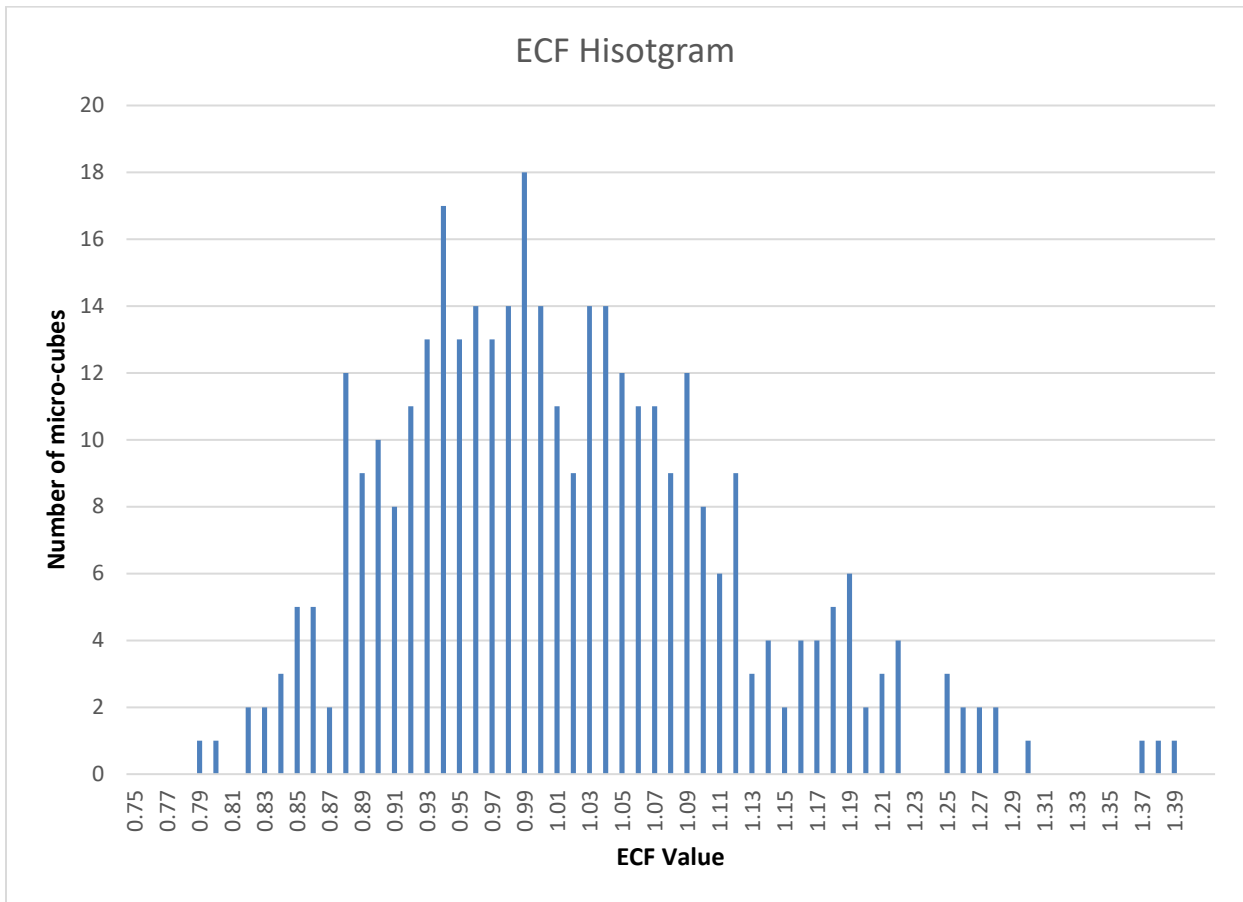


Figure 48: Histogram of ECF values for all TLD micro-cubes.

3.2.2 Linearity Correction Factor (K_L)

The linearity correction factor, K_L , gives insight as to how TLD-100 micro-cubes respond to different dose levels. In Figure 49 the TLD signal response versus dose is shown. As expected, we see a linear dose response to about 400 cGy, and highly correlated linear fit (R-squared value >0.99).

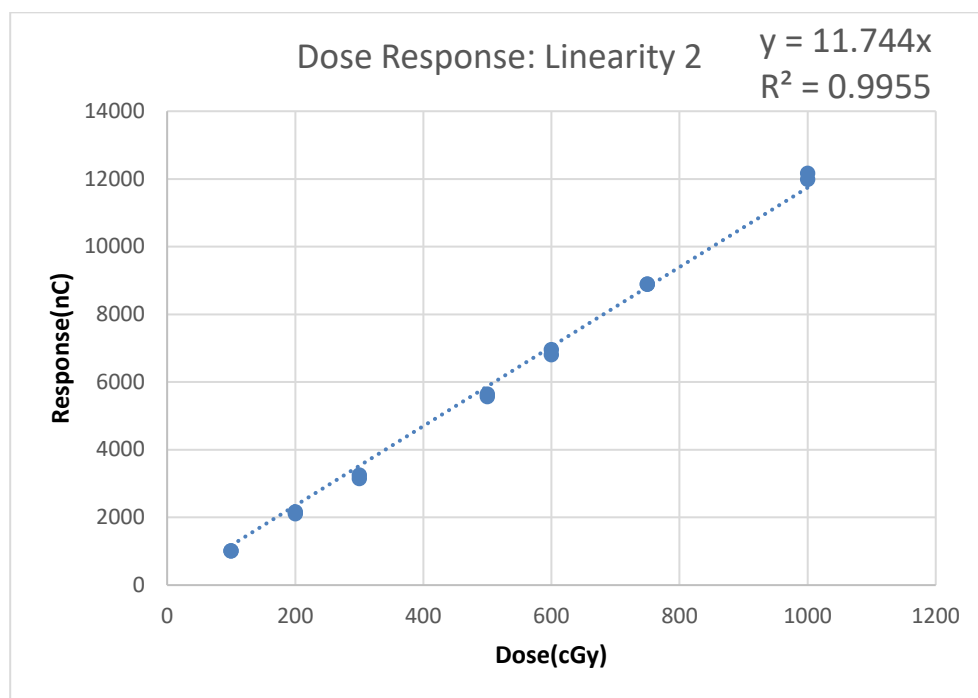
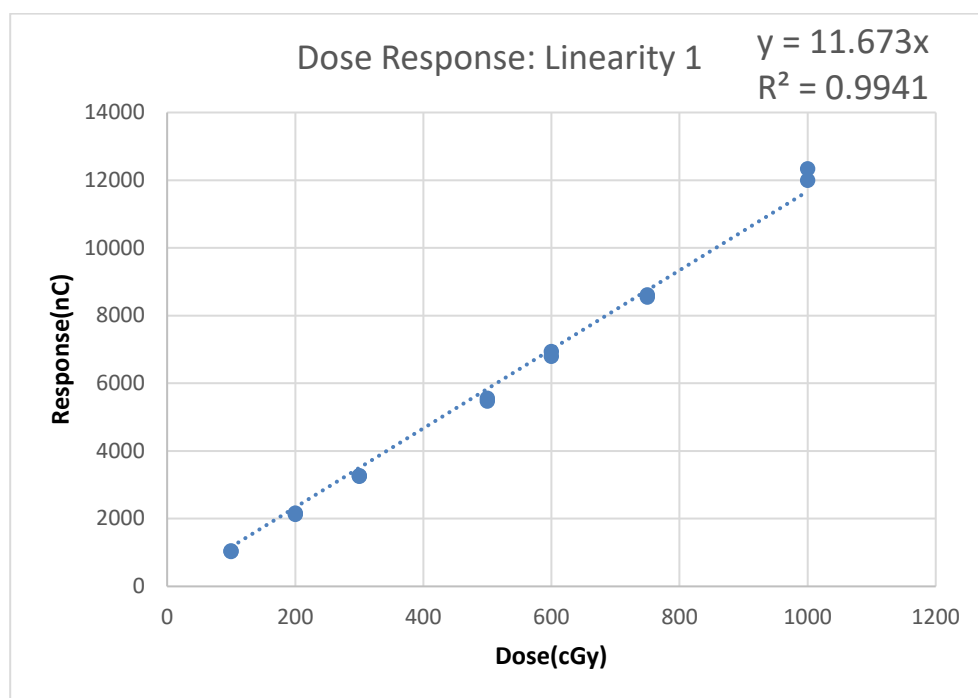
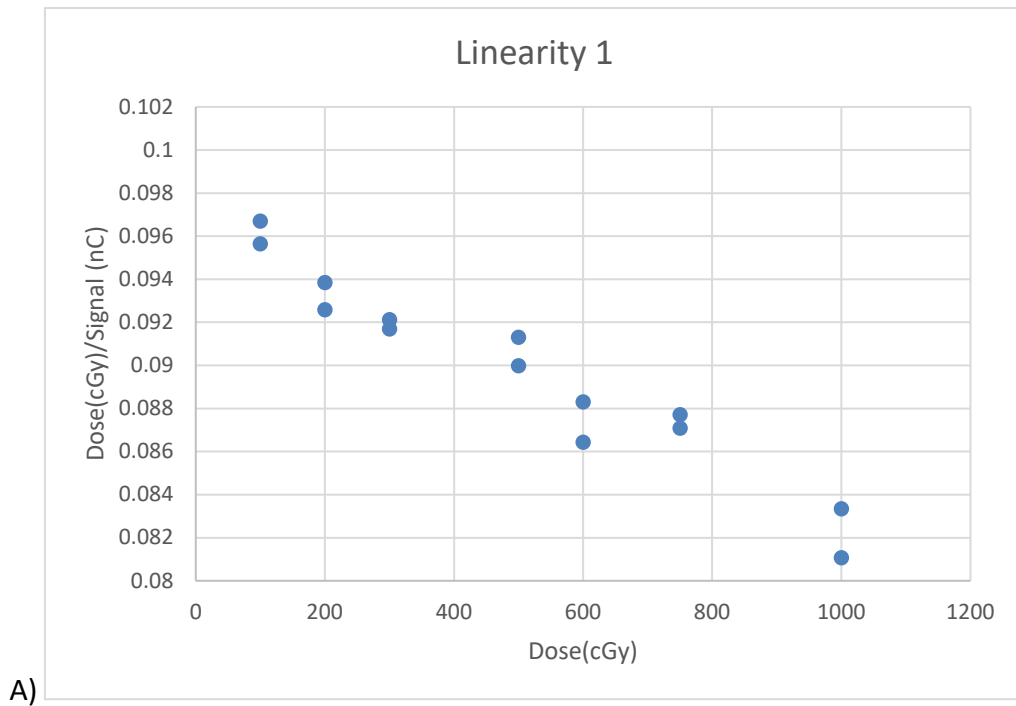


Figure 49: TOP) Linearity dose measurement 1 BOTTOM) Linearity measurement 2

To get actual correction factor K_L , the relationship between dose/signal and dose (Figure 50) was analyzed. These curves represent the linearity curves used by IROC Houston for TLD-100 powder. A linear curve was fit to each of the plots, after they were normalized to 600 cGy (Figure 51). For the first measurement, the slope was -1.60×10^{-4} , the intercept was 1.10, and the R^2 value was 0.935. For the second measurement, the slope was -1.95×10^{-4} , the intercept was 1.12, and the R^2 value was 0.913.



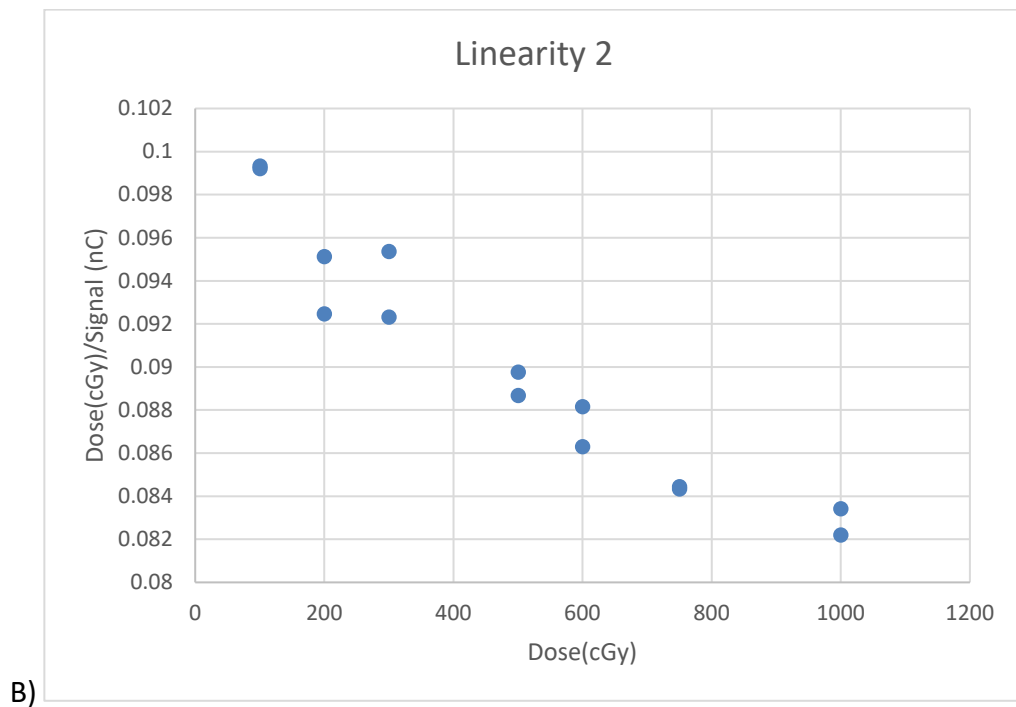
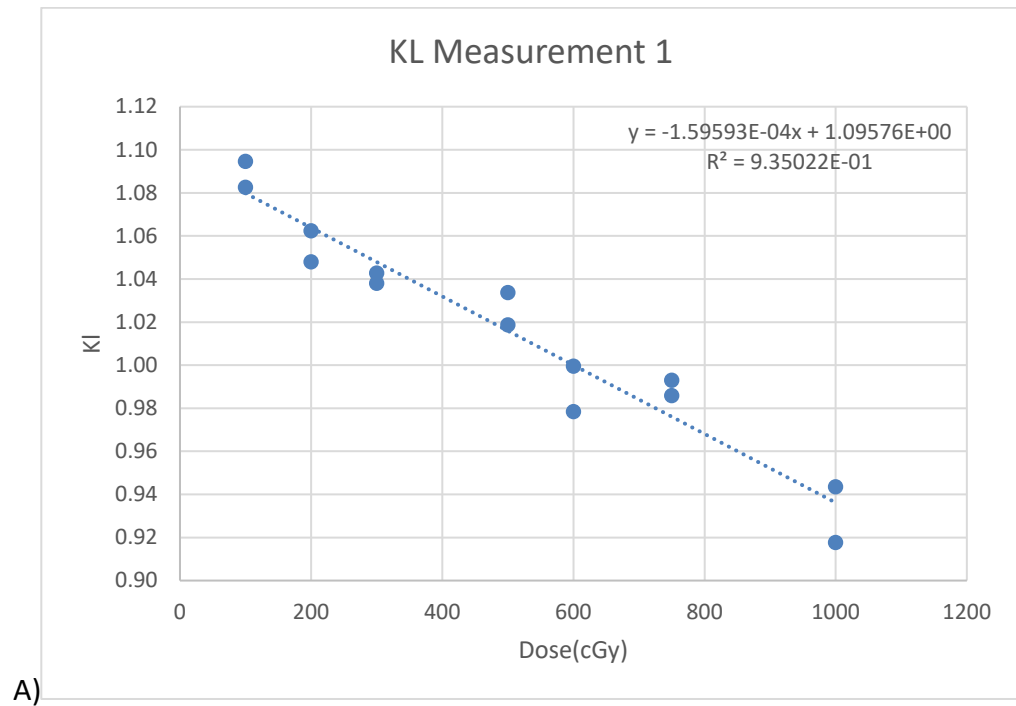


Figure 50: Dose/Signal (K_L) with respect to dose. 45A show the first experiment for linearity, while 45B shows the second experiment.



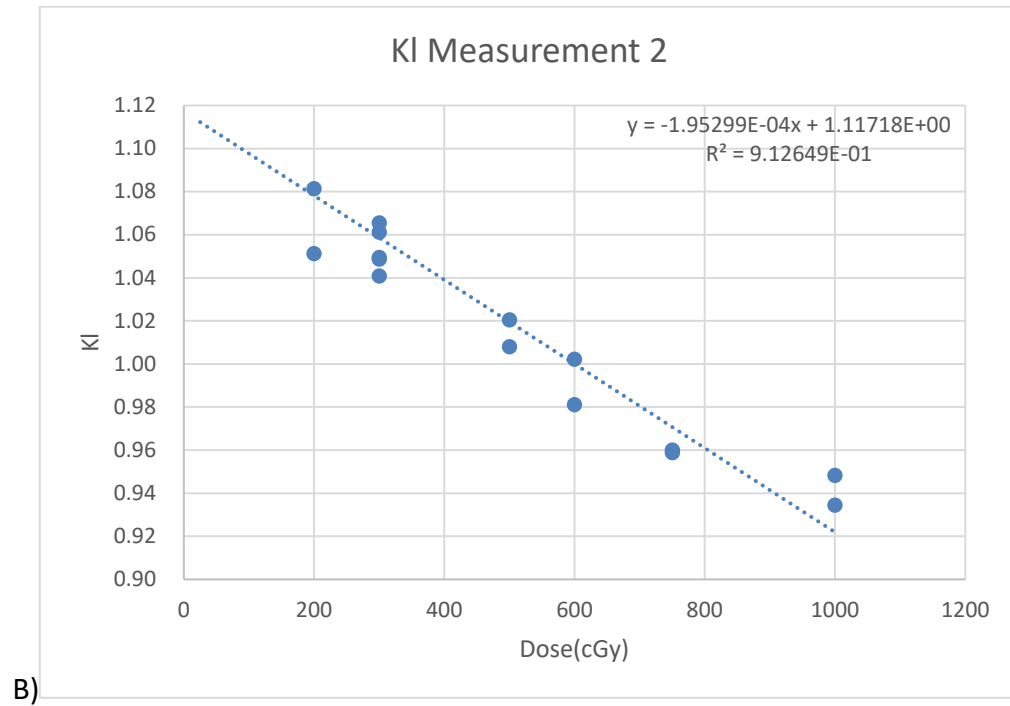


Figure 51: Normalized linearity plots. 46A show the first experiment for linearity, while 46B shows the second experiment.

To get the final K_L correction factor, the average of the slopes and intercepts was used to give the equation below, where X is the signal measured from a TLD in nano-Coulombs. A comparison of the individual slopes is depicted in Figure 52.

$$K_L = -1.774 \cdot 10^{-4}(nC^{-1}) \cdot X(nC) + 1.106$$

Equation 9: Measured Linearity Correction Factor

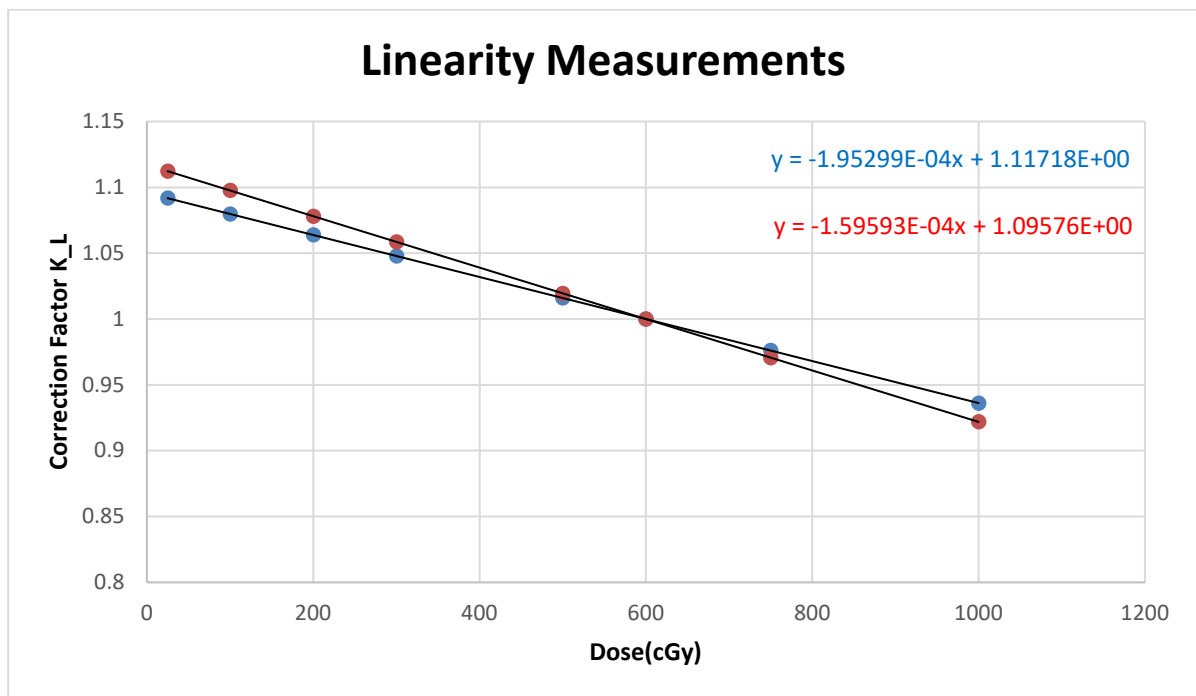


Figure 52: Linearity correction factors comparison from both measurements

3.2.3 Energy Correction Factor K_E

The energy correction factor, K_L , was evaluated using Equation 7. The results of the analysis are in the table below. The energy correction factors for 6 MV photons is about a 4% correction, 1.036.

Table 4: Energy Correction factors for $^{60}\text{Cobalt}$, 6MV, and 18MV photon beams.

Energy	K_E
$^{60}\text{Cobalt}$	1.0
6 MV	1.036

3.3 Uncertainty Analysis

The uncertainty in both standards and samples is estimated by evaluating the standard deviation in a large number of readings, irradiated to the same dose. The standard deviation in the thermoluminescent reading for the samples and the standards were both 0.30%.

The uncertainty in the dose to the standards, taken from Kirby et al. was 0.60%. This uncertainty is largely determined by the ion chamber setup uncertainty, taken to be $\pm 1\text{mm}$ for both source to chamber distance and the depth of the chamber in water.

The uncertainty in the linearity correction factor was estimated determining the standard error of the regression coefficient, which is taken from the regression line from the least-squares fit of the slope of the linearity measurement. Here, the standard error of the regression coefficient is defined in Equation 12 below. This was determined to be $5.82 \times 10^{-6} \%$, as we evaluated the uncertainty in the correction factor for dose within $\pm 3\%$ of the 600 cGy normalization dose.

$$s_L^2 = [s_{b_L}(D - D')a_L / (a_L + b_L D')^2]^2$$

Equation 10

The uncertainty in the energy correction factor stems from a combination in the uncertainty in the calibration of the photon beam as well as the uncertainty in the TLD readings themselves. The uncertainty in the energy correction factor was evaluated using Equation 13 below, and was determined to be $7.73 \times 10^{-3} \%$.

$$s_E^2 = K_E [2(\frac{s_D'}{D'})^2 + (\frac{s_T}{T})^2 / 2]$$

Equation 11

The uncertainty in the elemental correction factor was estimated from the average standard deviation of three ECF measurements from all TLD micro-cubes. This standard deviation was 1.0%.

Using each of the values described in section 2.3, the total uncertainty in the dose to the sample was determined to be 1.5%. This value is comparable to the uncertainty in OSLD and TLD powder used at IROC Houston, which are 1.6% and 1.3% at the one sigma level, respectively (Alvarez et al., 2017). This 1.5% uncertainty in TLD micro-cube dose determination is well suited for the $\pm 5\%$ accuracy tolerance that is desired.

3.4 Single Field Experiment Results

The data obtained from single field irradiation experiments is evaluated on agreement with TLD-100 powder, agreement with the expected beam output, and reproducibility of the measurements.

The expected beam output and the average measured doses at the location of the TLD for each field size are shown in Table 5. For each field size, the measurements differed from the expected dose by less than 4%, with a coefficient of variance of 0.53%, 0.98%, and 0.98% for the 10 x 10 cm², 3 x 3 cm², and 2 x 2 cm² fields, respectively. These results are summarized in Table 5 and Table 6 below.

Table 5: Single field output results

Field Size (cm ²)	Measured Dose (cGy)	Calculated Dose (cGy)	Ratio: Measured/Expected	% Difference
10 x 10 A	624	602	1.04	-3.65%
10 x 10 B	623	602	1.03	-3.39%
10 x 10 C	618	602	1.03	-2.59%
3 x 3 A	564	548	1.03	-2.92%
3 x 3 B	558	548	1.02	-1.81%
3 x 3 C	569	548	1.04	-3.69%
2 x 2 A	552	536	1.03	-3.01%
2 x 2 B	554	536	1.03	-3.40%
2 x 2 C	544	536	1.01	-1.49%

Table 6: Single filed output average dose, coefficient of variation, and average ratio of measured dose: expected dose

	10 x 10 cm ²	3 x 3 cm ²	2 x 2 cm ²
Average Dose (cGy)	622	564	550
Coefficient of Variation	0.53%	0.92%	0.98%
Average Difference from Expected Dose	-3.21%	-2.81%	-2.63%

To compare the results of the TLD micro-cubes to the results measured from the TLD powder is a final confirmation of the performance of micro-cube in the single field output experiment. The doses measured for each field size are shown in Table 7. These results agreed with what the TLD micro-cube measurements by 0.69% on average (Table 7).

Table 7: TLD micro-cube and TLD powder agreement

Field Size (cm ²)	TLD MicroCube (cGy)	TLD Powder (cGy)	% Difference
10 x 10	622	620	-0.28%
3 x 3	564	563	-0.10%
2 x 2	550	541	-1.70%

3.4.1 Single Field Film

Film analysis for the 3 x 3 cm² and 2 x 2 cm² fields showed that the fields were aligned well with respect to the single field phantom and the TLD micro-cubes. Below are the field line profiles for each of the field sizes. All field profiles showed similar results.

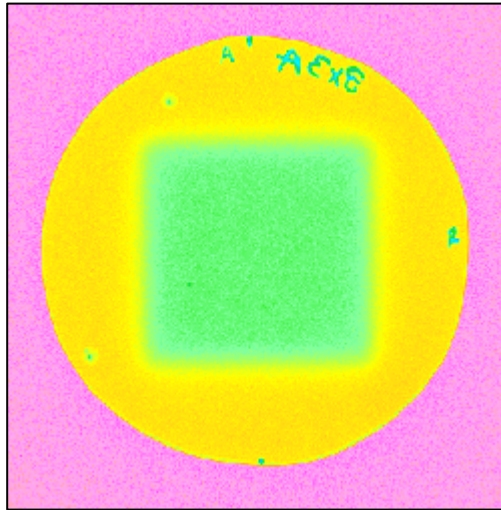


Figure 53: 3 x 3 cm² field film

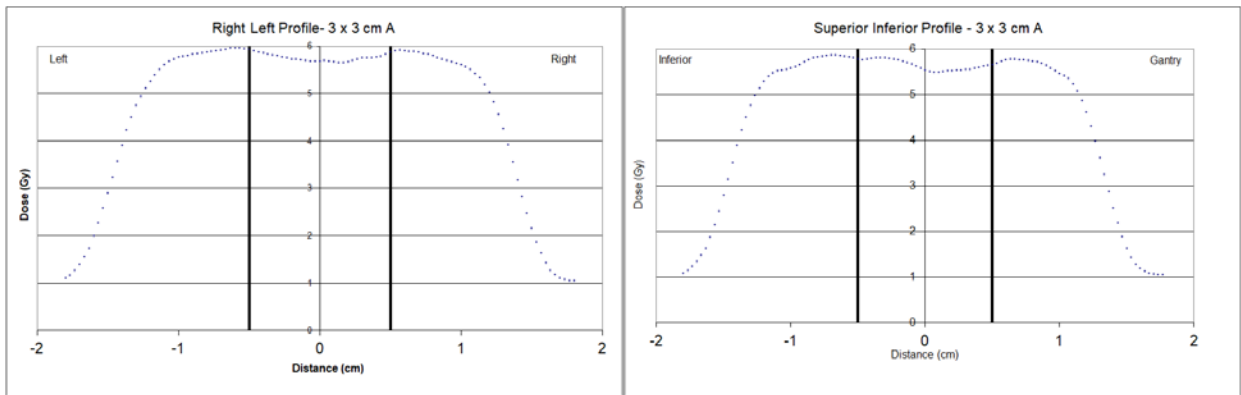


Figure 54: 3 x 3 cm² field line profiles, solid black lines indicate tumor boundaries

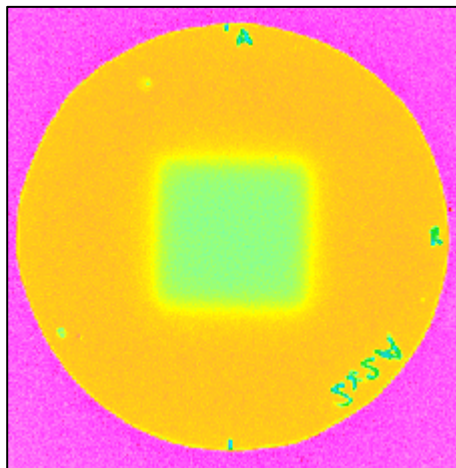


Figure 55: 2 x 2 cm² field film

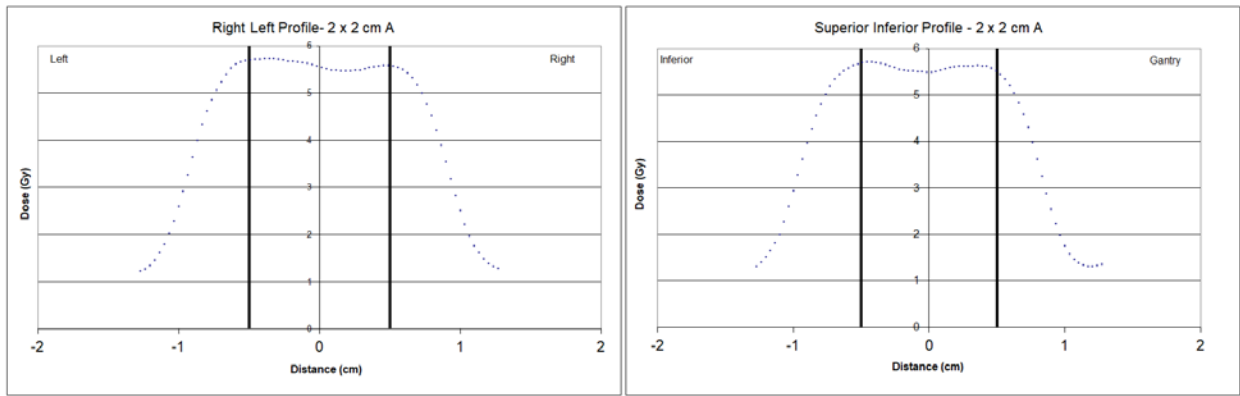


Figure 56: 2 x 2 cm² field line profiles, solid black lines indicate tumor boundaries

3.5 SRS Head Experiment Results

3.5.1 SRS Head Linac Experiment Results

The data for the TrueBeam SRS head phantom experiments was analyzed in multiple ways. The first was the agreement between the dose measured with the TLD micro-cubes, and the dose calculated by the TPS. Second was the agreement between what was measured with the TLD micro-cubes and what was measured with the standard TLD powder. Third was the reproducibility of the measurements, as the experiment was repeated for a total of three measurements.

The experiments were identified as A, B, and C, and were further divided into the superior TLD capsule and the inferior TLD capsule. The expected mean dose to the superior capsule, as calculated by the TPS was 608 cGy. The average dose measured was 612 cGy, and all measurements agreed with the expected dose within 1%. For the inferior capsule, the average dose to the capsule, as calculated by the TPS was 606 cGy, and the average dose measured by the TLD in the inferior capsule was 605 cGy. All measurements for the inferior capsule were also within 1% of the expected dose.

Table 8: Linac SRS head phantom dose measurement compared to TPS doses. Letter A, B, and C refer to the experiment trial.

Experiment	Measured Dose (cGy)	Calculated Dose (cGy)	Ratio: Measured/Expected
Linac A Superior	609	608	1.00
Linac B Superior	612	608	1.01
Linac C Superior	616	608	1.01
Linac A Inferior	606	606	1.00
Linac B Inferior	609	606	1.01
Linac C Inferior	600	606	0.99

With regards to the reproducibility of these measurements, the average dose to the superior capsule was 612 cGy, with a coefficient of variance of 0.59%. Second, the average dose to the inferior capsule as measured by the TLD micro-cubes was 605 cGy, where the coefficient of variance was 0.76%.

Table 9: Linac micro-cube reproducibility

	Superior Capsule	Inferior Capsule
Average Dose (cGy)	612	605
Coefficient of Variation (%)	0.59%	0.76%
Average Difference in Expected Dose (%)	-0.79%	0.15%

Table 10: TLD micro-cube and TLD powder comparison for SRS linac experiments

Capsule	TLD Micro-Cube (cGy)	TLD Powder (cGy)	% Difference
Superior	612	594	-3.10%
Inferior	605	593	-1.99%

3.5.1.1 SRS Linac Film Analysis

After registering the three pin pricks in each film plane, the software calculated a root mean square (RMS) error between the expected and actual distance between the registered points (Figure 57). The MatLab software checks the dose value on a pixel to pixel basis with a gamma pass/fail criteria of 5% dose difference, and 3mm distance to agreement (DTA). An RMS error less than 1mm was considered acceptable for use in analysis, which each of the film registrations met. Once location registration was completed, and the film dose was normalized to TLD dose, line dose profiles were taken from the film and compared to the TPS calculations (Figure 58).

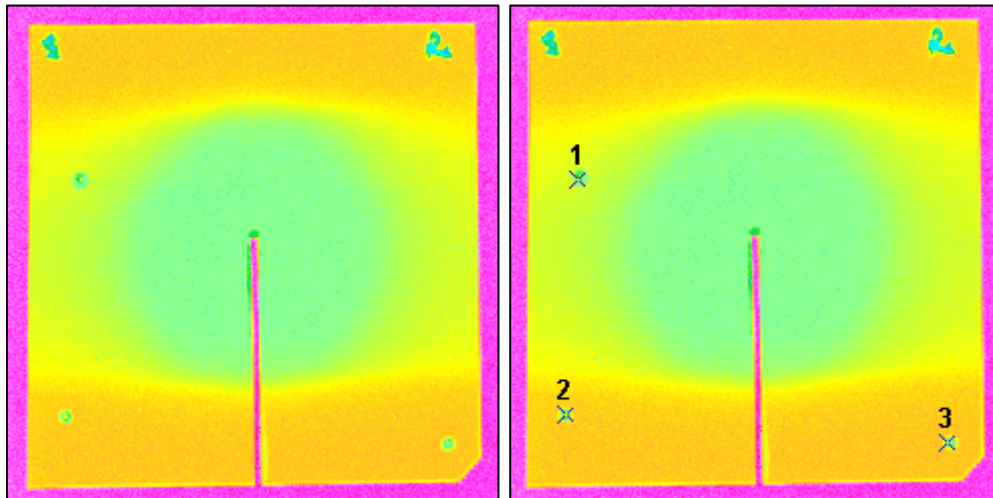


Figure 57: SRS linac film registration

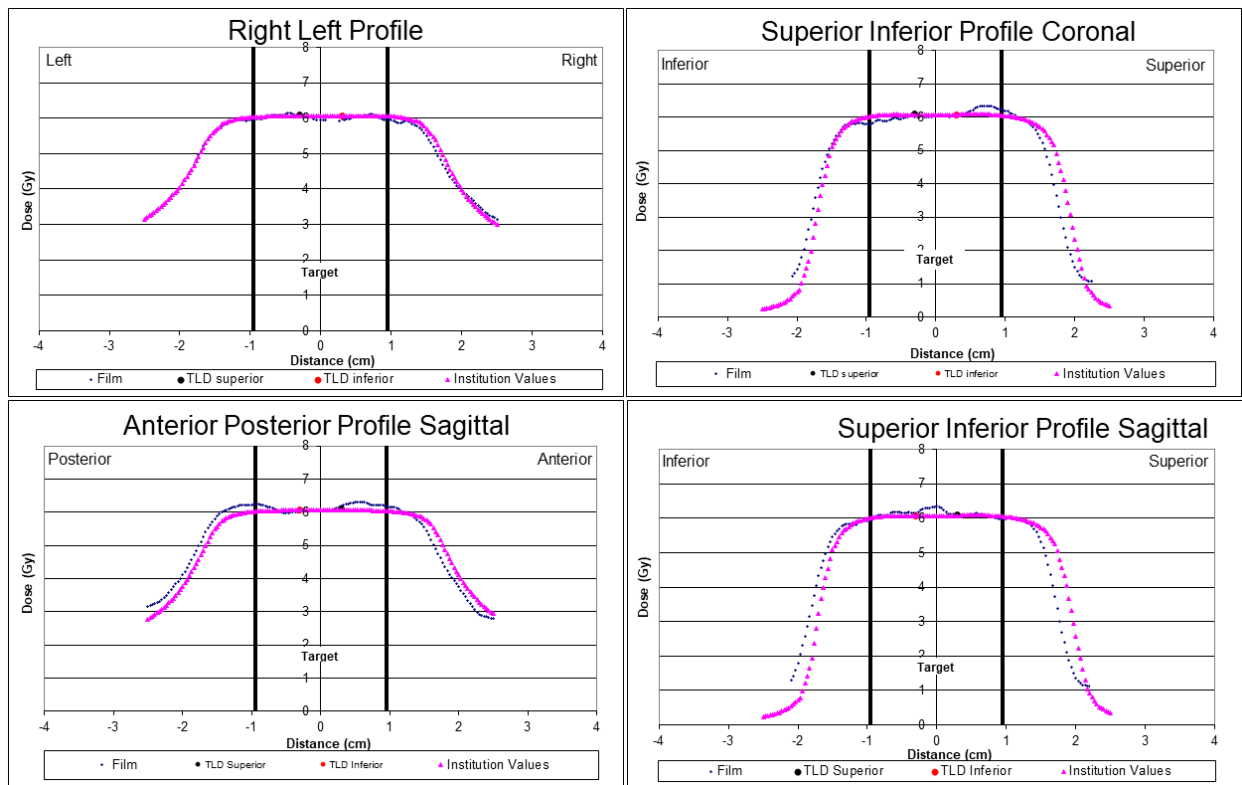


Figure 58: Film dose line profiles for Linac. See appendix for all profiles.

The film was analyzed for agreement between treatment planning system calculated dose profiles and measured dose profiles. The percent agreement was defined by the gamma (γ) evaluation (Figure 59). The MatLab software checks the dose value on a pixel to pixel basis with a gamma pass/fail criteria of 5% dose difference, and 3 mm distance to agreement (DTA). Films from sagittal and coronal planes for each of the three experiments were registered. From this data, a mean agreement of 83.6% with a coefficient of variance of 5.4% was obtained (see Figure 59 for an example, see Appendix for all gamma evaluations).

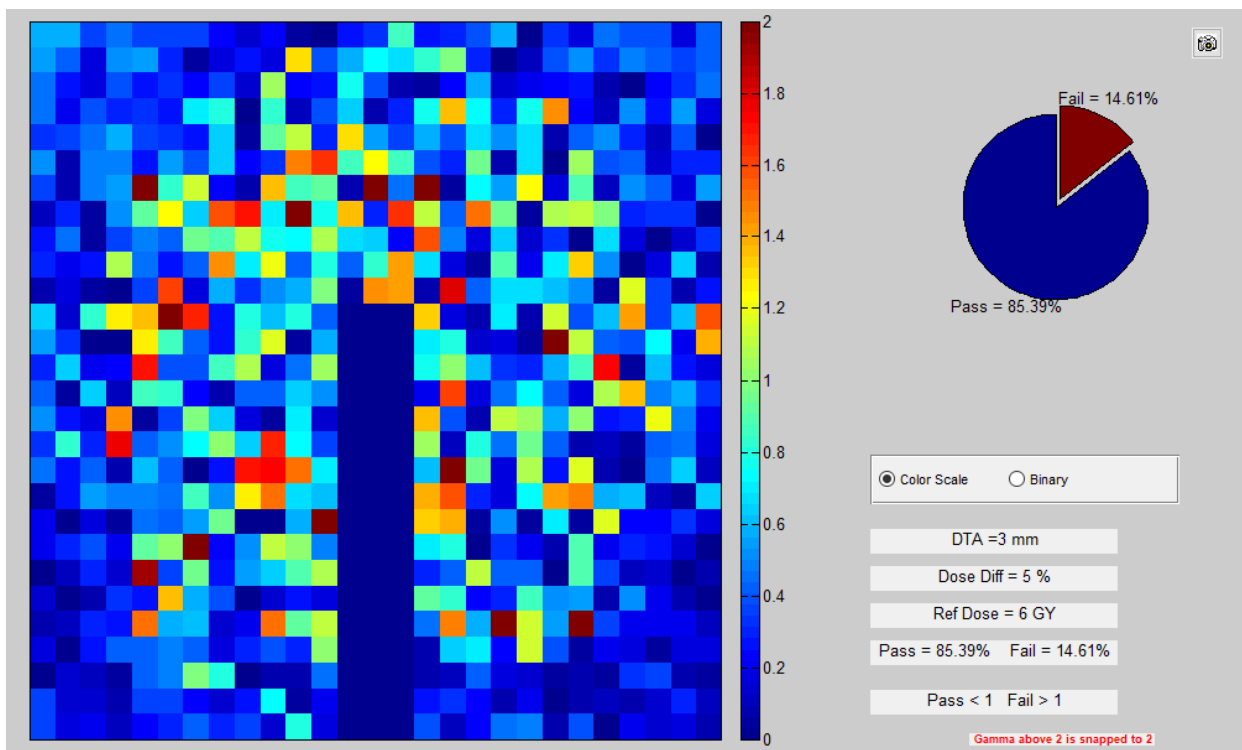


Figure 59: Gamma analysis for linac coronal plane

3.5.2 SRS Head Gamma Knife Experiment Results

The data for the Gamma Knife SRS head phantom experiments were analyzed following the same procedure as the linac data analysis. The average TPS dose to the active volume of the TLD capsules was 632 cGy and 628 cGy, for the superior and inferior capsules, respectively. The maximum dose to the active volume was 659 cGy and 665 cGy for the superior and inferior capsules, respectively.

The measured dose was taken to be the average of the three micro-cubes contained in the active volume of each capsule. For the superior capsule for experiment A, B, and C, the average dose to the volume was 618 cGy, 624 cGy, and 610 cGy, respectively. The average difference between calculated and measured dose to the TLD was 2.39%, where the maximum difference was 3.55% and the minimum difference was 1.35%. The average dose to the superior

capsule was measured to be 617 cGy, with a standard deviation of 6.7 cGy (1.08% coefficient of variance), for all three measurements.

For the inferior capsule for experiment A, B, and C, the average dose to the volume was 639 cGy, 636 cGy, and 626 cGy respectively. The average difference between calculated and measured dose to the TLD was 1.14%, where the maximum difference was 1.78% and the minimum difference was 0.40%. The average dose to the inferior capsule was measured to be 634 cGy, with a standard deviation of 7.2 cGy (1.14% coefficient of variance), for all three measurements.

Table 11: Summary of Gamma Knife experiment dose calculations. Letter A, B, and C refer to the experiment trial.

Experiment	Measured Dose (cGy)	Calculated Dose (cGy)	Ratio: Measured/Expected
A Superior	618	632	0.98
B Superior	624	632	0.99
C Superior	610	632	0.97
A Inferior	639	628	1.02
B Inferior	636	628	1.01
C Inferior	626	628	1.00

Table 12: Gamma Knife micro-cube reproducibility

	Superior Capsule	Inferior Capsule
Average Dose (cGy)	617	634
Coefficient of Variation (%)	1.08%	1.14%
Average Difference in Expected Dose (%)	2.33%	-0.89%

Table 13: TLD micro-cube versus TLD powder for Gamma Knife SRS head experiments

Capsule	TLD Micro-Cube (cGy)	TLD Powder (cGy)	% Difference
Superior	617	619	0.28%
Inferior	634	649	2.37%

To dive deeper into the analysis of these micro-cubes, the measured dose of the individual capsules (periphery of tumor volume, middle cube, and center of tumor volume) was reviewed. The dose of Gamma Knife treatments were inhomogeneous within the treatment volume, and there were hotspots over the active volume of the TLD micro-cube capsule (Figure 60 and Figure 61). In Figure 60, there is a visible hotspot of 650 cGy towards the periphery of the simulated tumor volume, local to the active volume of the TLD capsule. This 650 cGy hotspot encompasses the location of the outermost micro-cube. Likewise, there is a similar hotspot in the region of the inferior capsule. Figure 61 shows this 650 cGy hotspot also near the periphery of the tumor volume, in the vicinity of the active volume of the TLD capsule. This region high dose encompasses the most inferior micro-cube.

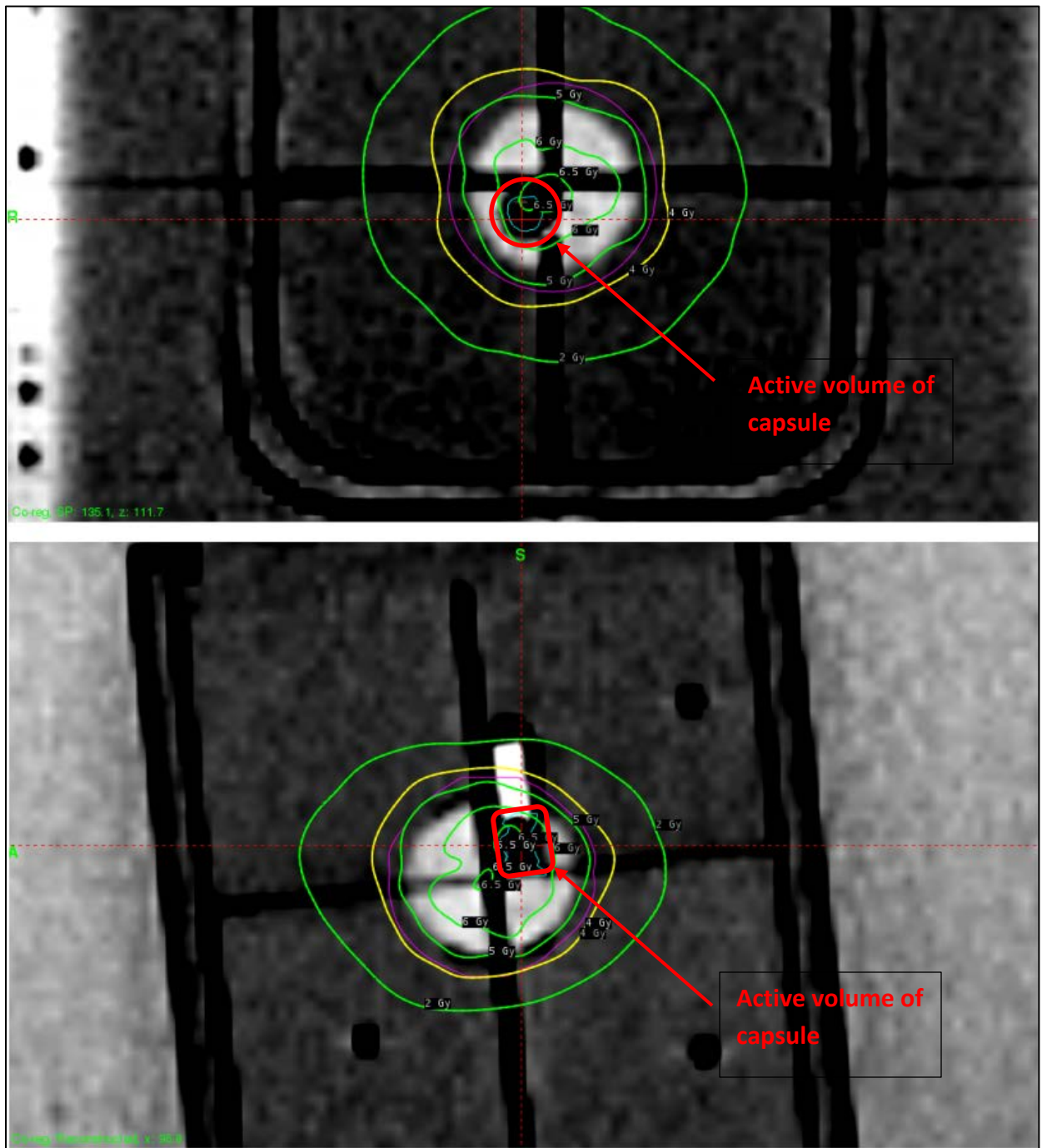


Figure 60: Superior Capsule

TOP: Axial view

BOTTOM: Sagittal View

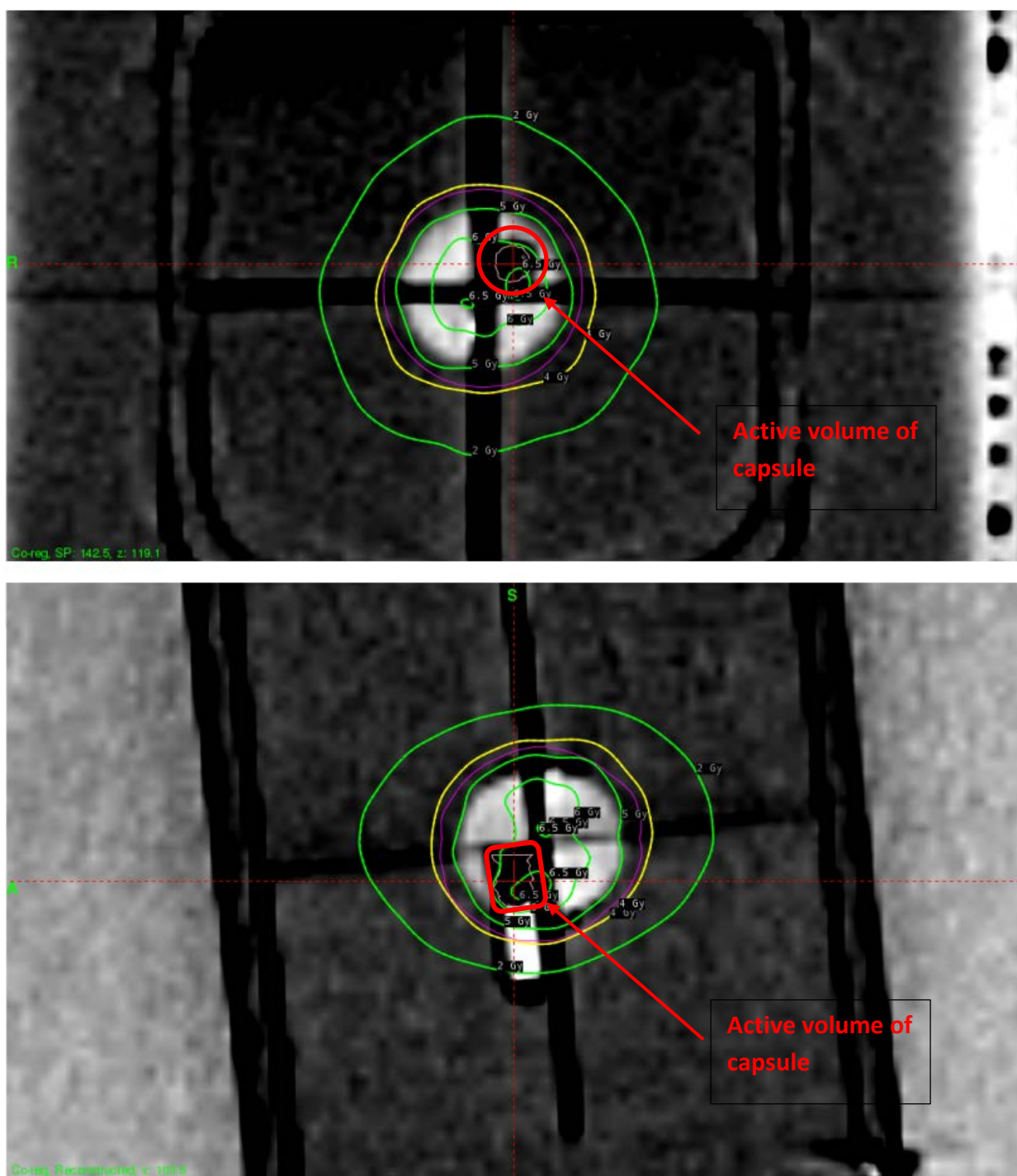


Figure 61: Inferior Capsule

TOP: Axial View

BOTTOM: Sagittal View

For the superior and inferior TLD capsules, the micro cubes are designated as “periphery of tumor”, “middle cube” and “center of tumor”. For the superior capsule, the average measured dose to the periphery, middle, and center micro-cubes was 627 cGy, 619 cGy, and 606 cGy, respectively, where the coefficient of variance was 0.65%, 1.49%, and 1.27% for the three measurements. The calculated dose to the superior periphery, middle, and center micro-cubes was 650, 630, and 620 cGy respectively. For the inferior capsule, the average measured dose to the periphery, middle, and center micro-cubes was 649 cGy, 640 cGy, and 611 cGy, respectively, where the coefficient of variance was 1.18%, 2.21%, and 1.83% for the three measurements. The calculated dose to the inferior periphery, middle, and center micro-cubes was 660, 640, and 620 cGy, respectively. The data regarding these measurements is shown in Table 14 below.

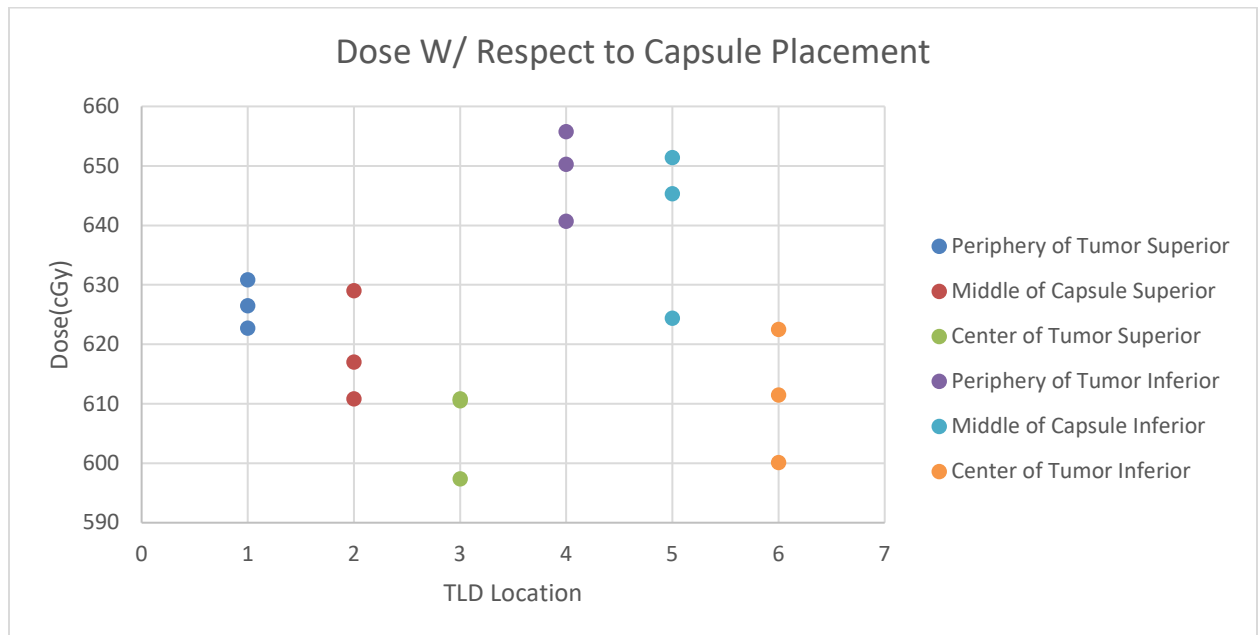


Table 14: TLD micro-cube differences in Gamma Knife experiment

Superior Capsule	Inferior Capsule
Average Dose to Superior Periphery (cGy)	Average Dose to Inferior Periphery (cGy)
627	649
Superior Periphery Coefficient of Variance (%)	Superior Periphery Coefficient of Variance (%)
0.65%	1.18%
Average Ratio in Expected Dose	Average Ratio in Expected Dose
0.96	0.98
Average Dose to Superior Middle (cGy)	Average Dose to Inferior Middle (cGy)
619	640
Superior Middle Coefficient of Variance (%)	Inferior Middle Coefficient of Variance (%)
1.49%	2.21%
Average Ratio in Expected Dose	Average Ratio in Expected Dose
0.98	1.00
Average Dose to Superior Center (cGy)	Average Dose to Inferior Center (cGy)
620	611
Superior Center Coefficient of Variance (%)	Inferior Center Coefficient of Variance (%)
1.24%	1.83%
Average Ratio in Expected Dose	Average Ratio in Expected Dose
0.98	0.99

3.5.2.1 Gamma Knife Film Analysis

After registering the three pin pricks in each film plane, an RMS error less than 1mm was considered acceptable, and each film registration achieved this requirement. Once location registration was completed, and the film dose was normalized to TLD dose, line dose profiles were taken from the film and compared to the TPS calculations (Figure 64).

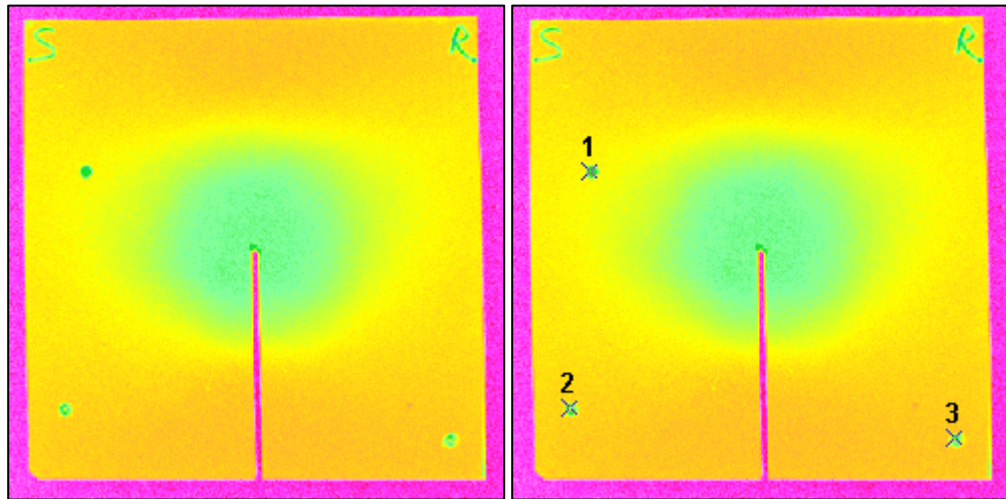


Figure 62: Film registration using 3 pin breaks for localization in the coronal plane

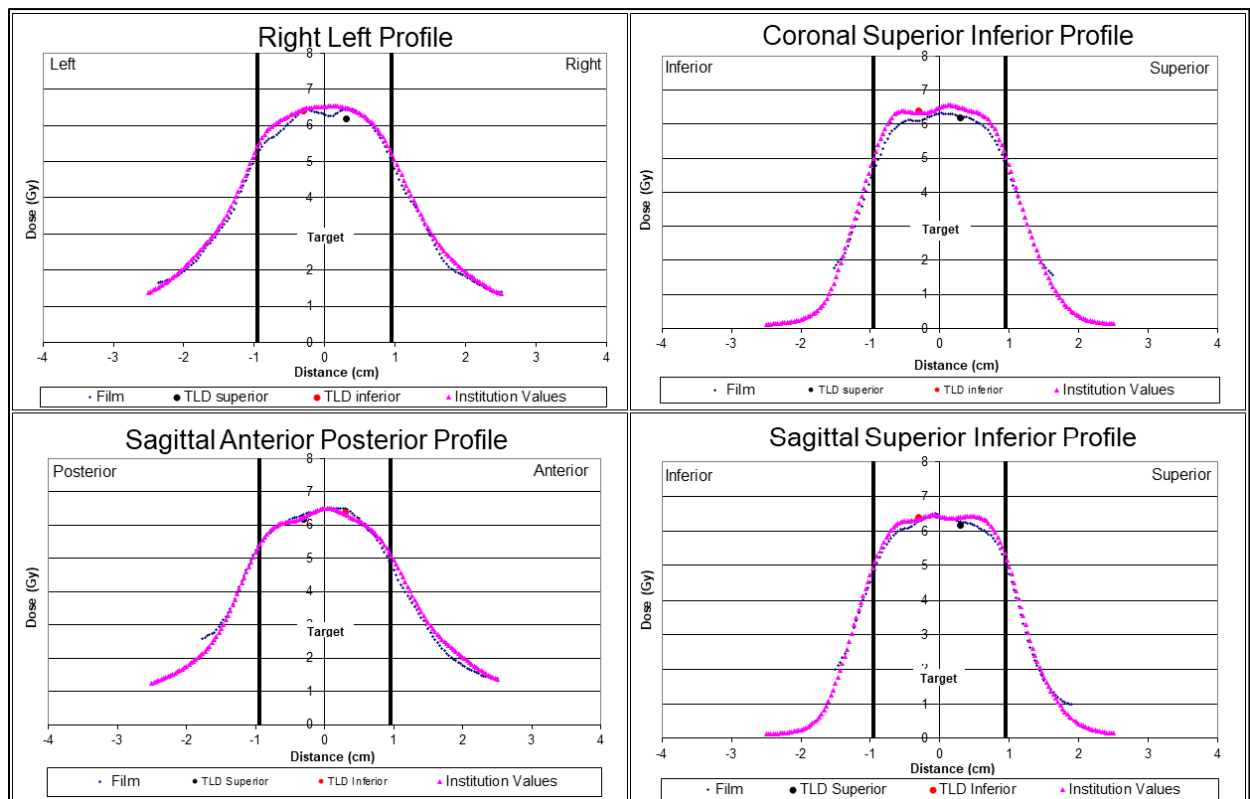


Figure 63: Film dose line profiles for Gamma Knife. See appendix for all profiles.

The film was analyzed for agreement between treatment planning system calculated dose profiles and measured dose profiles. The percent agreement was defined by the gamma (γ) evaluation (Figure 65). Films from sagittal and coronal planes for each of the three experiments were registered. From this data, a mean agreement of 98.94% with a coefficient of

variance of 0.35% was obtained (see Figure 65 for an example, see Appendix for all gamma evaluations).

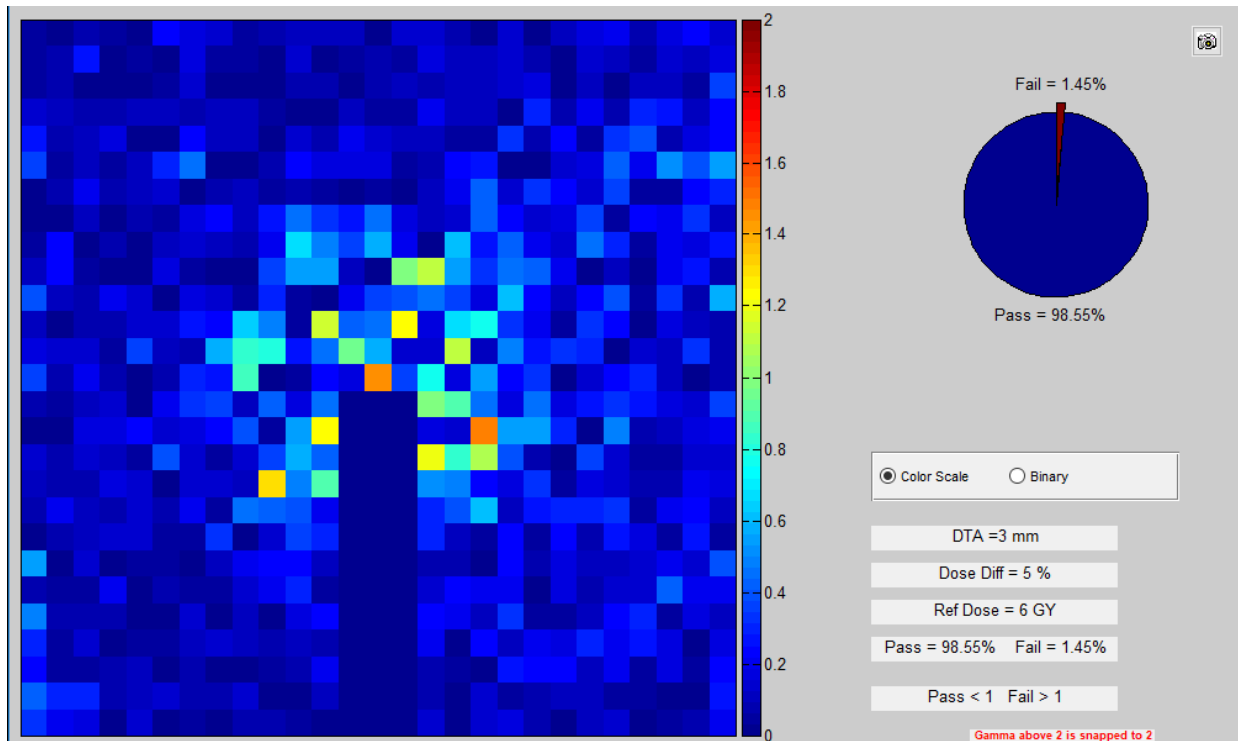


Figure 64: Film and TPS dose agreement

3.5.3 SRS Head CyberKnife Experiment Results

The data collected from the SRS CyberKnife experiments was evaluated on the same bases as the linac and Gamma Knife experiments. Agreement between TPS and micro-cube, TLD powder and micro-cube, and reproducibility were all considered. The expected dose as calculated by the TPS was 708 cGy to the superior TLD capsule, and 689 cGy to the inferior. The average measured dose to the superior capsule was 705 cGy, where the maximum difference in calculated to measured dose was 0.80% and the minimum was 0.13%. The average measured dose to the inferior capsule was 684 cGy, where the maximum difference in measured and calculated dose was 1.92% and the minimum difference was 0.05%. The difference between the

average measured dose and the calculated dose was 0.43% and 0.70% for the superior and inferior TLD capsules respectively. These results are contained in Table 15 and Table 16 below.

Table 15: CyberKnife measured dose evaluation

CyberKnife Experiment	Measured Dose (cGy)	Calculated Dose (cGy)	Ratio: Measured/Expected
A Superior	709	708	1.00
B Superior	704	708	0.99
C Superior	703	708	0.99
A Inferior	675	689	0.98
B Inferior	687	689	1.00
C Inferior	689	689	1.00

Table 16: CyberKnife experiment reproducibility

	Superior Capsule	Inferior Capsule
Average Dose (cGy)	705	684
Coefficient of Variation (%)	0.49%	1.07%
Average Difference in Expected Dose (%)	0.43%	0.70%

Table 17: Comparison of micro-cube and TLD powder

Capsule	TLD Micro-Cube (cGy)	TLD Powder (cGy)	% Difference
Superior	705	699	-0.90%
Inferior	684	637	-7.32%

3.5.3.1 CyberKnife film Analysis

Similar to the first two SRS experiments described, after registering the three pin pricks in each film plane, an RMS error less than 1mm was considered acceptable, and each film registration achieved this requirement. Once location registration was completed, and the film dose was normalized to TLD dose, line dose profiles were taken from the film and compared to the TPS calculations (Figure 67).

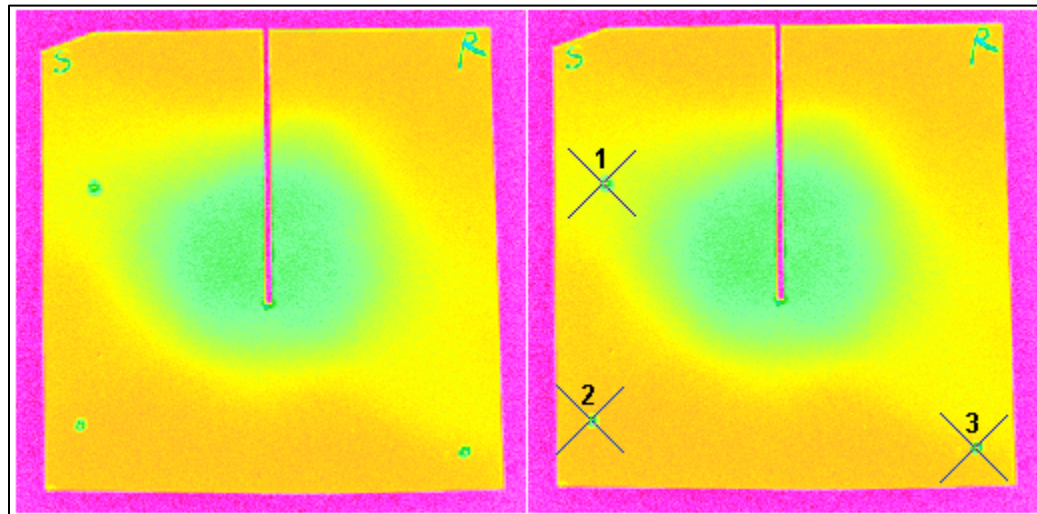


Figure 65: CyberKnife film registration in the sagittal plane

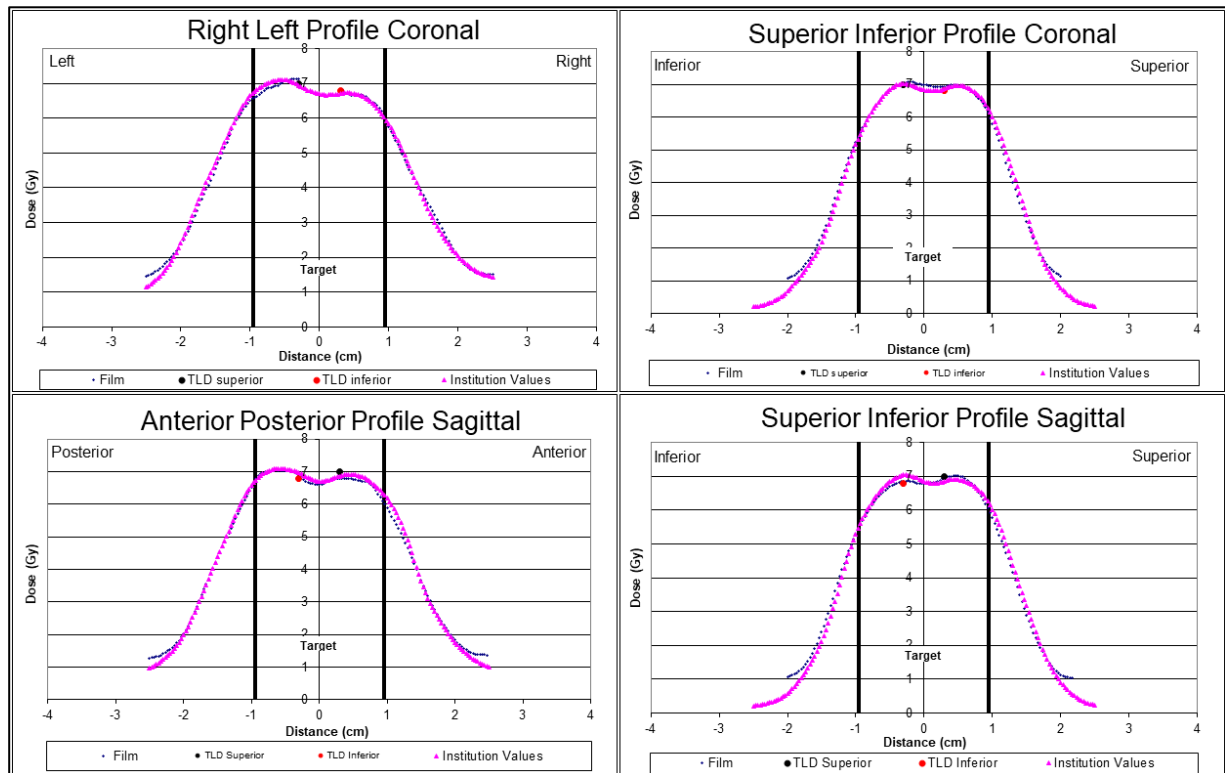


Figure 66: CyberKnife film line profiles

The film was analyzed for agreement between treatment planning system calculated dose profiles and measured dose profiles. The percent agreement was defined by the gamma (γ) evaluation (Figure 65). The MatLab software checks the dose value on a pixel to pixel basis

with a gamma pass/fail criteria of 5% dose difference, and 3mm distance to agreement (DTA). Films from sagittal and coronal planes for each of the three experiments were registered. From this data, a mean agreement of 96.37% with a coefficient of variance of 0.78% was obtained (Figure 68).

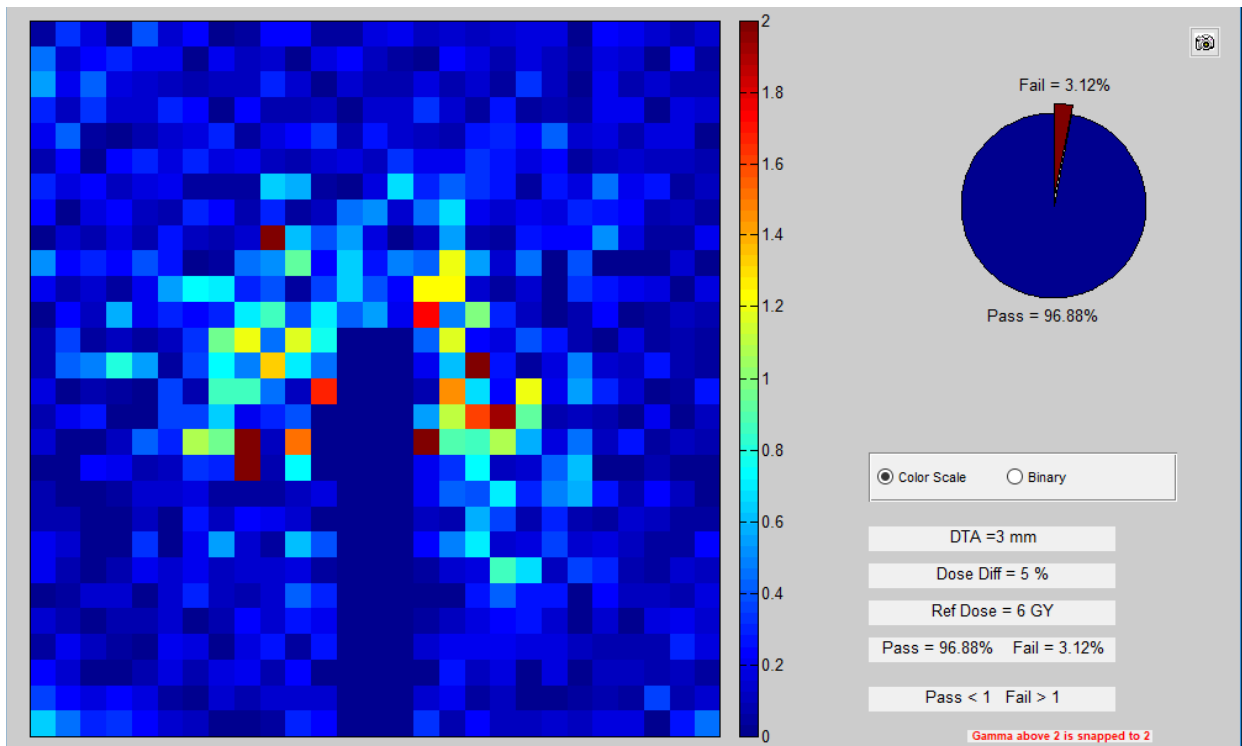


Figure 67: Gamma analysis for CyberKnife SRS experiments

3.6 Single Small Field Output Results

The average dose in cGy measured by the micro-cubes for the 60, 20, 15, 10, 7.5, and 5 mm fields was 594, 575, 559, 529, 498, and 411 respectively. The calculated dose for these fields were 600, 589, 572, 540, 514, and 428 cGy for the respective fields.

For the 60 mm field, the average ratio of measured dose to calculated dose is 0.99. The maximum and minimum difference in measured and calculated dose is 1.22% and 0.17%, where the coefficient of variance of the measurements is 0.67%. For the 20 mm field, the average ratio

of measured dose to calculated dose is 0.98. The maximum and minimum difference in measured and calculated dose is 2.95% and 1.90%, where the coefficient of variance of the measurements is 0.61%. For the 15 mm field, the average ratio of measured dose to calculated dose is 0.98. The maximum and minimum difference in measured and calculated dose is 2.49% and 1.91%, where the coefficient of variance of the measurements is 0.32%.

For the 10 mm field, the average ratio of measured dose to calculated dose is 0.98. The maximum and minimum difference in measured and calculated dose is 2.24% and 1.58%, where the coefficient of variance for the measurements is 0.37%. For the 7.5 mm field, the average ratio of measured dose to calculated dose is 0.97. The maximum and minimum difference in measured and calculated dose is 13.69% and 2.66%, where the coefficient of variance for the measurements is 0.56%. Finally, for the 5 mm field, the average ratio of measured dose to calculated dose is 0.97. The maximum and minimum difference in measured and calculated dose is 3.63% and 3.25%, where the coefficient of variance for the measurements is 0.21%.

These results are contained in the tables below:

Table 18: Single small field irradiation results

Field size	Measured Dose (cGy)	Calculated Dose (cGy)	Ratio Measured/Expected
60 mm A	593	600	0.99
60 mm B	592	600	0.99
60 mm C	592	600	1.00
20 mm A	577	589	0.98
20 mm B	571	589	0.97
20 mm C	577	589	0.98
15 mm A	558	572	0.98
15 mm B	558	572	0.98
15 mm C	561	572	0.98
10 mm A	528	540	0.98
10 mm B	528	540	0.98
10 mm C	532	540	0.98
7.5 mm A	495	514	0.96
7.5 mm B	499	514	0.97
7.5 mm C	500	514	0.97
5 mm A	414	428	0.97
5 mm B	413	428	0.96
5 mm C	412	428	0.96

Table 19: Single small field irradiation results

Field Size	60 mm	20 mm	15 mm	10 mm	7.5 mm	5 mm
Average Dose(cGy)	594	575	560	529	498	413
Coefficient of Variance (%)	0.67%	0.61%	0.32%	0.37%	0.56%	0.21%
Average Difference from Expected Dose	0.93%	2.26%	2.27%	2.00%	3.07%	3.49%

3.6.1 Small Field Film

Similar to the single field film data, there did appear to be a 1 mm shift inferiorly (away from the gantry) in the line profiles, which could have an effect on measured output of the fields

smaller than 15 mm. Figure 69 below depicts the film for field sizes 20 mm and smaller. Figure 70 shows the line profile for the 5 mm cone for Cyberknife small field irradiations. Figures for other field sizes are located in the appendix.

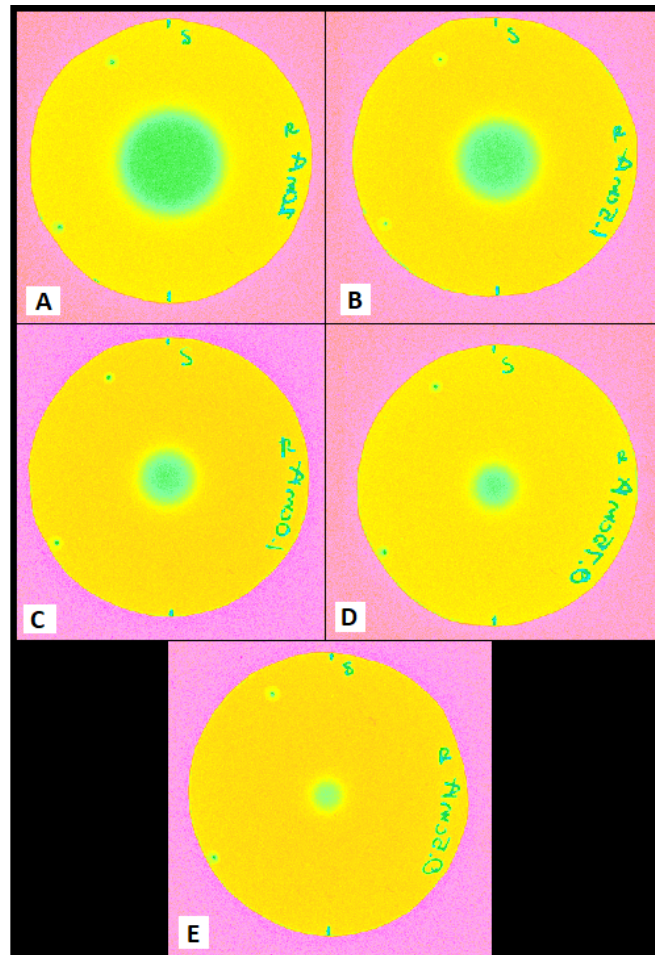


Figure 68: A) 20 mm B) 15 mm C) 10 mm D) 7.5 mm E) 5 mm

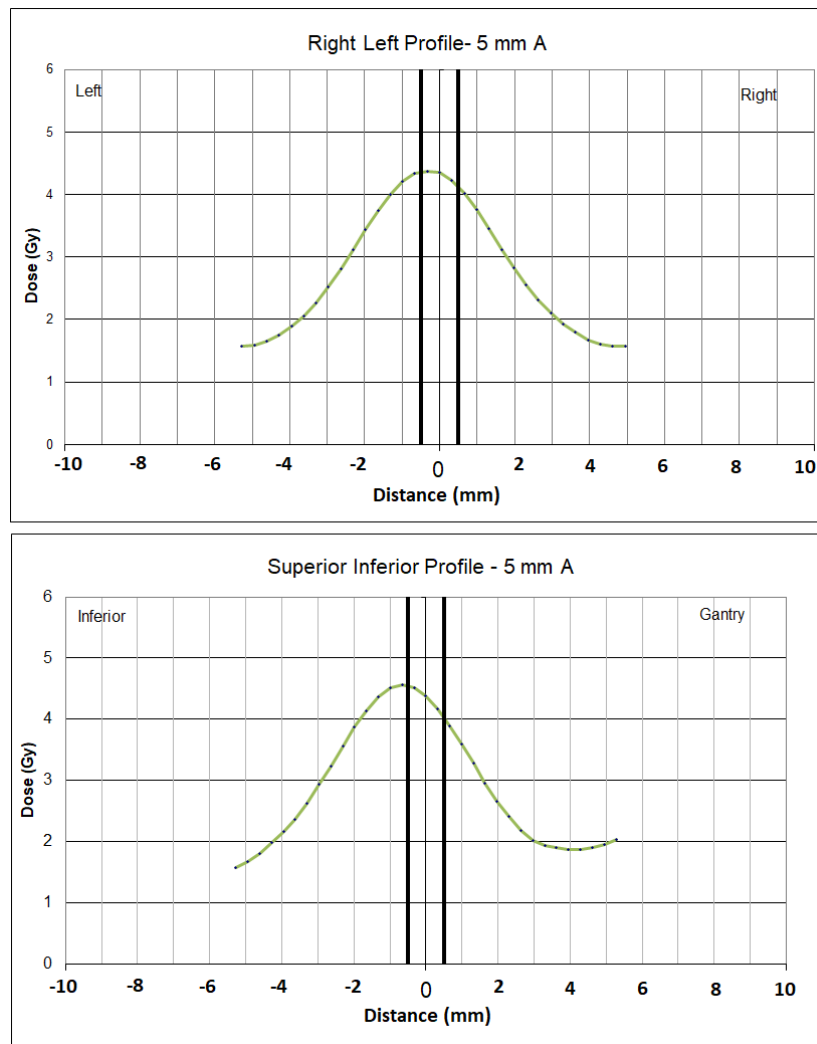


Figure 69: 5 mm field line profile, the thick vertical lines represent the boundaries of the micro cubes

3.7 Statistical Analysis

For each of the four populations, ((1) single field, n=9 (2), SRS experiments, n=18, (3) TLD micro-cube vs. TLD powder, n=8, and (4) small field, n=18), a TOST test of equivalence on the ratio of measured to expected dose was performed to assess statistical confidence that the ratios were within the equivalence bounds. A p-value of 6.72E-5, 7.34E-12, 6.3E-5, and 4.54E-10 was obtained for the respective populations, all showing statistical significance of the consistency of the measurements with expected values.

4 Discussion

4.1 Characterization

The values obtained for energy correction and linearity are similar to those which IROC Houston obtained for TLD-100 powder, although it is difficult to compare the correction factors for micro-cubes with powder. Not only are they different forms of TLD, but characterization of TLD is done on a batch-to-batch basis, so correction factors are expected to be somewhat different.

4.2 TLD Handling and Reading

The manner in which micro-cubes are handled and used is directly correlated with the performance they are able to achieve. Factors such as maintaining identity of each cube, annealing protocol, and careful reading placement of micro-cubes have a direct effect on measurements. Additionally, careful handling of the micro-cubes themselves is quite important. In the experience gained from this work, using tweezers and jeweler's glasses to handle the micro-cubes is necessary for manipulating micro-cubes with the dexterity needed for placing them in the reading planchet, as well as the frequent transfers from annealing trays to SRS and single field capsules. While tweezers are necessary to use, they add a risk of scratching the surface of the cubic faces, or chipping them from force used. If it is possible to file or coat the tips of the tweezers, that is recommended. Additionally, consistency in the reading technique of trained readers is a factor to be considered, as TLD placement is vital in obtaining reliable results.

There are multiple factors that must be considered in executing a successful micro-cube process. Implementing micro-cubes into a quality assurance program requires that these factors be carefully defined and adhered to in order to obtain satisfactory results.

4.3 Irradiation Experiments

4.3.1 Single Field Irradiations

When analyzing the accuracy of the single field experiments, all measurements for all three field sizes were within 4.1% of the documented beam output. The reproducibility showed a coefficient of variance of 0.81% was achieved. These data points are within the bounds for $\pm 5\%$ accuracy and $\pm 3\%$ reproducibility.

What these results suggest is that the measurements were systematically higher than expected. For the 10 x 10 cm² field, the average ratio of measured dose over calculated dose was 1.04 ± 0.01 . For the 3 x 3 cm² field, the average ratio of measured dose over calculated dose was 1.03 ± 0.01 . Lastly, for the 2 x 2 cm² field, the average ratio of measured dose over calculated dose was 1.03 ± 0.01 . These measurements show very good reproducibility, but the dose is further from the beam output dose than is expected, and repeatedly so. These output measurements were confirmed by the TLD-100 powder measurements, which are well trusted. In this experiment the difference in TLD micro-cube and TLD powder for 10 x 10, 3 x 3, and 2 x 2 cm² fields were 0.28%, 0.10%, and 1.70%, respectively. These results lead us to believe that the beam output for this linac was possibly 3 to 4% higher than documented, and that the measured results were valid. A review of the last annual machine output check by IROC Houston also showed a measurement that was several percent high, so these results follow the machine history.

4.3.2 SRS Linac, Gamma Knife, CyberKnife Experiments

For the SRS Linac experiments, all three measurements for the superior capsule and inferior capsules were within 1.4% of the TPS calculated dose. These measurements were

performed on a different linac than the one use for the single field output checks. In this experiment, the coefficient of variance of the superior and inferior capsule measurements was 0.59% and 0.76%, respectively. These results were well within the $\pm 5\%$ accuracy and $\pm 3\%$ reproducibility aims. Additionally, the agreement between the TLD micro-cube and TLD powder for this experiment was 3.1% and 2.0% for the superior and inferior capsules, respectively.

For the SRS Gamma Knife experiments, all three measurements for the superior capsule and inferior capsules were within 3.43% of the TPS calculated dose. In this experiment, the coefficient of variance for the superior and inferior capsule measurements was 1.08% and 1.14%, respectively. These results were within our aims of $\pm 5\%$ accuracy and $\pm 3\%$ reproducibility. Additionally, the agreement between the TLD micro-cube and TLD powder for this experiment was 0.28% and 2.4% for the superior and inferior capsules, respectively.

Lastly, for the SRS CyberKnife experiments, all three measurements for the superior capsule and inferior capsules were within 1.9% of the TPS calculated dose. In this experiment, the coefficient of variance for the superior and inferior capsule measurements was 0.49% and 1.07%, respectively. These results were within our aims of $\pm 5\%$ accuracy and $\pm 3\%$ reproducibility. Additionally, the agreement between the TLD micro-cube and TLD powder for this experiment was 0.90% and 7.3% for the superior and inferior capsules, respectively. The inferior capsule for powder measurements seems to be an outlier and is likely not an accurate measurement. An explanation for this could be that the capsule was reversed in the phantom, placing the powder outside of the treatment volume where the dose would agree. Regardless, no conclusion drawn from this single measurement would be valid.

For all SRS head phantom experiments, both our accuracy and reproducibility were within the aims of the experiment and showed very good agreement with TPS calculations and powder measurements.

4.3.3 Small Field Irradiations

The small field irradiation experiments embodied the goals of this thesis, as they helped to define the limitations and capabilities of micro-cube TLD. All other experiments in this thesis have been conducted using TLD powder, however, the smallest field size typically used for TLD powder is a 12.5 mm field. This small field experiment tested 4 fields small than this.

The measurements for small field irradiations were all within 3.69% of the documented beam output for the CyberKnife. The coefficient of variance for the 60, 20, 15, 10, 7.5, and 5 mm fields were all less than 0.67%, showing excellent reproducibility. This final test of the capabilities of micro-cube TLD showed that measurements were within the aims of $\pm 5\%$ accuracy and $\pm 3\%$ reproducibility.

A note regarding the smaller field sizes of this experiment: the ability to align the phantom perfectly under the central axis of the beam is of utmost importance. In looking at the films collected from these experiments, there appears to be a slight offset of a little less than one millimeter, which would be within the tolerance for CyberKnife laser alignment with the beam central axis (<1 mm). This likely explains the systematic under response of approximately 3% in the 7.5 mm and 5 mm fields, where the dose fall-off is quite sharp away from central axis.

4.3.4 Film Analysis

The main objective of film analysis is to evaluate alignment of the treatment plan with the actual treatment itself. In this sense, the most important information we gather from film

analysis is the line profiles with respect to the TPS line profiles. These gives us alignment information. The gamma analysis gives some further insight, however there are limitations to gamma analysis. In this work, this was particularly apparent in the linac SRS head experiments where the agreement was only 84%, which was much lower than expected. This is a result of noise in the treatment and film, and is not an indication of poor delivery or planning. The beam output shows very good agreement and the film profile distance-to-agreement is also very good, so we put more weight in those characteristics for this analysis.

4.4 Statistics

A p-value smaller than 0.05 indicates strong statistical evidence to reject the null hypothesis, which for each TOST test was that the true ratio was ≤ 0.95 and that the true ratio was ≥ 1.05 i.e. the result was outside of a $\pm 5\%$ accuracy bound. Because each p-value was much smaller than 0.05, we can confidently conclude that the TLD micro-cubes are capable of accuracy within $\pm 5\%$.

4.5 Small Field Considerations

An item of concern in small field dosimetry is the level of care needed in making irradiations. In this experiment, this particular consideration can be exemplified in the small field experiments of 1.5 cm and smaller. By looking at the dose profile (Figure 71), it is easy to see that a small shift off of central axis could result in a largely reduced output due to the extremely steep fall off of the beam. Essentially, there is no flat region of the beam that is sometimes seen in larger fields, and thus the likelihood of misalignment is increased substantially.

This may be evident in our own experiments where extreme care was taken in aligning the phantom with the central axis. It seems that our phantom placements were just a fraction

of a millimeter off axis, and this could be the reason for our systematic measurement under response of 3%.

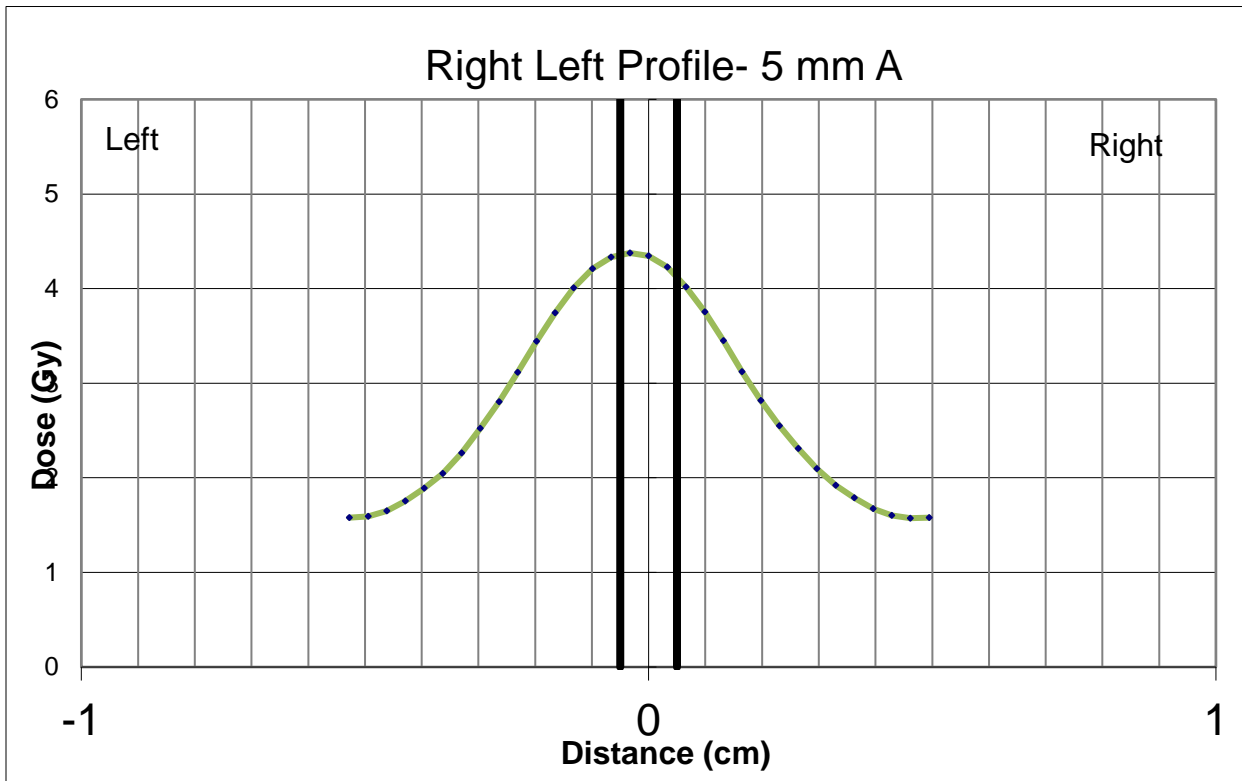


Figure 70: 5 mm field profile of CyberKnife

5 Conclusion

5.1 Conclusion

The aim of this study was to develop a remote dosimetry audit system using TLD micro-cubes to evaluate small radiation fields. More specifically, the hypothesis of this work was: *Micro-cube TLD can be commissioned to evaluate small field dosimetry, and provide reproducibility within $\pm 3\%$, as well as assure agreement between measured dose and calculated doses to within $\pm 5\%$.*

The first two experiments conducted in this work, single field output measurements and SRS head phantom measurements, served as an evaluation to answer the question: Can TLD micro-cubes perform as well as TLD powder and show equivalence in measurements? Intrinsically, if the micro-cubes could not show equivalence to TLD powder in these two audit test that are already implemented, then there could be little confidence that they would show promising results in small field dosimetry. Fortunately, the TLD micro-cubes did show close agreement with the TLD powder in each experiment. This gave confidence in the potential of the micro-cubes.

However, the backbone of this work was truly in the small field experiments. TLD powder and OSLD chips have been used extensively in the single field output checks and SRS head phantom measurements, and there is no reason to use micro-cubes to make these measurements. The novelty in this work is to define the limits of micro-cubes in small field dosimetry. This meant evaluating fields smaller than the 1.25 cm limit placed on TLD powder measurements.

This experiment proved, with confidence, that TLD micro-cubes can evaluate field sizes as small as 5 mm in diameter. For the CyberKnife, this is the smallest field size available. These measurements collected in the experiments surpassed the expectations of the hypothesis, showing that TLD micro-cubes are an appropriate tool for small field dosimetry. Additionally, the system developed proved effectively robust, allowing it to be implemented as an audit program.

5.2 Future Work

5.2.1 Fading Correction

One item that was not completed in this study was characterization of the fading correction factor. Because the standards defining reader system sensitivity and the experimental micro-cubes were both irradiated and read on the same day in each experiment, the fading correction factor was unnecessary. However, if this system is to be implemented as an audit program, it is unlikely that the standards and experimental micro-cubes will be irradiated on the same day. In this light, a fading correction factor for micro-cubes should be measured.

5.2.2 Future Applications

This study has shown the capabilities of TLD micro-cubes and opens a door to their routine use. One such avenue is in SRS head phantoms. A future application of TLD micro-cubes is to develop an SRS head phantom in which the simulated tumor volume is smaller than the current 1.9 cm. This would be a unique application of the micro-cubes, and would allow an audit of smaller targets for SRS.

A similar application would be to develop an SRS head phantom with multiple targets, as opposed to a single target in the center of the cranial region. This would be a more robust and inclusive audit for SRS treatments and likely more practical to SRS treating multiple brain metastases.

These applications of TLD micro-cubes are not only novel, but very applicable to a comprehensive SRS audit program. They would serve as a complete evaluation of possible treatments for brain metastasis to provide insight for institutions, aiding in the improvement of treatment delivery.

6 Appendix

6.1 SRS Head Phantom Instructions

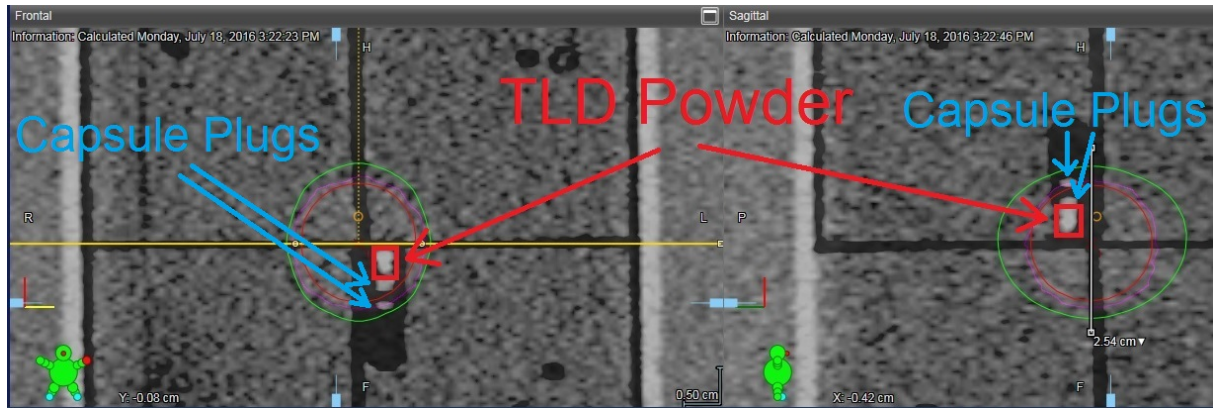
Imaging the Phantom:

1. *If you use immobilization, apply it on the phantom. For headframes, the target is located roughly between the upper parts of the ears. When positioning the phantom, please attempt to keep the head level and straight so that the mid-coronal and mid-sagittal film planes are not rotated (if applicable to your setup, two leveling screws are present on the base-plate of the phantom). This is optimal to compare these measured planes with the corresponding dose plane produced by your treatment planning system.*
2. *Locate the target with CT. This phantom is not compatible with MRI imaging and if MRI imaging is desired a different (water-filled) SRS phantom is necessary. Please provide axial, coronal and sagittal images through the target volume when submitting data to IROC.*
3. *Create a treatment plan according to the guidelines provided below.*

Treatment Planning:

1. *The target is the solid water ball that should be evident on the CT scan. The center of the ball defines the center of the target volume. Please treat the solid water ball as the PTV.*
2. *Contour the TLD powder inside both of the capsules. The powder is illustrated in the figure below. Please note that the powder is just the high contrast volume near the mid-plane of the insert – please do not include the capsule plugs in this contour (the TLD powder size is*

approximately 3 mm in diameter and 4 mm in length). Submit the TLD contour dose as determined by your treatment planning computer. Please also submit the point dose to the center of the TLD.



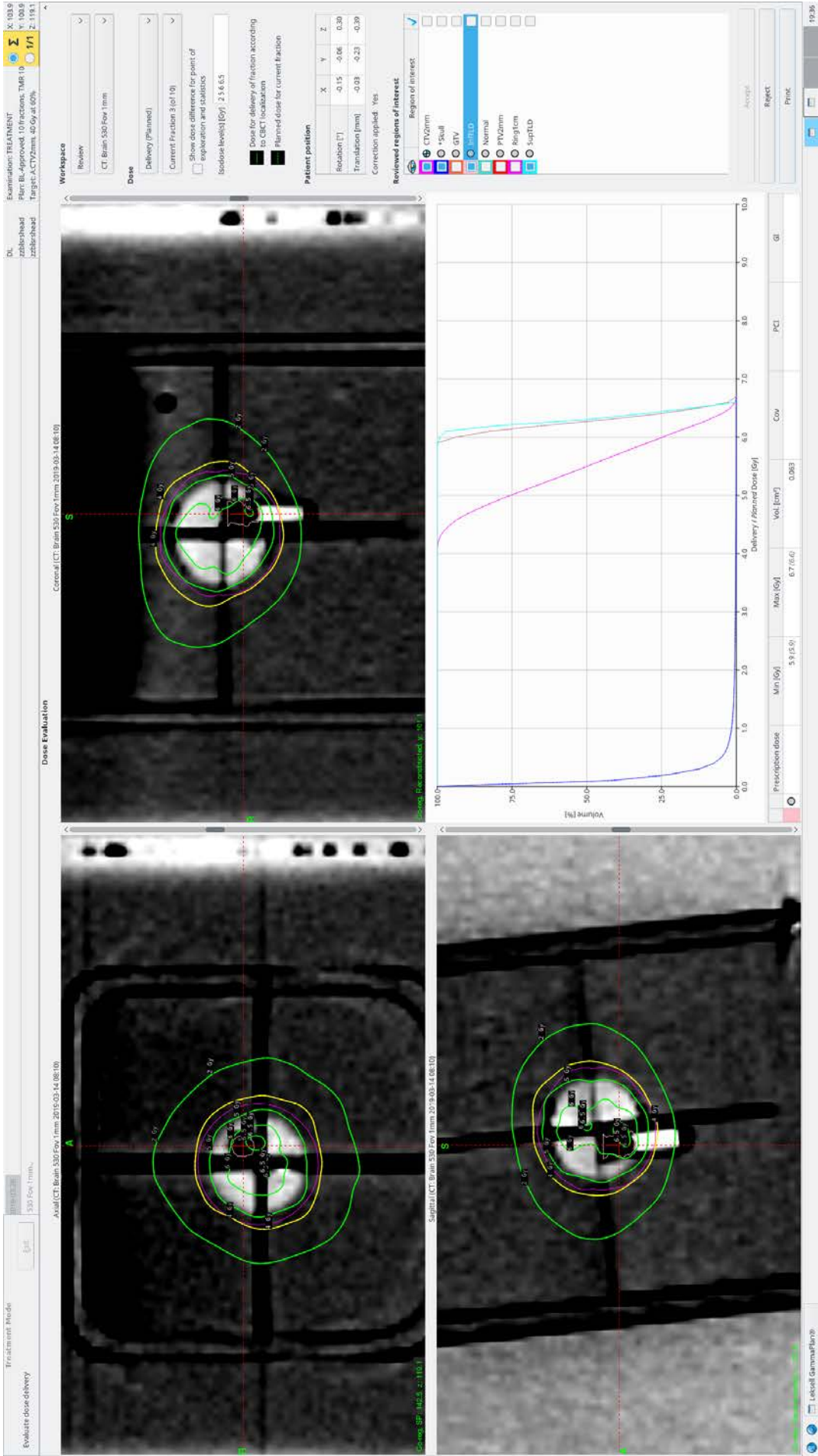
3. Plan a treatment that covers the target volume while sparing all other tissues. To achieve maximum precision, IROC would like the dose to the center of the target to be approximately 30Gy (100% isodose line). This should be achievable with the following dose guidelines:
 - a. GammaKnife: Cover the target with 15 Gy (prescription isodose line 40% - 60%)
 - b. CyberKnife: Cover the target with 20 Gy (prescription isodose line 60% - 80%)
 - c. C-arm linear accelerator: Cover the target with 25 Gy (prescription isodose line >85%)

Treatment

1. Align the phantom according to your clinical workflow.
2. Remove the ear TLD after imaging is complete and before treatment begins.
3. Irradiate the phantom according to your plan.

6.2 Gamma Knife

6.2.1 Gamma Knife Treatment Plan Snapshots



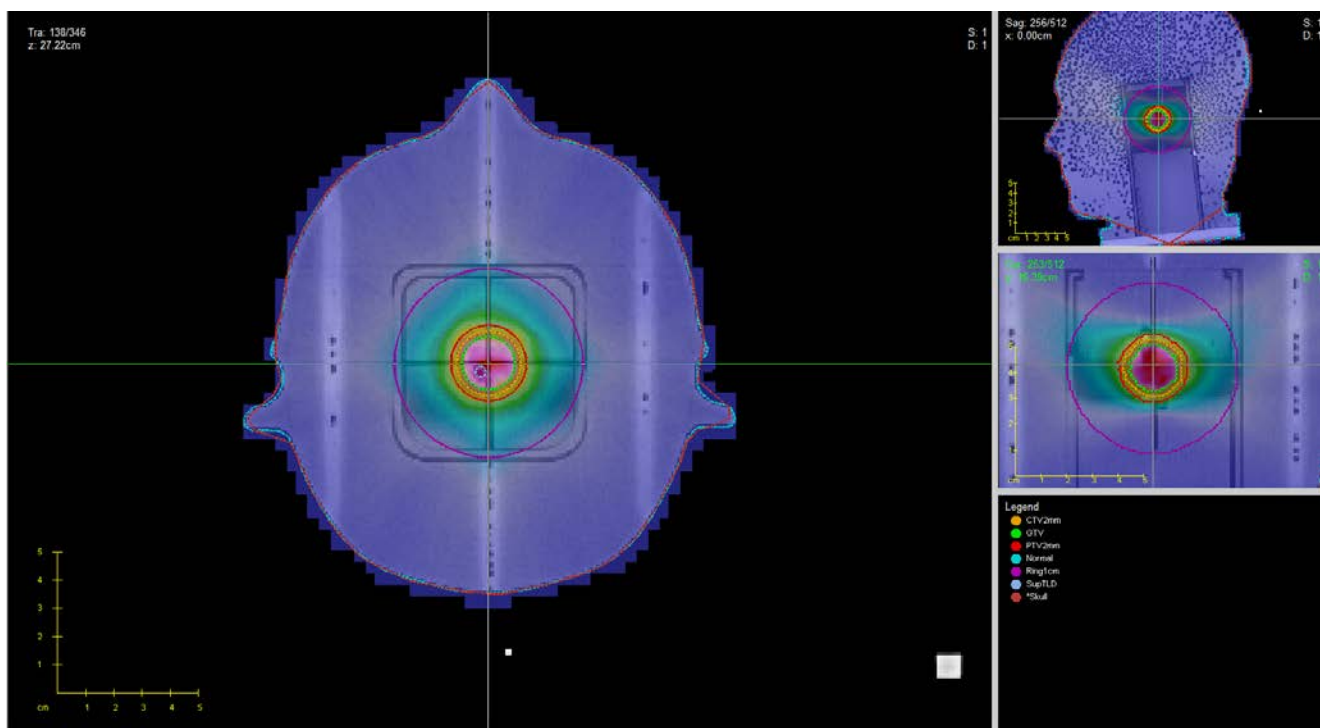
The screenshot displays the Leksell GammaPlan® software interface, showing three CT scan slices (Coronal, Axial, and Sagittal) with isodose lines and a DVH plot. The interface includes a top toolbar with icons for workspace, review, and dose evaluation. The left sidebar shows patient information and treatment details. The right sidebar displays patient position, rotation, and translation data. The main area shows the CT slices with isodose lines and a DVH plot on the right.

Top Toolbar: Workspace, Review, Dose Evaluation, Exam: TREATMENT, Plan: BL Approved, 10 fractions, TMR 19, Target: ACTV2mm, 40 Gy at 60%, 2.1116

Left Sidebar: Patient information, Treatment details, Dose evaluation details.

Right Sidebar: Patient position, Rotation, Translation, Correction applied, Reviewed regions of interest, Region of interest, CTV2mm, *scal, *GTV, *PTVLO, Normal, PTV2mm, Ring 1cm, Ring 1.5cm, Ring 2.0cm, Ring 2.5cm, Ring 3.0cm, Ring 3.5cm, Ring 4.0cm, Ring 4.5cm, Ring 5.0cm, Ring 5.5cm, Ring 6.0cm, Ring 6.5cm, Ring 7.0cm, Ring 7.5cm, Ring 8.0cm, Ring 8.5cm, Ring 9.0cm, Ring 9.5cm, Ring 10.0cm, Ring 10.5cm, Ring 11.0cm, Ring 11.5cm, Ring 12.0cm, Ring 12.5cm, Ring 13.0cm, Ring 13.5cm, Ring 14.0cm, Ring 14.5cm, Ring 15.0cm, Ring 15.5cm, Ring 16.0cm, Ring 16.5cm, Ring 17.0cm, Ring 17.5cm, Ring 18.0cm, Ring 18.5cm, Ring 19.0cm, Ring 19.5cm, Ring 20.0cm, Ring 20.5cm, Ring 21.0cm, Ring 21.5cm, Ring 22.0cm, Ring 22.5cm, Ring 23.0cm, Ring 23.5cm, Ring 24.0cm, Ring 24.5cm, Ring 25.0cm, Ring 25.5cm, Ring 26.0cm, Ring 26.5cm, Ring 27.0cm, Ring 27.5cm, Ring 28.0cm, Ring 28.5cm, Ring 29.0cm, Ring 29.5cm, Ring 30.0cm, Ring 30.5cm, Ring 31.0cm, Ring 31.5cm, Ring 32.0cm, Ring 32.5cm, Ring 33.0cm, Ring 33.5cm, Ring 34.0cm, Ring 34.5cm, Ring 35.0cm, Ring 35.5cm, Ring 36.0cm, Ring 36.5cm, Ring 37.0cm, Ring 37.5cm, Ring 38.0cm, Ring 38.5cm, Ring 39.0cm, Ring 39.5cm, Ring 40.0cm, Ring 40.5cm, Ring 41.0cm, Ring 41.5cm, Ring 42.0cm, Ring 42.5cm, Ring 43.0cm, Ring 43.5cm, Ring 44.0cm, Ring 44.5cm, Ring 45.0cm, Ring 45.5cm, Ring 46.0cm, Ring 46.5cm, Ring 47.0cm, Ring 47.5cm, Ring 48.0cm, Ring 48.5cm, Ring 49.0cm, Ring 49.5cm, Ring 50.0cm, Ring 50.5cm, Ring 51.0cm, Ring 51.5cm, Ring 52.0cm, Ring 52.5cm, Ring 53.0cm, Ring 53.5cm, Ring 54.0cm, Ring 54.5cm, Ring 55.0cm, Ring 55.5cm, Ring 56.0cm, Ring 56.5cm, Ring 57.0cm, Ring 57.5cm, Ring 58.0cm, Ring 58.5cm, Ring 59.0cm, Ring 59.5cm, Ring 60.0cm, Ring 60.5cm, Ring 61.0cm, Ring 61.5cm, Ring 62.0cm, Ring 62.5cm, Ring 63.0cm, Ring 63.5cm, Ring 64.0cm, Ring 64.5cm, Ring 65.0cm, Ring 65.5cm, Ring 66.0cm, Ring 66.5cm, Ring 67.0cm, Ring 67.5cm, Ring 68.0cm, Ring 68.5cm, Ring 69.0cm, Ring 69.5cm, Ring 70.0cm, Ring 70.5cm, Ring 71.0cm, Ring 71.5cm, Ring 72.0cm, Ring 72.5cm, Ring 73.0cm, Ring 73.5cm, Ring 74.0cm, Ring 74.5cm, Ring 75.0cm, Ring 75.5cm, Ring 76.0cm, Ring 76.5cm, Ring 77.0cm, Ring 77.5cm, Ring 78.0cm, Ring 78.5cm, Ring 79.0cm, Ring 79.5cm, Ring 80.0cm, Ring 80.5cm, Ring 81.0cm, Ring 81.5cm, Ring 82.0cm, Ring 82.5cm, Ring 83.0cm, Ring 83.5cm, Ring 84.0cm, Ring 84.5cm, Ring 85.0cm, Ring 85.5cm, Ring 86.0cm, Ring 86.5cm, Ring 87.0cm, Ring 87.5cm, Ring 88.0cm, Ring 88.5cm, Ring 89.0cm, Ring 89.5cm, Ring 90.0cm, Ring 90.5cm, Ring 91.0cm, Ring 91.5cm, Ring 92.0cm, Ring 92.5cm, Ring 93.0cm, Ring 93.5cm, Ring 94.0cm, Ring 94.5cm, Ring 95.0cm, Ring 95.5cm, Ring 96.0cm, Ring 96.5cm, Ring 97.0cm, Ring 97.5cm, Ring 98.0cm, Ring 98.5cm, Ring 99.0cm, Ring 99.5cm, Ring 100.0cm, Ring 100.5cm, Ring 101.0cm, Ring 101.5cm, Ring 102.0cm, Ring 102.5cm, Ring 103.0cm, Ring 103.5cm, Ring 104.0cm, Ring 104.5cm, Ring 105.0cm, Ring 105.5cm, Ring 106.0cm, Ring 106.5cm, Ring 107.0cm, Ring 107.5cm, Ring 108.0cm, Ring 108.5cm, Ring 109.0cm, Ring 109.5cm, Ring 110.0cm, Ring 110.5cm, Ring 111.0cm, Ring 111.5cm, Ring 112.0cm, Ring 112.5cm, Ring 113.0cm, Ring 113.5cm, Ring 114.0cm, Ring 114.5cm, Ring 115.0cm, Ring 115.5cm, Ring 116.0cm, Ring 116.5cm, Ring 117.0cm, Ring 117.5cm, Ring 118.0cm, Ring 118.5cm, Ring 119.0cm, Ring 119.5cm, Ring 120.0cm, Ring 120.5cm, Ring 121.0cm, Ring 121.5cm, Ring 122.0cm, Ring 122.5cm, Ring 123.0cm, Ring 123.5cm, Ring 124.0cm, Ring 124.5cm, Ring 125.0cm, Ring 125.5cm, Ring 126.0cm, Ring 126.5cm, Ring 127.0cm, Ring 127.5cm, Ring 128.0cm, Ring 128.5cm, Ring 129.0cm, Ring 129.5cm, Ring 130.0cm, Ring 130.5cm, Ring 131.0cm, Ring 131.5cm, Ring 132.0cm, Ring 132.5cm, Ring 133.0cm, Ring 133.5cm, Ring 134.0cm, Ring 134.5cm, Ring 135.0cm, Ring 135.5cm, Ring 136.0cm, Ring 136.5cm, Ring 137.0cm, Ring 137.5cm, Ring 138.0cm, Ring 138.5cm, Ring 139.0cm, Ring 139.5cm, Ring 140.0cm, Ring 140.5cm, Ring 141.0cm, Ring 141.5cm, Ring 142.0cm, Ring 142.5cm, Ring 143.0cm, Ring 143.5cm, Ring 144.0cm, Ring 144.5cm, Ring 145.0cm, Ring 145.5cm, Ring 146.0cm, Ring 146.5cm, Ring 147.0cm, Ring 147.5cm, Ring 148.0cm, Ring 148.5cm, Ring 149.0cm, Ring 149.5cm, Ring 150.0cm, Ring 150.5cm, Ring 151.0cm, Ring 151.5cm, Ring 152.0cm, Ring 152.5cm, Ring 153.0cm, Ring 153.5cm, Ring 154.0cm, Ring 154.5cm, Ring 155.0cm, Ring 155.5cm, Ring 156.0cm, Ring 156.5cm, Ring 157.0cm, Ring 157.5cm, Ring 158.0cm, Ring 158.5cm, Ring 159.0cm, Ring 159.5cm, Ring 160.0cm, Ring 160.5cm, Ring 161.0cm, Ring 161.5cm, Ring 162.0cm, Ring 162.5cm, Ring 163.0cm, Ring 163.5cm, Ring 164.0cm, Ring 164.5cm, Ring 165.0cm, Ring 165.5cm, Ring 166.0cm, Ring 166.5cm, Ring 167.0cm, Ring 167.5cm, Ring 168.0cm, Ring 168.5cm, Ring 169.0cm, Ring 169.5cm, Ring 170.0cm, Ring 170.5cm, Ring 171.0cm, Ring 171.5cm, Ring 172.0cm, Ring 172.5cm, Ring 173.0cm, Ring 173.5cm, Ring 174.0cm, Ring 174.5cm, Ring 175.0cm, Ring 175.5cm, Ring 176.0cm, Ring 176.5cm, Ring 177.0cm, Ring 177.5cm, Ring 178.0cm, Ring 178.5cm, Ring 179.0cm, Ring 179.5cm, Ring 180.0cm, Ring 180.5cm, Ring 181.0cm, Ring 181.5cm, Ring 182.0cm, Ring 182.5cm, Ring 183.0cm, Ring 183.5cm, Ring 184.0cm, Ring 184.5cm, Ring 185.0cm, Ring 185.5cm, Ring 186.0cm, Ring 186.5cm, Ring 187.0cm, Ring 187.5cm, Ring 188.0cm, Ring 188.5cm, Ring 189.0cm, Ring 189.5cm, Ring 190.0cm, Ring 190.5cm, Ring 191.0cm, Ring 191.5cm, Ring 192.0cm, Ring 192.5cm, Ring 193.0cm, Ring 193.5cm, Ring 194.0cm, Ring 194.5cm, Ring 195.0cm, Ring 195.5cm, Ring 196.0cm, Ring 196.5cm, Ring 197.0cm, Ring 197.5cm, Ring 198.0cm, Ring 198.5cm, Ring 199.0cm, Ring 199.5cm, Ring 200.0cm, Ring 200.5cm, Ring 201.0cm, Ring 201.5cm, Ring 202.0cm, Ring 202.5cm, Ring 203.0cm, Ring 203.5cm, Ring 204.0cm, Ring 204.5cm, Ring 205.0cm, Ring 205.5cm, Ring 206.0cm, Ring 206.5cm, Ring 207.0cm, Ring 207.5cm, Ring 208.0cm, Ring 208.5cm, Ring 209.0cm, Ring 209.5cm, Ring 210.0cm, Ring 210.5cm, Ring 211.0cm, Ring 211.5cm, Ring 212.0cm, Ring 212.5cm, Ring 213.0cm, Ring 213.5cm, Ring 214.0cm, Ring 214.5cm, Ring 215.0cm, Ring 215.5cm, Ring 216.0cm, Ring 216.5cm, Ring 217.0cm, Ring 217.5cm, Ring 218.0cm, Ring 218.5cm, Ring 219.0cm, Ring 21

6.2.2 Gamma Knife Dose Profile



6.2.3 GammaKnife Film

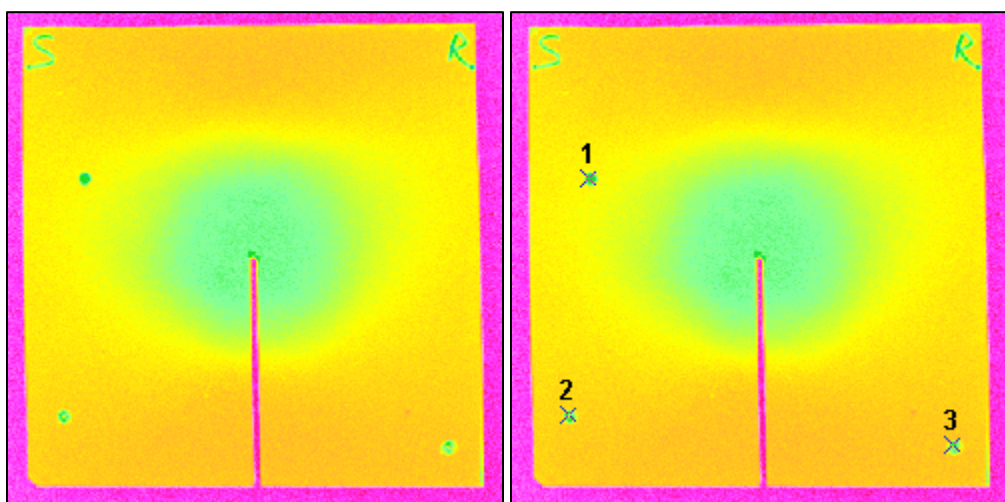


Figure 71 Gamma Knife coronal plane film registration

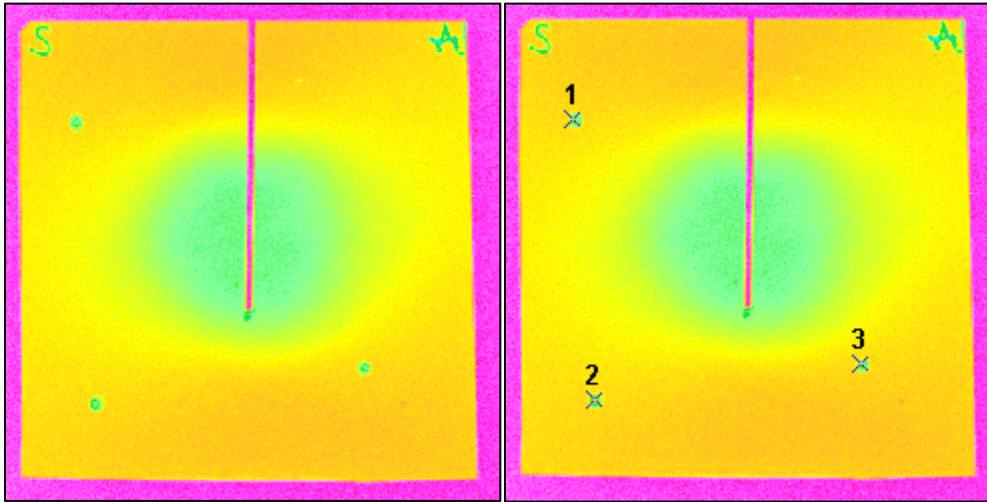


Figure 72 Gamma Knife sagittal plane film registration

6.2.4 Gamma Knife Film Gamma Analysis

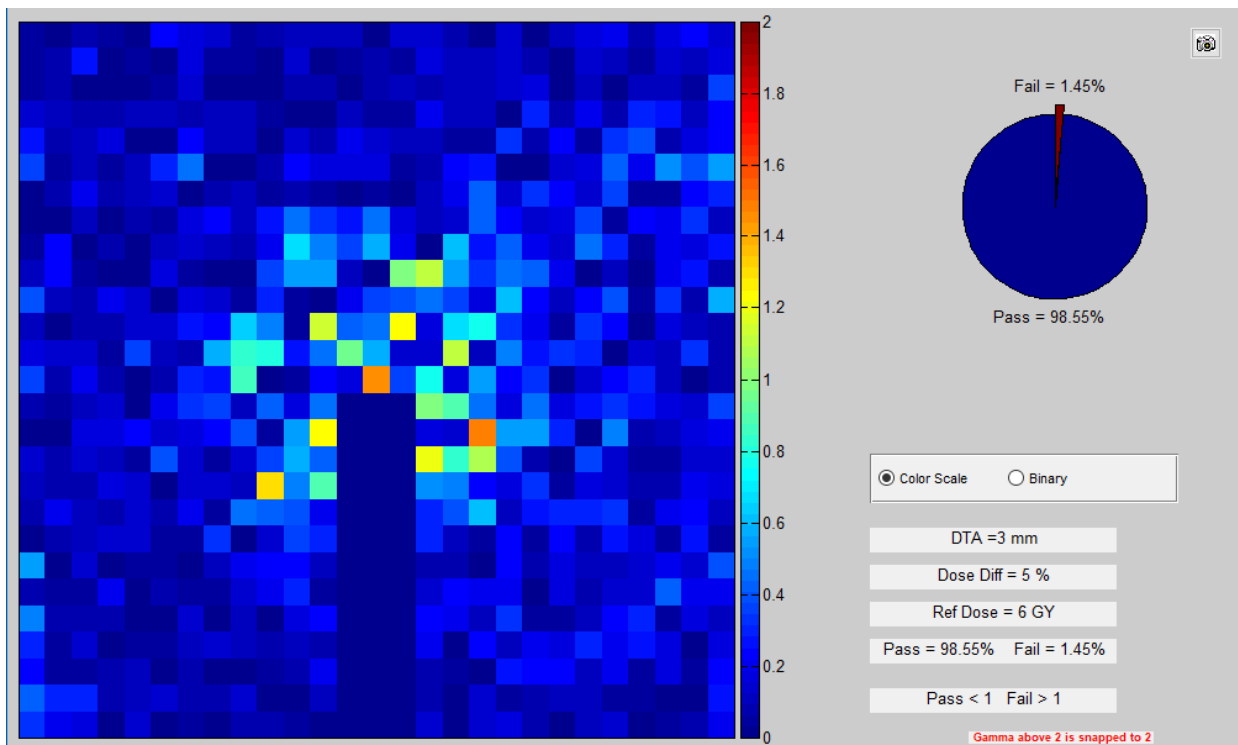


Figure 73 Gamma Knife A Coronal

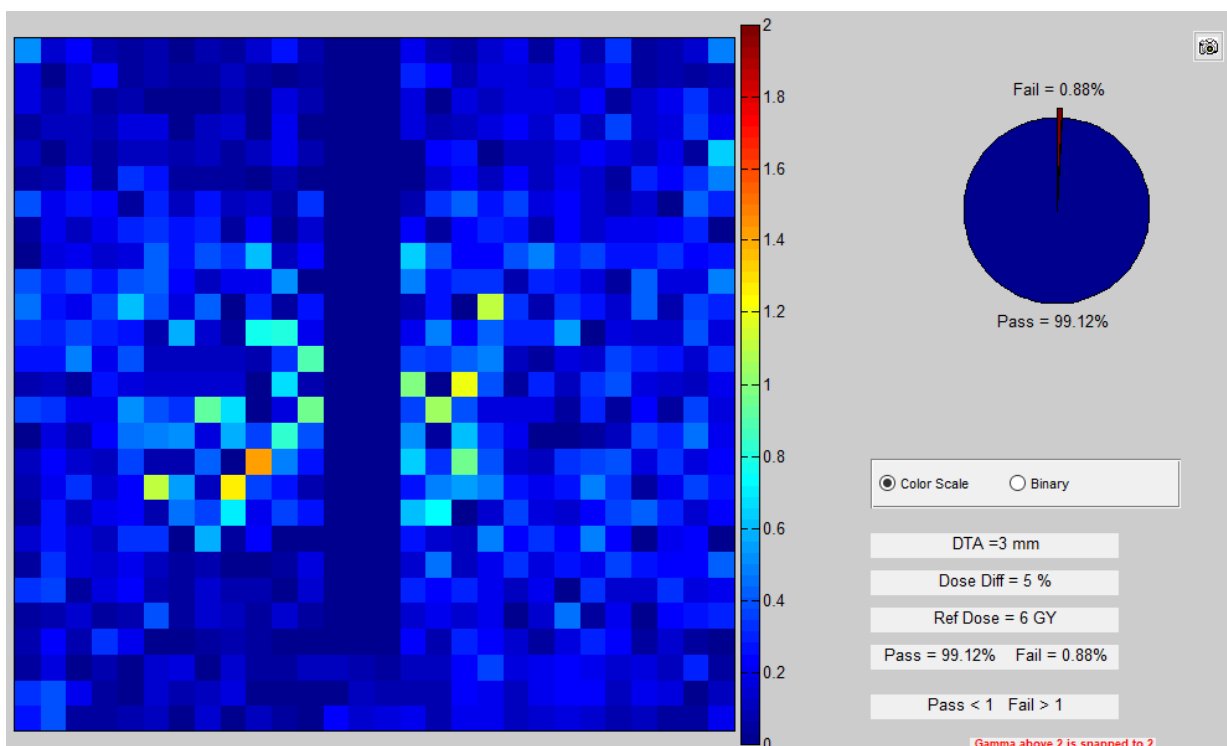


Figure 74 Gamma Knife A sagittal

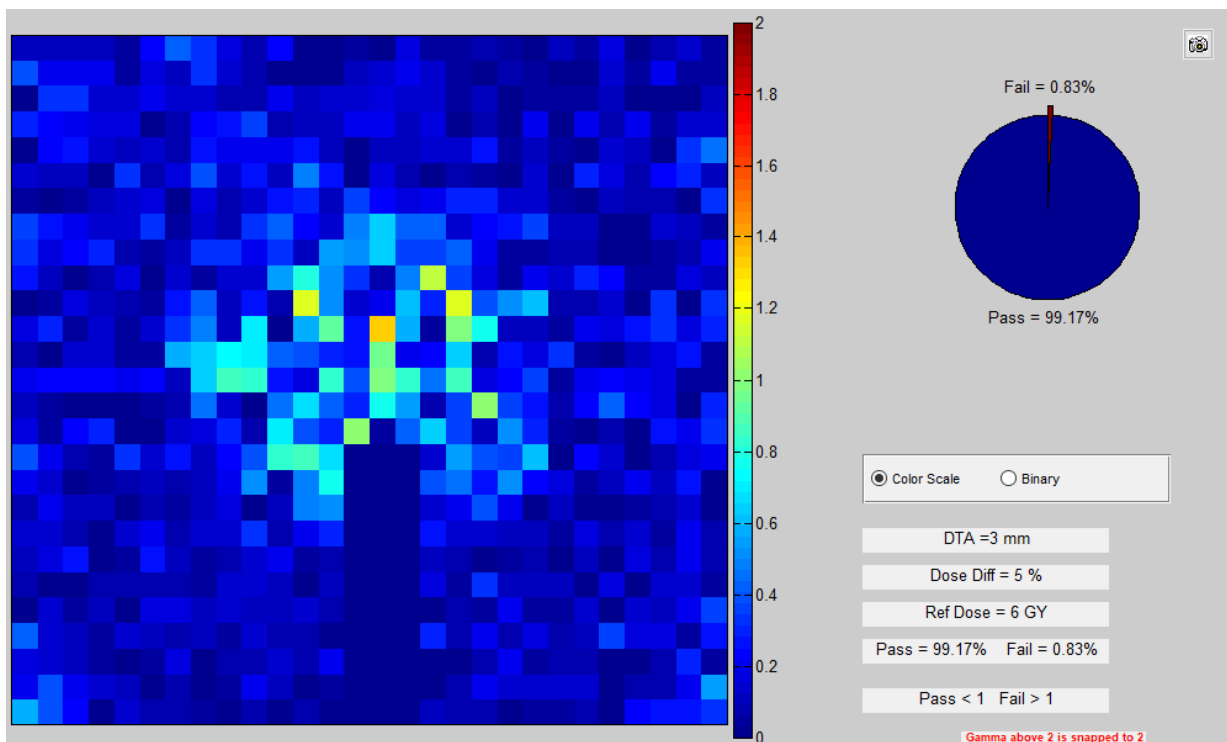


Figure 75 Gamma Knife B coronal

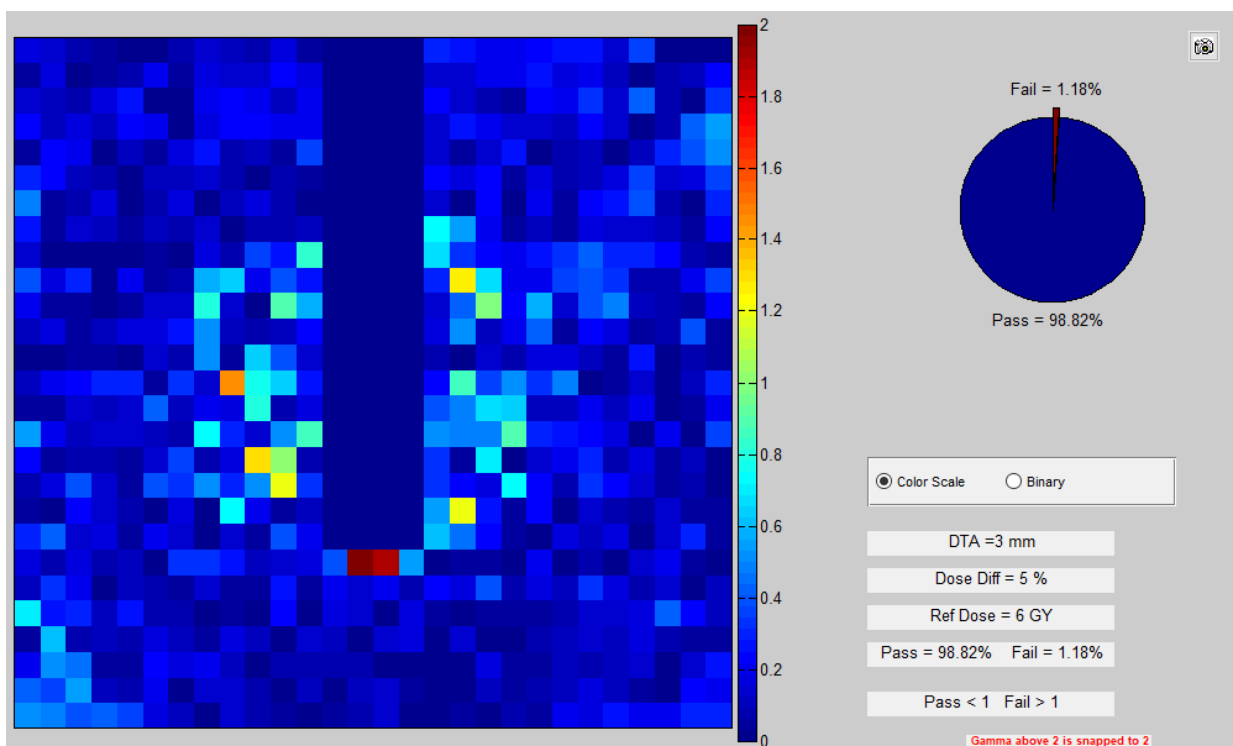


Figure 76 Gamma Knife B sagittal

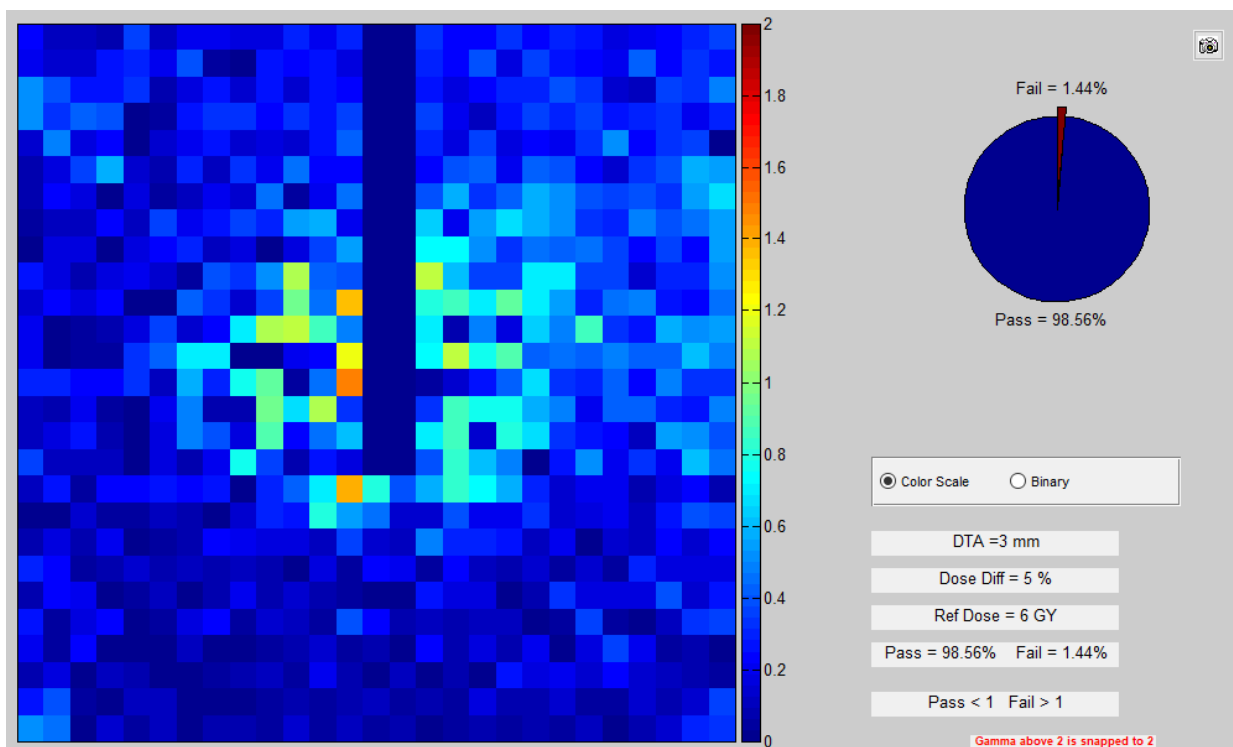


Figure 77 Gamma Knife C coronal

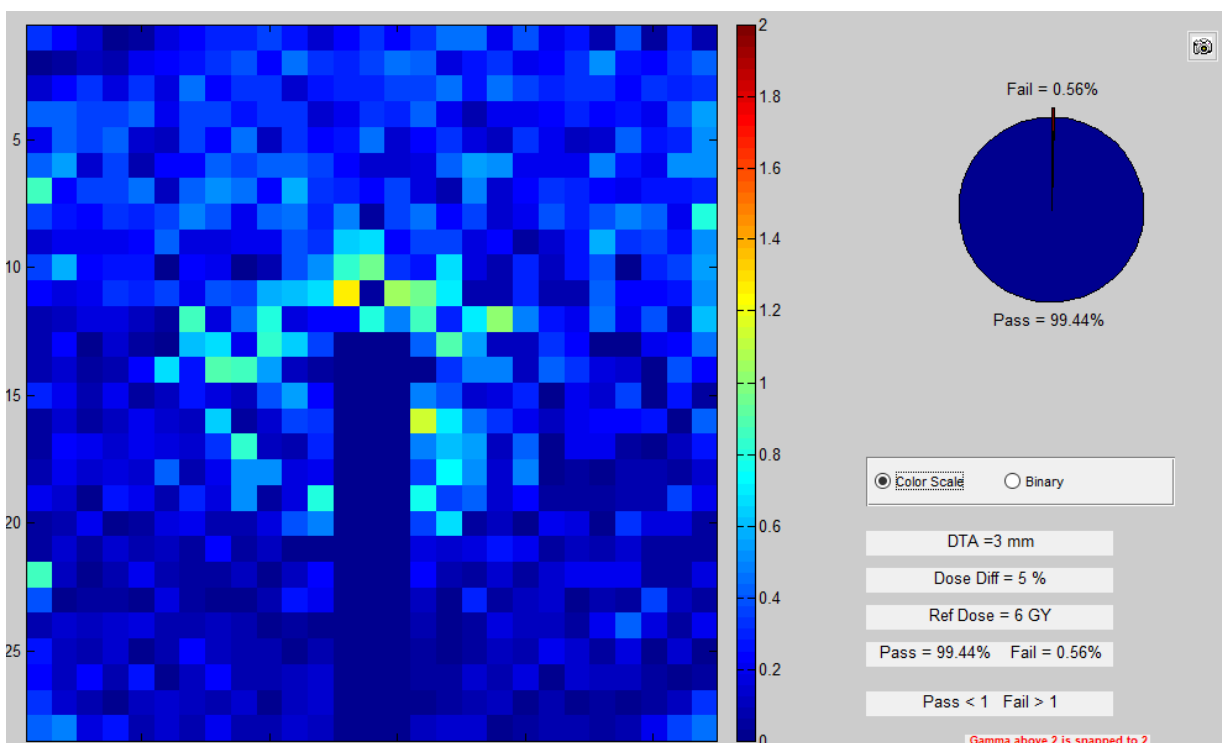
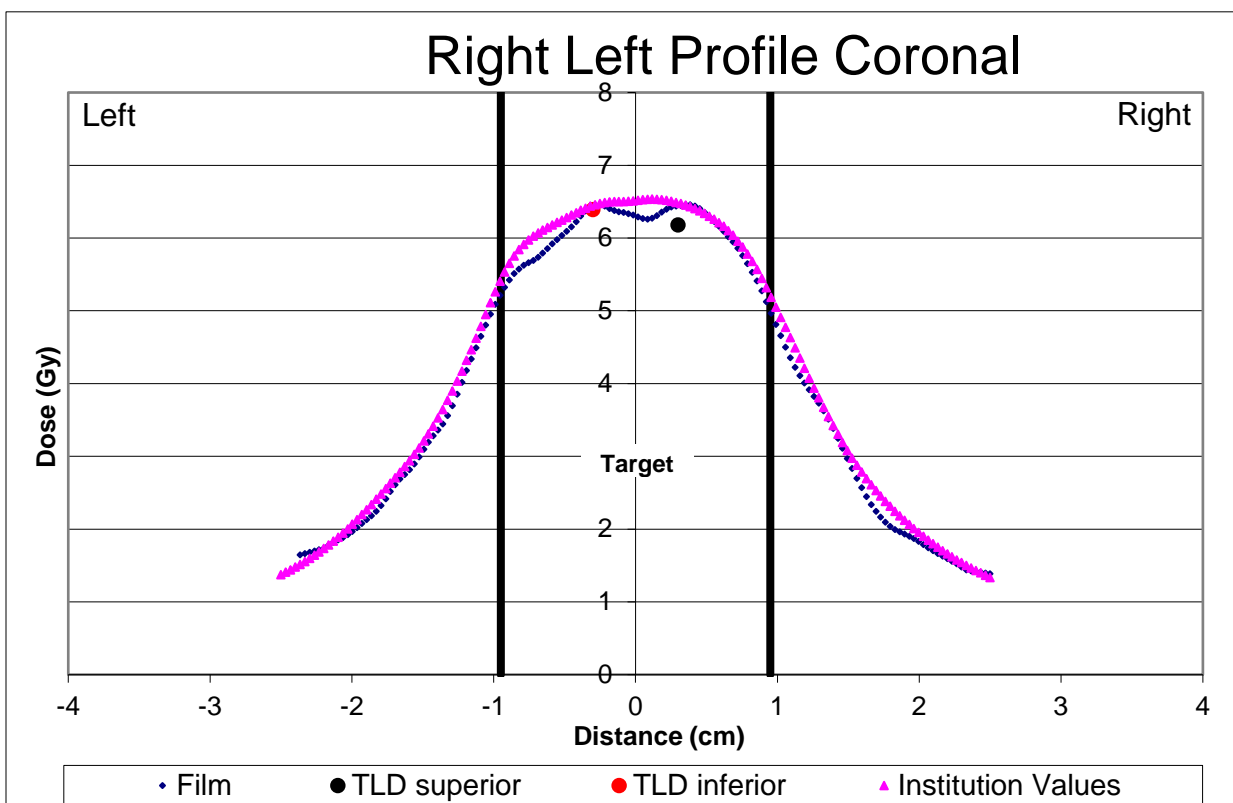
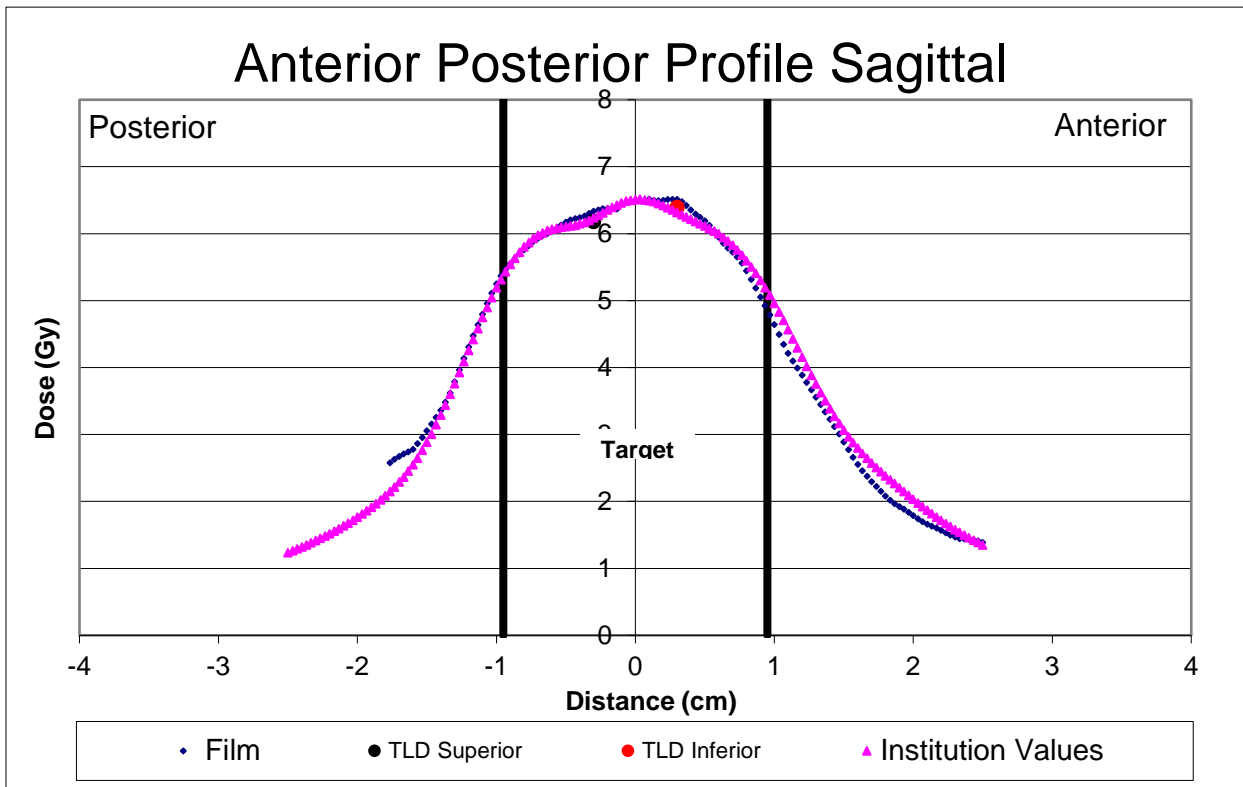
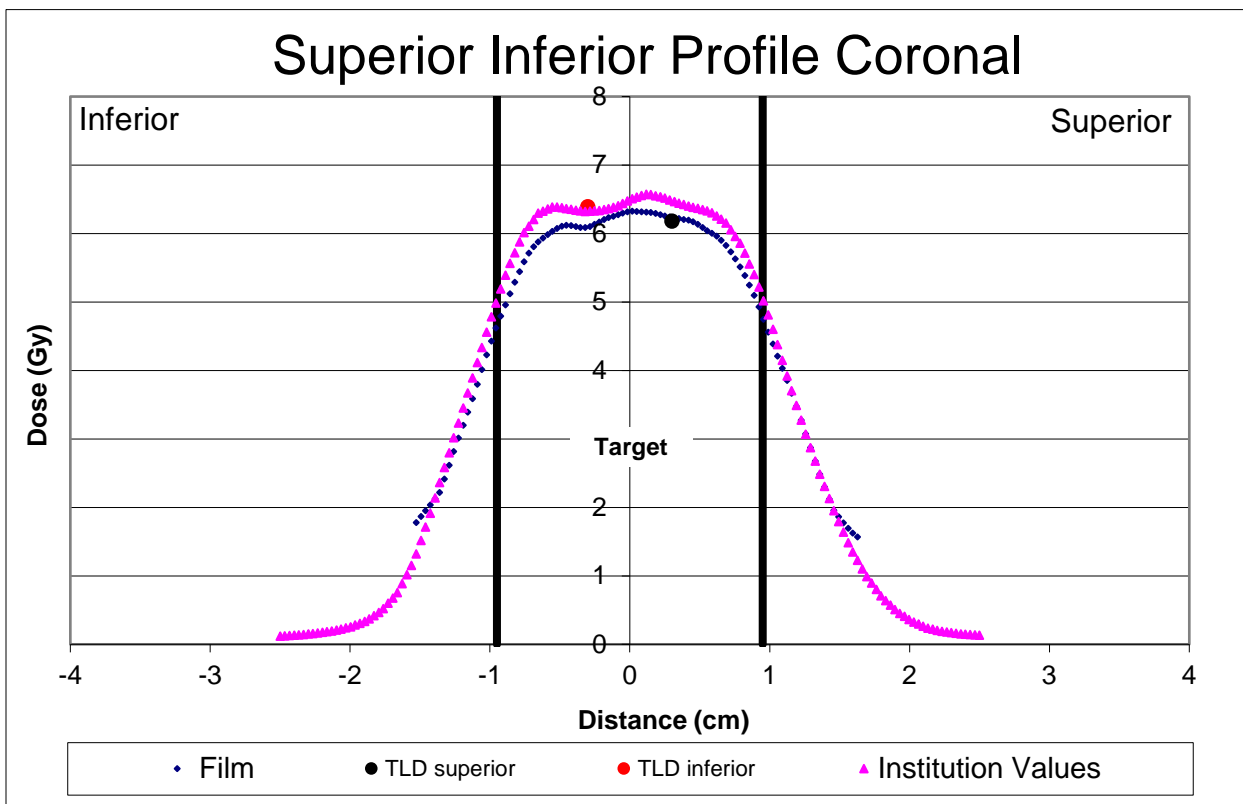


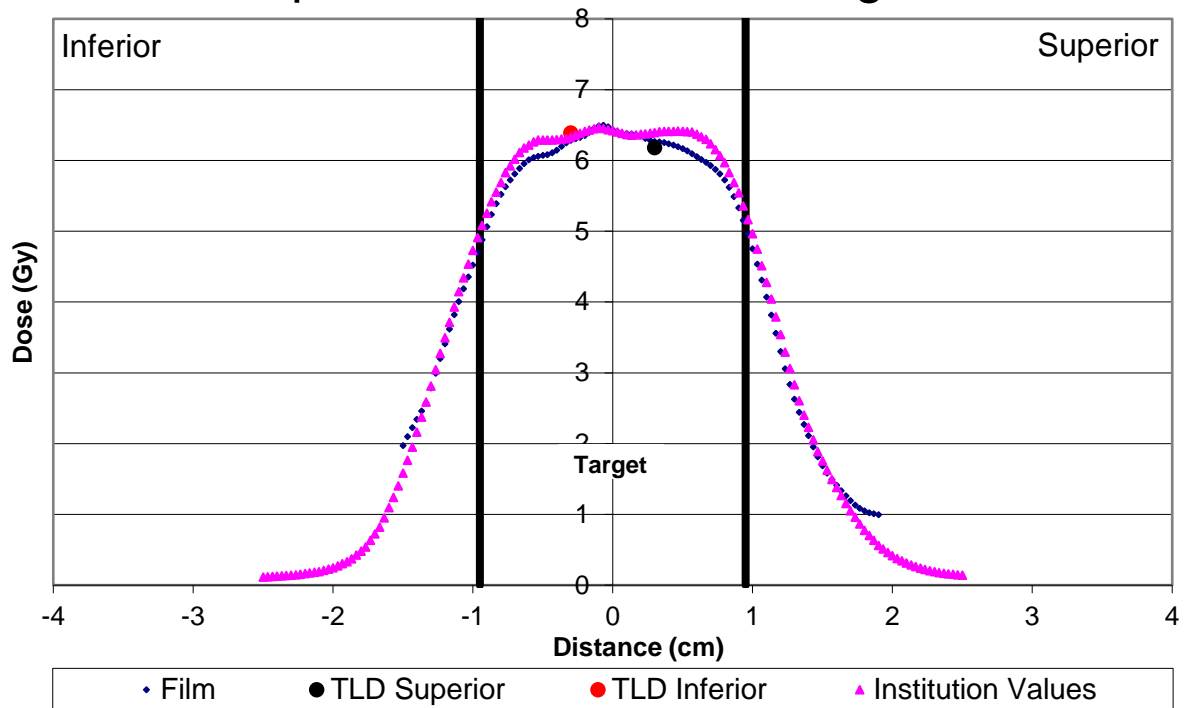
Figure 78 Gamma Knife C sagittal

6.2.5 Gamma Knife Film/TPS dose Line Profiles

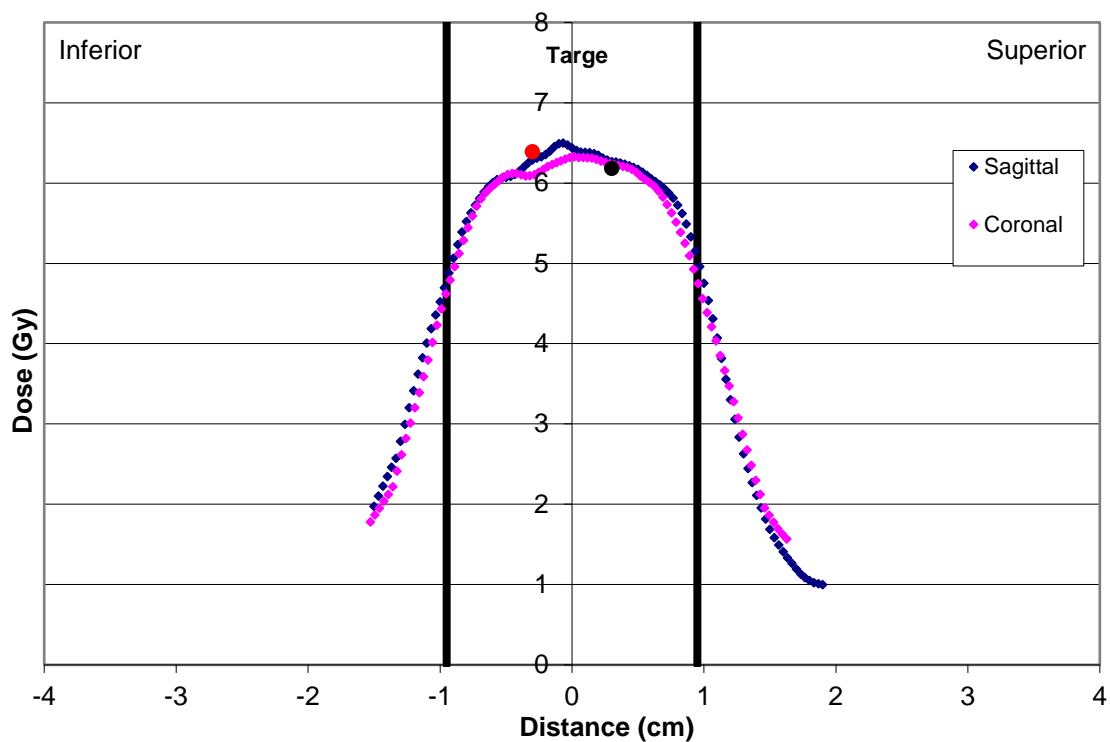




Superior Inferior Profile Sagittal

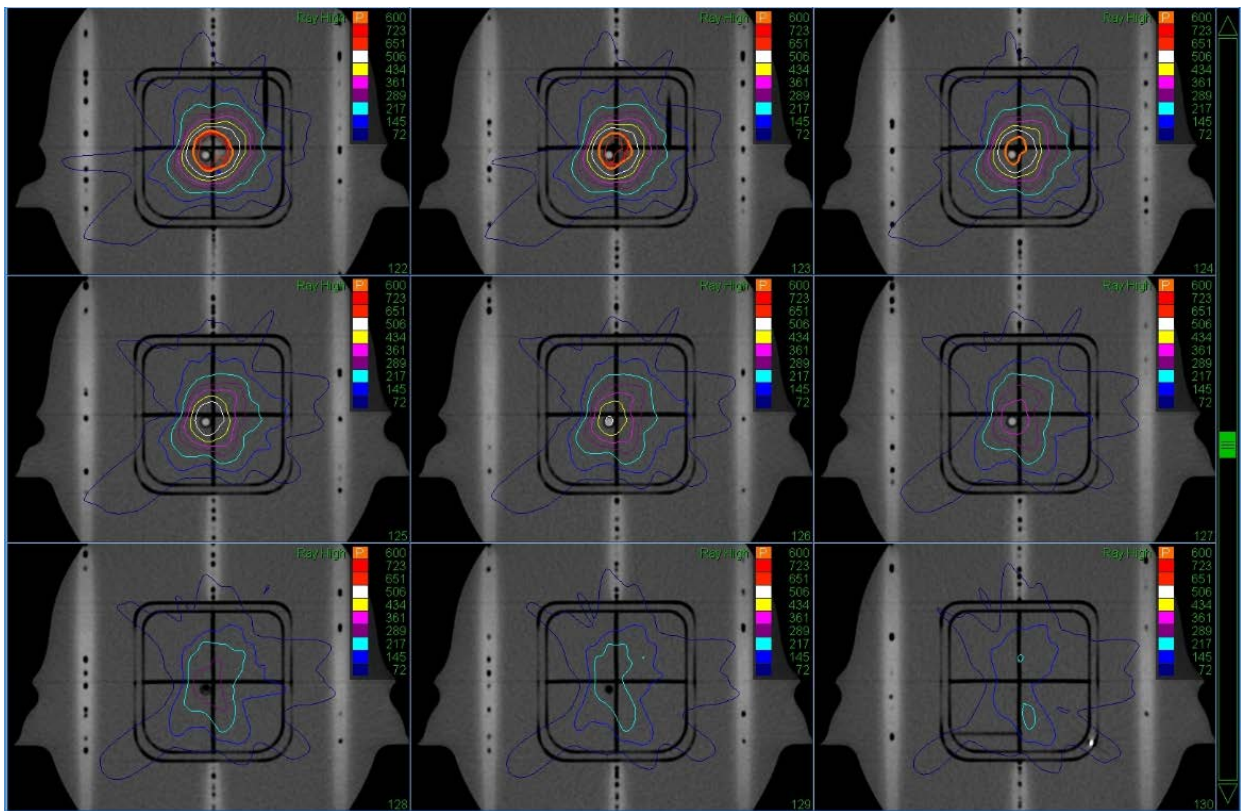


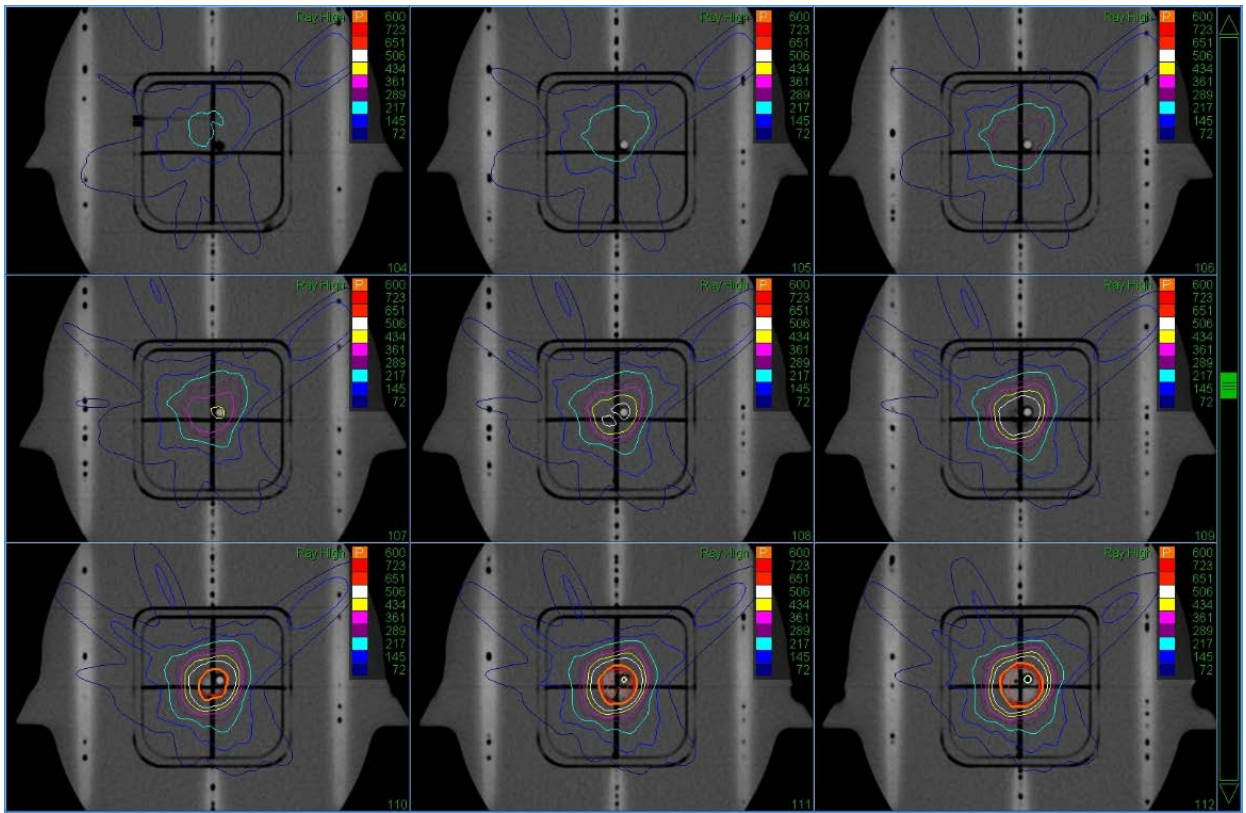
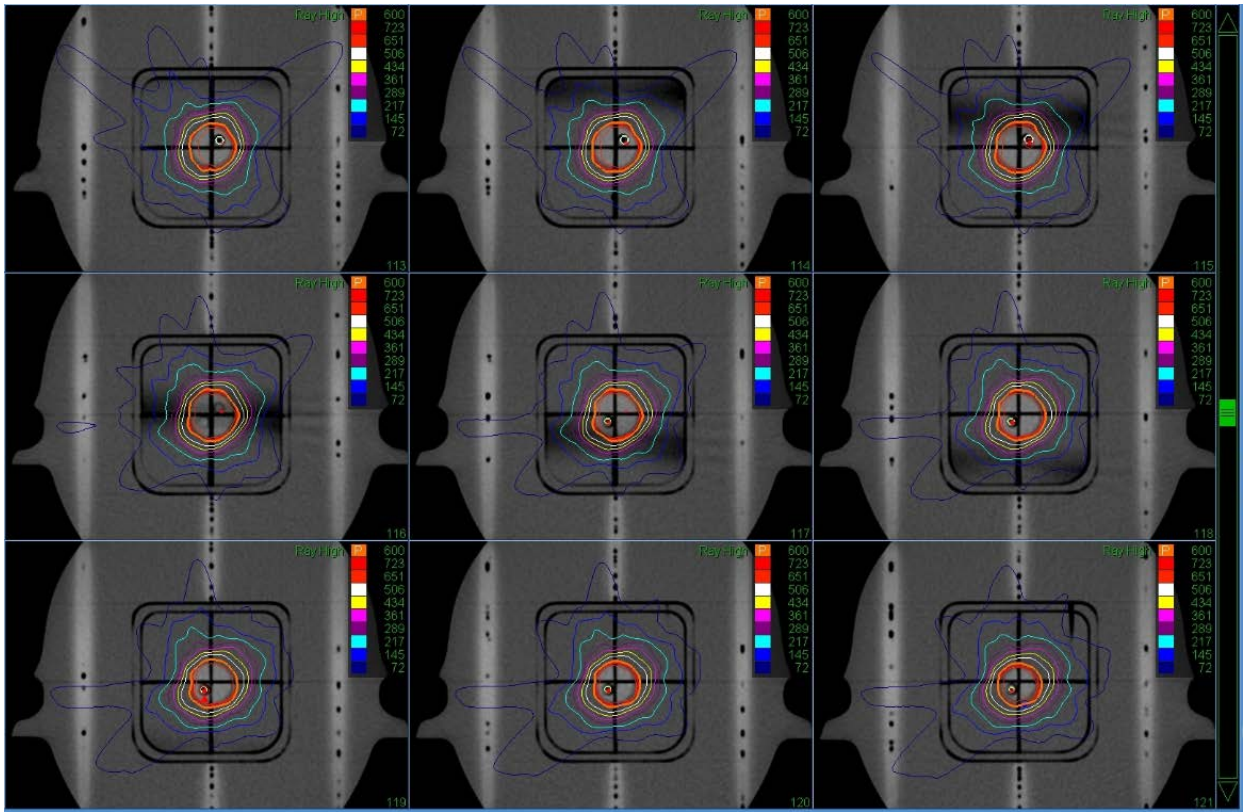
Superior Inferior - Comparison

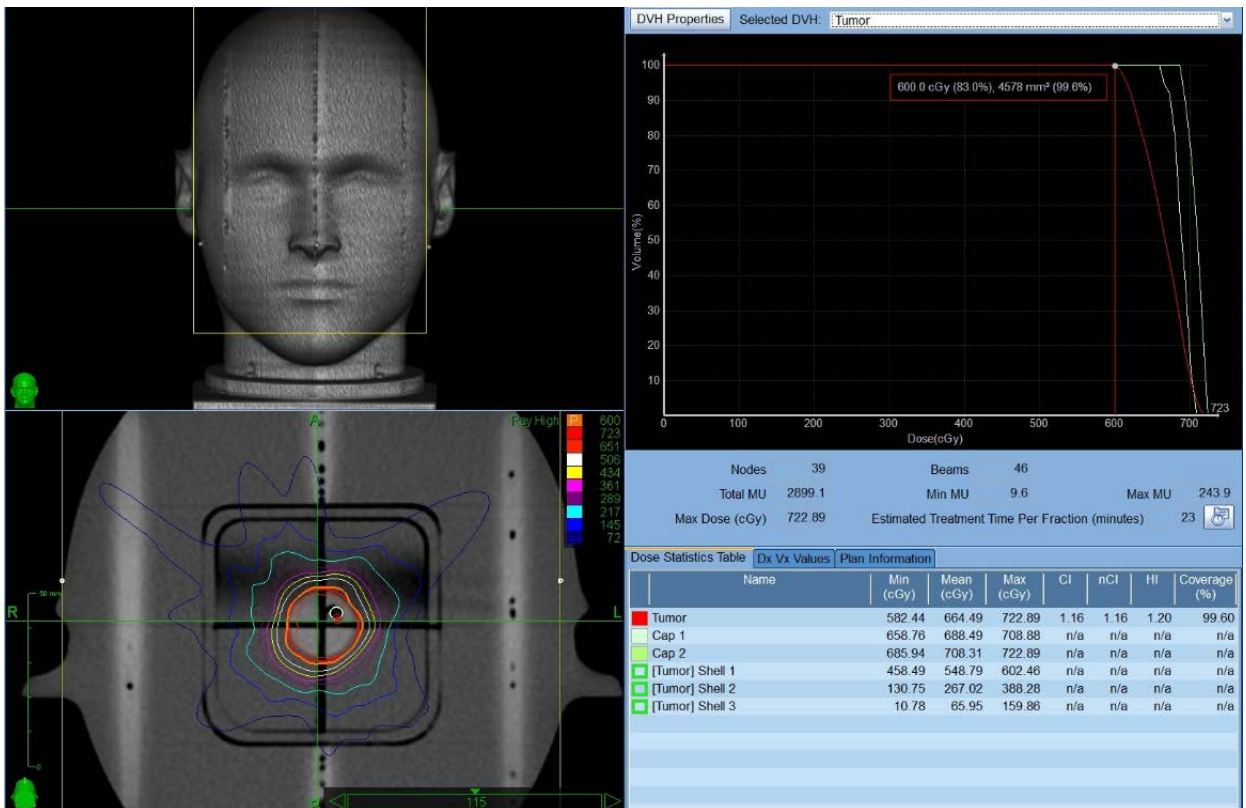
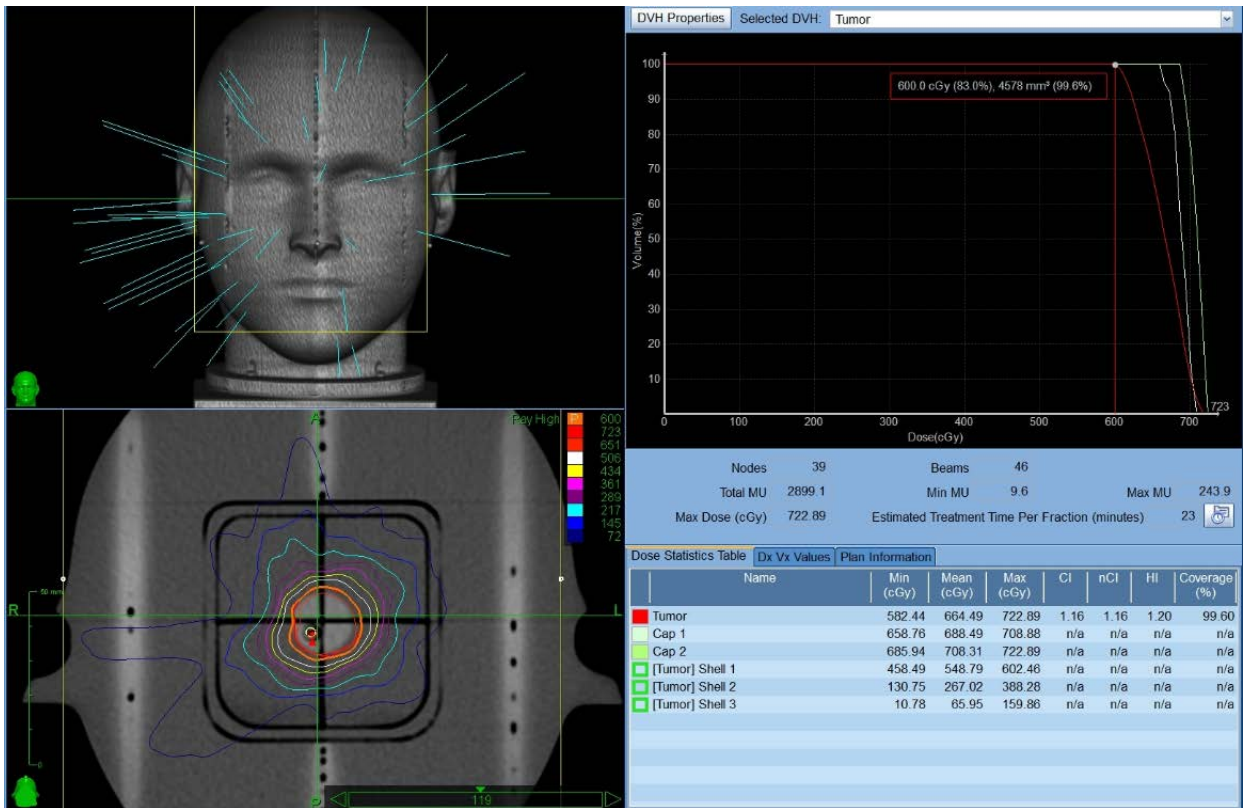


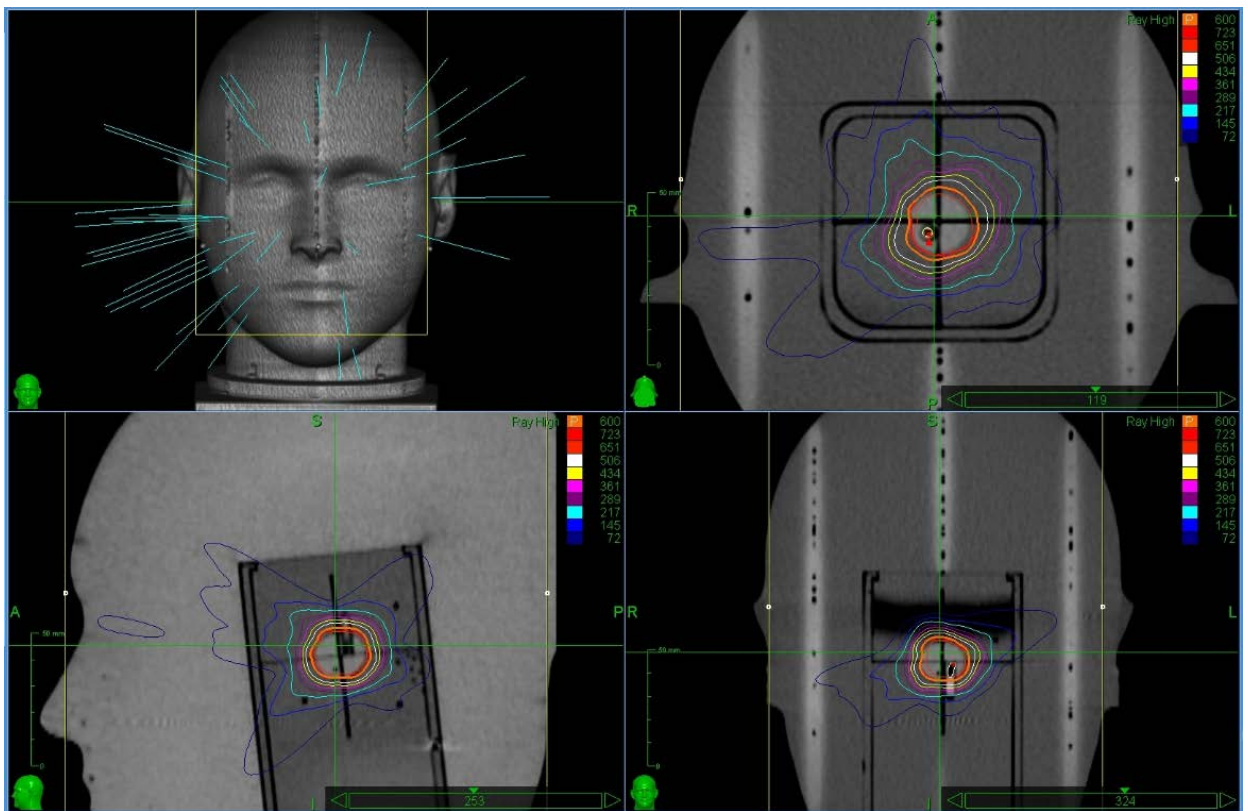
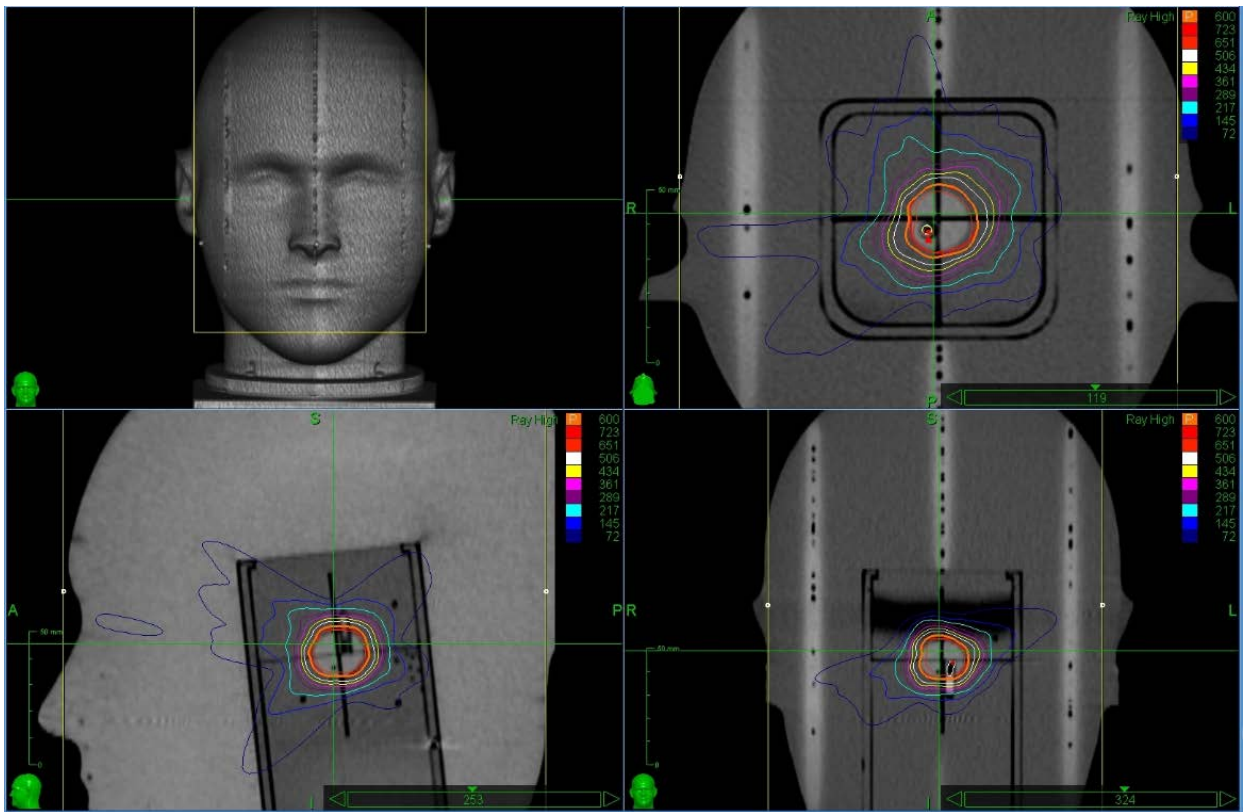
6.3 CyberKnife

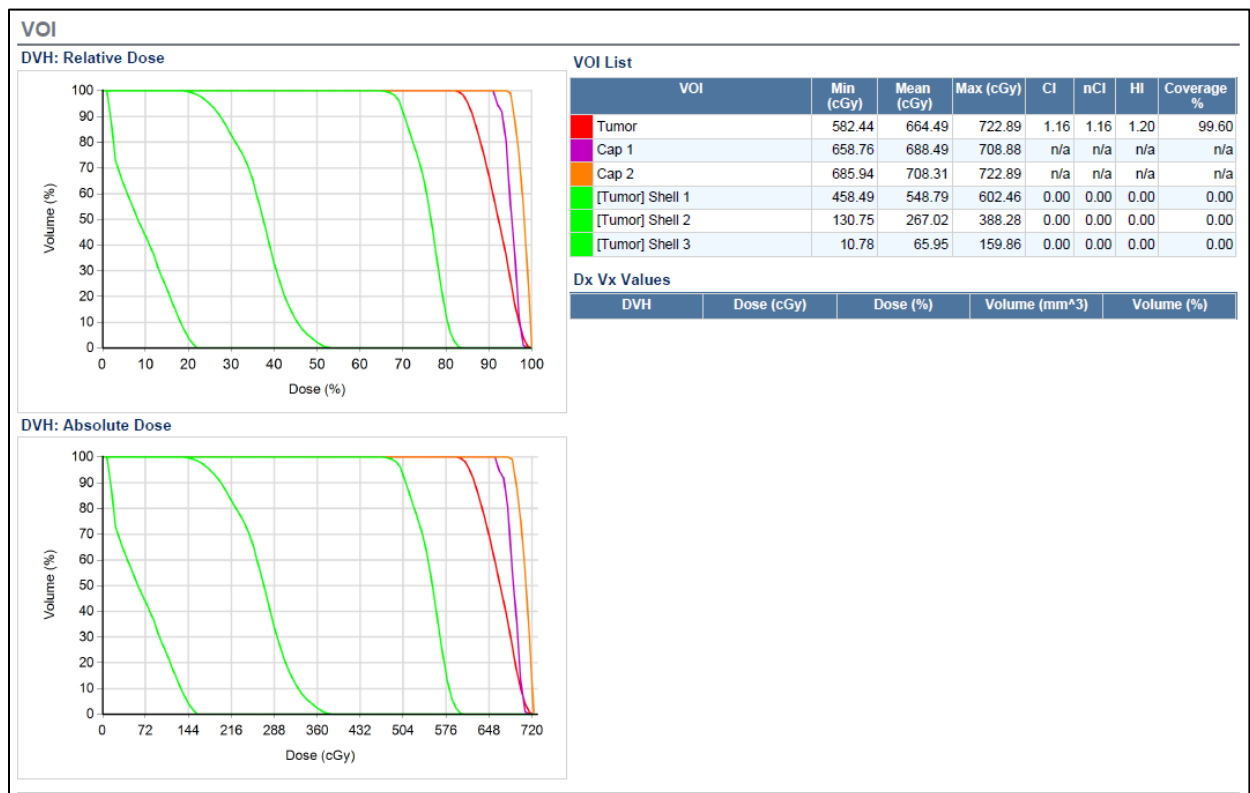
6.3.1 CyberKnife Treatment Plan Snapshots











6.3.2 CyberKnife Film

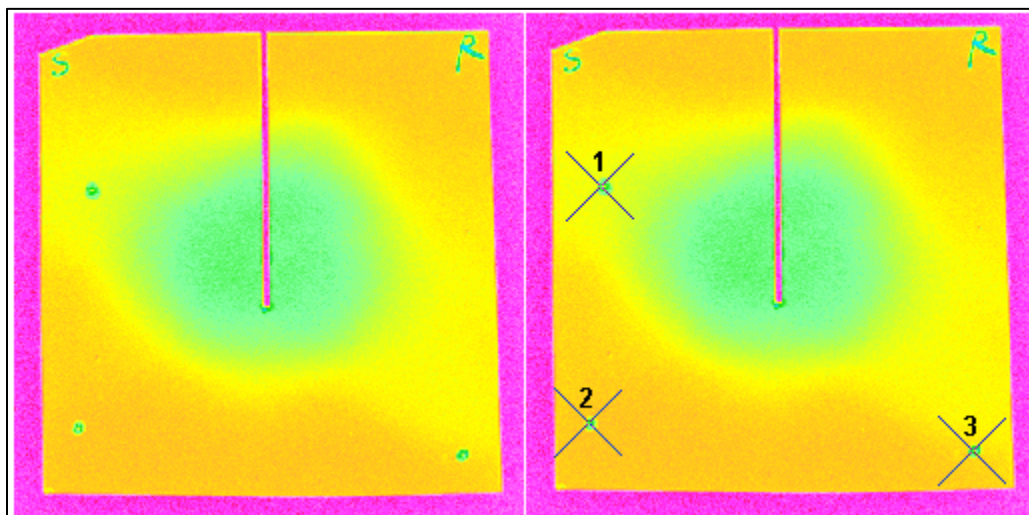


Figure 79: CyberKnife Coronal Film

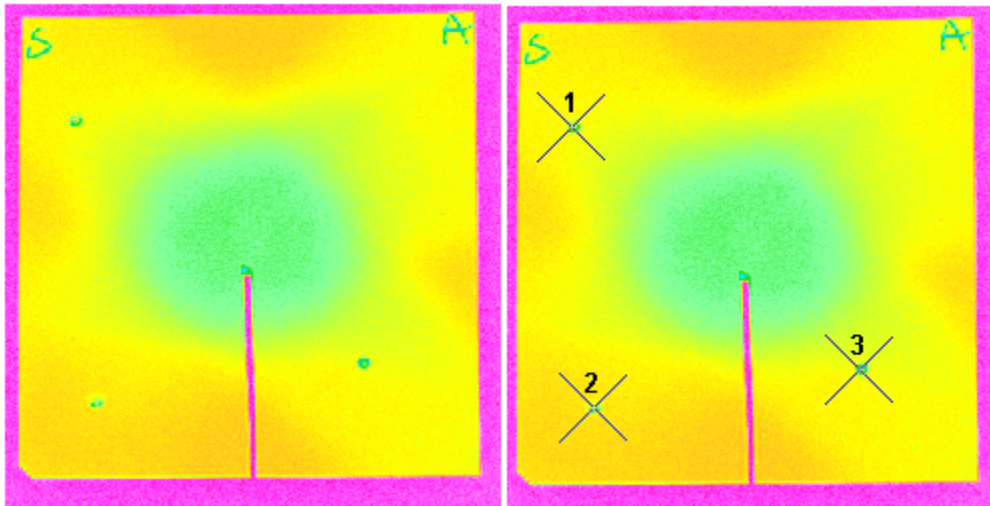


Figure 80: CyberKnife Sagittal Film

6.3.3 CyberKnife Film Gamma Analysis

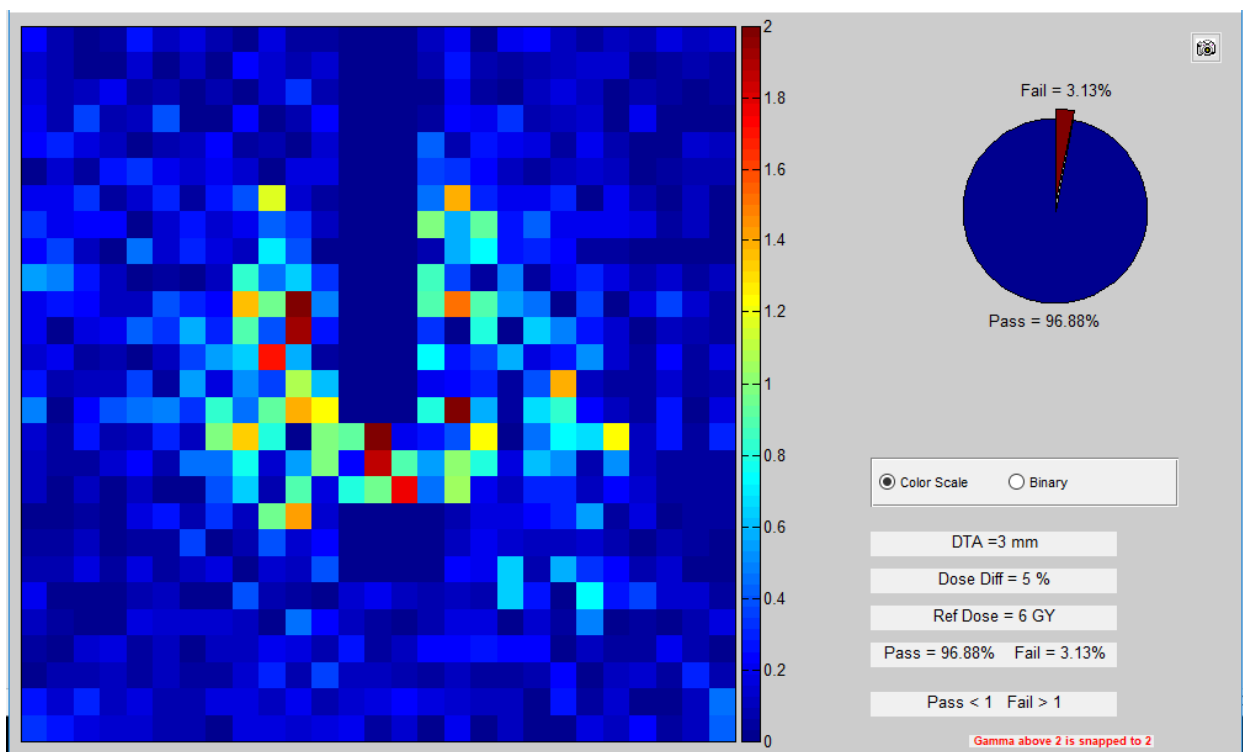


Figure 81. Coronal A

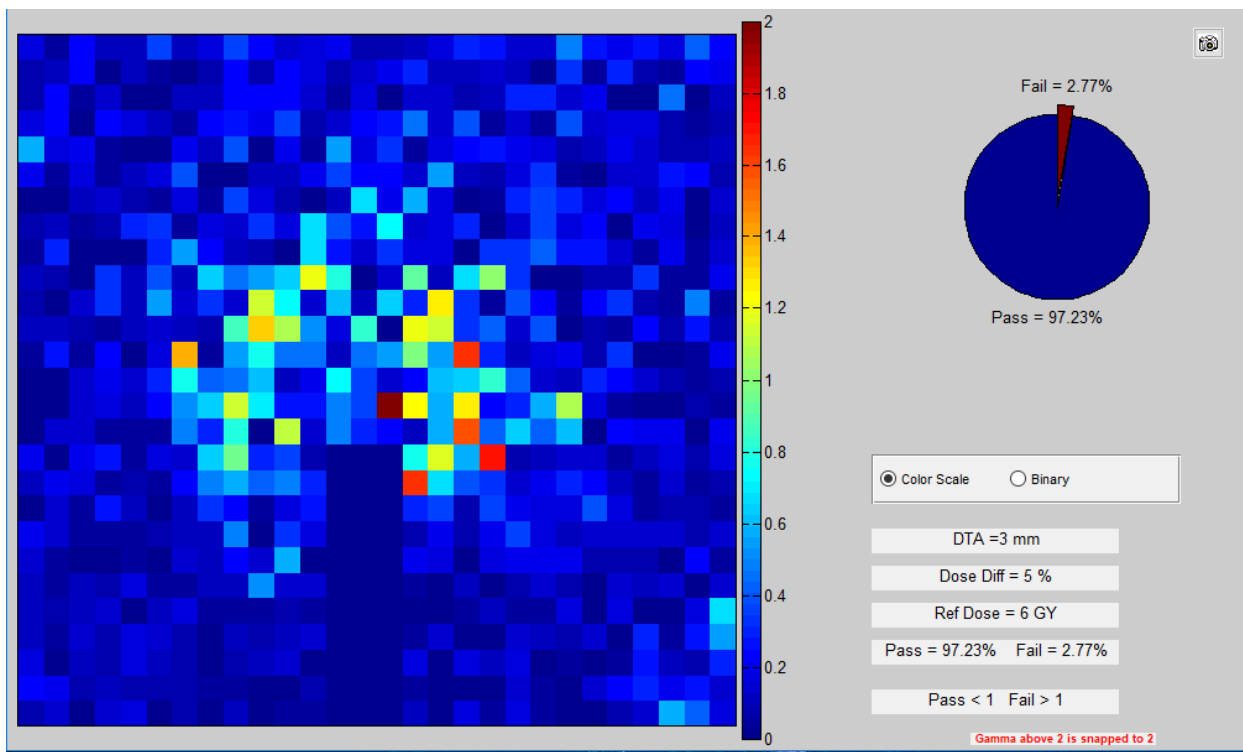


Figure 82. Sagittal A

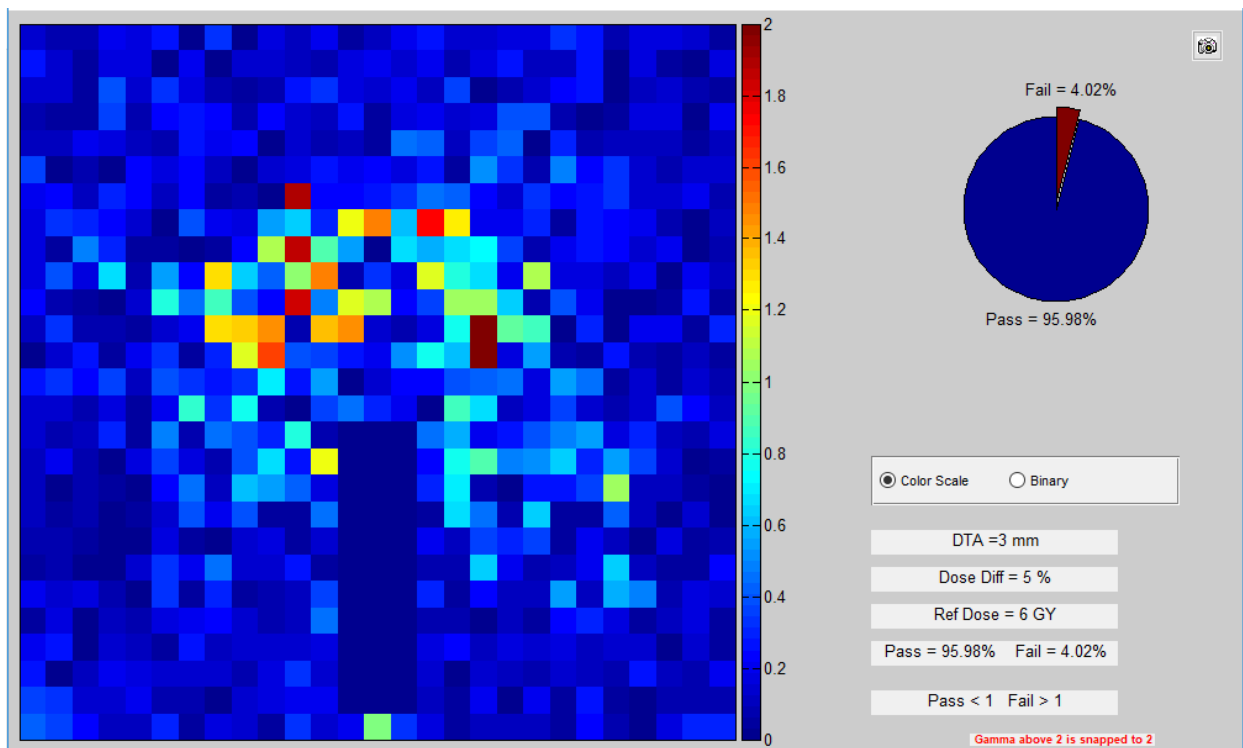


Figure 83. Coronal B

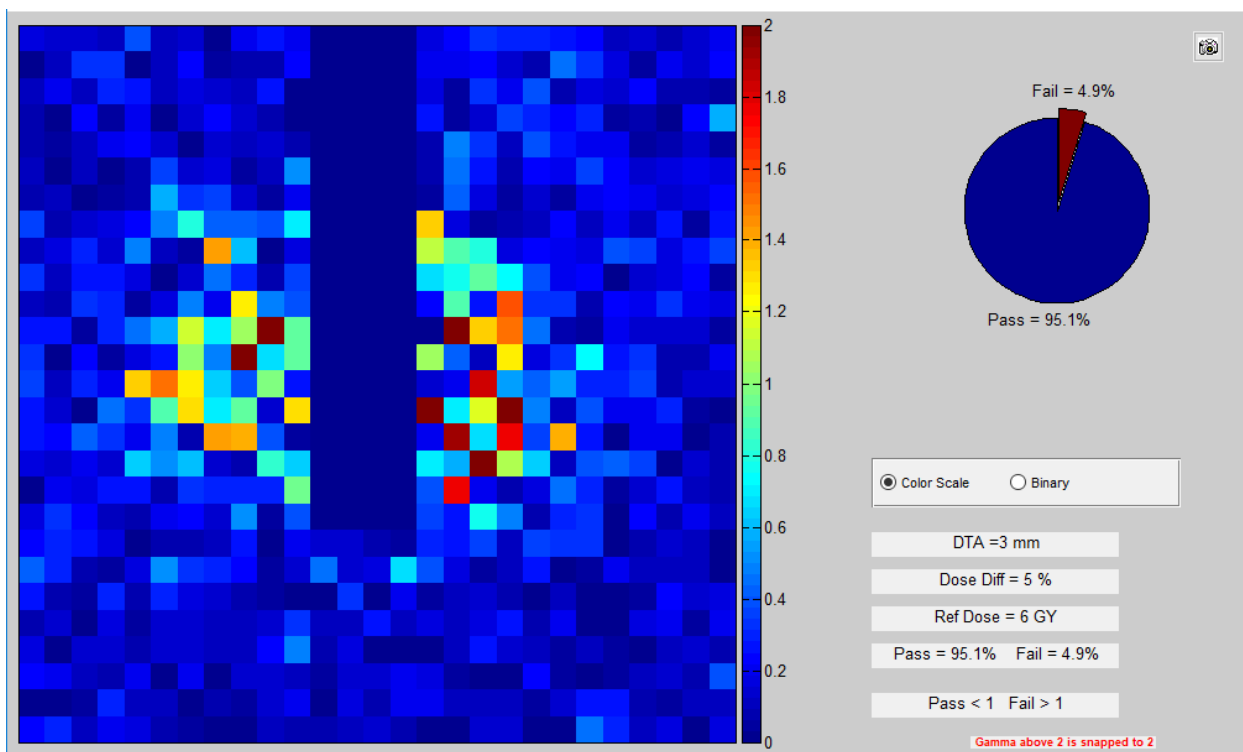


Figure 84. Sagittal B

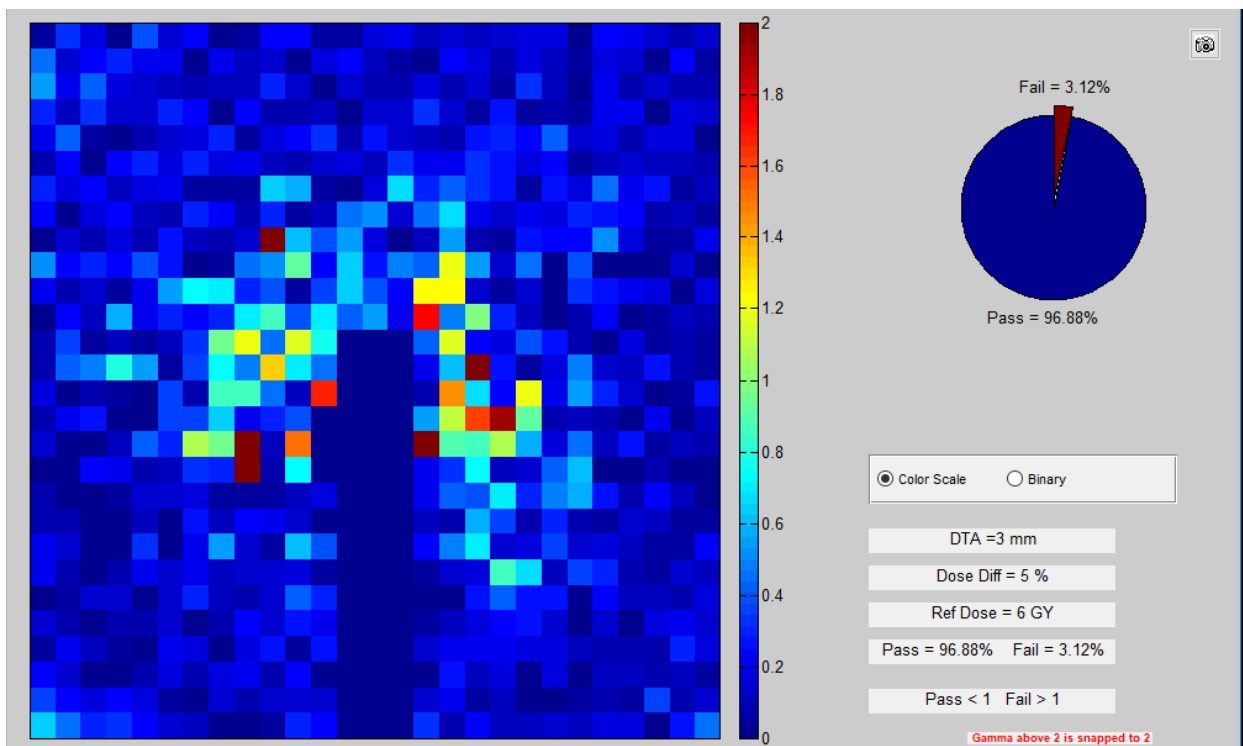


Figure 85. Coronal C

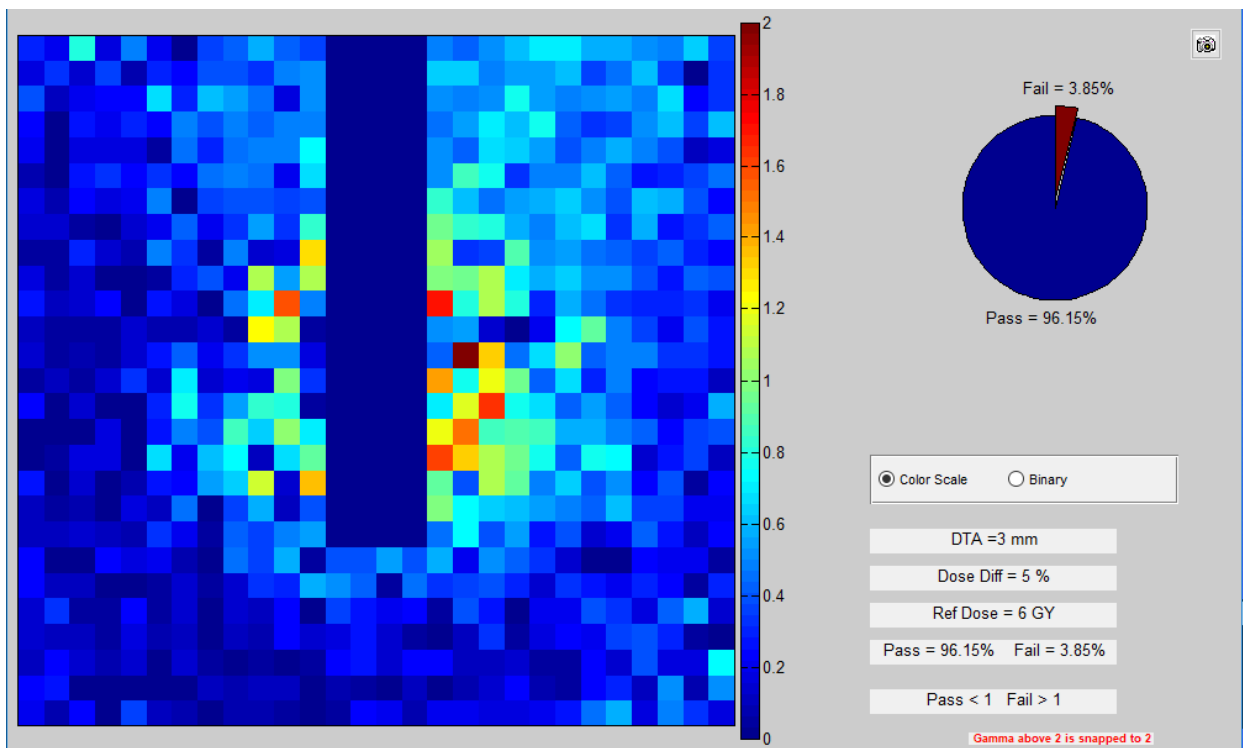
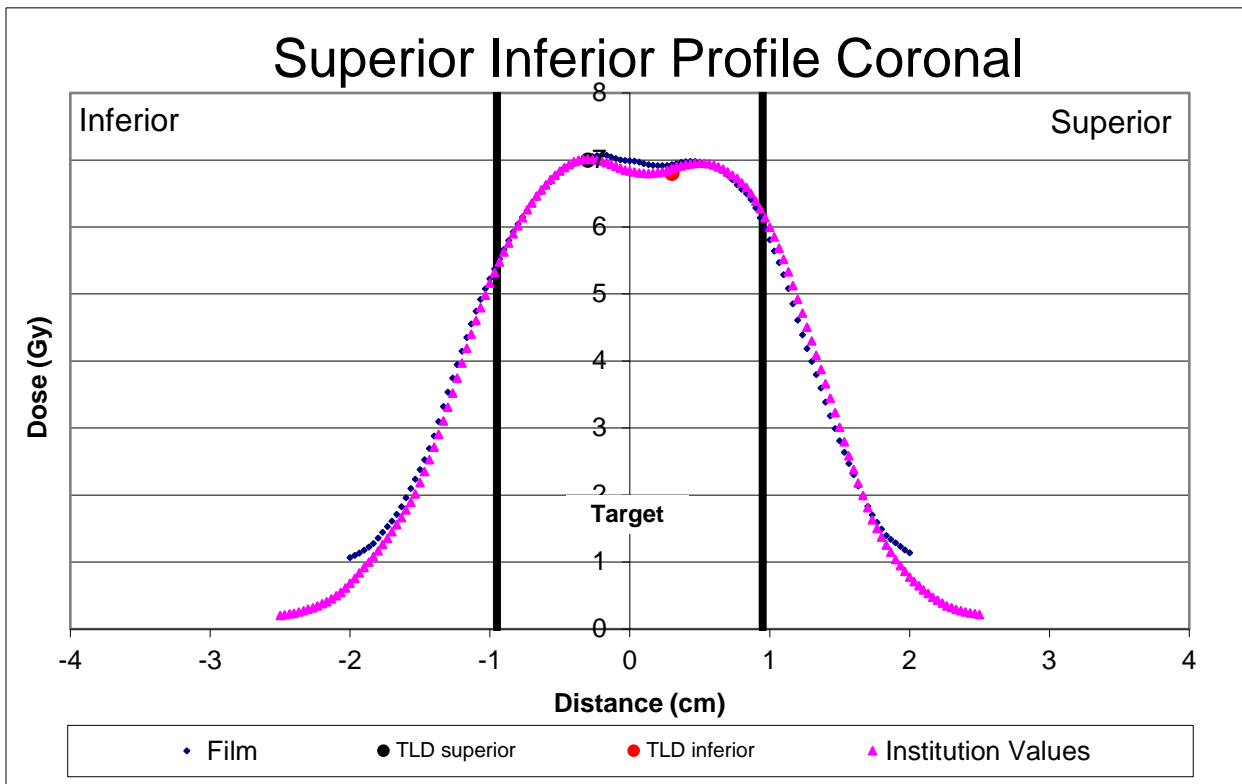
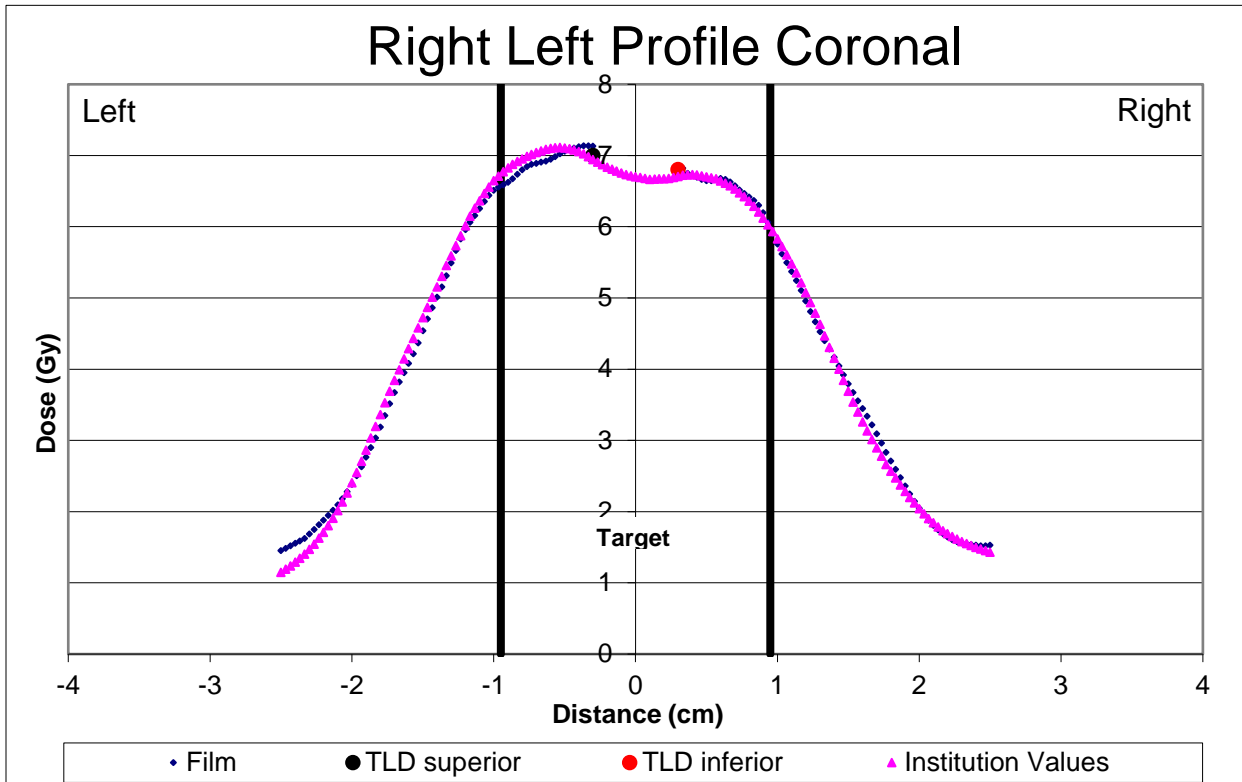
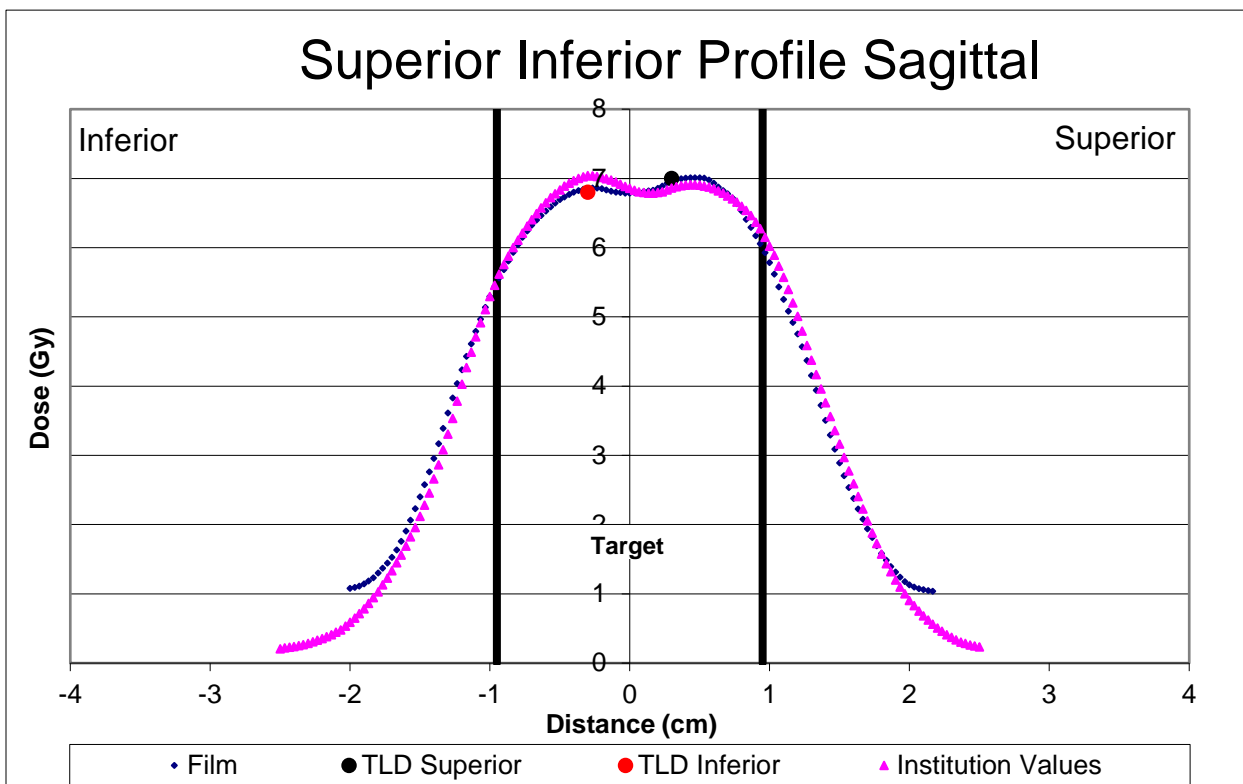
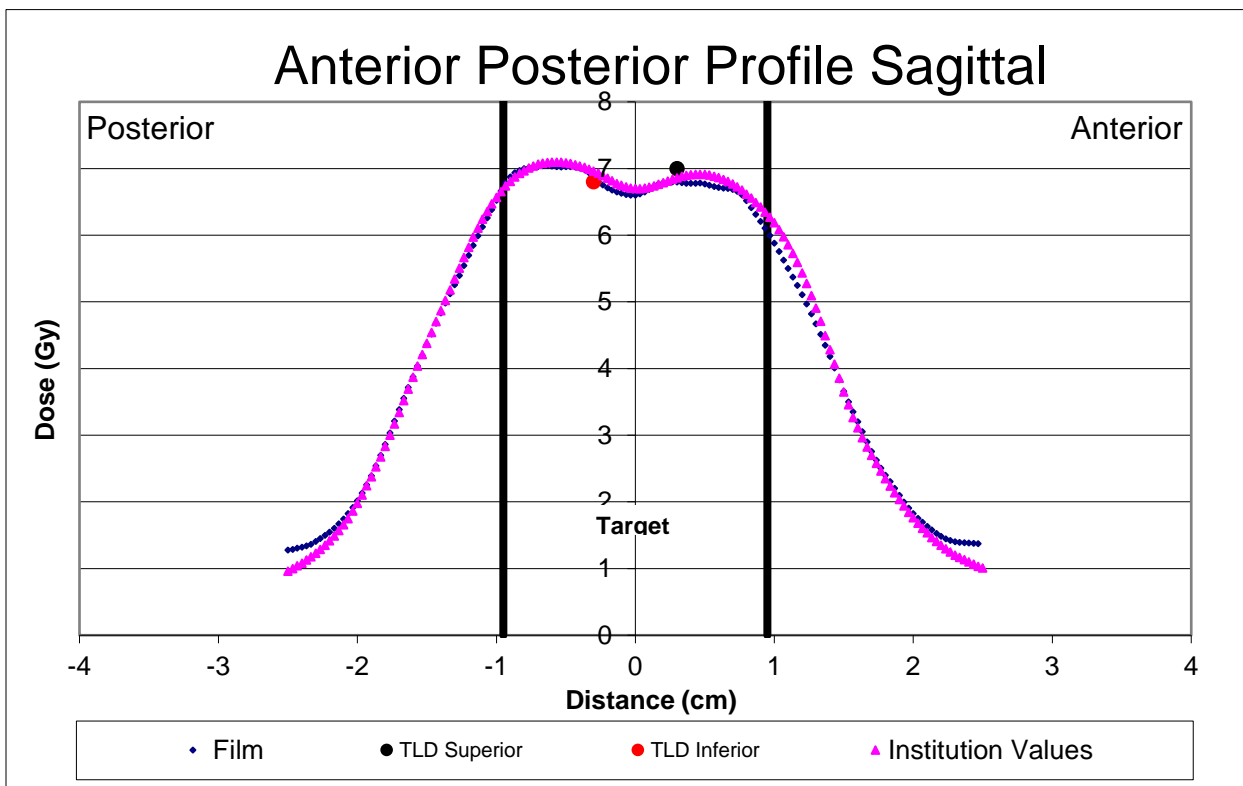
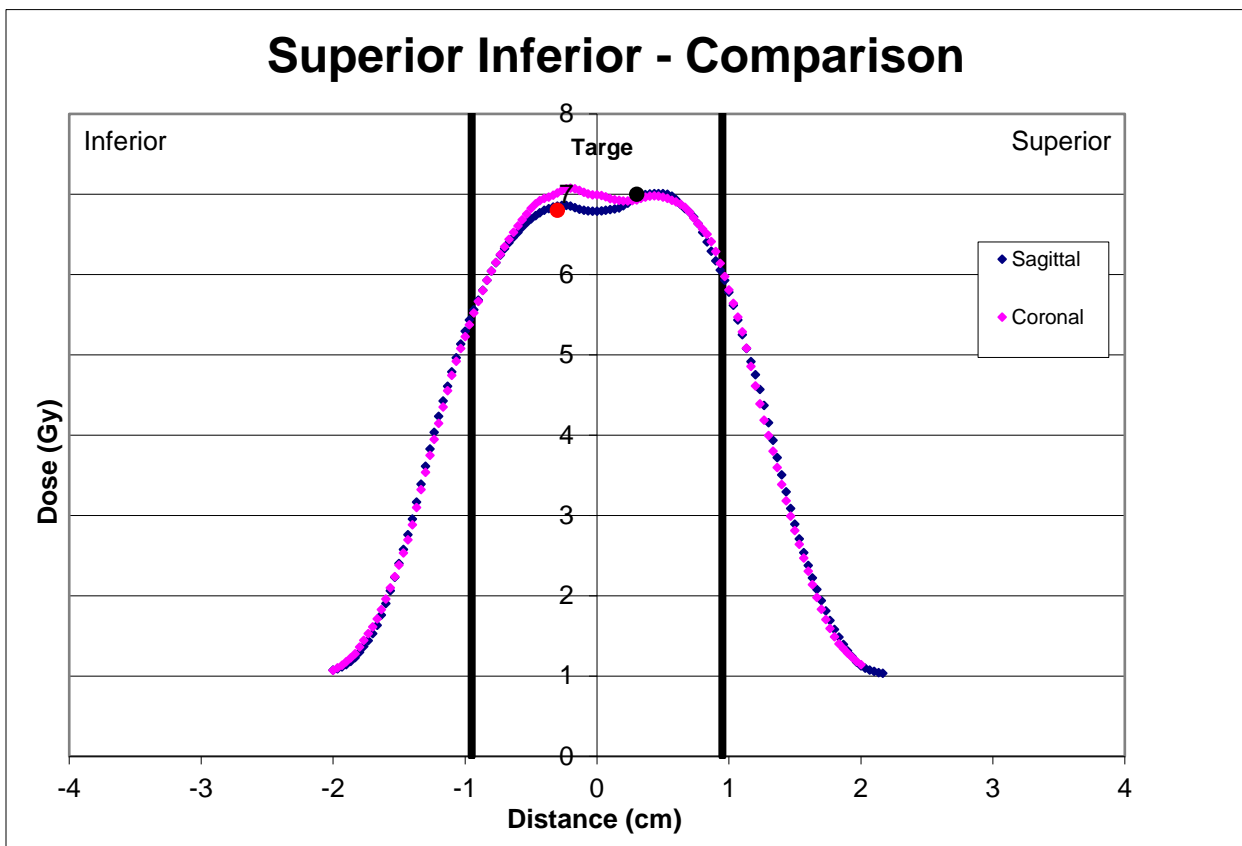


Figure 86. Sagittal C

6.3.4 CyberKnife Film/TPS dose Agreement

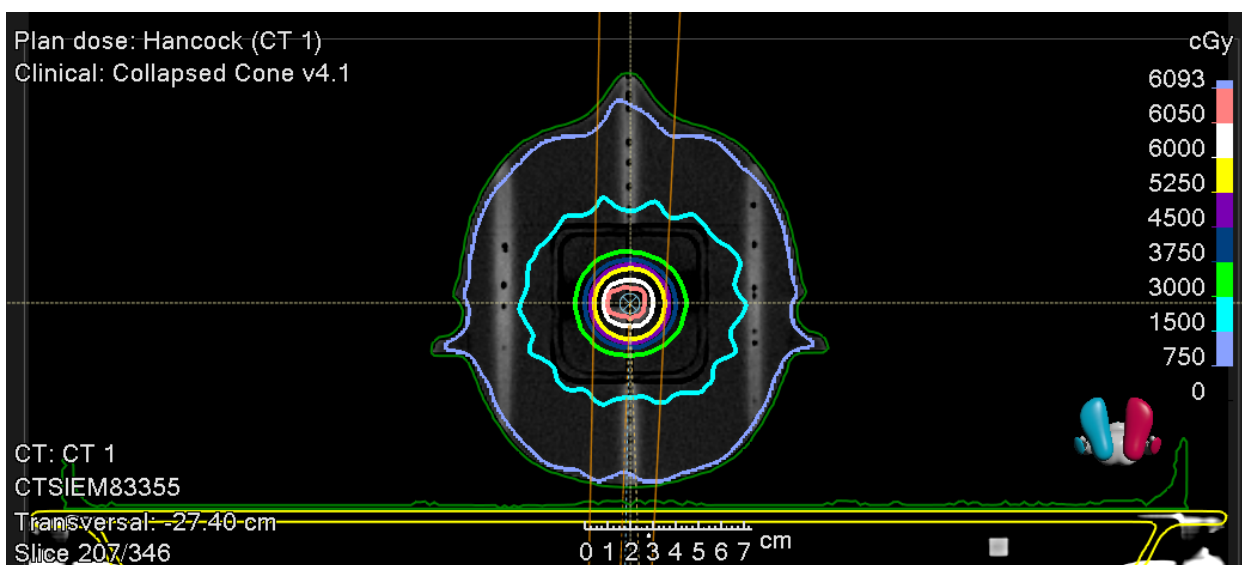


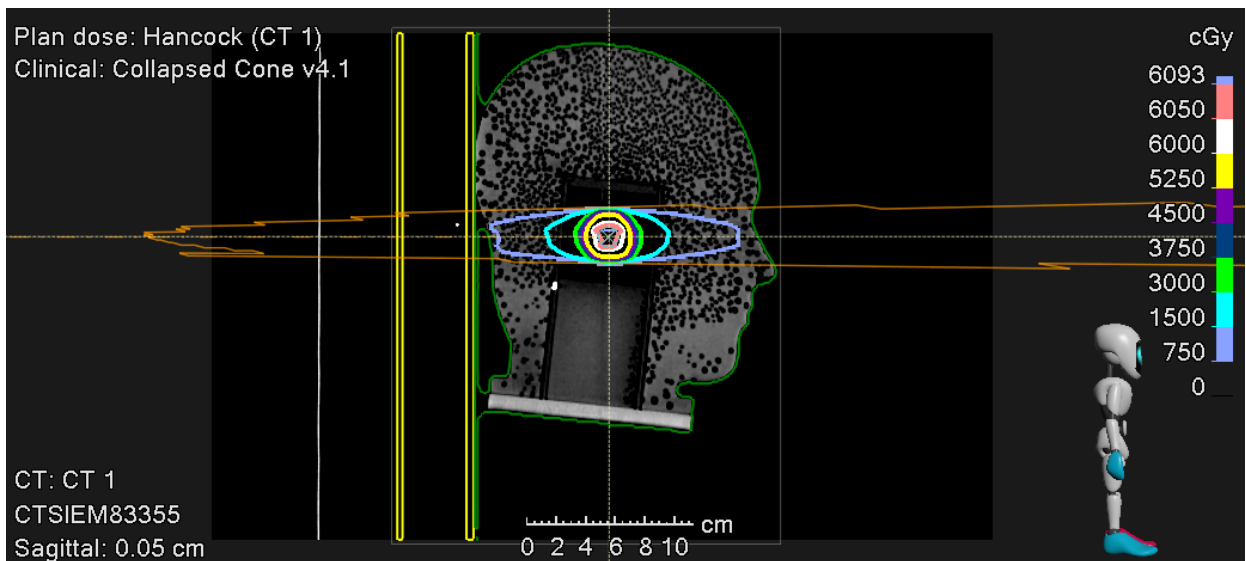
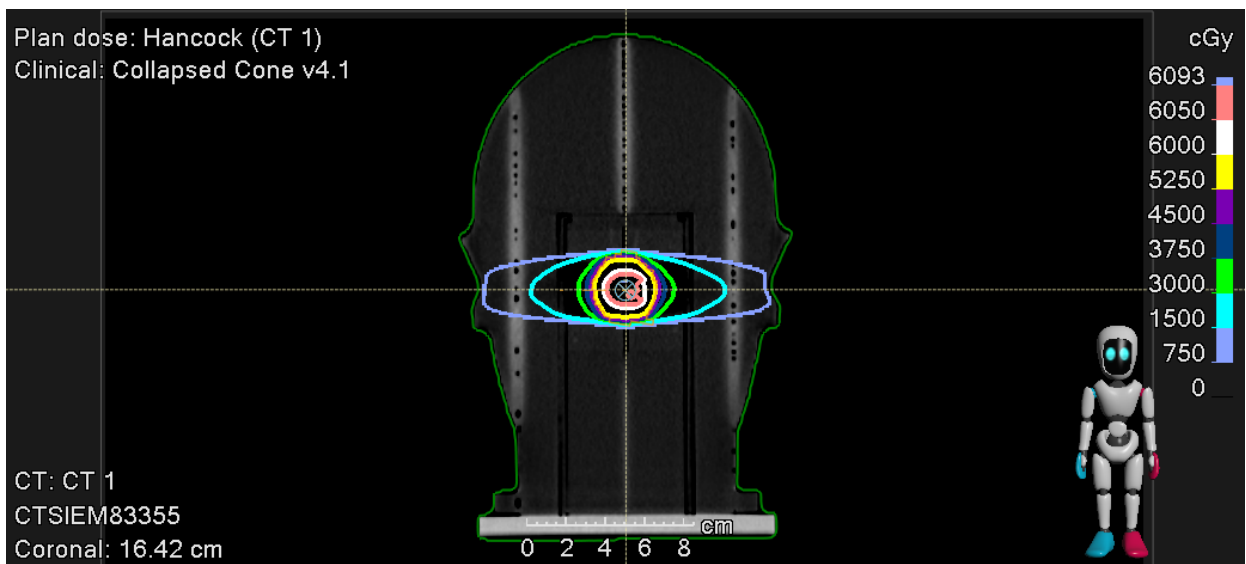




6.4 Linac

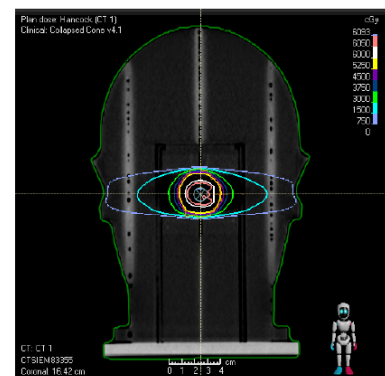
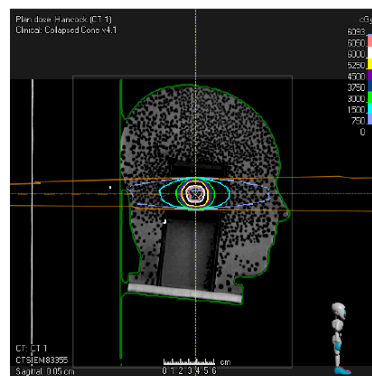
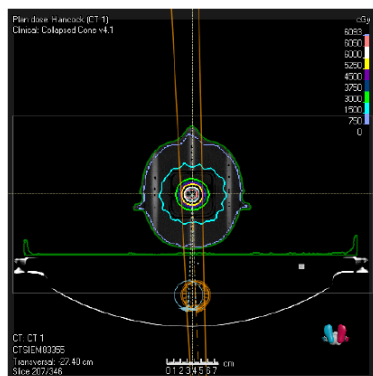
6.4.1 Linac Treatment Plan Snapshots and Isodose Lines

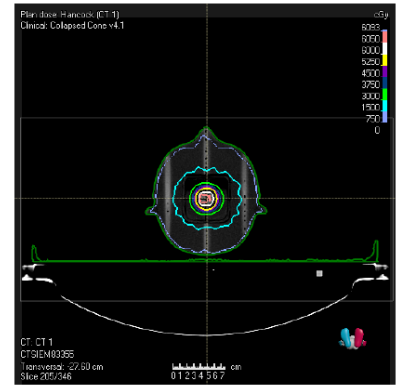
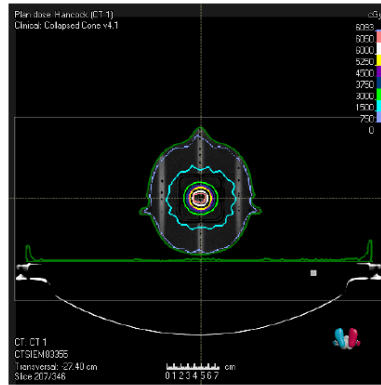
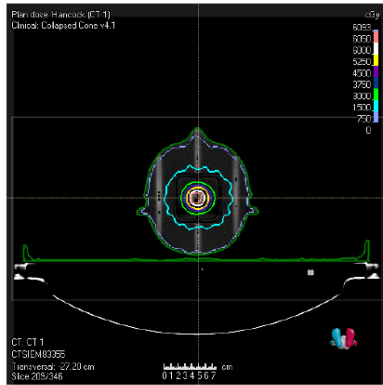
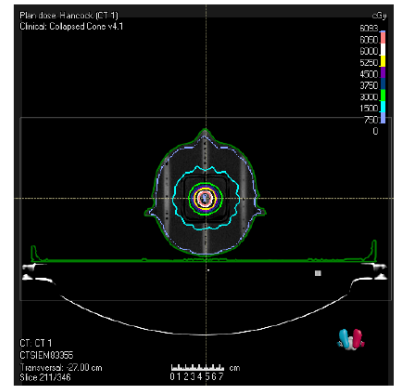
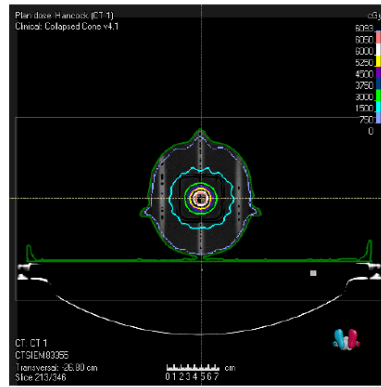
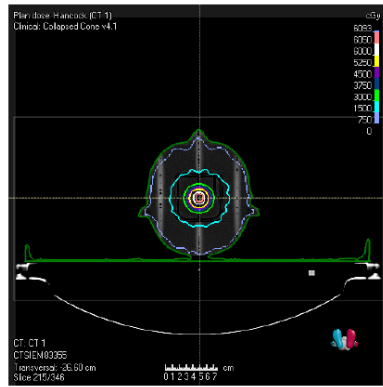
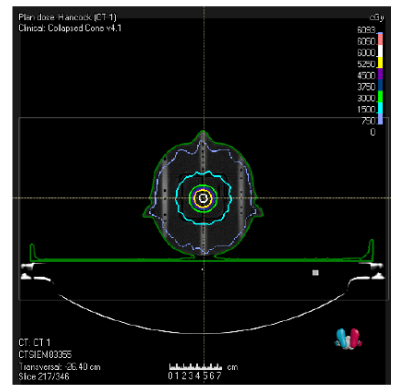
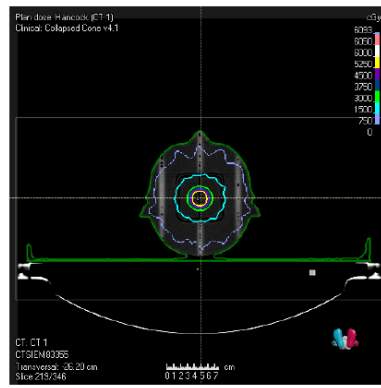
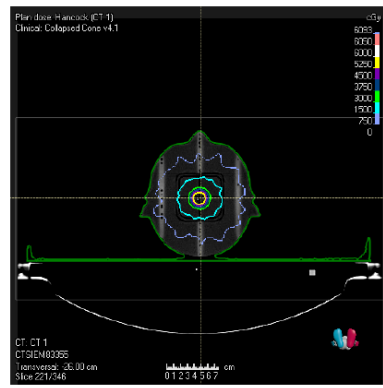
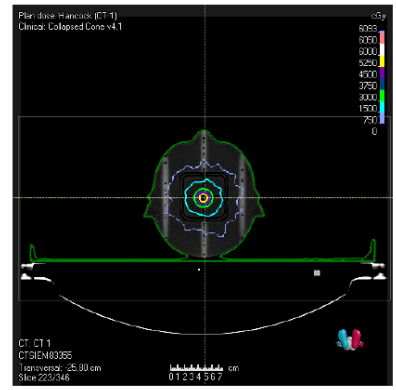
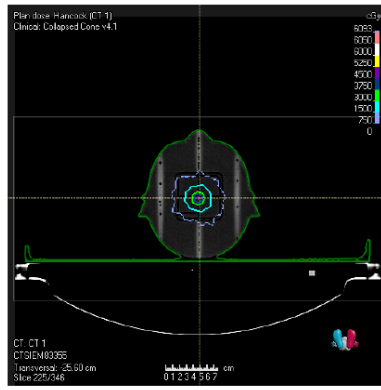
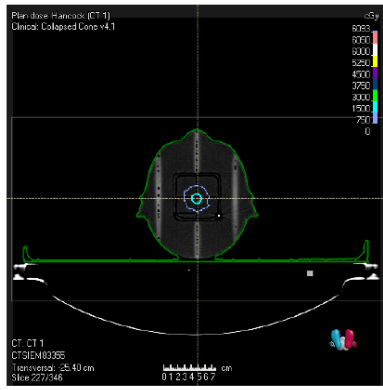


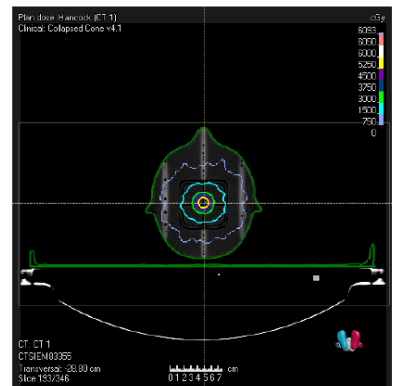
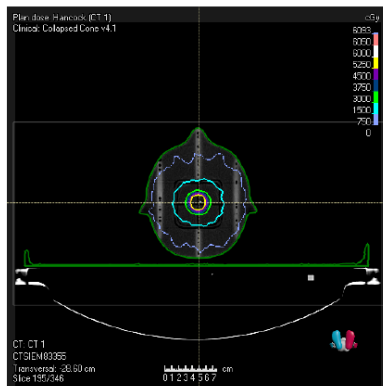
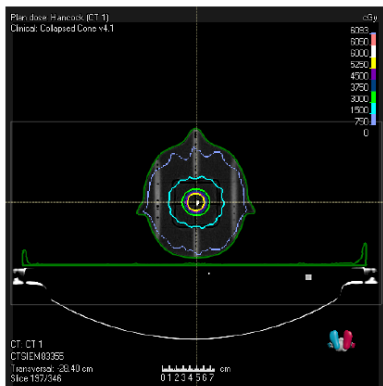
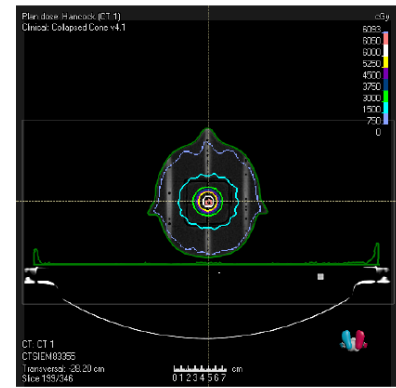
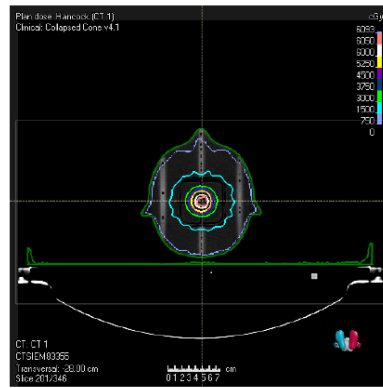
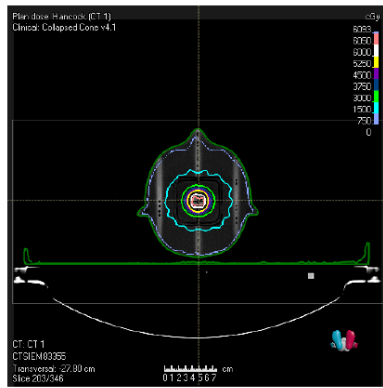


Modality: Photons
Energy: 6.0 MV
Treatment Device: DynamicArc
Number of Beams: 2

Hancock: 6000 cGy (600 cGy @ 10 Fx) to 99.0% of the Average for GTV





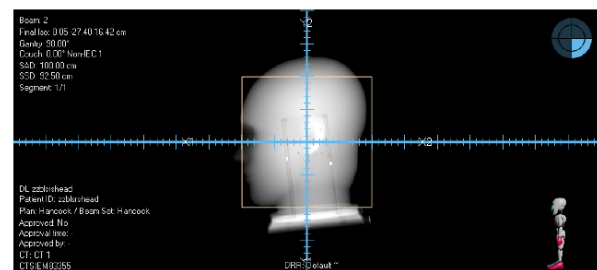
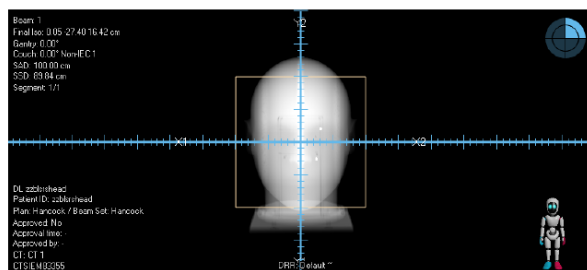


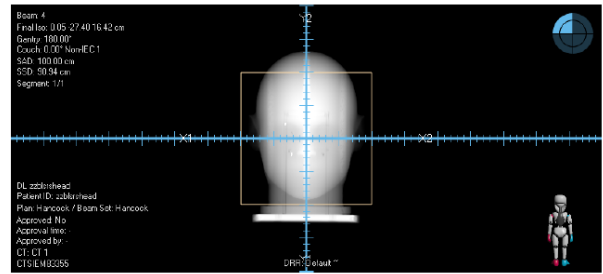
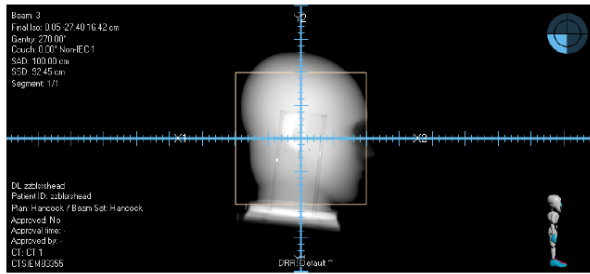
ROI Dose statistics [Beam Set dose]

Name	Volume [cm³]	D99 [cGy]	D98 [cGy]	D95 [cGy]	Average [cGy]	D50 [cGy]	D2 [cGy]	D1 [cGy]	% outside grid
*Skull									
CTV2mm	5.95	5999	6005	6016	6053	6055	6092	6094	0
External	4891.53	0	0	0	231	19	2028	2969	0
fsBody	4430.31	0	0	0	251	21	2137	3147	0
GTV	3.32	6036	6039	6043	6064	6061	6094	6095	0
infLAntTLD	0.02	6047	6047	6049	6054	6053	6067	6069	0
InfTLD	0.06	6049	6049	6050	6057	6055	6078	6079	0
Normal	4378.39	0	0	0	202	20	1707	2090	0
PTV2mm	9.69	5905	5921	5944	6026	6037	6089	6093	0
Ring1cm	99.86	129	141	164	1555	1880	3055	3137	0
supRpostTLD	0.04	6060	6060	6061	6081	6084	6093	6094	0
SupTLD	0.06	6055	6056	6057	6076	6079	6094	6094	0

 External

This ROI is set as the external ROI that defines the outer border of the patient





6.4.2 Linac Film

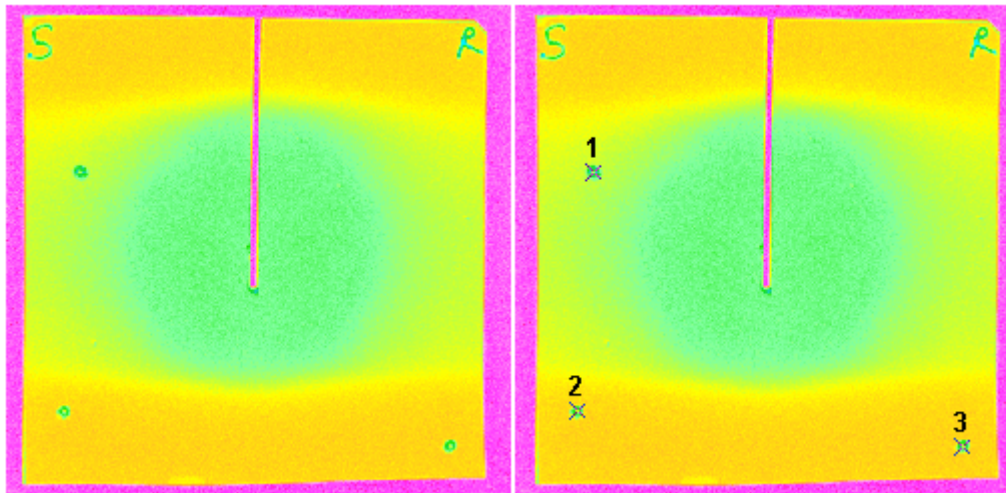


Figure 87: Linac Coronal Film

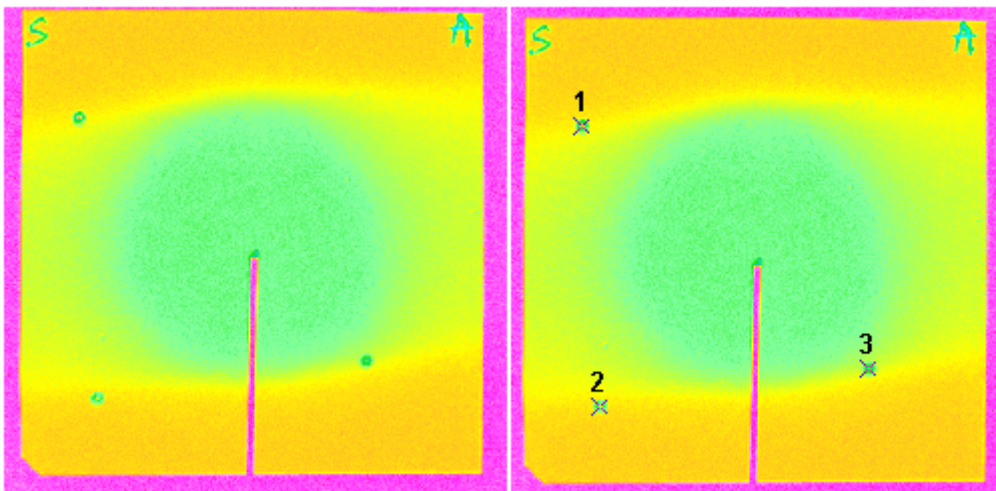


Figure 88: Linac Sagittal Film

6.4.3 Linac Film Gamma Analysis

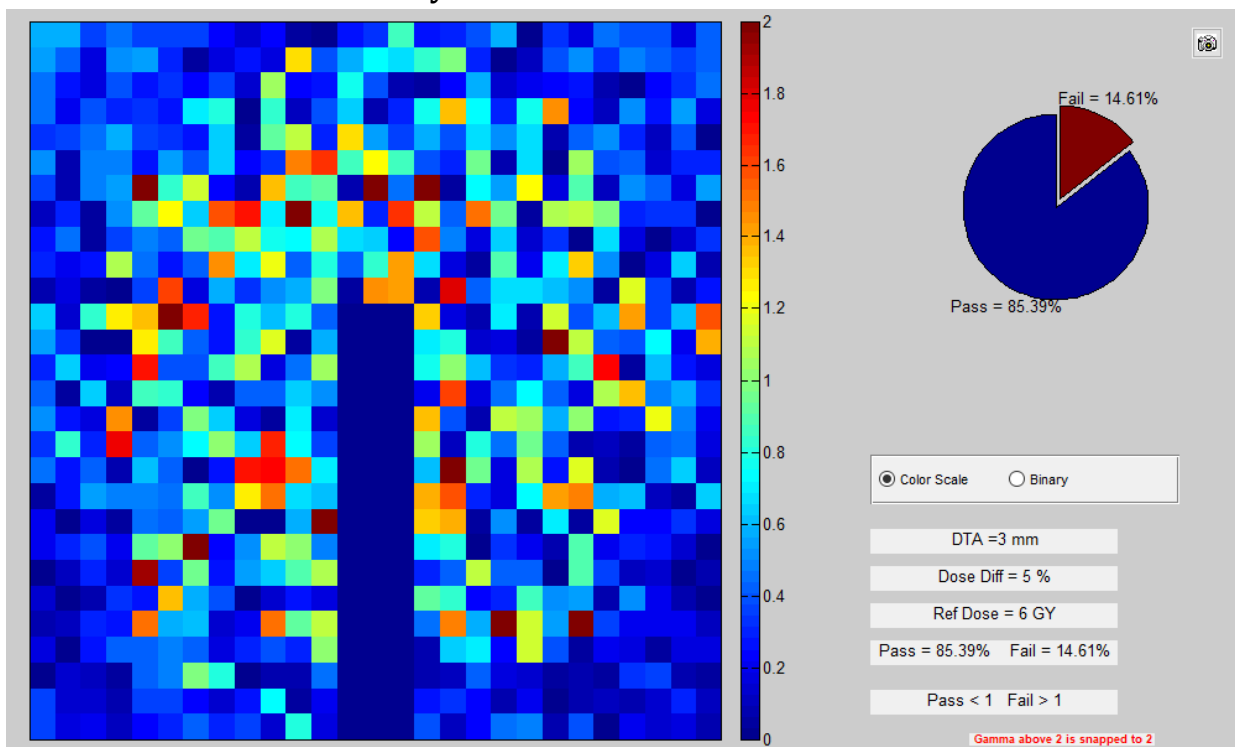


Figure 89: Linac Coronal A

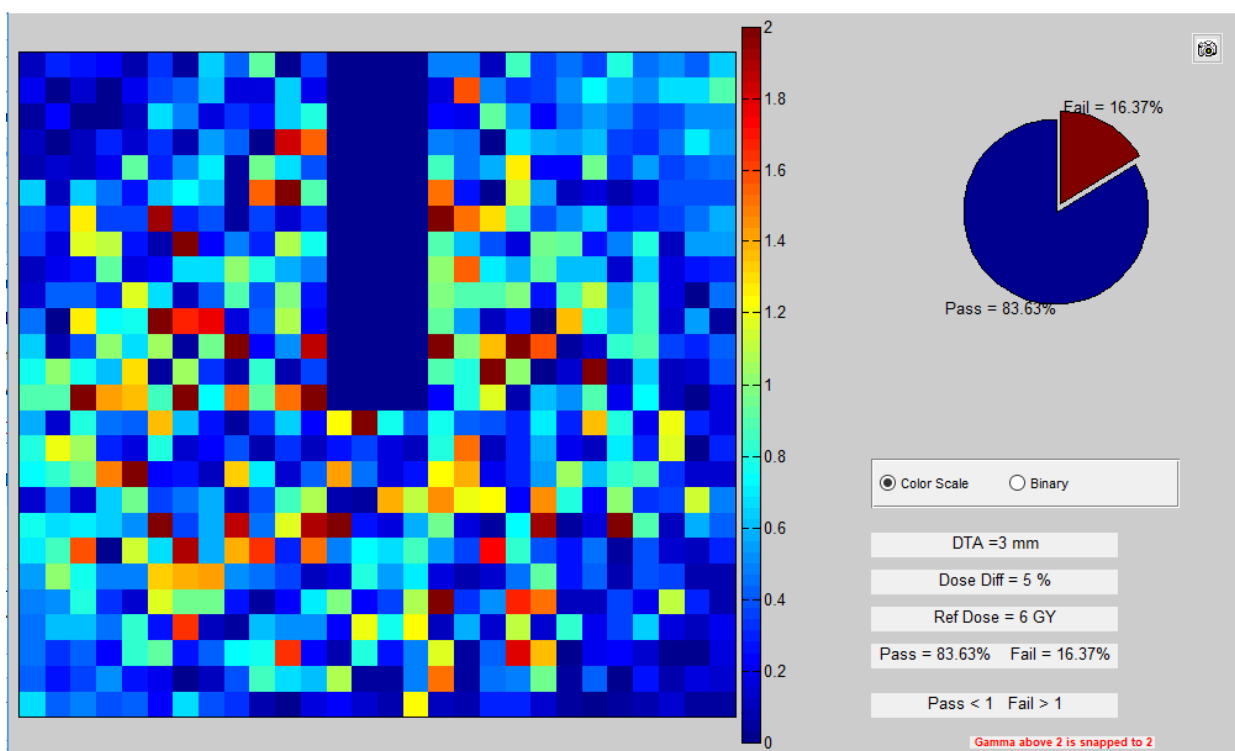


Figure 90: Linac Sagittal A

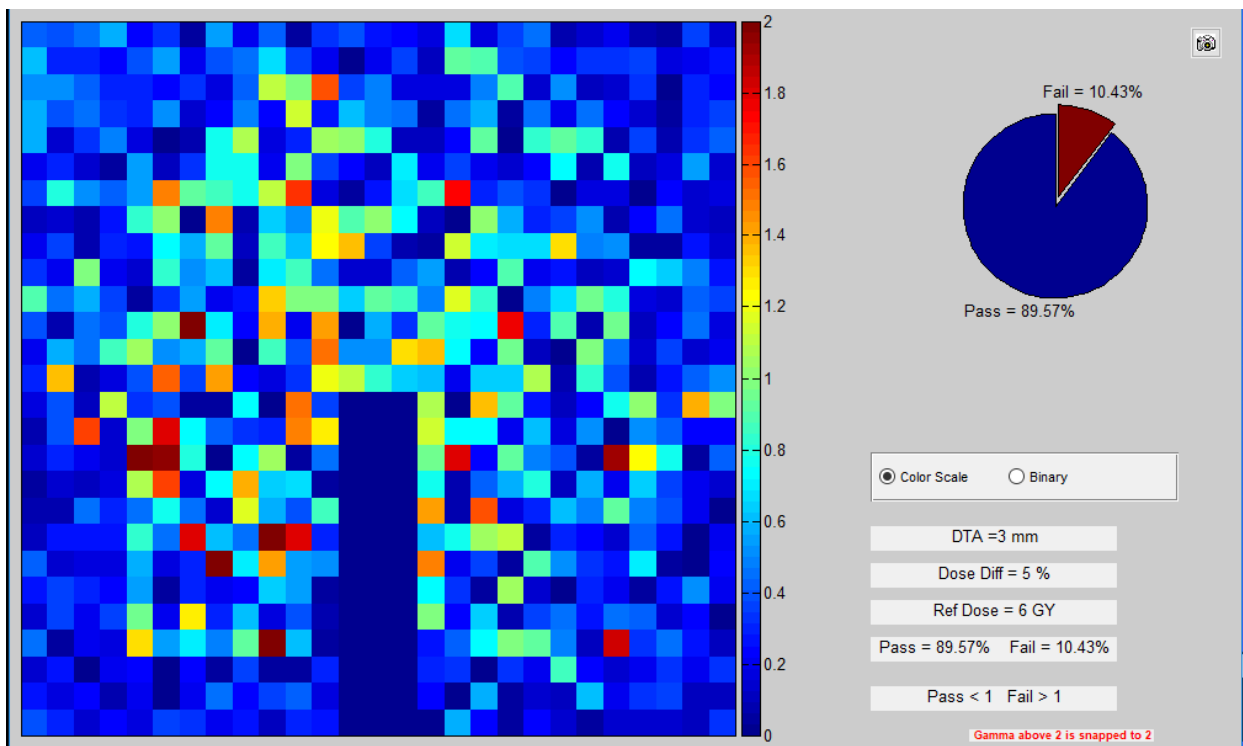


Figure 91: Coronal B

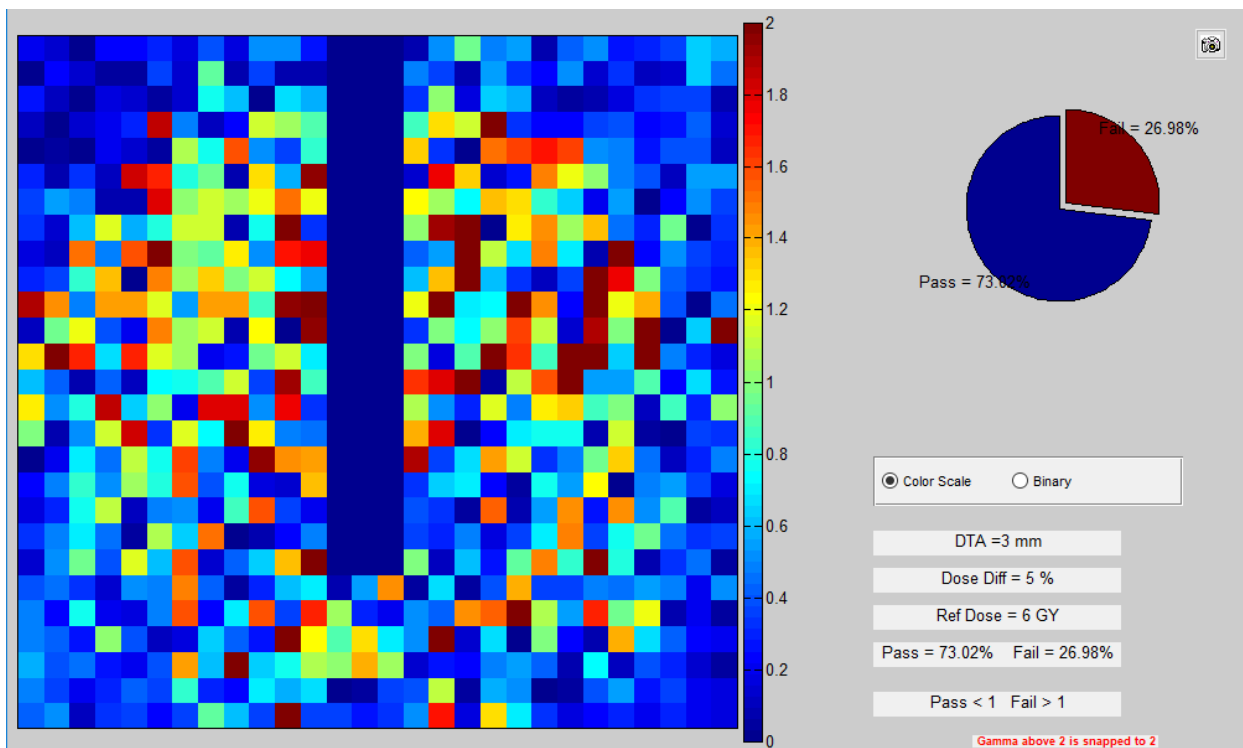


Figure 92: Sagittal A

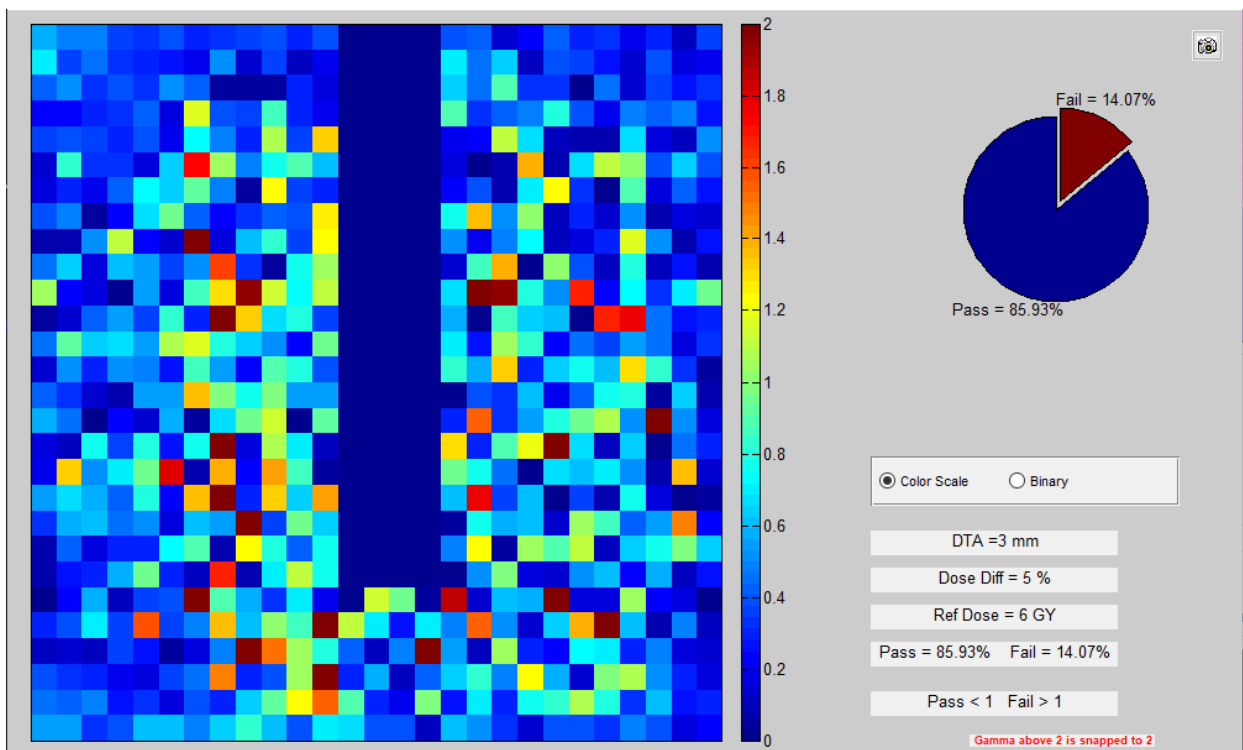


Figure 93: Coronal C

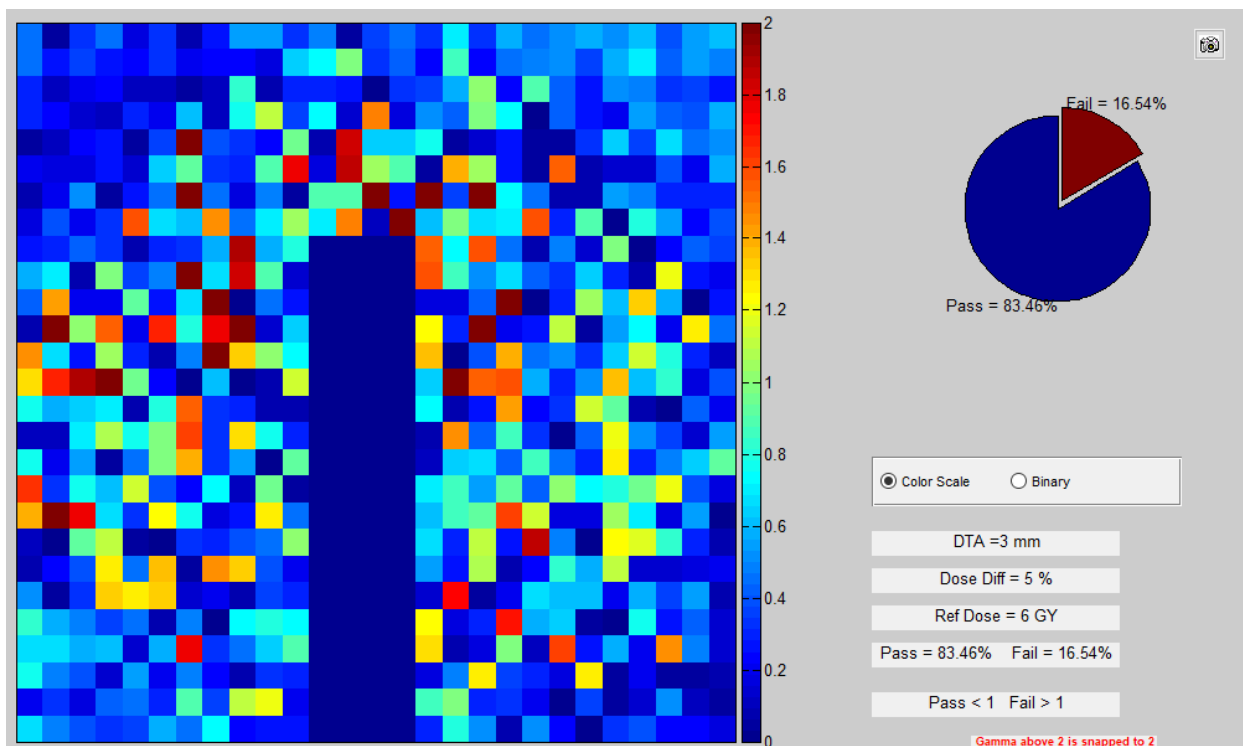
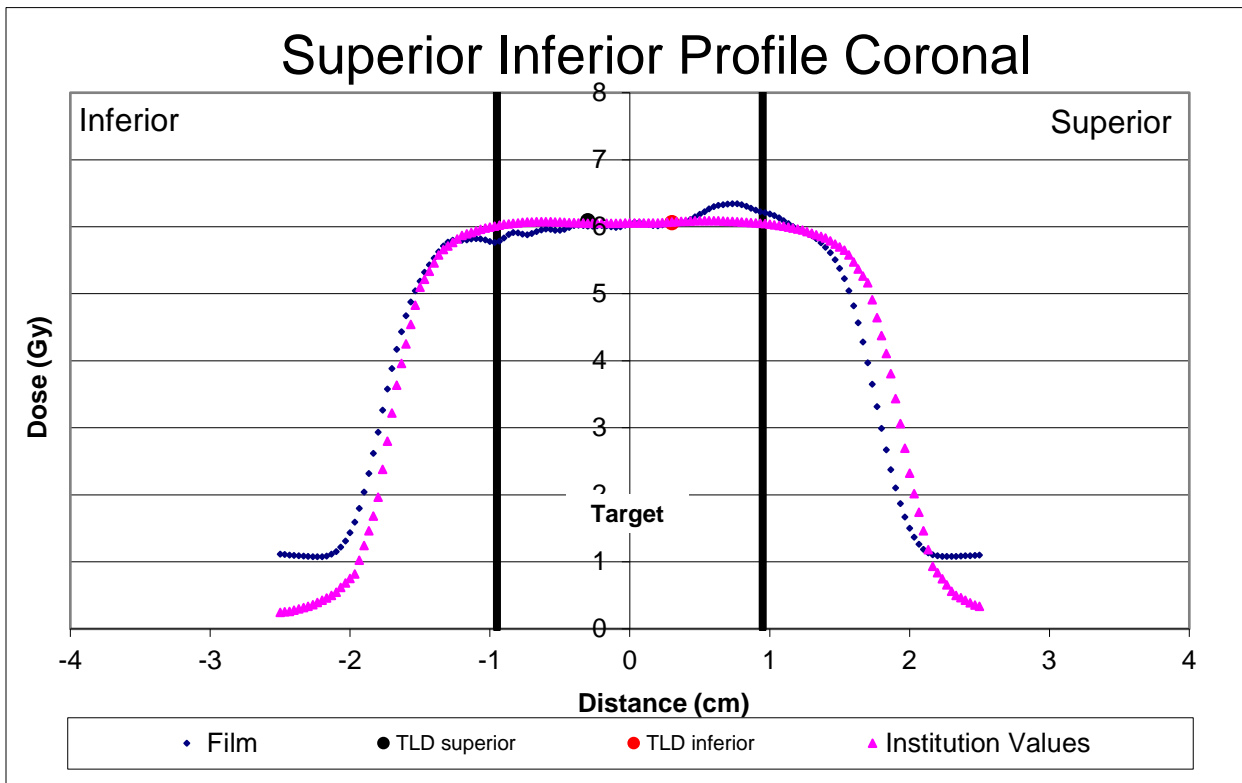
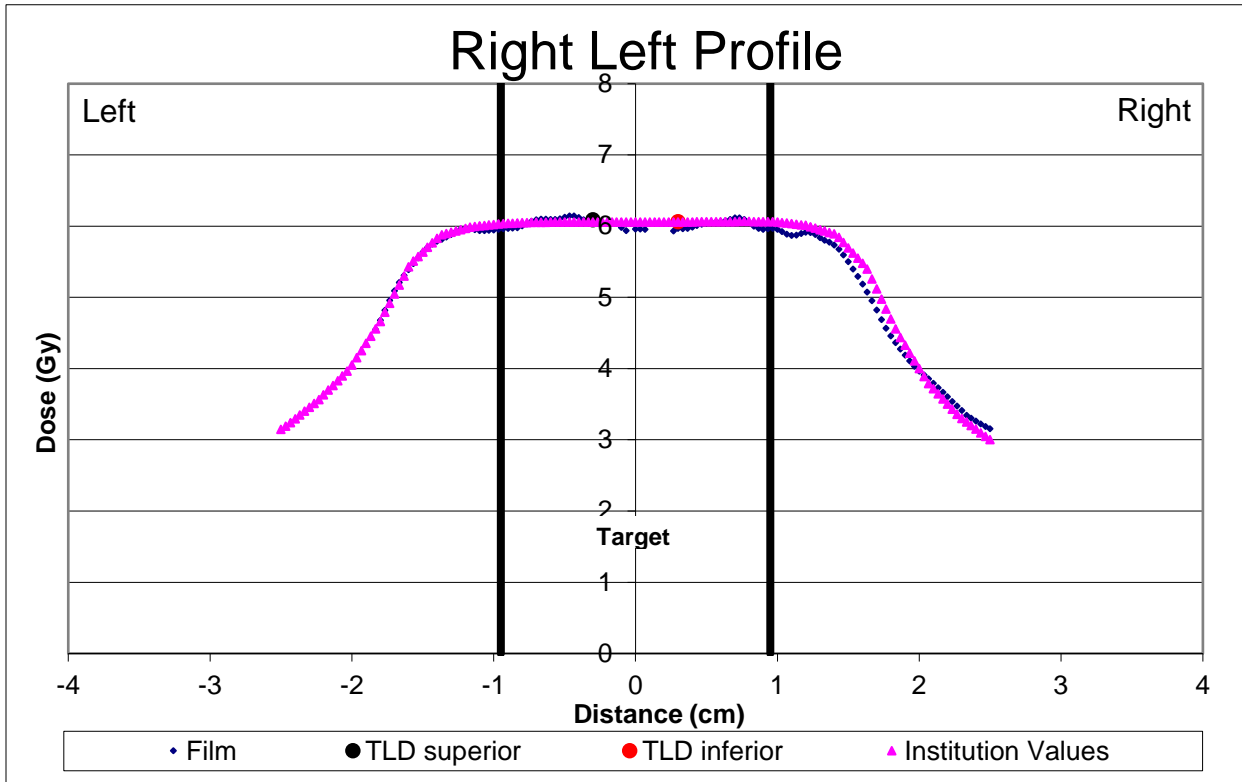
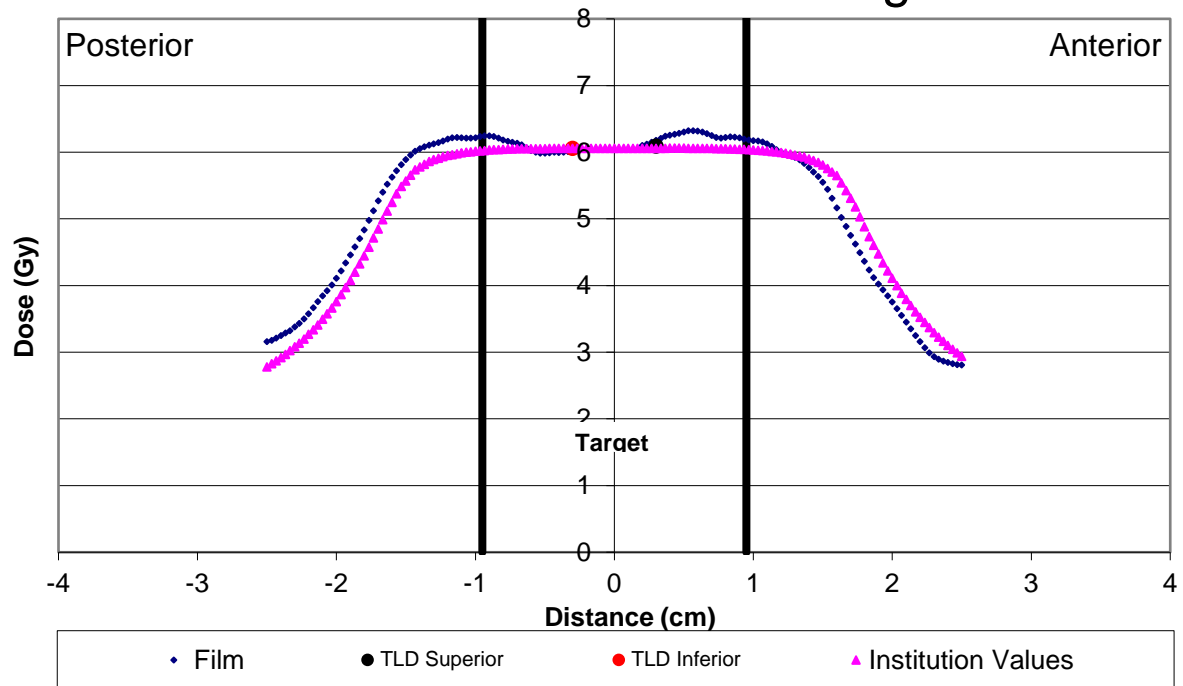


Figure 94: Sagittal C

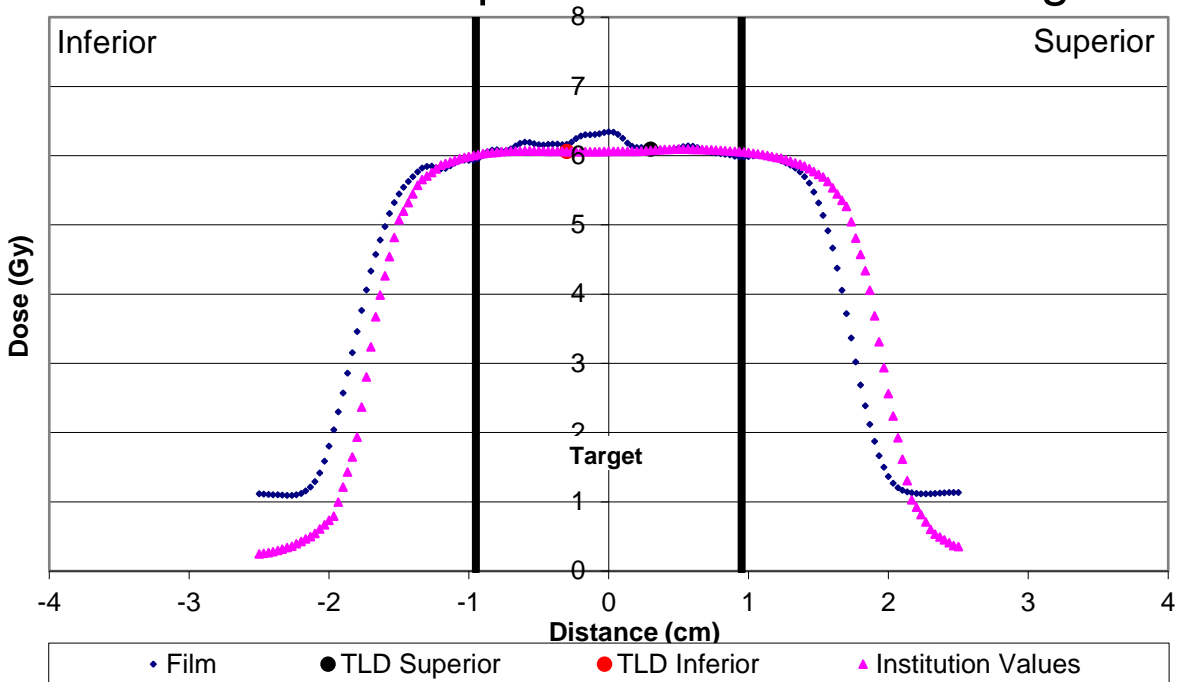
6.4.3 Linac Film/TPS dose Line Profiles

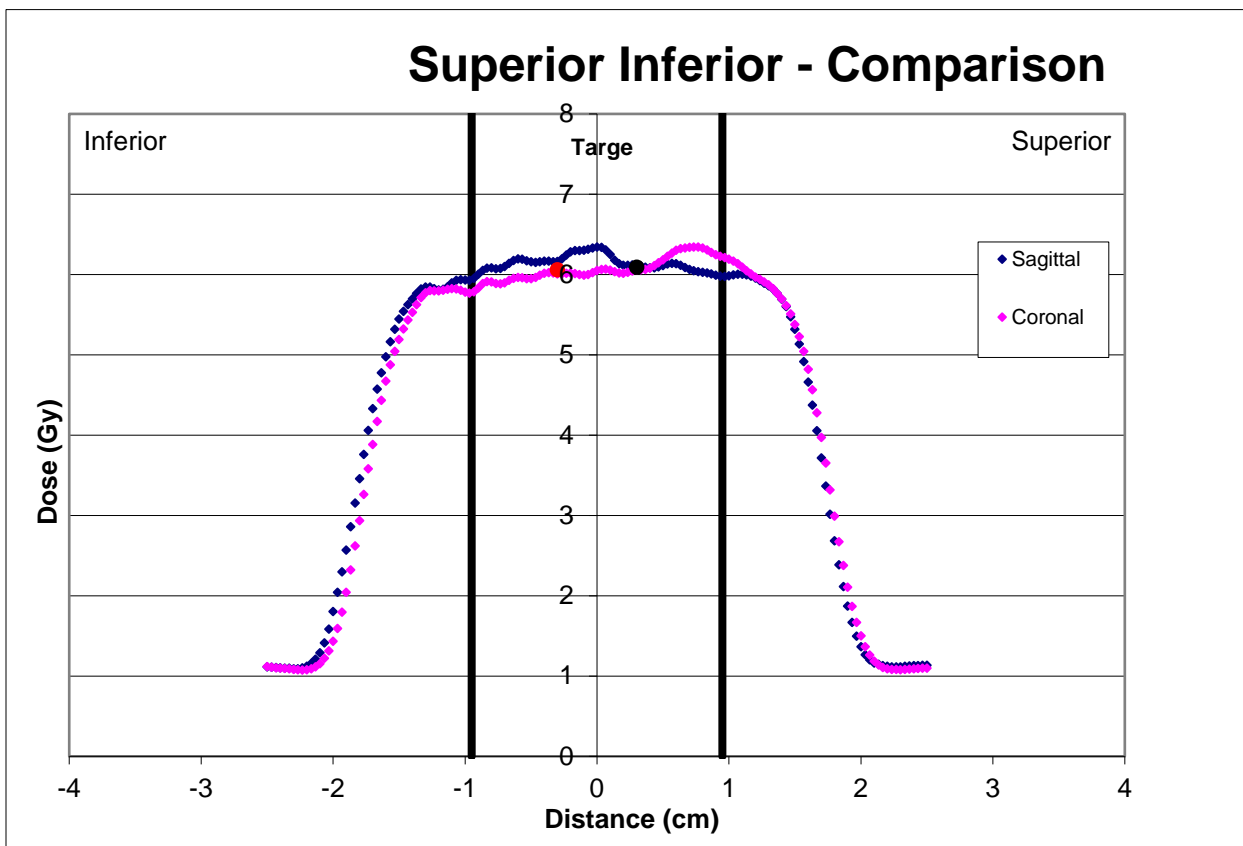


Anterior Posterior Profile Sagittal

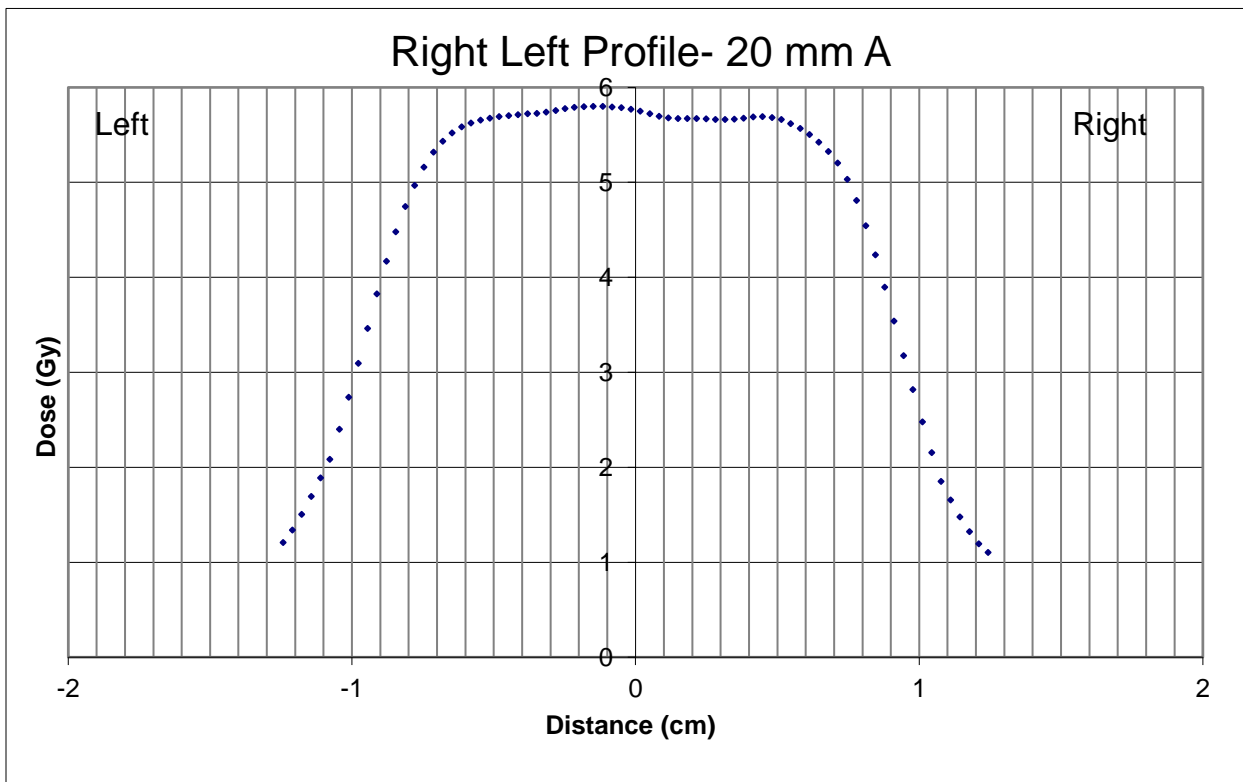


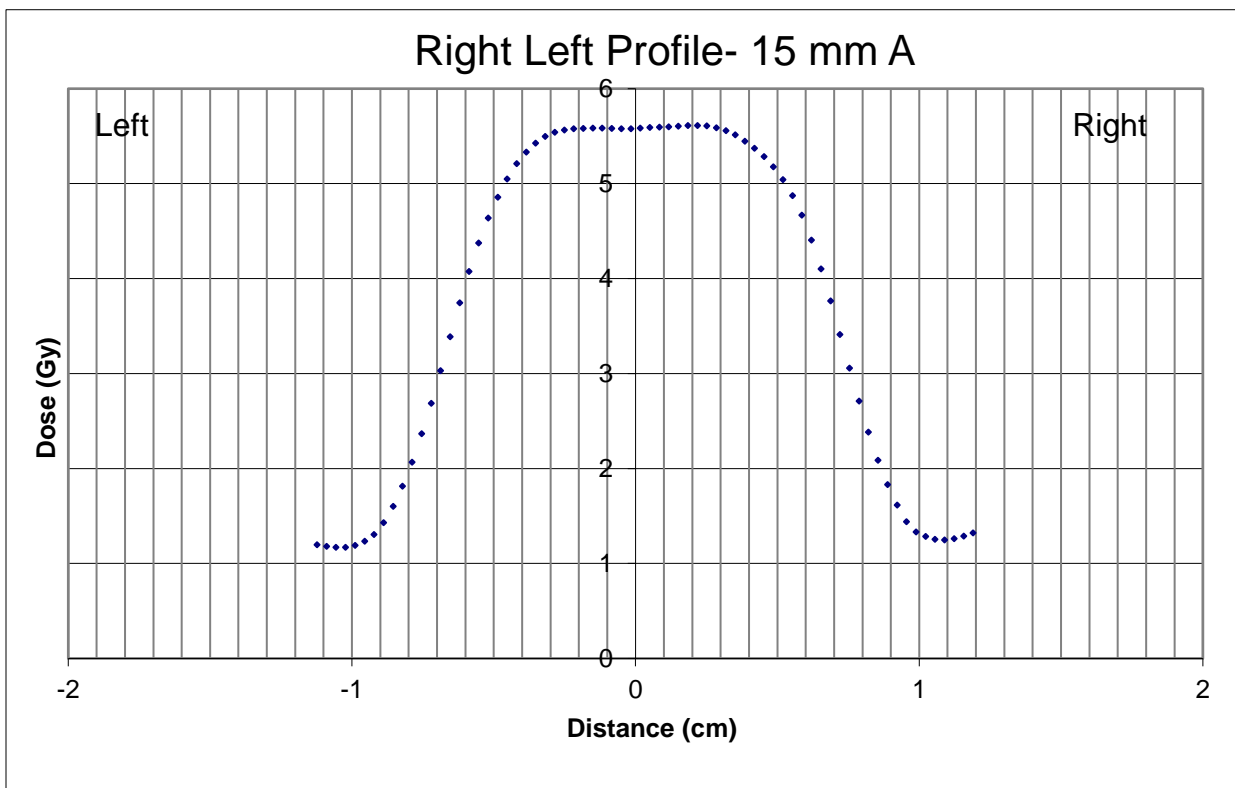
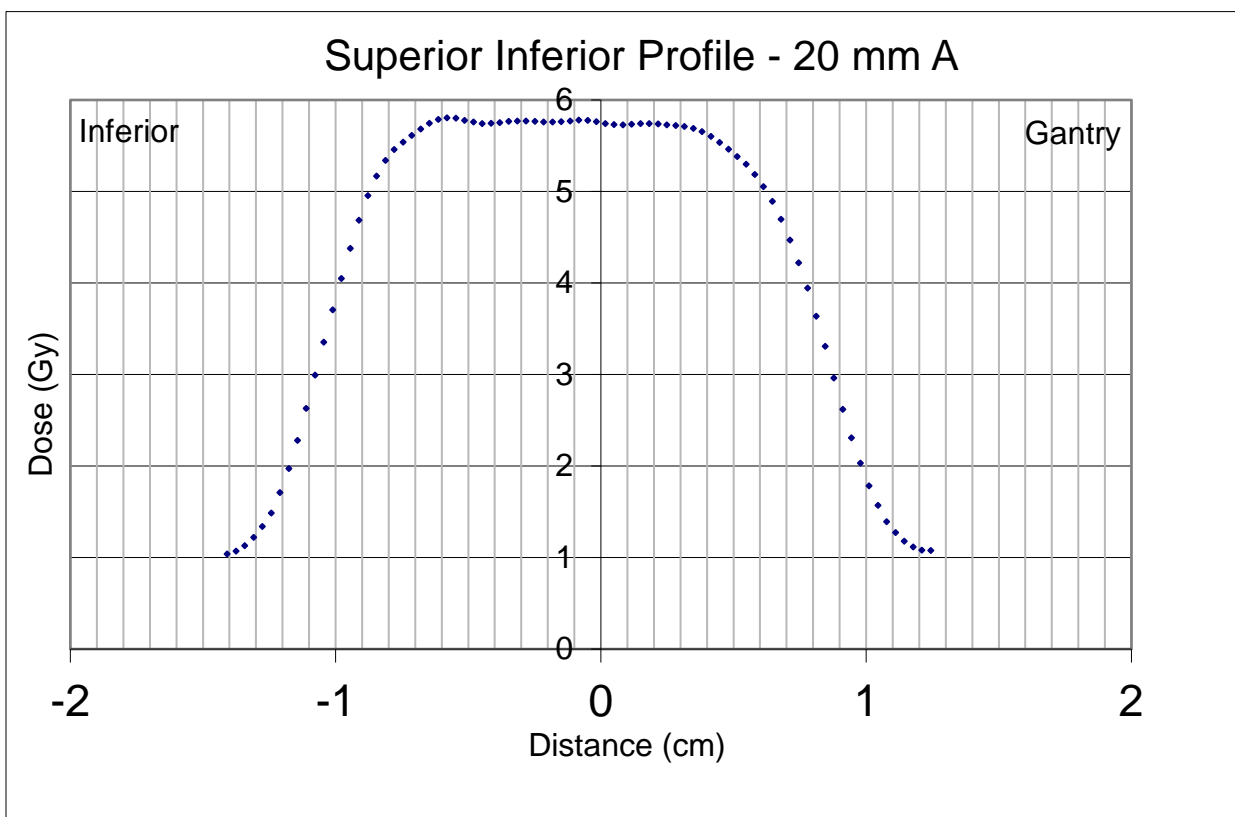
Superior Inferior Profile Sagittal

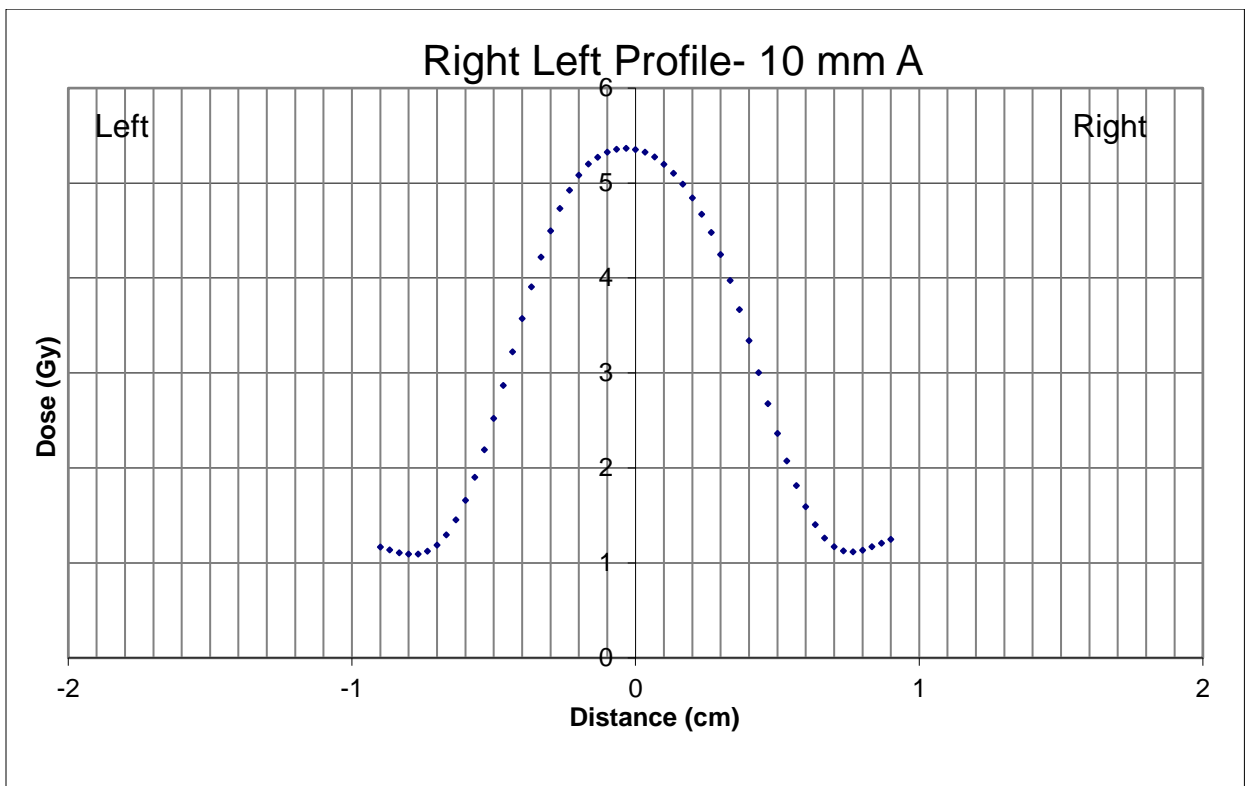
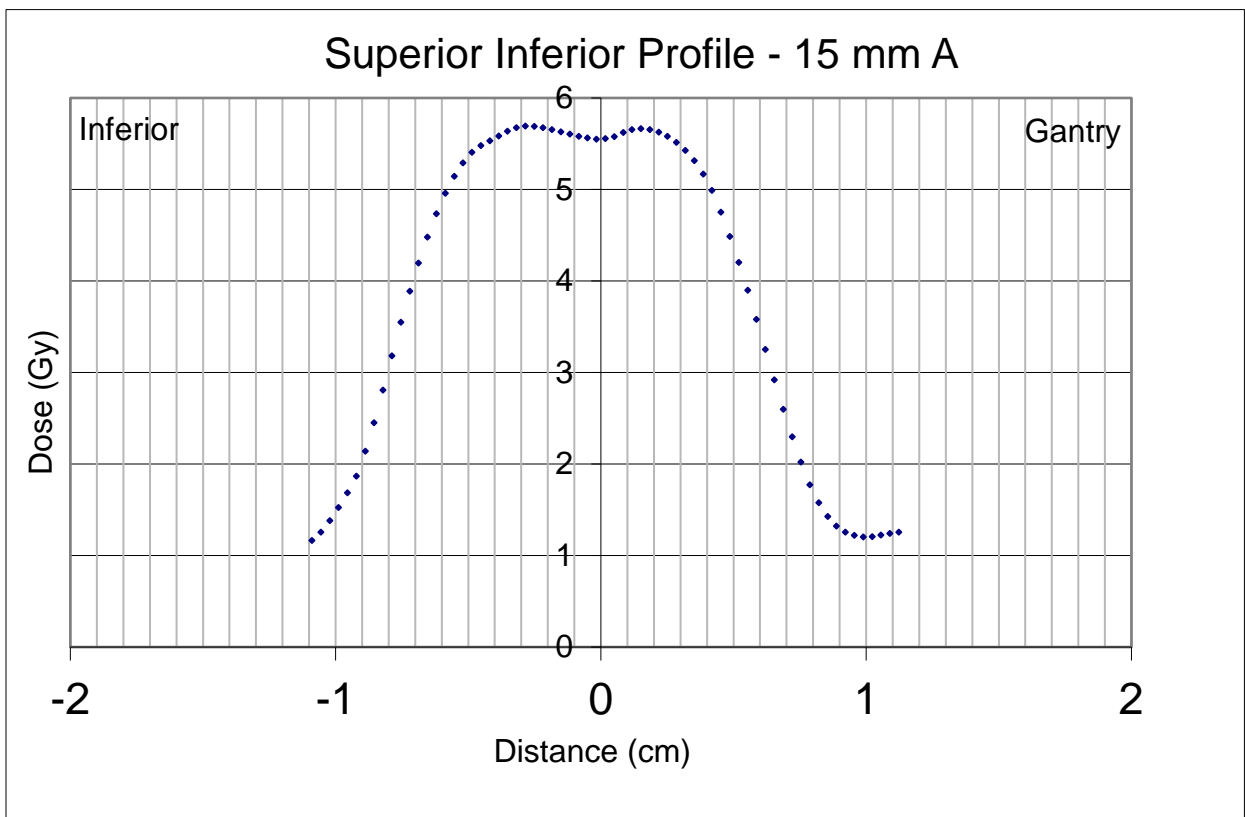


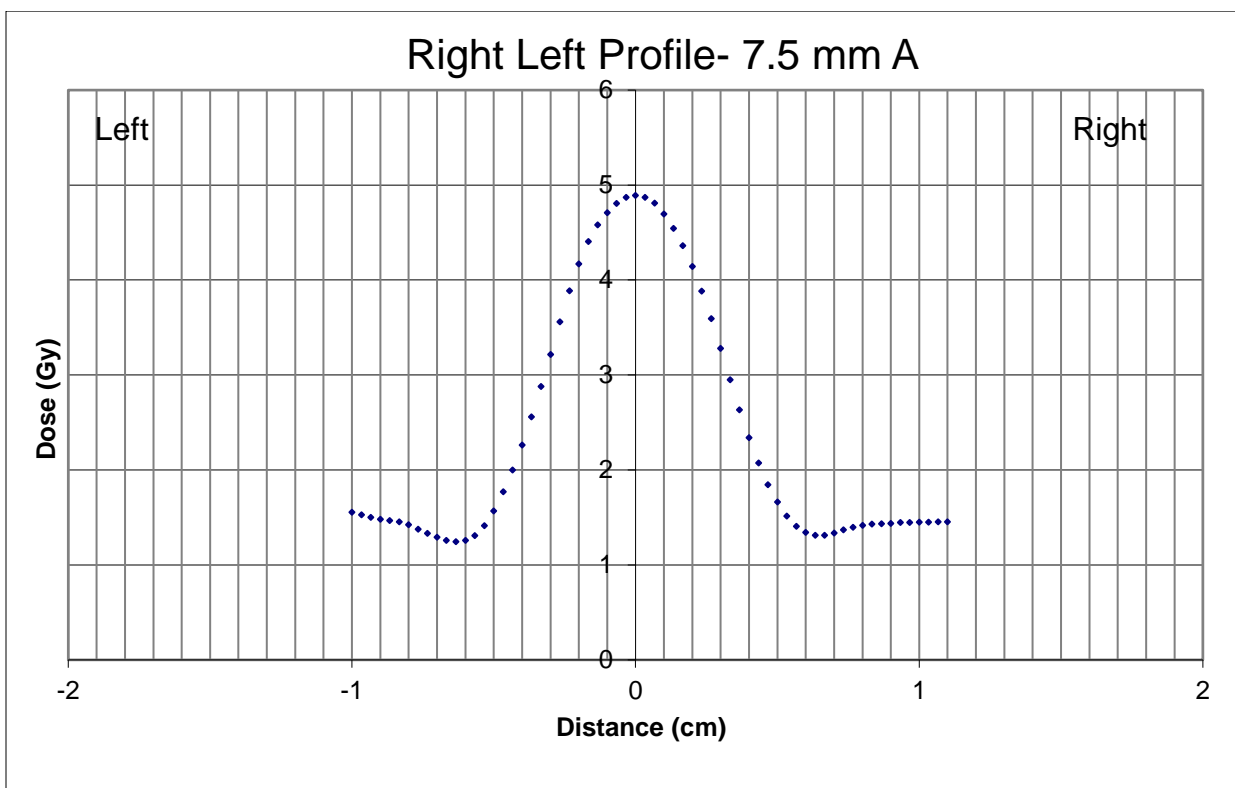
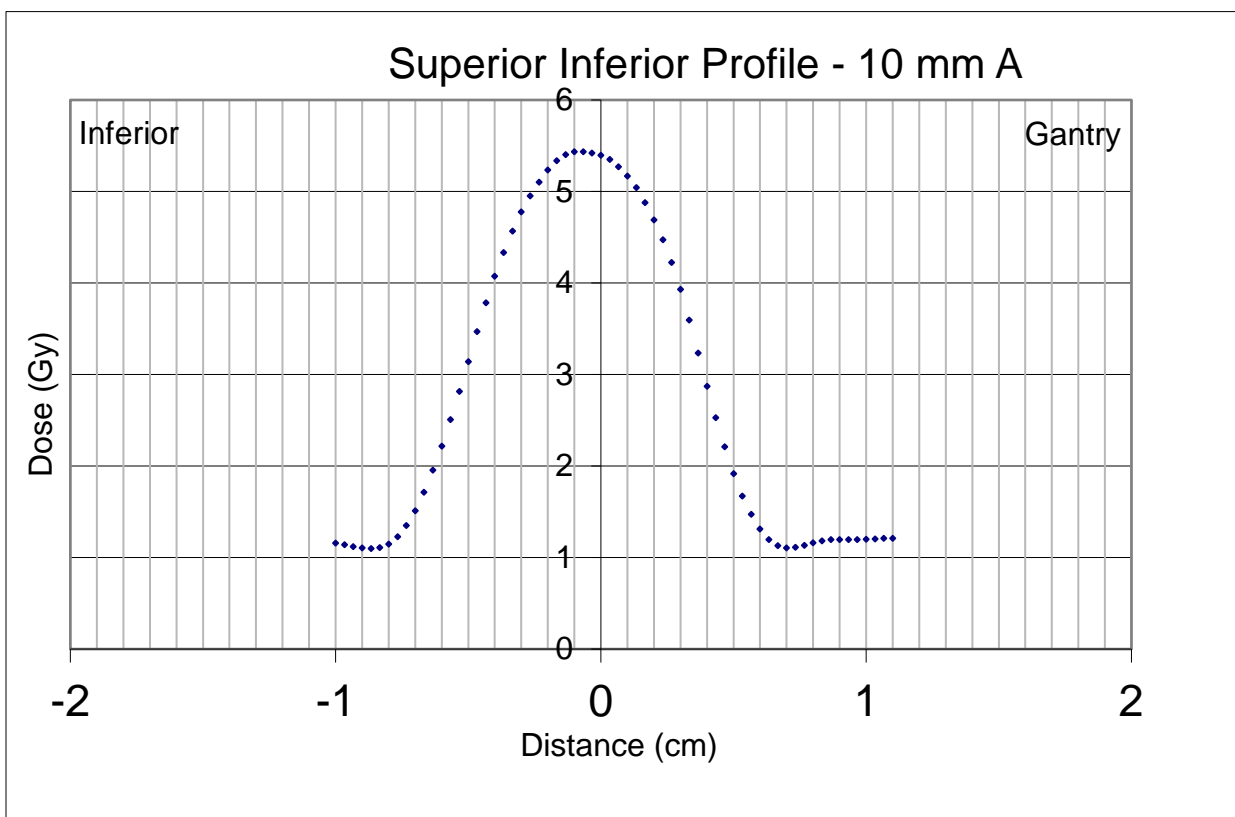


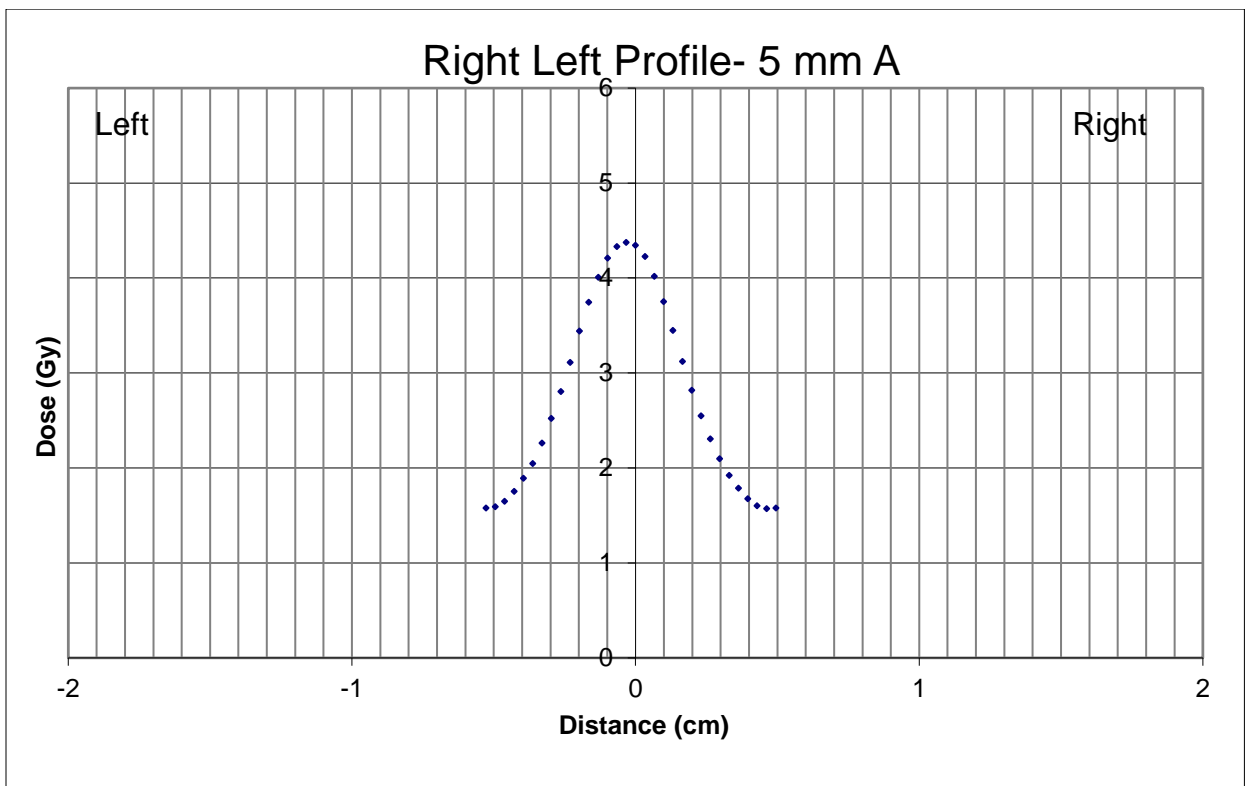
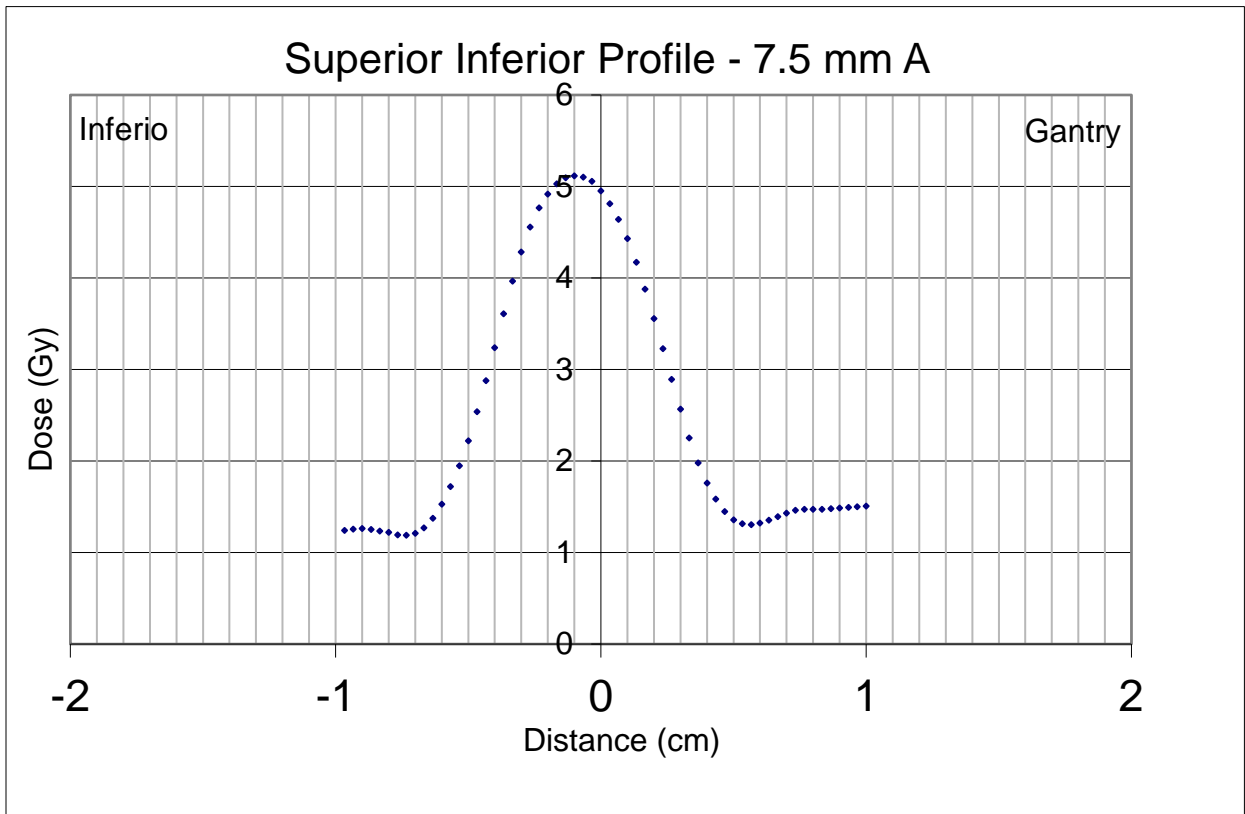
6.5 Small Field Film Line Profiles

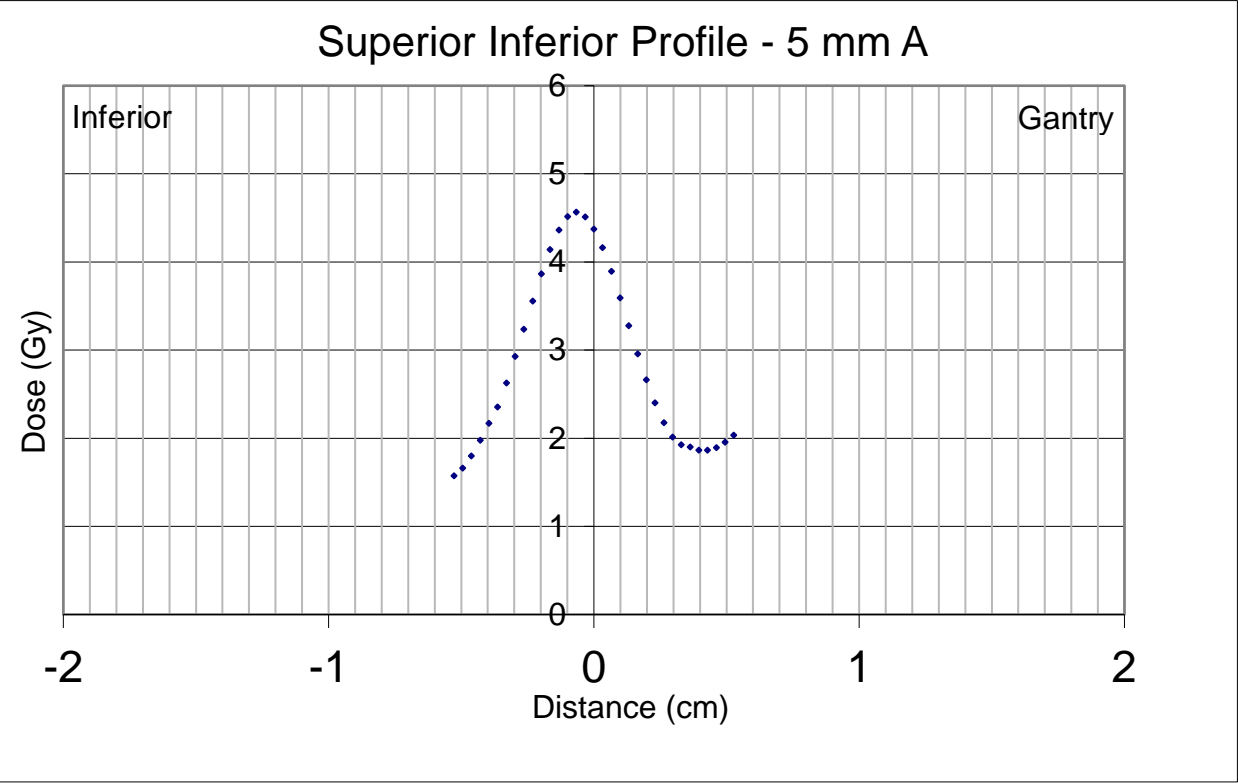












Bibliography

References

Agency, I. A. E. (2017). *Dosimetry of Small Static Fields Used in External Beam Radiotherapy*. Vienna:

INTERNATIONAL ATOMIC ENERGY AGENCY.

Almond, P. R., Biggs, P. J., Coursey, B. M., Hanson, W. F., Huq, M. S., Nath, R., & Rogers, D. W. O. (1999).

AAPM's TG-51 protocol for clinical reference dosimetry of high-energy photon and electron beams. *Medical Physics*, 26(9), 1847-1870. doi:10.1118/1.598691

Alvarez, P., Kry, S. F., Stingo, F., & Followill, D. (2017). TLD and OSLD dosimetry systems for remote audits of radiotherapy external beam calibration. *Radiation Measurements*, 106, 412-415.

doi:<https://doi.org/10.1016/j.radmeas.2017.01.005>

Aspradakis, M. M., Byrne, J. P., Palmans, H., Duane, S., Conway, J., Warrington, A. P., & Rosser, K.

(2010). *IPEM report 103: Small field MV photon dosimetry*. Retrieved from International Atomic

Energy Agency (IAEA): http://inis.iaea.org/search/search.aspx?orig_q=RN:42026432

Azangwe, G., Grochowska, P., Georg, D., Izewska, J., Hopfgartner, J., Lechner, W., Anderson, E.,

Beierholm, R., Helt-Hansen, J., Mizuno, H., Fukumara, A., Yajima, K., Gouldstone, C., Sharpe, P.,

Meghzifene, A., Palmans, H. (2014). Detector to detector corrections: A comprehensive

experimental study of detector specific correction factors for beam output measurements for

small radiotherapy beams. *Medical Physics*, 41(7), 072103. doi:10.1118/1.4883795

Bassinet, C., Robbes, I., Barbier, L., Baumann, M., Kernisant, B., & Trompier, F. (2010). Characterization

of 7LiF:Mg,Ti TLD micro-cubes. *Radiation Measurements*, 45(3-6), 646-648.

doi:DOI:101016/jradmeas200912005

- Crop, F., Reynaert, N., Pittomvils, G., Paelinck, L., De Wagter, C., Vakaet, L., & Thierens, H. (2009). *The influence of small field sizes, penumbra, spot size and measurement depth on perturbation factors for microionization chambers* (Vol. 54).
- da Rosa, L. A. R., Regulla, D. F., & Fill, U. A. (1999). Reproducibility study of TLD-100 micro-cubes at radiotherapy dose level. *Applied Radiation and Isotopes*, 50(3), 573-577.
doi:[https://doi.org/10.1016/S0969-8043\(98\)00068-2](https://doi.org/10.1016/S0969-8043(98)00068-2)
- DeWerd, L. A. (1983). Applied Thermoluminescent Dosimetry edited by M. Oberhofer and A. Scharmann. *Medical Physics*, 10(3), 377-378. doi:10.1118/1.595381
- Flickinger, J. C., Dade, Lunsford, L., Wu, A., Maitz, A. H., & Kalend, A. M. (1990). Treatment planning for gamma knife radiosurgery with multiple isocenters. *International Journal of Radiation Oncology • Biology • Physics*, 18(6), 1495-1501. doi:10.1016/0360-3016(90)90326-F
- Gildenberg, P. L. (2001). Spiegel and Wycis - the early years. *Stereotact Funct Neurosurg*, 77(1-4), 11-16.
doi:10.1159/000064587
- Girard, F., Bouchard, H., & Lacroix, F. (2012). Reference dosimetry using radiochromic film. *Journal of Applied Clinical Medical Physics*, 13(6), 339-353. doi:10.1120/jacmp.v13i6.3994
- Godson, H. F., Ravikumar, M., Sathiyar, S., Ganesh, K. M., Ponmalar, Y. R., & Varatharaj, C. (2016). Analysis of small field percent depth dose and profiles: Comparison of measurements with various detectors and effects of detector orientation with different jaw settings. *J Med Phys*, 41(1), 12-20. doi:10.4103/0971-6203.177284
- Grant, R. M., & Cameron, J. R. (1966). Effects of Pre-Irradiation Annealing on the Thermoluminescence and Dielectric Loss of LiF:Mg. *Journal of Applied Physics*, 37(10), 3791-3795.
doi:10.1063/1.1707926
- Ibbott, G. (2010). MO-A-BRA-01: Credentialing for Clinical Trials. *Medical Physics*, 37(6Part14), 3334-3334. doi:10.1118/1.3469035

- Kano, H., Niranjana, A., Kondziolka, D., Flickinger, J. C., & Lunsford, L. D. (2009). Stereotactic radiosurgery for pituitary metastases. *Surgical Neurology*, 72(3), 248-255.
doi:<https://doi.org/10.1016/j.surneu.2008.06.003>
- Kirby, T. H., Hanson, W. F., & Johnston, D. A. (1992). Uncertainty analysis of absorbed dose calculations from thermoluminescence dosimeters. *Medical Physics*, 19(6), 1427-1433.
doi:10.1118/1.596797
- Knoll, G. F. *Radiation Detection and Measurement* (Fourth ed.). New York: John Wiley and Sons, Inc.
- Kron, T. (1995). *Thermoluminescence dosimetry and its applications in medicine-Part 2: History and applications* (Vol. 18).
- Lasak, J. M., & Gorecki, J. P. (2009). The History of Stereotactic Radiosurgery and Radiotherapy. *Otolaryngologic Clinics of North America*, 42(4), 593-599.
doi:<https://doi.org/10.1016/j.otc.2009.04.003>
- Li, S., Medin, P., Pillai, S., & Solberg, T. (2006). SU-EE-A1-02: Analysis of Photon Beam Data From Multiple Institutions: An Argument for Reference Data. *Medical Physics*, 33(6Part2), 1991-1991.
doi:10.1118/1.2240156
- Li, W., Cho, Y.-B., Ansell, S., Laperriere, N., Ménard, C., Millar, B.-A., . . . Chung, C. (2016). The Use of Cone Beam Computed Tomography for Image Guided Gamma Knife Stereotactic Radiosurgery: Initial Clinical Evaluation. *International Journal of Radiation Oncology • Biology • Physics*, 96(1), 214-220. doi:10.1016/j.ijrobp.2016.04.011
- Mathieu, D., Flickinger, J. C., Kondziolka, D., Niranjana, A., Martin, J. J., Lunsford, L. D., & Madhok, R. (2008). RADIOSURGERY AS DEFINITIVE MANAGEMENT OF INTRACRANIAL MENINGIOMAS. *Neurosurgery*, 62(1), 53-60. doi:10.1227/01.NEU.0000311061.72626.0D
- Michael C. Schell, F. J. B., David A. Larson, Dennis D. Leavitt, Wendell R. Lutz, Ervin B. Podgorsak, Andrew Wu. (1995). AAPM Report No. 54 Stereotactic Radiosurgery. *American Association of Physicists in Medicine*.

- Ogunleye, O. T., Richmond, R. G., Cash, B. L., & Jones, K. L. (1987). Effects of Annealing on the Sensitivity of LiF TLD-100 After Repeated Use for Low Dose Measurements. *Radiation Protection Dosimetry*, 18(2), 101-104. doi:10.1093/oxfordjournals.rpd.a079891
- Palmans, H., Andreo, P., Huq, M. S., Seuntjens, J., Christaki, K. E., & Meghzifene, A. (2018). Dosimetry of small static fields used in external photon beam radiotherapy: Summary of TRS-483, the IAEA–AAPM international Code of Practice for reference and relative dose determination. *Medical Physics*, 45(11), e1123-e1145. doi:10.1002/mp.13208
- Schulz, R. J., Maryanski, M. J., Ibbott, G. S., & Bond, J. E. (1993). Assessment of the accuracy of stereotactic radiosurgery using Fricke-infused gels and MRI. *Medical Physics*, 20(6), 1731-1734. doi:10.1118/1.597126
- Wowra, B., Muacevic, A., & Tonn, J.-C. (2009). Quality of radiosurgery for single brain metastases with respect to treatment technology: a matched-pair analysis. *Journal of Neuro-Oncology*, 94(1), 69. doi:10.1007/s11060-009-9802-y

Vita

Brandon Michael Lockett was born in Baton Rouge, Louisiana, the son of Suzanne Shaye and John Paul Lockett. After completing his studies at Catholic High School in Baton Rouge, Louisiana, he entered Louisiana State University in Baton Rouge. He received his degree of Bachelor of Sciences with a major in physics and a concentration in medical physics in May 2017. In August of 2017, he entered the Master of Science in Medical Physics program at the University of Texas MD Anderson Cancer Center UTHealth Graduate School of Biomedical Sciences.